UNIVERSITY OF NOTTINGHAM

DEPARTMENT OF CIVIL ENGINEERING

THE BEHAVIOUR OF A GRANULAR MATERIAL UNDER REPEATED LOADING

by

John R. Boyce

May 1976

UNIVERSITY OF NOTTINGHAM

DEPARTMENT OF CIVIL ENGINEERING

THE BEHAVIOUR OF A GRANULAR MATERIAL UNDER REPEATED LOADING

by

JOHN RODNEY BOYCE, M.A.

Thesis submitted to the University of Nottingham

for the degree of Doctor of Philosophy

May 1976

CONTENTS

ACKNOWLEDGEMENTS

The author wishes to express his thanks to all those who assisted in this research project and in the preparation of the thesis, including:

Professor R.C. Coates, Head of Department, for providing all the facilities in the Department,

Dr. S.F. Brown and Professor P.S. Pell for their constructive criticism and helpful supervision throughout the work.

Mr. R.C. Collins for his advice and expert workmanship in the construction and maintenance of the equipment and for his help in carrying out the test programme.

Mrs. E.M. Nickeas for efficiently dealing with orders for external supplies.

Miss R. Allen for preparation of the diagrams in the thesis.

Miss J.L. Clerbaut, who undertook all the typing, for her competence and for her ability to decipher my illegible handwriting,

and to all the other members of staff in the Department and in the Faculty Workshops who have willingly given advice and assistance whenever it was requested.

This research project would not have been possible without the generous financial support of the Transport and Road Research Laboratory and this is gratefully acknowledged.

Finally, the author wishes to thank all the friends he has made in Nottingham for their tolerant attitude at a time when he was even more absent-minded than usual.

ABSTRACT

A large number of repeated load triaxial tests were carried out on samples of a well graded crushed limestone, maximum particle size 38 mm. This material is commonly used for the base or sub-base layers of flexible highway pavements in the United Kingdom. The aim of the research was to measure the strains which occurred when the material was subject to a wide range of stresses similar to those expected to occur in a pavement structure due to traffic loading. A review of previous work is presented and several new experimental techniques which were developed to achieve this aim are described.

Resilient strain tests were performed in which a few cycles of load only were applied at each stress condition, including conditions of cyclic confining stress, in order to measure the resilient behaviour of the material without subjecting it to large permanent strains. The primary factors influencing resilient strain response were found to be the mean normal stress and the ratio of deviator stress to normal stress. Permanent strain tests were then performed in which large numbers of load cycles were applied at each stress condition. The permanent strain which developed was found to be largely dependent on the applied stress ratio and it was also found that large numbers of load cycles caused some anisotropy in the resilient behaviour. A model for the resilient strain response of the material is proposed, and the application of the results to pavement design is discussed.

LIST OF SYMBOLS

φ'	angle of shearing resistance
E_r	resilient modulus of elasticity
ν_r	resilient Poisson's ratio
θ	sum of the principal stresses
N	number of load cycles

In the triaxial test:

σ_1	axial stress
σ_3	radial stress
ϵ_1	axial strain
ϵ_3	radial strain
p	normal stress $(\sigma_1/3 + 2\sigma_3/3)$
q	deviator stress $(\sigma_1 - \sigma_3)$
ϵ	shear strain $(\frac{2}{3}(\epsilon_1 - \epsilon_3))$
v	volumetric strain $(\epsilon_1 + 2\epsilon_3)$
S	stress ratio (q/p)
T_A, T_B	special stress parameters } see Section 8.3
W_A, W_B	special strain parameters } see Section 8.3

In three dimensions:

σ_1, σ_2, σ_3	principal stresses
ϵ_1, ϵ_2, ϵ_3	principal strains
T_A, T_B, T_C	special stress parameters } see Section 10.2.2
W_A, W_B, W_C	special strain parameters } see Section 10.2.2

Note:

Suffix m indicates a mean value of stress.

Suffix r indicates a repeated amplitude of stress or a resilient amplitude of strain measured from peak to peak.

Suffix p indicates a value of permanent strain.

Compressive stresses and strains are taken as positive.

Other symbols are defined and used in restricted conditions as the need arises.

LIST OF FIGURES

CHAPTER ONE

INTRODUCTION

The term "granular material" covers a variety of naturally occurring and artificially graded aggregates, and in the context of this investigation refers particularly to those used in the base and sub-base layers of a flexible pavement. The materials used include sand, gravel and crushed rock with the maximum particle size often being as large as 38 mm. All of these materials exhibit some similarities in their mechanical behaviour, because their strength is derived from interlock between the aggregate particles. The object of this research project was to investigate the behaviour of such a material on a macroscopic level as if it were a uniform solid, although this behaviour is clearly determined by the properties of the aggregate particles themselves.

The compaction of granular materials and their strength under a slowly applied load have been the subject of experimental study for many years, and are now fairly well understood. More recently, the behaviour of these materials under repeated loading has been investigated. This aspect of the behaviour is important because the granular layer of a highway pavement is subject to a repeated application of stress as each wheel load passes on the surface above. The role of the granular layer is essentially that of an intermediary between the surfacing which is relatively stiff, even in a flexible pavement, and the subgrade which is often relatively soft. The purpose of the previous studies (Hicks, 1970; Barksdale, 1972; Allen and Thompson, 1974; and Kennedy, 1974) was to compare the behaviour of a variety of granular materials under repeated loading; but it can also

be inferred from this work that the stress dependent stiffness of the materials make an important contribution to their role in a pavement. It is desirable to have a gradual transition from the stiff surfacing to the softer subgrade to avoid the tensile stress which occurs at the bottom of stiff layers and to spread the load more evenly over the lower layers of the pavement.

In this project it was decided to look in more detail at the stress-strain characteristics of a particular granular material. The material chosen was a well graded, crushed limestone commonly used as the base or sub-base in road construction in the United Kingdom. To obtain a fundamental understanding of the properties of the aggregate the test programme was formulated in terms of stress invariants, and the material was tested dry so that the effective stress could be directly related to the applied loads.

In order to achieve well defined stress conditions in the material, the tests were carried out in a triaxial apparatus, and repeated stresses were applied by servo-controlled hydraulic actuators generally at a frequency of 1 Hz. The stresses which can be applied in a triaxial test are similar to those which occur in a pavement under a wheel load; except that in a pavement the directions of principal stress rotate as the wheel passes, whereas in a triaxial apparatus they are always the same. Before embarking on the test programme, it was necessary to develop new techniques for sample preparation and for strain measurement. Locating points were embedded in the material during sample preparation so that axial and radial strain could be measured over the central part of the sample away from possible end effects. When carrying out repeated load tests, it is useful to measure separately the permanent (or plastic) strain which develops after a number of complete load cycles,

and the resilient (or elastic) strain which occurs with each load cycle. After some preliminary tests, the main test programme was in two parts designed to investigate the resilient response and the permanent strain response of the material. A wide range of repeated stresses were applied and the strains which occurred were measured so that the effect of different stress conditions on the material could be fully defined.

Although the form of a flexible pavement structure is relatively simple, the nature of the loading makes a rigorous stress-strain analysis very difficult if the non-linear behaviour of any layer is to be correctly represented. Current methods of pavement design are largely based on empirical rules which determine the thickness of each layer without considering the stresses in the structure. These methods are satisfactory when considerable experience has been built up of a certain type of construction in certain conditions. However, when designing pavements in unusual environmental conditions such as developing countries, when designing for different types of loading, or when using new materials in the interests of economy, it is necessary to adopt a more rational approach which takes into consideration the mechanical properties of the materials and the loads applied to the structure.

Analytical methods are available at the present time (Peutz et al, 1968; Thrower, 1968; and Warren and Dieckman, 1963) which treat the pavement as a semi-infinite structure of three or four layers, each layer being isotropic with constant elastic properties. Such methods give a good indication of the stresses in pavements with a considerable thickness of bituminous material (greater than 150 mm) but doubts have been expressed (Dehlen, 1969; and Hicks and Monismith, 1972) about their ability to predict the stresses in pavements with a thin asphalt

surfacing (say 50 mm) and a thick granular base (say 300 mm) because of the non-linear characteristics of the granular layer. This type of construction is commonly used in developing countries where traffic densities are low and initial cost is a prime consideration, and it is therefore important that the properties of granular materials should be defined under a wide range of conditions so that appropriate analytical methods can be used to predict the behaviour of such pavements. The finite element method at present appears to have the best possibilities and it is hoped that the results of this investigation will be useful in formulating suitable techniques. However, further theoretical and experimental work is required before such a procedure can be incorporated into a design method with any degree of confidence.

This work was directed specifically towards the behaviour of granular materials in a highway pavement, but the results may also find application in other situations where granular materials are subject to repeated loading. These include the ballast under a railway track, and natural sand and gravel deposits under the foundations of structures subject to earthquakes, or to wave action in the case of off-shore structures.

CHAPTER TWO

REVIEW OF PREVIOUS WORK - STRESS-STRAIN BEHAVIOUR OF GRANULAR MATERIALS

The majority of laboratory tests on coarse grained, granular materials have been carried out in the triaxial apparatus. This apparatus employs a cylindrical sample subjected to an all round confining stress (σ_3) and an axial deviator stress ($\sigma_1 - \sigma_3$). Granular materials have been tested in the dry, saturated and partially saturated condition, and it will be made clear in the text when the stresses referred to are total stresses or effective stresses.

2.1 SINGLE LOAD TESTS

This form of test is much used in soil mechanics to determine the strength and stress-strain response of soils. For a given confining stress, the deviator stress is increased until failure or excessive deformation occurs.

It is important when studying granular materials to pay attention to the density and moisture content at which the test takes place. Beavis (1969) tested 20 different granular materials used in Australia, and states: "Each of the twenty materials tested has the same type of stress-strain curve when moulded and tested within a similar zone of density and moisture content expressed in terms of compactive effort. .... The stress-strain curves of each material vary more over the range of conditions examined than do all 20 materials under equivalent conditons." In other words, the condition of the material can have as much effect on its behaviour as the type of aggregate and the grading used.

Dunn (1966) reported work on crushed aggregates, maximum particle

size 19 mm, to study the effect of fines content on compaction and stability. He found that up to 6% fines aided compaction, but that the material with only 1% fines had the highest shear strength in the undrained triaxial test. He also noted that increased plasticity of the fraction passing a No. 36 sieve reduced the undrained shear strength. This work indicates that material graded for maximum density may not have the best stress-strain behaviour.

Thompson (1969) comes to similar conclusions, and notes that the density achieved by a given compactive effort is dependent upon:

(1) particle index (shape),

(2) gradation and maximum particle size,

(3) fines content and plasticity of these fines,

and that the same factors affect the strength and stiffness of the material, but not in the same way. He found that maximum density occurred at 13% fines content and maximum strength at 8%. With regard to repeated loading, he says that work has shown that aggregates consisting of rounded particles are not as satisfactory in dynamic* conditions as those with angular particles.

Kennedy (1974) performed single load triaxial tests (drained) on partially saturated aggregate. He worked with each of the following factors at two levels:

(1) Aggregate type (limestone and granite)

(2) Grading (open and dense)

(3) Density (achieved by compaction at -2% and +2% of O.m.c.)

(4) Cell pressure (5 p.s.i. and 15 p.s.i.)

---

* The term "dynamic" is used by some workers when referring to tests with rapid repeated loading. It does not imply that the material is experiencing large accelerations.

The secant modulus at various values of axial strain was used as a parameter of strength and stiffness. This parameter was found to increase markedly with cell pressure and density. Aggregate type was not significant, and grading was only significant in that it affected the density which could be achieved during compaction.

The stress-strain behaviour of the material is interesting, and typical curves for granite (dense grading) are shown in Fig. 2.1. The behaviour is similar to that found for dense cohesionless soils. Initially, a volume contraction occurs but this changes to a dilation with the material still dilating rapidly at maximum axial stress.

2.2 REPEATED LOAD TESTS (RESILIENT STRAIN)

Some of the first reported research on repeated loading of granular materials was by Williams (1963). This work was an attempt to define the stiffness of granular material so that appropriate parameters could be used in layered system theory to calculate stresses in the overlying bituminous material of a pavement. It was recognised that this would require the measurement of resilient strains as the material was subjected to repeated loading in the laboratory. Williams did some work using successive applications of a single load on sand, and reported that the stiffness reached a more or less constant value after only 50 applications. He concluded:

(1) "Repeated cyclic loading of granular soils causes an increase in elastic modulus and a decrease in non-recoverable strain. These changes cannot be attributed simply to densification, but perhaps to some rearrangement of the particles which does not give rise to a significant volume change."

(2) ".... the elastic modulus is linearly related to the cell pressure raised to the one third power."

(3) ".... rate of loading has only a small effect on the elastic modulus."

Since 1960, much work has been done in various parts of the world to establish the resilient properties of granular materials. Work done in the United States, and especially at the University of California, is well reviewed by Hicks (1970). From this research, it emerges that the following factors can influence the resilient response of granular materials subject to repeated loads:

(1) Stress level (mean normal stress or confining stress)

(2) Density

(3) Grading, aggregate type and particle shape

(4) Moisture content

(5) Frequency of loading and number of load applications

Each of these factors is dealt with separately below, except for moisture content which is considered later (Section 2.4).

Considerable work has also been done on the dynamic properties of sand to establish its behaviour under the conditions set up by earthquakes. This work has included strain controlled, repeated load, triaxial tests on dry and saturated samples of sand at frequencies and stresses similar to those applicable to pavement design (e.g. Silver and Park, 1975). The results have shown that shear modulus varies in very much the same way as for the resilient modulus described below, and that the hysteretic damping factor is in the range of 10% to 30%.

2.2.1 Stress Level

Every study in this field has recorded an increase in the stiffness of granular material with stress level, expressed in terms of confining stress (σ_3) or mean normal stress (p). Stiffness is usually expressed as the resilient modulus which is analogous to Young's Modulus in linear elastic materials. The resilient modulus (E_r) is defined by:

$$E_r = \frac{\sigma_{1r}}{\epsilon_{1r}}^{*} \qquad (2.1)$$

where ϵ_{1r} is the resilient axial strain caused by a repeated axial stress, σ_{1r}.

The relationships between E_r and stress level found from different studies are shown in Table 2.1. These results were usually obtained from a single sample, about 100 loading cycles being applied at each stress level in order to obtain a constant resilient strain before taking measurements. It has been shown that the resilient strain does not vary appreciably after larger numbers of loading cycles (Lashine et al, 1971; Morgan, 1966).

It can be seen from Table 2.1 that the majority of studies have indicated that the resilient modulus is affected by stress level as follows:

$$E_r = K_1(\sigma_3)^{K_2} \quad \text{or} \quad E_r = K_1'(p)^{K_2'} \qquad (2.2)$$

From his extensive investigation, Hicks (1970) found higher correlation coefficients when resilient modulus was expressed as a function of mean normal stress (p) than in terms of confining stress (σ_3).

Certain workers, including Morgan (1966) and Lashine et al (1971), have noted that the resilient modulus (E_r) also appears to be dependent on the axial deviator stress ($\sigma_1 - \sigma_3$). However, there is not sufficient

---

* For tests with constant confining stress.

information available at present to assess the significance of these observations.

Table 2.1

Effect of Stress Level on Resilient Modulus

Worker	Material	Relationship
Biarez (1962)	Uniform sand	$E_r = K_1'(p)^{K_2'}$ $(0.5 < K_2' < 0.6)$
Dunlap (1963)	Partially saturated, well graded aggregate	$E_r = K_1 + K_2(\sigma_3)$
Williams (1963)	Uniform sand (1)	$E_r = K_1 + K_2(\sigma_3)^{\frac{1}{3}}$
Hicks (1970) and others at Berkeley	Aggregate base	$E_r = K_1(\sigma_3)^{K_2}$ or $K_1'(p)^{K_2'}$
Moore et al (1970)	Crushed limestone base (1)	$E_r = K_1 + K_2(\sigma_3)^2$
Lashine et al (1971)	Crushed stone	$E_r = K_1(\sigma_3)^{K_2}$ $(K_2 = 0.54)$
Allen and Thompson (1973)	Gravel and crushed stone	$E_r = K_1(\sigma_3)^{K_2}$ or $K_1'(p)^{K_2'}$
Hardin and Black (1966)	Dry sand (2)	$E_r = K_1(p)^{K_2}$
Robinson (1974)	Uniform dry sand (2)	$E_r = K_1'(p)^{K_2'}$ $K_2' = 0.48 - 0.60$

(1) These relationships are based on a limited number of results.

(2) These results were obtained from vibration tests, the others are from repeated load tests.

2.2.2 Density

Trollope et al (1962) reported slow repeated load tests on a uniform sand, and found that the resilient modulus increased by up to 50% between loose and dense samples. Robinson (1974) also worked with a uniform sand, and measured stiffness by resonance. He found that the

coefficient K_1' (see Eqn 2.2) increased linearly by 50% between the loosest and densest samples (void ratios of 0.67 and 0.50 respectively) but that K_2' was unaffected.

Some work has also been done on the way in which density affects graded aggregate. Coffman et al (1964) reported creep tests on base and sub-base material used in the AASHO road test and Kennedy (1974) reported repeated load tests on aggregate base material. Both noted that stiffness increased with density. Hicks (1970) performed fairly extensive tests on aggregate base material and observed a general trend of increasing resilient modulus with dry density. Even his results do not show any consistent relationship between density and stiffness, and it must be concluded that such a relationship is yet to be established.

2.2.3 Grading, Aggregate Type and Particle Shape

These variables have a marked effect on the density of material which can be achieved with a given compactive effort. However, if results are compared on the basis of material at the same relative density*, there appears to be little effect on stiffness.

Hicks (1970) compared results of a crushed and partially crushed aggregate, and found that the coefficients K_1 and K_2 (see Eqn 2.2) were similar at comparable relative densities. Robinson (1974) noted that K_2' (see Eqn 2.2 again) was 0.48 for angular sands and 0.60 for a rounded sand. This would indicate that rounded particles are even more dependent than angular ones on the level of confining stress to achieve their stiffness.

---

* Relative density is here defined as the density of the material being investigated compared with the maximum and minimum densities which can be achieved for material of that type and grading.

If relative density is the criterion which determines the stiffness of different granular materials, it indicates that a poorly graded material, such as railway ballast, and a well graded material, such as road base, would have similar resilient properties.

2.2.4 Frequency of Loading and Number of Load Applications

A few workers have attempted to measure the effect of frequency on the stiffness of granular materials (Williams, 1963; Lashine et al, 1971; and Robinson, 1974). They all come to the conclusion that frequency of loading has little or no effect.

Some change in the resilient modulus of granular material after a large number of load applications (up to 10^6) have been recorded in a few instances (Morgan, 1966; Lashine et al, 1971; and Kennedy, 1974). However, there is no data given to correlate these changes with any other effect. Moore et al (1970) observed that the resilient modulus of a crushed limestone was still increasing after 2.5×10^6 load applications, but they suggested that this may have been due to a gradual loss of moisture leading to high suction forces. It has been observed in the field that a cementitious bonding action can occur in crushed limestone in the presence of moisture, and this may lead to an increase in stiffness. There is no evidence that large numbers of load applications have any direct effect on the stiffness of granular materials.

2.2.5 Radial Strain

For a triaxial test with constant confining stress, the resilient Poisson's ratio (ν_r) can be defined as:

$$\nu_r = -\epsilon_{3r}/\epsilon_{1r} \qquad (2.3)$$

where ϵ_{1r} and ϵ_{3r} are resilient strains in the axial and radial

directions. As the definition implies, measurements of resilient radial strain are required to determine this parameter, and techniques for this have only recently been developed (see Section 3.4.4).

The first worker to obtain measurements of radial strain was Morgan (1966). He found that ν_r varied in the range 0.2 - 0.4. More complete data is supplied by Hicks (1970) and he found that the resilient Poisson's ratio (ν_r) varied with the stress ratio (σ_1/σ_3) as shown in Fig. 2.2. These tests employed a constant confining stress (σ_3) and a repeated axial stress (σ_1), and similar results were obtained for other samples. The values of secant Poisson's ratio are lower than the tangent values, and this is as one would expect for a parameter which increases with stress level. It is interesting to note that if his results are plotted in terms of the ratio of the stress invariants (q/p), ν_r is directly proportional to q/p. An attempt is made later (Section 2.4.1) to explain the scatter in the Poisson's ratio plot for the partially saturated case.

Hicks also determined the Poisson's ratio for materials with different gradings and densities, and found a wide variation but no discernable pattern (average values of secant Poisson's ratio varied from 0.23 to 0.50).

Robinson (1974) measured resilient Poisson's ratio indirectly by considering the natural vibration of samples in torsional and longitudinal modes. He obtained low values ($\nu_r \approx 0.1$) which is as one would expect, because the stress ratios applied by vibration are low.

No work has yet been done to establish the degree of anisotropy in triaxial specimens, and it is therefore difficult to assess the significance of these values of Poisson's ratio.

2.2.6 Variable Confining Stress

There have been two studies of the effect of variable confining stress on granular materials (Allen and Thompson, 1974; Brown and Hyde, 1975). Both recognise the difficulty in defining the resilient modulus (E_r) and resilient Poisson's ratio (ν_r) for a material which is non-linear. However, they both use the linear-elastic equations with E_r and ν_r as pseudo-elastic constants.

$$\epsilon_{1r} = (\sigma_{1r} - 2\nu_r\sigma_{3r})/E_r$$
$$\epsilon_{3r} = (\sigma_{3r} - \nu_r(\sigma_{1r} + \sigma_{3r}))/E_r \qquad (2.4)$$

Allen and Thompson compared the results of constant confining stress (CCP) tests and variable confining stress (VCP) tests in which the confining stress is cycled from zero at the same time as the deviator stress is applied. They conclude: "Compared with the VCP test data, the CCP data consistently over-estimated Poisson's ratio and generally overestimated E_r by varying amounts."

Typical results are shown in Fig. 2.3. Any interpretation of these results based on pseudo-elastic theories may be misleading and is not attempted here.

Brown and Hyde presented results which are broadly similar for a crushed stone (Breedon gravel). They found that there was a unique relationship between resilient volumetric strain (v_r) and the repeated normal stress (p_r) and between the resilient shear strain (ϵ_r) and repeated deviator stress (q_r) if the stresses were expressed as ratios of the mean normal stress (p_m). These relationships are shown in Figs 2.4 and 2.5. In a discussion of Allen and Thompson's work, Brown (1975) suggested that the apparent difference between their constant

confining stress and variable confining stress tests might be resolved by analysing the results in this way, with due regard to the difference in mean normal stress in the two types of test.

2.3 REPEATED LOAD TESTS (PERMANENT STRAIN)

Compared with the data available on the resilient behaviour of granular materials, information on the build up of permanent strain shows less agreement. This is because the resilient behaviour of the material is not appreciably affected by the previous loading history of the sample, and behaviour at a range of stresses can be measured on a single sample. However, the permanent strain is considerably reduced by any previous loading applied to the sample (Hyde, 1974) and investigation of permanent strain behaviour must begin with a new sample for each stress path applied. Therefore, much less data is available.

2.3.1 Well Graded Material

Lashine et al (1971) carried out repeated load tests on a crushed stone in the partially saturated and drained condition, and found that the permanent axial strain settled down to a constant level (ϵ_f) after about 2 x 10^4 cycles. ϵ_f was found to be dependent on stress ratio:

$$\epsilon_f = 0.9[(\sigma_1 - \sigma_3)_{p-p}/\sigma_3]\% \qquad (2.5)$$

where $(\sigma_1 - \sigma_3)_{p-p}$ = "peak to peak" deviator stress.

There was an exception of one test at a high stress ratio where strain continued to increase to failure. In the case of a few undrained tests, the axial strains were higher but because no pore pressure measurements were taken, interpretation of the results is

difficult. Hyde (1974) tested the same material and showed that Eqn 2.5 is also applicable to tests with variable confining stress if the value of σ_3 chosen is the mean value.

Barksdale (1972) has performed the most comprehensive study to date on the build up of permanent strain in granular base materials. He found that the permanent axial strain (ϵ_{1p}) was proportional to the log of the number of load cycles (N) after a settling down period of about 10 cycles:

$$\epsilon_{1p} = K \log(N) \qquad (2.6)$$

The constant (K) was found to vary with the stress ratio $[(\sigma_1 - \sigma_3)_{p-p}/\sigma_3]$ in a complicated hyperbolic law, but the results exhibited a large degree of scatter.

After testing different materials under various conditions, Barksdale concluded that the accumulation of permanent strain was strongly dependent on the aggregate type and was increased somewhat by low density, increased fines content and by soaking the material. The results showed too much scatter to be interpreted as any more than general trends.

Morgan (1966) performed a few repeated load tests on a well graded angular sand at low stress ratios. His results, together with those of Barksdale and Lashine et al are shown in Fig. 2.6. Lau (1975) also performed repeated load tests on sand and his results are very similar to those reported by Morgan, except that he found that for repeated stresses above a certain proportion of the single load failure stress (0.5 to 0.625) failure eventually took place.

2.3.2 Railway Ballast

A considerable amount of work has been done at the British

Railways Research Department on the behaviour of railway ballast under repeated loading, especially its permanent strain behaviour (Shenton, 1974). The main conclusions are:

(1) Permanent axial strain, ϵ_{1p} increases with the number of load cycles, N, according to the relationship:

$$\epsilon_{1p} = \epsilon_I(1 + 0.2 \log_{10}N) \qquad (2.7)$$

where ϵ_I is the strain after the first load cycle.

(2) Permanent axial strain increases markedly with applied stress ratio:

$$\epsilon_{1p} = K[(\sigma_1 - \sigma_3)_{max}/\sigma_3]^{\alpha} \qquad (2.8)$$

where the exponent α varies between 1 and 3.

Permanent lateral strain was measured and found to be approximately equal magnitude to the permanent axial strain showing that the material was rapidly dilating. Frequency of loading on the range 0.1 to 30 Hz was found to have little effect.

Much work has also been done at Queen's University, Kingston, Ontario, on the behaviour of railway ballast. Their results (e.g. Olowokene, 1975) are similar to those of British Rail.

2.3.3 Mechanism of Permanent Strain

There is no information available at present to suggest what mechanism determines the rate of accumulation of permanent strain in granular materials. There is evidence that the build up of permanent strain with cyclic loading in cohesive soils and in bituminous materials is a creep phenomenon (Hyde 1974; and Snaith, 1973); however, other factors may be responsible in the case of granular materials, as their

stress-strain behaviour is not dependent on the rate of loading. From Fig. 2.6 it can be seen that different types of granular material behave in different ways, but at present the reason for this is not clear.

2.4 EFFECT OF MOISTURE CONTENT ON GRANULAR MATERIALS

The effect which moisture has on the density of soil and granular materials which can be achieved by compaction is well known, and is considered in detail in Section 3.2. However, the effect which moisture has on the stress-strain behaviour of granular materials is more difficult to define.

Repeated loading of granular materials has been carried out on material at various moisture contents from dry to saturated and many workers have used partially saturated material at the moisture content used for compaction.

There are two factors which must be born in mind when considering moisture in granular materials. Firstly, water exerts a pore pressure (U) or suction (S) on the particles of granular material. The pore pressure in a saturated material can be measured (see Section 3.3.6) but it is virtually impossible to measure the suction in partially saturated material during a triaxial test.

Secondly, there may not be sufficient time during a rapid repeated load test on granular material for pore pressures within the material to equalise. This will be dependent on the permeability of the material. According to Barber (1959) the permeability of a granular base can be between 10 ft/day and 3000 ft/day* depending on grading and density.

---

* 1 ft/day = 3.5×10^{-6} m/s.

2.4.1 Effect of Moisture on Resilient Behaviour

Hicks (1970) reviewed previous work at California on the effect of moisture content on the resilient response of granular materials and stated that ".... the resilient modulus decreases as the degree of saturation increases, so long as comparisons are made on the basis of total confining pressures. Comparisons on the basis of effective stresses indicate that the resilient moduli for 100% saturated samples differ only slightly from those of dry samples." As a result of his own tests, Hicks concluded that the degree of saturation affects primarily the parameter K_1 (see Eqn 2.2). In every case, K_1 was lower for a partially saturated sample than for the corresponding dry sample. The value of K_1 for saturated samples (based on effective stresses) was almost the same as for corresponding dry samples.

Haynes and Yoder (1963) reported similar results from undrained repeated load tests on gravel and crushed stone from the AASHO road test, and these are shown in Table 2.2. Increasing the moisture content was found to reduce the resilient modulus.

Hicks (1970) presented some results for the Poisson's ratio of a coarse, partially saturated aggregate, and his results are replotted in terms of the tangent Poisson's ratio (ν_r) and stress parameters (p and q) in Fig. 2.7. In this particular case, ν_r is lower than for the equivalent dry sample (see Fig. 2.2) but this was not found to be a general rule. The interesting point is that if a reasonable value of suction is assumed in the pores of the sample (2 p.s.i.), a much better correlation occurs between the results for different confining stresses. It seems possible, therefore, that the behaviour of the sample is being influenced by soil suction.

Table 2.2

Influence of Degree of Saturation and Grading on Resilient Properties of Granular Materials

(after Haynes and Yoder (1963))

Material tested	Fraction passing No. 200 sieve	Resilient Modulus MN/m^2		
		70% sat.	80% sat.	90% sat.
Gravel	6.2%	385	315	235
	9.1%	-	275	215
	11.5%	395	310	255
Crushed stone	6.2%	290	270	-
	9.1%	270	200	-
	11.5%	275	230	-

2.4.2 Effect of Moisture on Permanent Strain

Morgan (1966) found that the behaviour of drained saturated sand samples was only slightly different from that of dry samples, although there was a tendency for saturated samples to show larger permanent and resilient strains. Lashine et al (1971) found that much greater permanent strains developed in undrained repeated load tests than in corresponding drained tests and concluded that this was due to the build up of excess pore pressures. Barksdale (1972) found that up to 50% greater permanent strains developed in soaked samples as compared with those tested in the "as compacted" condition, i.e. partially saturated.

Apart from these indications, there is little information to assess what effect moisture content has on the build up of permanent strain in granular materials. It seems reasonable to suppose that its

effect must be linked to the existence of pore pressures, either transient in a drained test or permanent in an undrained test. This in turn must be dependent on the grading of the material which determines its permeability in the saturated condition and the level of suction forces in the partially saturated condition. The situation is further complicated by the fact that in a flexible pavement, the drainage conditions are rather different and hence the material may be subjected to pore pressures rather different to those occurring in a triaxial test.

2.5 SUMMARY

The foregoing can be briefly summarised as follows:

(a) The stiffness of granular materials is principally determined by the applied stress level. The resilient modulus (E_r) varies with the mean normal stress (p),

$$E_r = K_1'(p)^{K_2'}$$

There is some evidence that K_1' is dependent on the relative density of the material and that K_2' is dependent on particle shape. Frequency and number of load applications have little effect.

(b) The lateral strain of a sample of granular material in a triaxial test increases with the applied stress ratio. Poisson's ratio (ν_r) can vary between 0 and 1, but most investigations have shown 0.3 to be a typical value under conditions of constant confining stress.

(c) The build up of permanent strain in granular materials is dependent on the ratio of repeated deviator stress to confining stress:

$$(\sigma_1 - \sigma_3)_{p-p}/\sigma_3$$

The rate at which permanent strain is accumulated decreases with the number of load applications.

(d) There is some evidence that the effect of moisture content on granular material is dependent on the pore pressure (or suction) acting on the particles.

(e) In general, a high degree of correlation occurs when a single sample is tested under different conditions; however, there is often much scatter evident when results from different samples are compared. This accounts for much of the uncertainty about the permanent strain response of granular materials and about the effects of density and moisture content. Little work has been done to determine the degree of variation in the results of similar samples under identical conditions, and in the absence of this information, it can only be assumed that the scatter in the results is due to the random and particulate nature of the material.

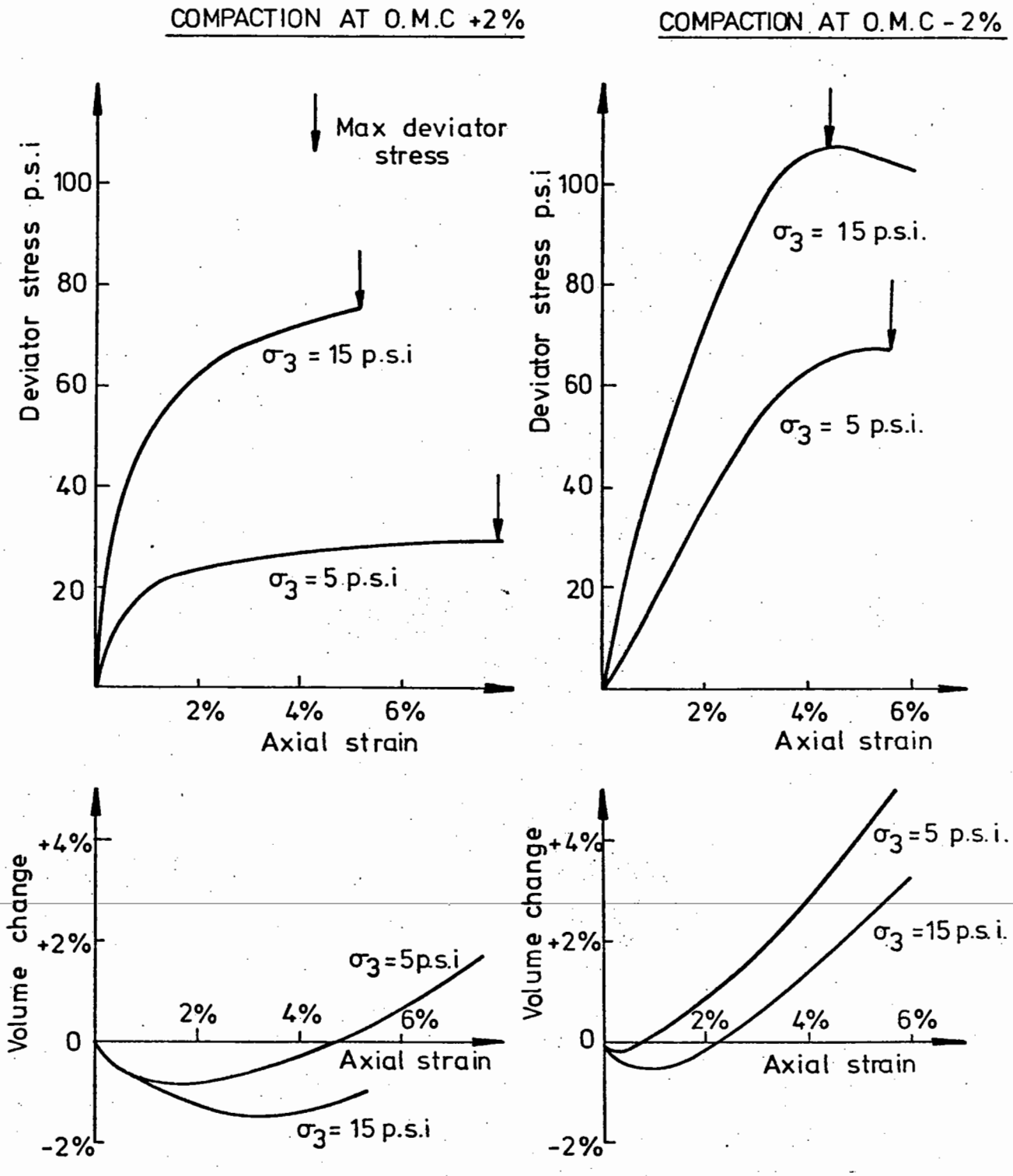

FIG. 2.1 SINGLE LOAD TESTS ON A CRUSHED GRANITE AGGREGATE (AFTER KENNEDY, 1974)

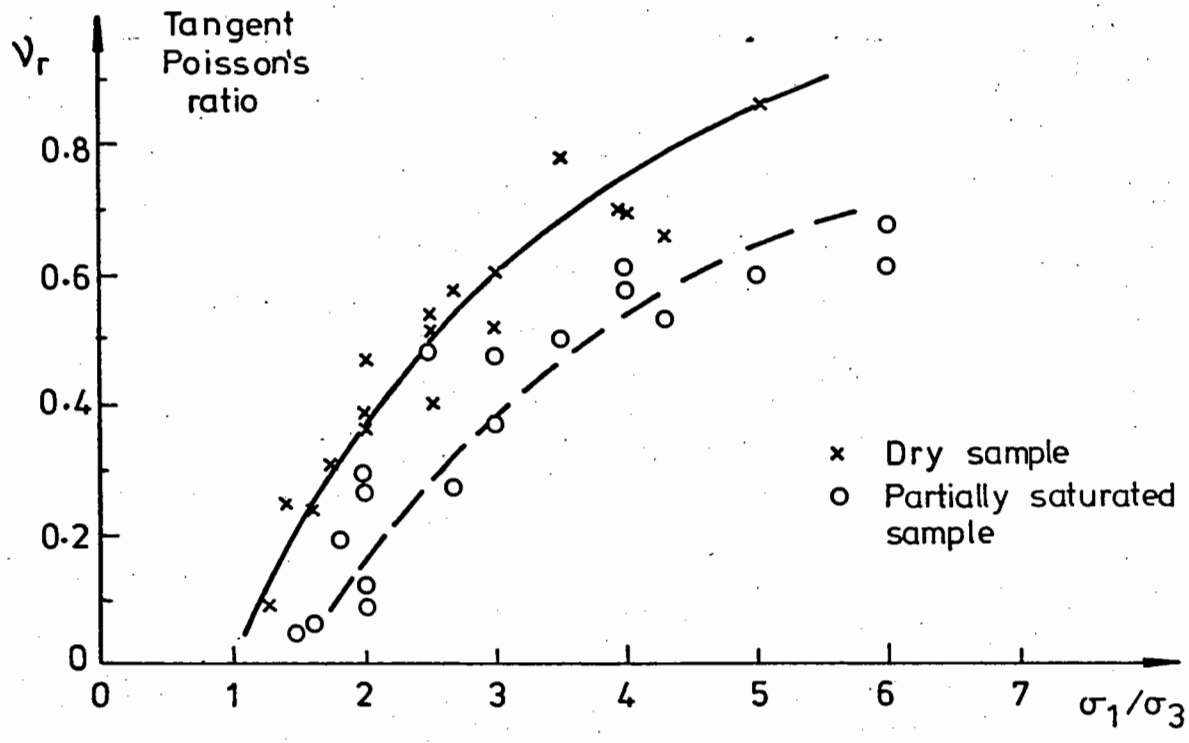

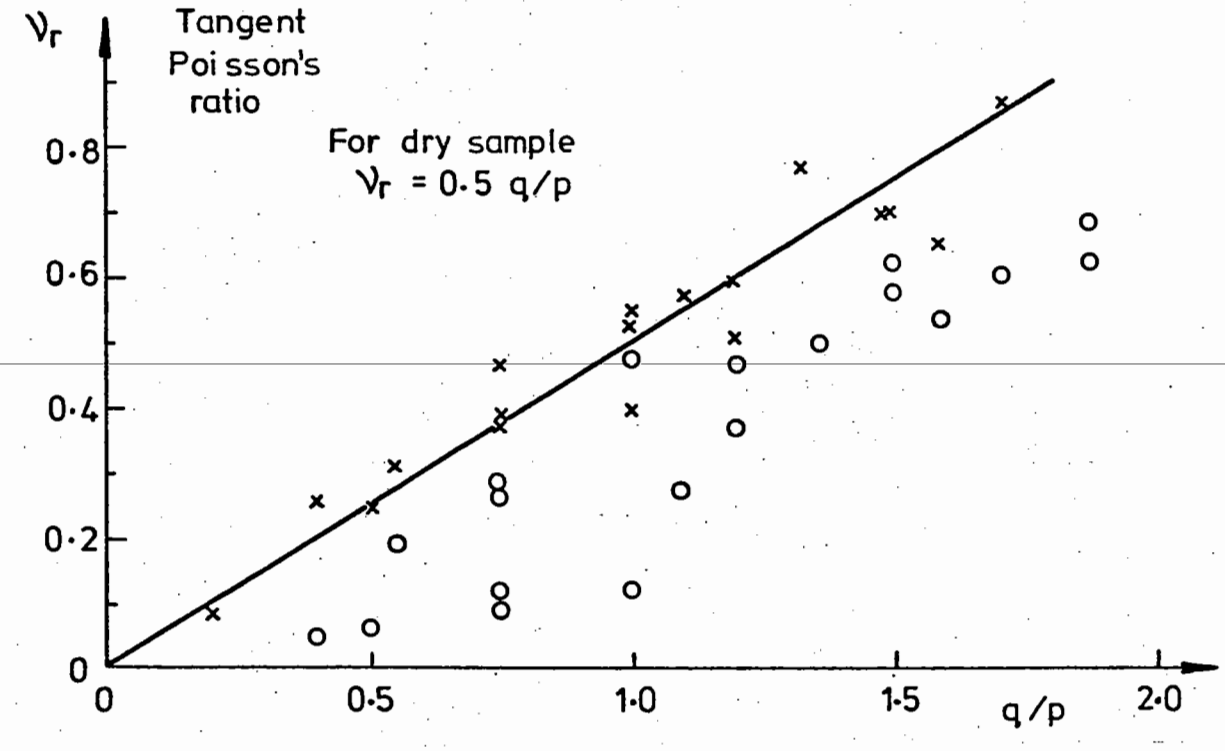

FIG. 2.2 RESILIENT POISSON'S RATIO FOR A PARTIALLY CRUSHED AGGREGATE (AFTER HICKS, 1970)

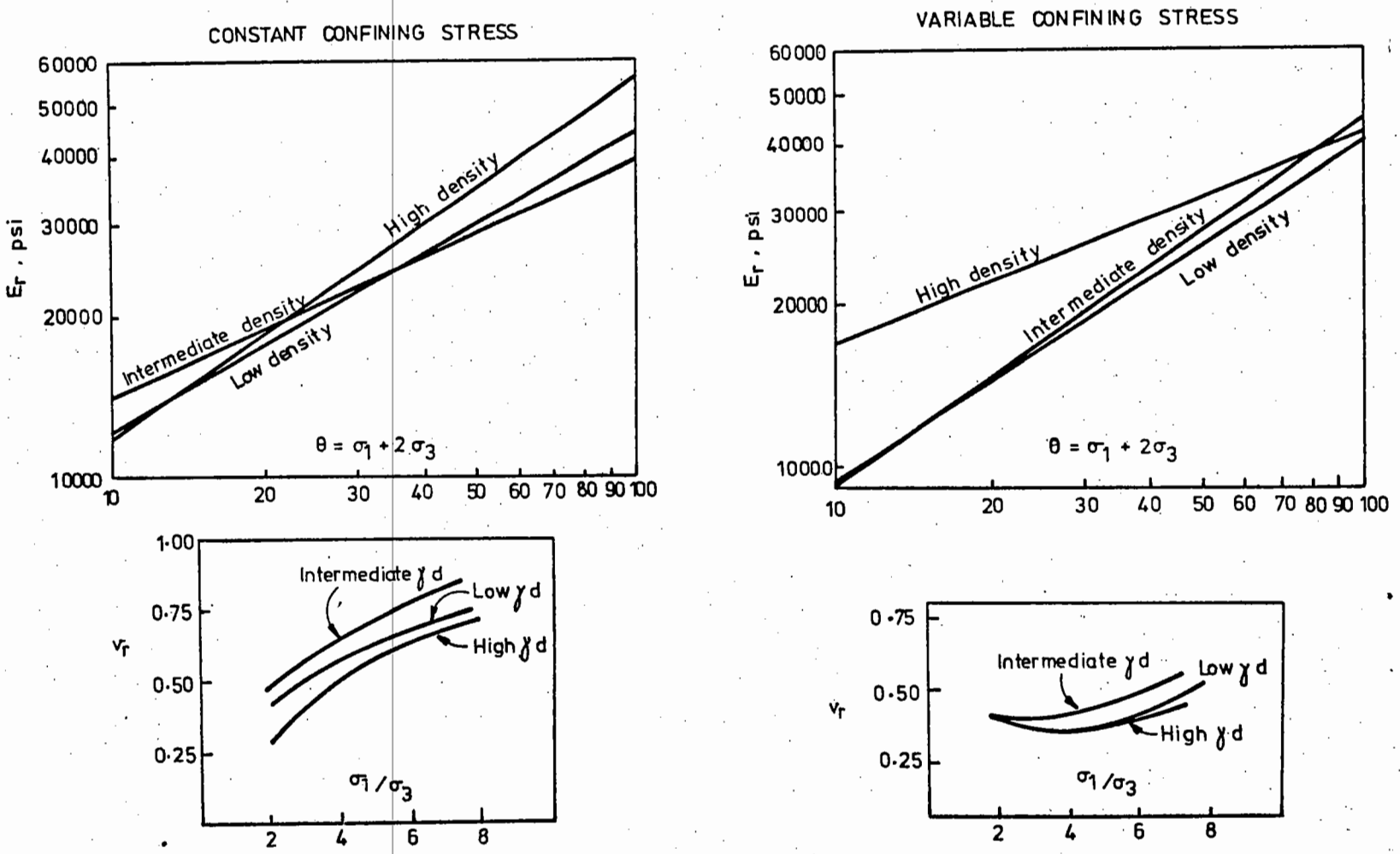

FIG. 2.3 EFFECT OF VARIABLE CONFINING STRESS ON A CRUSHED STONE (AFTER ALLEN AND THOMPSON, 1973)

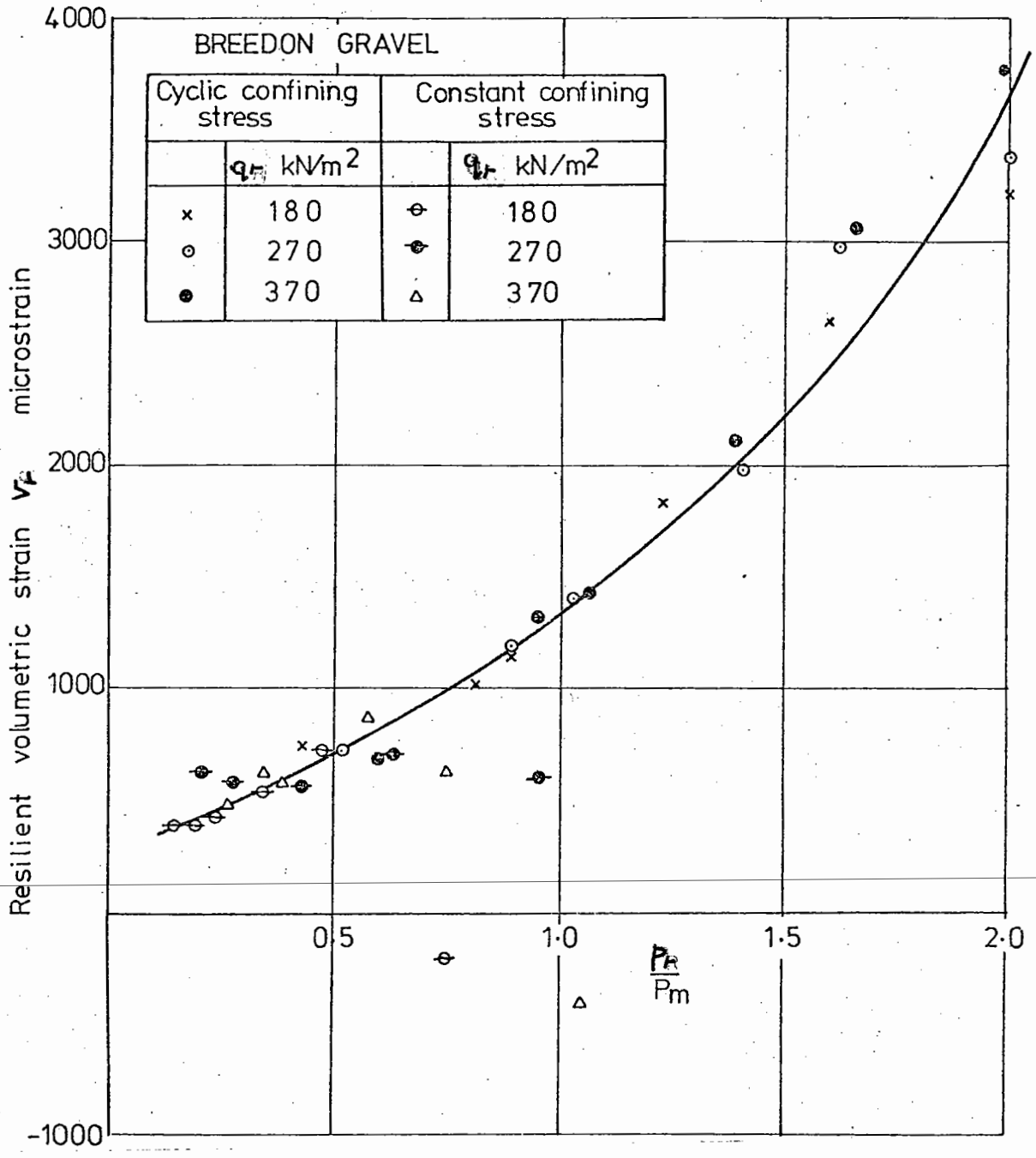

FIG. 2.4 RELATIONSHIP BETWEEN RESILIENT VOLUMETRIC STRAIN AND REPEATED NORMAL STRESS FOR A FINE CRUSHED STONE (AFTER HYDE, 1974)

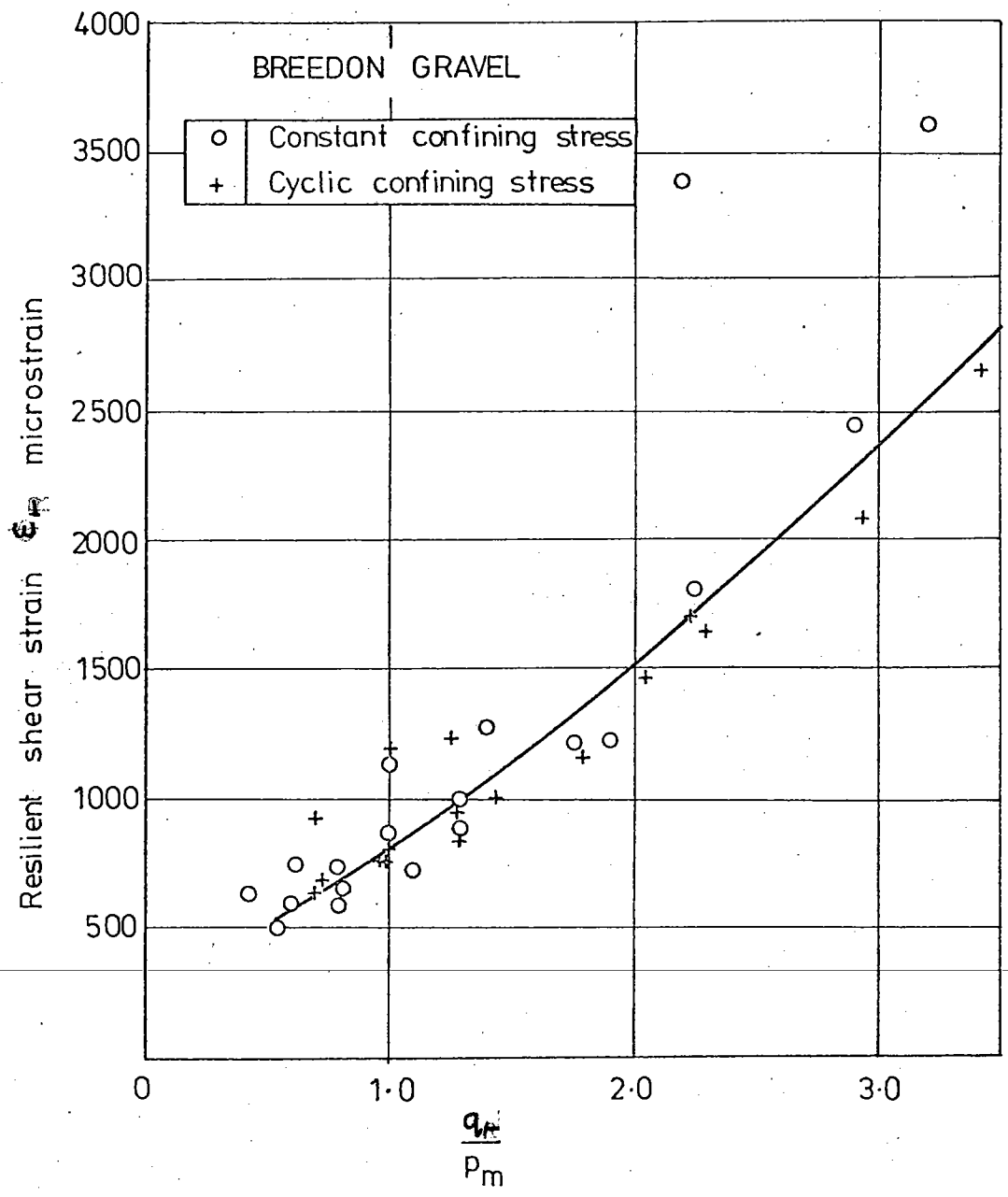

FIG. 2.5 RELATIONSHIP BETWEEN RESILIENT SHEAR STRAIN AND REPEATED DEVIATOR STRESS OF A FINE CRUSHED STONE (AFTER HYDE, 1974)

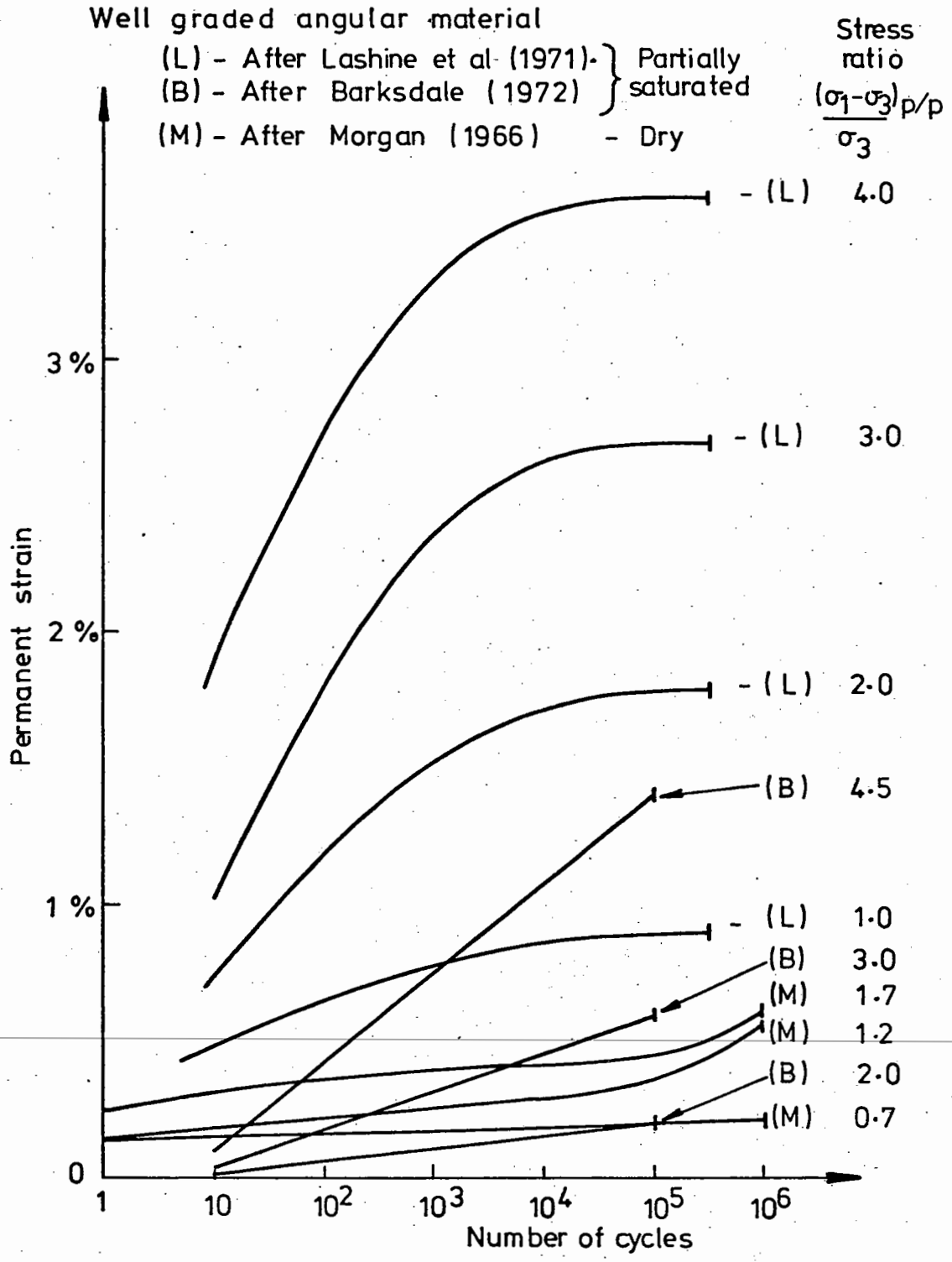

FIG. 2.6 DEVELOPMENT OF PERMANENT STRAIN IN WELL GRADED MATERIAL

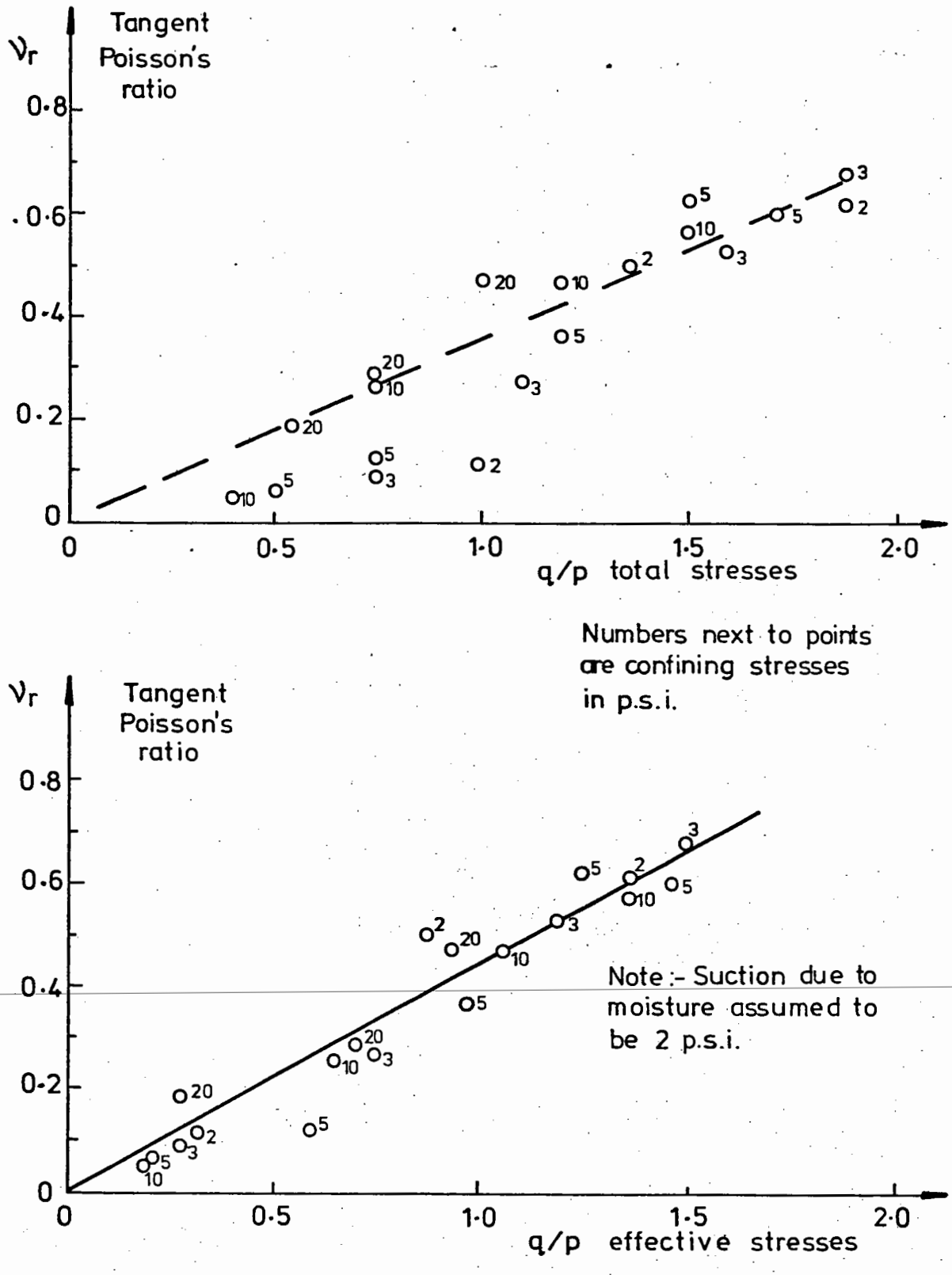

FIG. 2.7 EFFECT OF SUCTION ON THE RESILIENT POISSON'S RATIO OF A PARTIALLY CRUSHED AGGREGATE (AFTER HICKS, 1970)

CHAPTER THREE

REVIEW OF PREVIOUS WORK - EXPERIMENTAL TECHNIQUES

Most repeated load testing of granular materials has been carried out in the triaxial apparatus as used in conventional soil mechanics. However, the nature of the material and the type of loading makes several unusual features desirable including special techniques for sample preparation, loading and deformation measurement.

Other work on granular materials has used vibratory techniques or a simple shear apparatus and this is also described.

3.1 SAMPLE PREPARATION

There are a number of different ways of compacting granular materials to a density appropriate for testing:

(1) Falling hammer

(2) Vibrating hammer

(3) Vibrating table

(4) Gyratory compaction

Falling hammer

A standard falling hammer method of compaction is described in BS 1377 (1975). As mentioned, this method is not satisfactory for granular materials containing coarse aggregate because:

(a) Larger particles are liable to break.

(b) Densities achieved are low and not uniform.

(c) The top of the sample is left in a rough condition, and must be smoothed by other means.

In spite of these drawbacks, the method has been widely used because it requires no special equipment, and the compactive effort can be easily varied. Barksdale (1972) used this method for material with a maximum particle size of 38 mm with the following levelling off procedure: "The specimens were prepared about $\frac{1}{16}$" greater than the required height of 12" and while still in the mold, they were compressed in a testing machine to the desired height". This procedure may have been expedient, but it may also have produced undesirable side effects, such as crushing of some particles, and influenced the behaviour of the material during subsequent repeated loading.

Vibrating hammer

This is a better method for granular materials and results in denser samples with a smoother top surface; a standard method is described in BS 1377 (1975). Hicks (1970) used a vibrating air hammer, and was able to achieve a range of densities by using different layer thicknesses.

Vibrating table

This is a relatively new method in which the whole sample former is vibrated. It is based on work by Kolbuszewski and Alyanak (1964) who studied the effect of vibration on the density of sand. They found that there is an optimum acceleration for maximum density and that this acceleration depends on the depth of the sample, that is, it depends on the mean pressure at any level with the material above acting as a surcharge. However, the maximum density which can be achieved is the same for any depth as shown in Fig. 3.1.

This method of compaction was used by Kennedy (1974), and the technique is to slowly reduce the level of vibration from a high level

to zero so as to compact successive layers of the sample to maximum density.

Gyratory compaction

A gyratory compactor developed at the Texas Transportation Institute is described by Moore et al (1968). It is claimed that ".... (the compactor) produces more uniform specimens over a wider range of moisture content and density than was previously possible." However, the device is large and complicated, and this claim is yet to be verified.

An interesting method was developed for assessing the uniformity of compacted samples. The fines content of partially saturated samples was replaced with cement, and after curing, they were sawn into sections and the density of each section determined.

3.2 DENSITY/MOISTURE CONTENT RELATIONSHIP

If a soil is compacted with a certain compactive effort, the density which can be achieved is dependent on the moisture content. This relationship is usually expressed as a plot of dry density (or percentage volume occupied by solids) against moisture content, and the standard procedure for obtaining this relationship is given in BS 1377 (1975). For most soils including granular materials compacted by the falling hammer method, there is an optimum moisture content at which the material achieves the maximum dry density. However, for granular materials compacted by vibration, the relationship is rather different as shown in Fig. 3.2. High densities are obtained when the material is dry and when nearly saturated with lower values in between.

An extensive study was made by Pike (1972) into the compactability of graded aggregate with a vibrating hammer. He found that, in almost

all cases, the dry density of oven-dry material is about the same as that obtained at the "optimum moisture content" near saturation. Investigating different materials and gradings, he found that the maximum density expressed as the percentage volume occupied by solids (V_s) is influenced by the grading and angularity of the material. V_s decreases with angularity number, showing that gravel can be compacted to higher densities than crushed stone, and increases with coefficient of uniformity showing that well graded material can be compacted to higher densities. Similar results were obtained by Lees and Kennedy (1971) who used a vibrating table to compact graded limestone and granite aggregates.

Lees (1968) studied the design of aggregate gradings required for maximum density and found that the optimum grading was dependent on:

(1) Shape of particles

(2) Shape of container

(3) Lubrication (e.g. water content)

(4) Method of compaction

All these factors affect the density which can be achieved by compaction, but it must be remembered that density is not the only factor which influences the stress-strain behaviour of the material.

3.3 LOADING

Although the behaviour of granular materials is not appreciably influenced by the frequency of loading (see Section 2.2.4), it is desirable in repeated load testing to use a fairly rapid loading rate (1 - 20 Hz) in order that the frequency is similar to that applicable in pavement design, and that a test is completed in a reasonable length of time.

3.3.1 Axial Load

The majority of studies on granular materials have used the triaxial test, usually with a constant confining stress, and a deviator stress cycled in compression. Mechanical, pneumatic and hydraulic systems have been developed for the application of this repeated axial load.

Kennedy (1974) describes a mechanical loading system operating at about 1000 cycles per hour. The system is controlled by reversing the loading motor when a load cell detects that the limited load (maximum or minimum) has been reached. This produces a triangular load pulse with adjustable null periods at the peaks and troughs (0.2 - 10 secs) to allow the data logging system to take a reading.

Much of the repeated load work in the United States has used a pneumatic loading system developed by Seed and Fead (1959). The system produces load pulses of about 0.1 seconds duration at intervals of 3 seconds by applying accurately regulated air pressures to a loading cylinder. When properly controlled, the system will apply a rectangular pulse without shock effects. Load can be measured by a load cell incorporated in the top platen of the sample (Hicks, 1970), or indirectly by prior calibration of the system (Barksdale, 1972).

Williams (1963) describes a simple hydraulic loading system based on the sudden release of pressure from one side of the piston in a hydraulic cylinder. The drawback with this arrangement is that the load generated is dependent on the deformation produced.

In Nottingham, Cullingford et al (1972) developed a servo-controlled, hydraulic loading system. The system is complex, but extremely flexible, and can produce any desired shape or frequency of loading pulse within wide limits. The system is activated by an

electronic oscillator, and the servo-loop may be completed by either a load cell or a displacement transducer so that the test is load controlled or displacement controlled. Further, allowance can be made for the increase in load which must be applied in order to maintain the stress applied to the sample as its area of cross-section increases.

3.3.2 Confining Stress

A confining stress is applied to a triaxial sample by pressurising a fluid in the surrounding cell. Air is a convenient fluid, if the test is performed at a constant confining stress, and has been widely used; however, if the confining stress is to be varied, the cell fluid must be a liquid.

Water has been used by Hyde (1974) and by Allen and Thompson (1974) but problems arise when electrical transducers are placed inside the cell. It is interesting that both workers independently adopted induction coils for the measurement of radial strain, and measured axial strains from outside the cell - Hyde used an LVDT on the loading rod, and Allen and Thompson used an optical tracker.

Snaith (1973) performed triaxial tests on bituminous materials with cyclic confining stress. Mineral oil was used as a cell fluid, but as this attacks latex, the samples were enclosed in neoprene membranes.

Hicks (1970) and Dehlen (1969) performed some tests on clay and on asphalt with varying confining stress and used a silicone electronic oil as cell fluid. This is claimed to have no effect on electrical transducers or on latex membranes.

Application of varying pressure to the confining liquid is achieved by a hydraulic cylinder. This can be controlled in a similar way to the axial load.

3.3.3 Stress Conditions

The triaxial test is designed to apply a uniform state of stress to a cylindrical sample. The major principal stress is along the axis of the sample, and the minor principal stresses are equal and act radially. The radial stress is applied through a flexible membrane enclosing the sample and, therefore, is equal to the cell pressure at all points on the surface. The axial stress is applied through rigid end platens which effectively ensure uniform axial deformation, and hence the axial stress will initially be uniform over the cross-section of the sample.

However, as the test progresses, and the sample deforms under load, there is a tendency for radial expansion. This expansion may be restrained at the ends of the sample by friction on the platens causing the sample to take on a barrelled shape, and complicating the stress regime in the sample by introducing:

(1) Radial shear stresses at the ends of the sample.

(2) A variation in cross-sectional area causing non-uniform axial stress over the length of the sample.

Taylor (1971) analysed this problem by a finite element method and showed that for a linear elastic material the error introduced by end restraint into measurements of Young's modulus may be up to 10%, depending on the height to depth ratio, and Poisson's ratio of the sample. For non-linear materials at high strains, the errors may be larger than this.

Experimental measurements of the variation of moisture content, axial strain and radial strain over the length of the sample were obtained by Rowe and Barden (1964) and by Lee and Morgan (1966). The improvement

in strain distributions which resulted when free (frictionless) ends were used is shown in Fig. 3.3. The use of enlarged polished end platens covered with a layer of silicone grease, and separated from the sample by a latex rubber disc, as advocated by Rowe and Barden, has now become standard procedure in research projects but not in commercial testing.

British Rail have studied the effect of repeated loading on railway ballast - a large single size aggregate. They replaced the latex disc by a thin stainless steel disc cut into many segments because it was found that the greased latex disc would not provide adequate lubrication at the point contacts between the platens and the sample. It may be that this method is an improvement for material containing large aggregate particles (Cooper, 1973).

3.4 MEASUREMENT OF STRESS AND STRAIN

Assuming that uniform conditions of stress and strain exist in a triaxial sample, there are four quantities which define the stress-strain state of the material at any time. They are:

(a) confining stress (σ_3),

(b) deviator stress ($\sigma_1 - \sigma_3$),

(c) axial strain (ϵ_1),

and (d) radial strain (ϵ_3).

It is often convenient to measure these quantities with electrical transducers, which can be designed to have a frequency response high enough to cope with the rapid changes occurring in a repeated load test. The electric signals are easily processed for automatic recording, and can be used for control purposes if required.

If electrical transducers are positioned inside the cell, care must be taken in selecting a confining fluid, and in ensuring adequate sealing of the electrical connections carrying signals from inside the cell.

3.4.1 Confining Stress (σ_3)

As the radial stress is equal to the cell pressure, it can be conveniently measured by a pressure transducer connected to the cell fluid. Various transducers are available for this, usually based on strain gauged diaphragms (Lashine et al, 1971).

3.4.2 Deviator Stress ($\sigma_1 - \sigma_3$)

Deviator stress is usually measured by a strain gauged load cell placed either in the top platen (Hicks, 1970) or on the cell base (Snaith and Brown, 1972). If the load cell is placed outside the cell (Lashine et al, 1971), problems occur because it will also measure any friction between the loading rod and the top of the cell, leading to errors which are difficult to assess. Care must also be taken in designing the load cell to ensure that it is sensitive only to deviator stress ($\sigma_1 - \sigma_3$) and not to confining stress (σ_3) as well.

3.4.3 Axial strain (ϵ_1)

Axial deformation in triaxial samples is most conveniently measured by LVDT's (linear variable differential transformers) and these have been widely used, the only point of difference being where they are mounted.

Parr (1972) and Lashine et al (1971) measured movement outside the cell between the frame and the loading rod. Errors were introduced because of the deflection of the frame under load, but these were allowed for by calibration with a dummy specimen of known stiffness

(aluminium or perspex). If the LVDT's are positioned inside the cell to measure deflection between the platens (Kennedy, 1974), these errors are removed, but there is still an unknown error present due to bedding irregularities at the ends of the sample, and the presence of a greased rubber disc for lubrication.

These errors were demonstrated by Moore et al (1969) by using an optical measuring system sighted onto targets glued to the sample. Typical results for a dummy plastic sample are shown in Fig. 3.4. The optical tracker was believed to give an accurate measurement of boundary strain on the sample, readings from the strain gauges being lower because of their stiffening effect on the relatively flexible plastic. The principal drawback of the optical system is that it must be manually sighted onto a target which makes it too slow for repeated load work. However, Allen and Thompson (1974) have recently reported the use of two Physitech optical trackers to measure axial strain in a repeated load test from the movement of tapes stuck on to the membrane.

Terrel (1967) measured axial strain by placing two circular clamps around the sample and measuring their relative movement with a pair of small LVDT's. This eliminates the errors described above, but he expressed concern that the rigid encirclement of the sample by these clamps would prevent radial strain, and lead to errors.

Dehlen (1969) modified Terrel's clamps so that they only contacted the sample (or to be precise, the surface of the membrane surrounding the sample) over two short lengths at opposite ends of a diameter, and were held in contact by light springs. Hicks (1970) and Barksdale (1972) used similar arrangements for measuring resilient axial strain. However, Barksdale observed that there was a "scatter" in the permanent axial strain at large numbers of load repetitions when

these clamps were used, and his permanent deformation results are based on measurements taken outside the cell. He concluded that this scatter may have been due to slip between the sample and the membrane or between the membrane and the clamps.

3.4.4 Radial Strain (ϵ_s)

Various methods have been employed to measure radial strain, all involving attachment of transducers to the sample. This is a difficult problem, and none of the methods is entirely satisfactory, but no work has been done to compare the results.

Hicks (1970) measured radial strains by mounting horizontal LVDT's on the clamps used for axial strain. These measured the extension of a spring which held the clamps across a diameter of the sample. The same principal was used by Brown and Snaith (1974).

Coffman et al (1964) used a thin metal clip which was sprung across the diameter of a sample. Changes in sample diameter caused output from strain gauges in the middle of the clip. Lee and Morgan (1966) encircled the sample with an aluminium foil band separated from the membrane by a layer of grease. Any increase in circumference of the sample was measured by the relative movement of the ends of the foil band. This method has been used successfully for single load tests, but Kennedy (1974) was unable to measure resilient radial strain when using a similar foil band in repeated load tests.

A method has recently been developed at Nottingham for the measurement of radial strain with induction coils (Hyde, 1974). Any radial deformation of the sample changes the mutual inductance between a coil attached to the sample, and a similar one placed just outside the cell. The method is promising, and has the advantage that the moving coil is in direct contact with the sample, inside the membrane.

3.4.5 On-Sample Measurement

There are two contrasting approaches to the measurement of strain in granular materials. Firstly, measurement of average deformation across the whole sample, for instance axial deformation measured across the end platens and lateral deformation measured by means of a band around the circumference of the sample. This approach is susceptible to errors from edge effects, and from the presence of a flexible membrane between the sample and the measuring device. Secondly, measurement of the relative movement of points fixed onto the sample, for instance strain collars (Brown and Snaith, 1974). Errors in this case arise from the particulate nature of the material and the consequent non-uniformity of strain throughout the material. Kennedy (1971) preferred the first approach in which the errors are systematic and it may be that this approach is better when attempting to compare the behaviour of different materials under similar conditions. However, it is considered that the second approach, in which the errors are random, provides a better basis for determining the behaviour of a single material under different conditions.

3.4.6 Pore Pressure

It is well established in soil mechanics (Terzaghi, 1943) that the behaviour of a soil is dependent upon the effective stress between the particles. The importance of this concept for granular materials can be judged when it is remembered that their strength and stiffness are primarily dependent on the normal stress (see Section 2.2.1).

In order to measure pore pressure, a sample, and any probe used, must be completely de-aired because any meniscus present at an air-water interface will cause unknown pressure differentials (Scott, 1963). A technique for completely saturating a sample of granular material is

described by Hicks (1970); the sample is evacuated and de-aired water drawn into it through porous end platens.

Assuming that complete saturation of the sample and the measuring system has been achieved, other errors may still be present in cyclic pore pressure measurement under rapid repeated loading.

(a) The compliance of the transducer may cause pressure differentials to occur around the porous probe (or platen) as water flows into it.

(b) Pore pressure is measured in a local area of the sample, and if stress conditions are not uniform (say around a non-lubricated platen) this may not be representative of the pore-pressure in the bulk of the sample.

These errors will not occur when considering the permanent build up of pore pressure, because pressures will have time to equalise. However, other errors in undrained tests may be caused by leaks or by diffusion through the membrane.

Hicks (1970) measured pore pressure through large porous discs on the end platens and recorded transient pore pressures of 5-10% of the repeated deviator stress. He reported no build up of permanent pore pressure and that drained and undrained samples behaved in the same way.

Hyde (1974) measured pore pressure during rapid repeated load tests on Keuper Marl (10 Hz). He used a porous ceramic probe in the base platen and could measure the build up of permanent pore pressures but not transient pore pressures.

Brown and Brodrick (1973) investigated the performance of various stress and strain transducers for incorporation into experimental

pavements, and they also investigated a piezoelectric pressure transducer which could be incorporated into a pavement or a triaxial sample. This device measures transient variation in pore pressures ($\geq$ 0.5 Hz) in coarse and medium grained soils. They summarised the important design requirements of such a transducer as:

(a) The compliance must be low to reduce flow requirements.

(b) The filter system between the soil and the transducer must be efficient in blocking soil particles but allowing the passage of water.

(c) The transducer must be insensitive to external stresses other than pore pressure.

(d) The system must be completely de-aired and the electrical connections fully waterproofed.

This piezoelectric transducer is promising, but further development is required before rapidly varying pore pressures can be measured with confidence.

3.5 VIBRATORY TESTING OF GRANULAR MATERIALS

The elastic properties of granular materials can be determined by subjecting a sample to vibration (Hardin and Black, 1966; and Robinson, 1974). Any solid body has various natural frequencies of vibration in different modes and the frequency of resonance in any mode depends on the geometry, density and elastic constants of the material. A sample of sand or granular material subjected to a certain confining stress can be considered to be a solid body, and its elastic constants (E and G) calculated from the resonant frequencies observed in different modes.

A method of measuring these frequencies was described by Robinson, but, as he pointed out, the method has limitations:

"(a) The test frequencies used are unrealistically high for base and sub-base materials in a pavement (250 to 1000 Hz).

(b) Although the isotropic stress can be set at realistic values (up to about 100 kN/m^2), the deviator stresses due to vibration are small. They are also inhomogeneous throughout the specimen."

The results obtained by this method are similar to the resilient behaviour measured in the triaxial test. Vibration may provide a quick and simple way of assessing the relative stiffness of different granular materials, and of determining the parameters K_1' and K_2' in Eqn 2.2.

3.6 SIMPLE SHEAR APPARATUS

Work is at present in progress at the University of Nottingham on a simple shear apparatus capable of applying shear reversals to samples of a single size limestone aggregate resembling railway ballast (Ansell and Brown, 1975). Difficulties in achieving uniform stresses within the sample have so far prevented any repeated load shear tests being conducted with the apparatus.

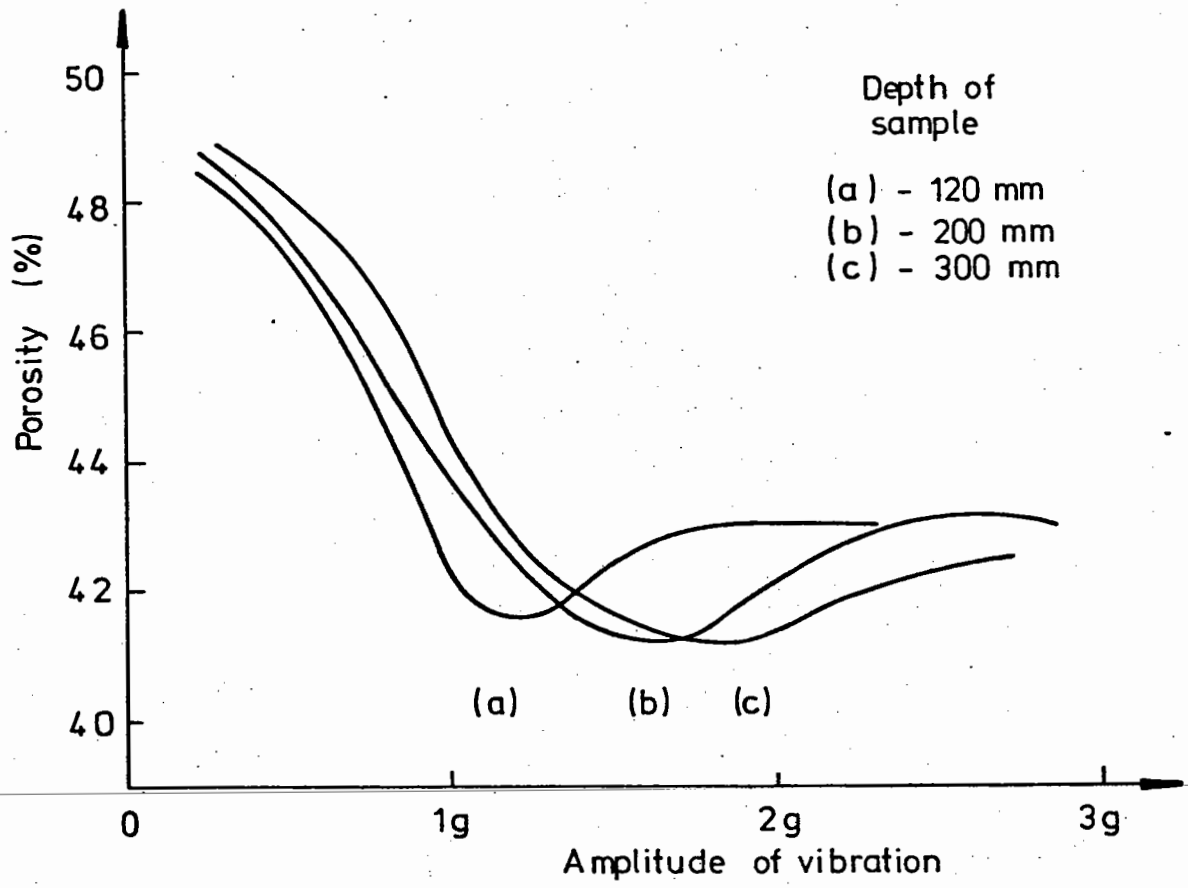

FIG. 3.1 DENSITY OF SAND SUBJECT TO VIBRATION (AFTER KOLBUSZEWSKI AND ALYANAK, 1964)

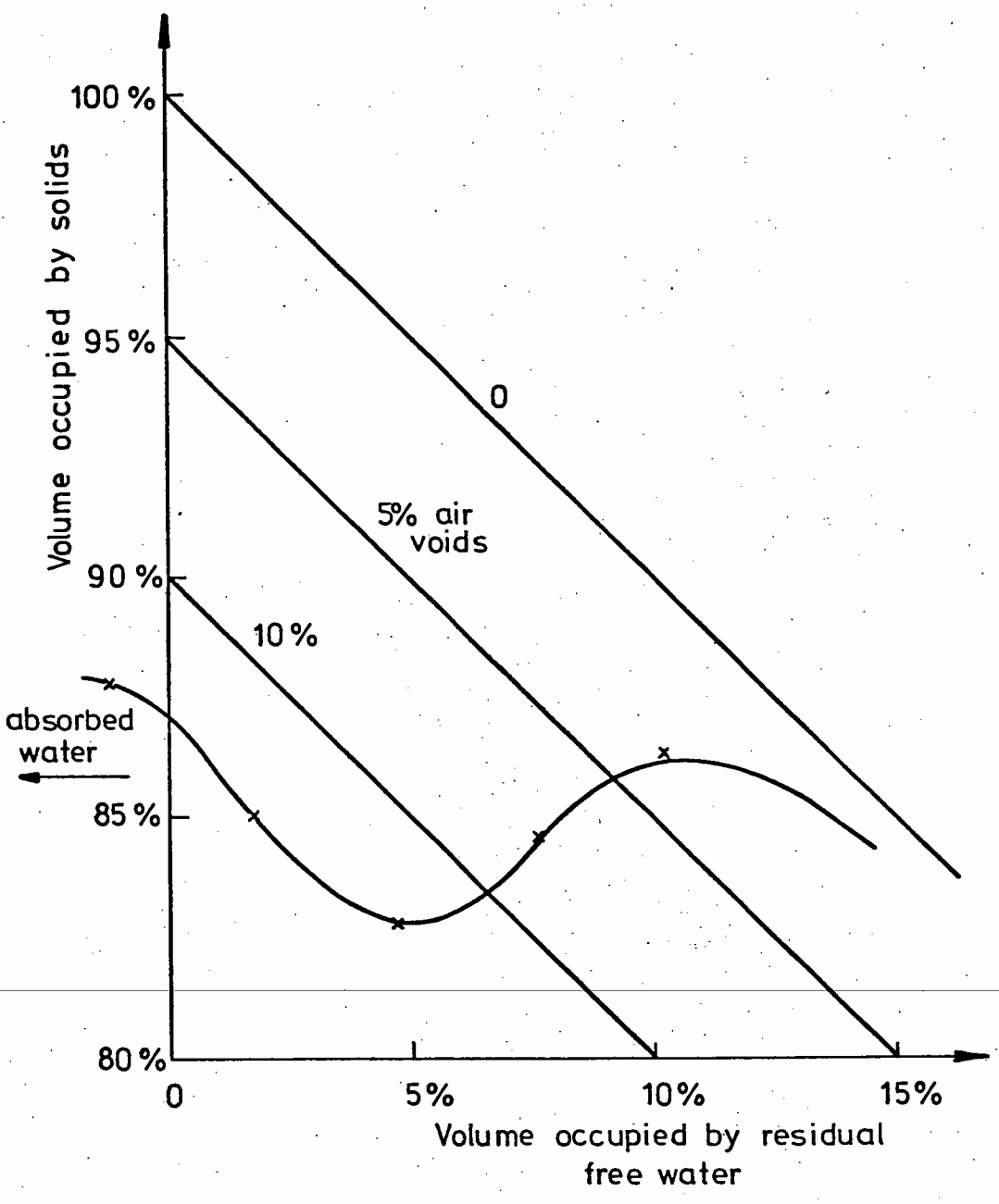

FIG. 3.2 RELATIONSHIP BETWEEN DRY DENSITY AND MOISTURE CONTENT FOR A WELL GRADED CRUSHED ROCK COMPACTED BY VIBRATING HAMMER (AFTER PIKE, 1972)

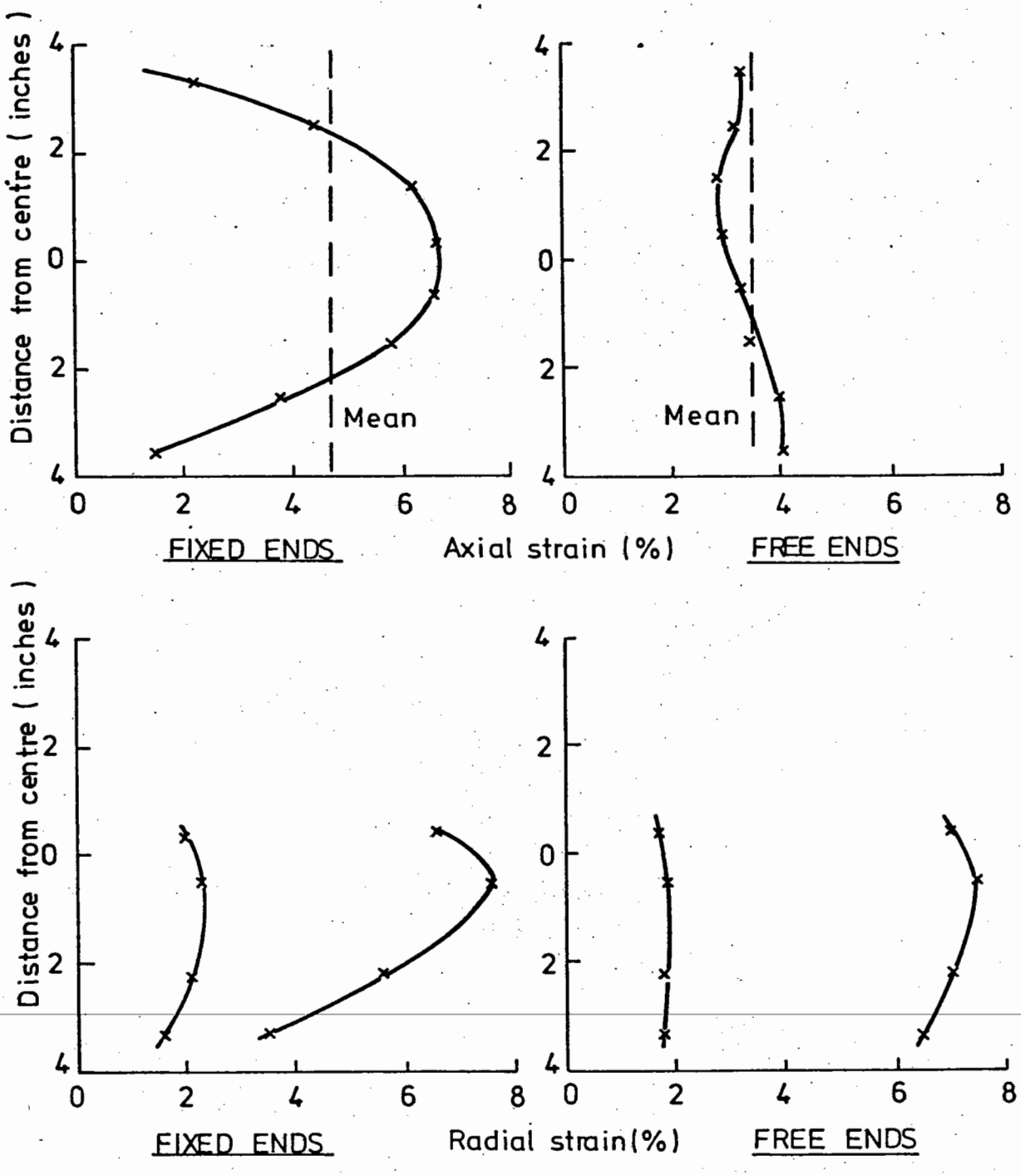

FIG. 3.3 EFFECT OF FREE ENDS ON STRAIN DISTRIBUTION DURING A TRIAXIAL TEST ON A SAMPLE OF SAND, 8" HIGH AND 4" DIAMETER (AFTER LEE AND MORGAN, 1966)

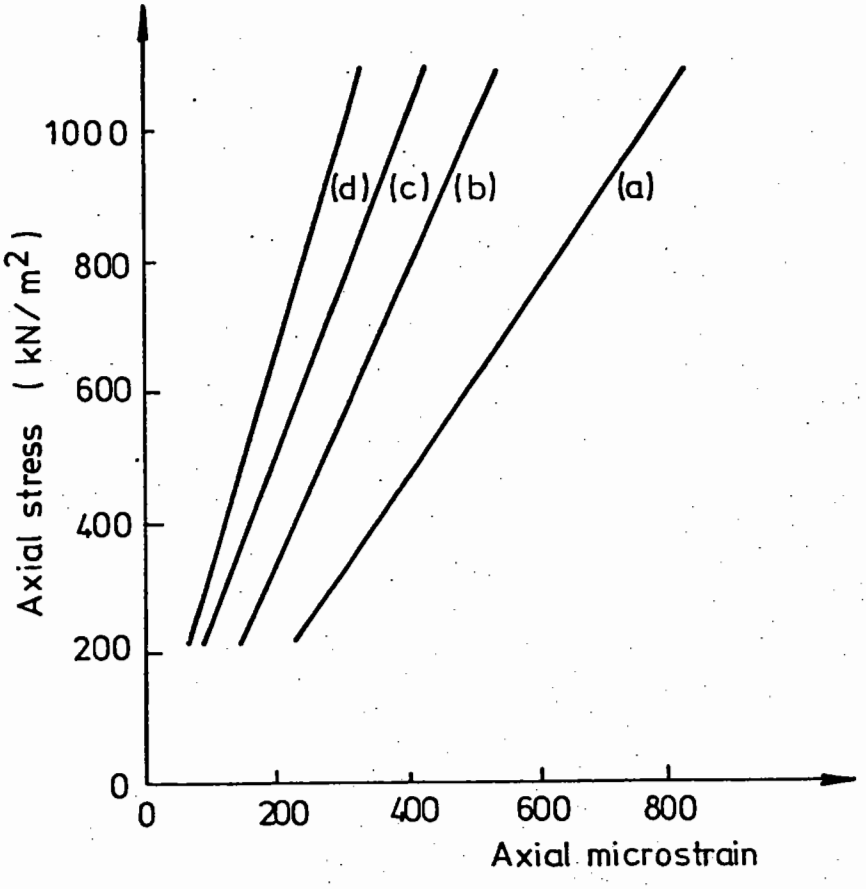

Strain measurements from a repeated loading test on a plastic cylinder (8" high × 4" dia.)

(a) From rod displacement
(b) From relative movement of platens
(c) From targets on the specimen with optical tracker
(d) From strain gauge measurements

FIG. 3.4 ERRORS IN RESILIENT STRAIN MEASUREMENT (AFTER MOORE ET AL, 1969)

CHAPTER FOUR

OBJECTIVES

The overall aim of this research project was to characterise the behaviour of granular materials used in highway pavements during the life of the pavement. The stresses which are imposed on the material have been estimated from analytical studies (Dehlen, 1969; and Taylor, 1971) and from the results of repeated load tests on model and full scale pavements (Brown and Bush, 1972).

The method of achieving this overall aim was to take samples of the material in the laboratory, apply to them stresses which are as near as possible to those occurring in a pavement and then measure their response.

4.1 CHOICE OF EQUIPMENT - THE REPEATED LOAD TRIAXIAL TEST

Roads are subjected to repeated loading from traffic, and hence repeated stress pulses are induced in the pavement structure, in addition to small stresses already present due to overburden pressure. Each stress pulse has three components, shown in Fig. 4.1:

(1) A vertical compressive stress.

(2) A lateral stress, smaller but of longer duration, which is normally compressive but which can be tensile at the bottom of a stiff layer.

(3) A shear stress which is reversed as the load passes, and can be considered as a roation of the planes of principal stress.

The magnitude of the stress pulse decreases, and its duration increases with depth in the pavement. The range in the granular layer

for a standard wheel load (40 kN) is a magnitude of 5-200 kN/m^2 for a duration of 0.01 - 0.2 seconds.

The repeated load triaxial test can produce similar stress conditions with the exception of the shear reversal. In practice, the use of vertical and horizontal stresses of different duration and the use of pulses as short as 0.01 sec is difficult. Tensile lateral stresses cannot be applied in the triaxial test but this is not important when testing a granular material which cannot sustain such stresses.

These drawbacks are not serious, and the triaxial apparatus has several points in its favour:

(1) If lubricated end platens are used, samples can be subjected to a uniform state of stress.

(2) There is access to the sides of the sample for strain measurement.

(3) Comprehensive servo-hydraulic and pneumatic control systems have been developed for repeated loading (see Section 3.3).

The repeated load triaxial apparatus which was developed for this project is described in Chapter 6. The only obvious alternative to the triaxial test was the repeated load shear test. This had the attraction that the shear reversal mentioned above could be investigated, but this was outweighed by several drawbacks including the difficulty of achieving uniform stress conditions in the sample, the sample being enclosed, and the need for contact stress transducers for stress measurement.

4.2 THE NEED FOR A THEORETICAL FRAMEWORK

Although the stress conditions which can be achieved in a triaxial test are similar to those in a pavement, there are differences. Shear reversal is not possible and drainage conditions, even if the sample is at the correct moisture content, are different. The only way in which these differences can be overcome is to develop a sound theoretical framework within which the results can be expressed. Such a framework will also enable simple tests to be devised to define the basic characteristics of different granular materials, and enable engineers to ensure that the material is being used to the best advantage. For example, considering another material used in road pavements, the strain criterion (Pell, 1962) enables the fatigue life of bituminous materials at various temperatures and speeds of loading to be found from only a few tests.

A theoretical framework must be based on the measurement of material properties over a wide range of conditions and this may well include conditions which are not strictly relevant to the problem (in this case pavement design) which gave rise to the research. The breadth of the investigation is particularly important when there are differences between laboratory and site conditions (see Section 10.4) and the significance of these differences can only be properly assessed from tests carried out in well defined conditions.

4.2.1 Theories in Related Fields

When considering a theoretical framework for granular materials under repeated loading, it is useful to consider the theories which have been developed for granular materials under other types of loading, and for other materials under repeated loads.

Table 4.1 summarises the way in which granular materials behave under different conditions. There is a wide range of behaviour, and different theories have been developed to cover some of these situations. The boundaries between different types of behaviour, expressed on the table in terms of strain and frequency, are somewhat arbitrary and in practice one type of behaviour will merge into another as conditions change.

Behaviour under repeated loading (centre of Table 4.1) is complex as there are two components of strain, resilient and permanent. Different treatment may be required for each component but it would be useful if a single unifying theory could be developed.

Other materials commonly subjected to repeated loading are cohesive soils in a pavement subgrade and bituminous material in the surface. Both of these show a time dependent behaviour in which resilient strain can be treated by rheological models (Murayama and Shibata, 1961) and in which permanent strain appears to be analogous to creep (Snaith, 1973; and Glynn and Kirwan, 1969). These theories are not applicable to granular materials, and this may be because they lack cohesion and derive their strength from particle interlock. Discussing cohesionless soils, Krizak (1971) states that "many observed phenomena in soil mechanics can be explained by the use of time-independent, but hysteric, models". However, these have not been used for granular materials in pavement design.

To date, no overall framework for the stress-strain behaviour of granular materials under repeated loading has emerged from research which has been carried out in this field. This may be because the behaviour of the material under these conditions is much more complex than was originally suspected. Useful relationships have been found, especially

for resilient modulus under certain conditions (see Section 2.2), but the overall picture is not clear.

Table 4.1

Behaviour of Granular Materials under Various Types of Loading

Strain / Freq.	Small $< 10^{-4}$	Intermediate 10^{-4} -10^{-2}	Large $> 10^{-2}$
Low < 1 Hz	Elastic	Permanent deformation e.g. consolidation, foundations	Plastic flow e.g. slope failure, single load triaxial test
Intermediate 1-100 Hz	Elastic	Resilient and permanent strain e.g. pavement in service	Progressive failure e.g. failed pavement
High > 100 Hz	Elastic and resonant vibration e.g. siesmic investigation	Compaction e.g. pavement construction	Liquefaction e.g. materials handling

4.3 THIS RESEARCH IN THE CONTEXT OF EXISTING KNOWLEDGE

Part of the information required for this overall framework is available, but there are gaps which need to be filled. The degree of success with which this project has filled these gaps is discussed in later chapters.

4.3.1 The Material

Granular material is a two-phase continuum, an aggregate phase -

hard particles of various shapes and sizes - surrounded by a pore fluid - air and/or water. The behaviour of the material is affected by the pressure of this pore fluid and it is accepted in conventional soil mechanics that this can be modelled by the concept of effective stress (Terzaghi, 1943). This concept will form part of any theoretical framework for granular materials, but the main part, which this project is concerned with, is the stress-strain behaviour of the aggregate phase. Therefore, dry material was used so that the effective stress could be measured directly.

Many materials which behave in a similar way are included in the term "granular material"; however, only a few are currently used for road construction in Britain. Only one previous study has been concerned specifically with these materials (Kennedy, 1974), but other related work has been carried out on sand, on unbound base materials used in America, or on a wide variety of granular materials to compare their performance. This project has been concentrated on one material typical of those currently used in Britain. Details of this material and the methods used for sample preparation are given in Chapter 5.

4.3.2 Resilient Strain Tests

Measurements of the resilient deformation of granular material have previously concentrated on finding the resilient modulus (E_r) and Poisson's ratio (ν_r) under different conditions. These are pseudo-elastic parameters which can be used to describe material behaviour under a constant lateral stress. However, difficulties are encountered under conditions of variable lateral stress such as occur in a pavement. In this project, a much greater range of stresses has been applied than previously and this enabled a model to be developed which will predict the resilient strain in the material under a wide variety of stress conditions (see Chapter 8).

4.3.3 Permanent Strain Tests

In Chapter 2, several studies of permanent deformation of granular materials were reviewed, and the main point to emerge from them was that the build up of permanent deformation is dependent on the applied stress ratio (repeated deviator stress/confining stress). The way in which permanent strain varies with the number of load applications and with the applied stress ratio was not well defined. To clarify these details was the objective of the permanent strain test programme (see Chapter 9).

4.3.4 Random Variation in Results

Granular materials are more or less random arrangements of discrete particles, and random variations will inevitably occur between samples, especially when particles in the larger size ranges are included. These statistical variations will be reflected in the stress-strain behaviour of the material and it is important to determine the magnitude of the effect by testing several samples under identical conditions. This is especially important when measuring permanent strain, where it is necessary to use separate samples for each stress condition. Failure to consider this point may have contributed to the lack of consistency in the work so far reported on permanent deformation.

In this project more than one sample has been tested at each stress condition and strain measurements have been taken from three or four gauge lengths on each sample.

4.4 FORMULATION OF TEST PROGRAMME

For the purpose of formulating a test programme, the objectives set out at the beginning of this chapter can be restated: to measure the strain which occurs in samples of granular material subject to repeated

loading at a wide range of different stresses. Before proceeding, it is worth considering in some detail the stress regimes possible in the repeated load triaxial test, and the type of strain measurements required.

4.4.1 Stress Paths in the Repeated Load Triaxial Test

In the triaxial test, stress conditions in the central part of the sample are assumed to be uniform (see Section 3.3.3). It can be considered that each repetition of load takes the sample to and fro along a particular "stress path".

Throughout this project, the test programme and the behaviour of the material has been formulated in terms of the stress invariants, normal stress, p, and deviator stress, q. In a drained triaxial test with axial stress, σ_1, and radial stress, σ_3, these stress invariants (taking compressive stresses positive) are defined as:

$$p = \tfrac{1}{3}(\sigma_1 + 2\sigma_3) \qquad (4.1)$$

and

$$q = \sigma_1 - \sigma_3 \qquad (4.2)$$

In the repeated load triaxial test, both p and q can be cycled so that in general four stress parameters are required to define the stress path applied to the sample. These parameters are shown in Fig. 4.2 and represent the mean (p_m and q_m) and the double amplitude (p_r and q_r) of the stress invariants. The mean stress ratio ($S_m = q_m/p_m$) and the repeated stress ratio ($S_r = q_r/p_r$) are also useful terms when describing the stresses applied to the material. This notation is an extension of that developed by Schofield and Wroth (1968).*

In the triaxial test, the stress regime is always symmetrical about the vertical axis and so no rotation of the principal stresses is possible.

---

* Schofield and Wroth refer to p as the 'mean normal stress' whereas in this work p is referred to as the 'normal stress' and p_m as the 'mean normal stress'.

4.4.2 Need for Preliminary Tests

In repeated load triaxial tests with variable confining stress a wide range of stress paths is possible represented by different values of the parameters p_m, q_m, p_r and q_r. Each stress repetition along a particular stress path will cause a certain resilient (recoverable) strain and a certain permanent (irrecoverable) strain, as shown in Fig. 4.3. The way in which permanent strain develops can only be established by applying a large number of cycles on each stress path and by starting with a fresh sample for each one. Allowing for replicate samples, the number of stress paths which can be investigated in a reasonable time scale is somewhat limited. The permanent strain test programme (Section 9.1) called for three replicate tests on each of ten stress paths.

There were indications from previous work (Hicks, 1970; Lashine et al, 1971) that, after an initial settling down period, resilient strain was not affected by the number of load repetitions. In that case, it would be possible to measure the resilient strain over a large number of different stress paths on the same sample, and resilient strain data could be obtained much more rapidly. The main function of the preliminary tests was to establish if this was the case, and to decide how many load repetitions should be applied to take each reading of resilient strain. When a satisfactory proceedure had been established, the programme of six resilient strain tests was carried out, each one involving resilient strain measurements over about 200 different stress paths. At this time it was realised that the range of applied stresses could be increased by including stress paths which involved triaxial extension (see Fig. 4.4). In three further tests the axial load, σ_1, though still compressive, was reduced to values less than the

confining stress, σ_3. Results from these tests made an important contribution to the development of a resilient strain model (Section 8.3).

Other preliminary tests were carried out to investigate the single loading behaviour of the material and to check that frequency had no influence on the resilient behaviour under repeated loading.

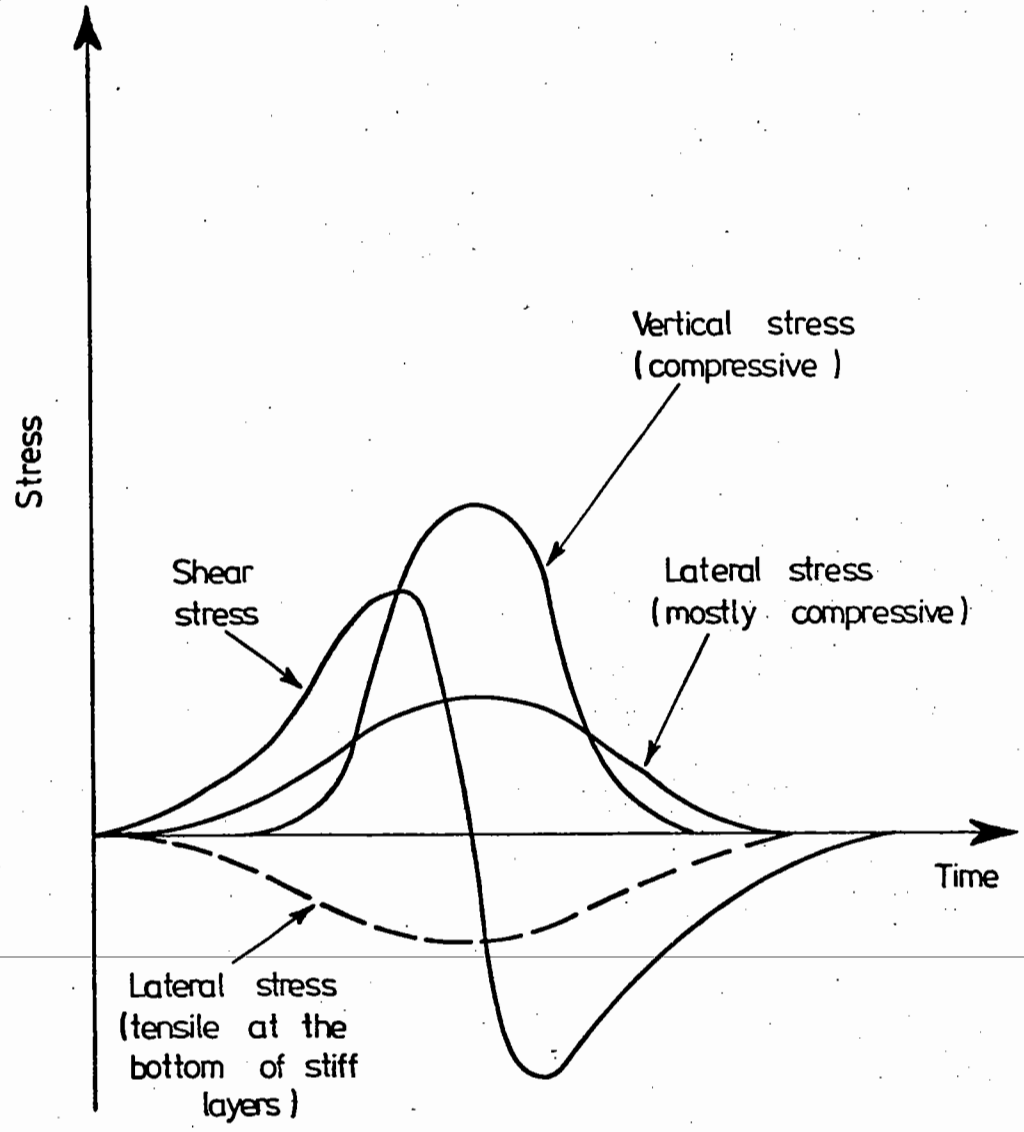

FIG. 4.1 TYPICAL STRESS PULSE IN A PAVEMENT STRUCTURE DUE TO A PASSING WHEEL LOAD

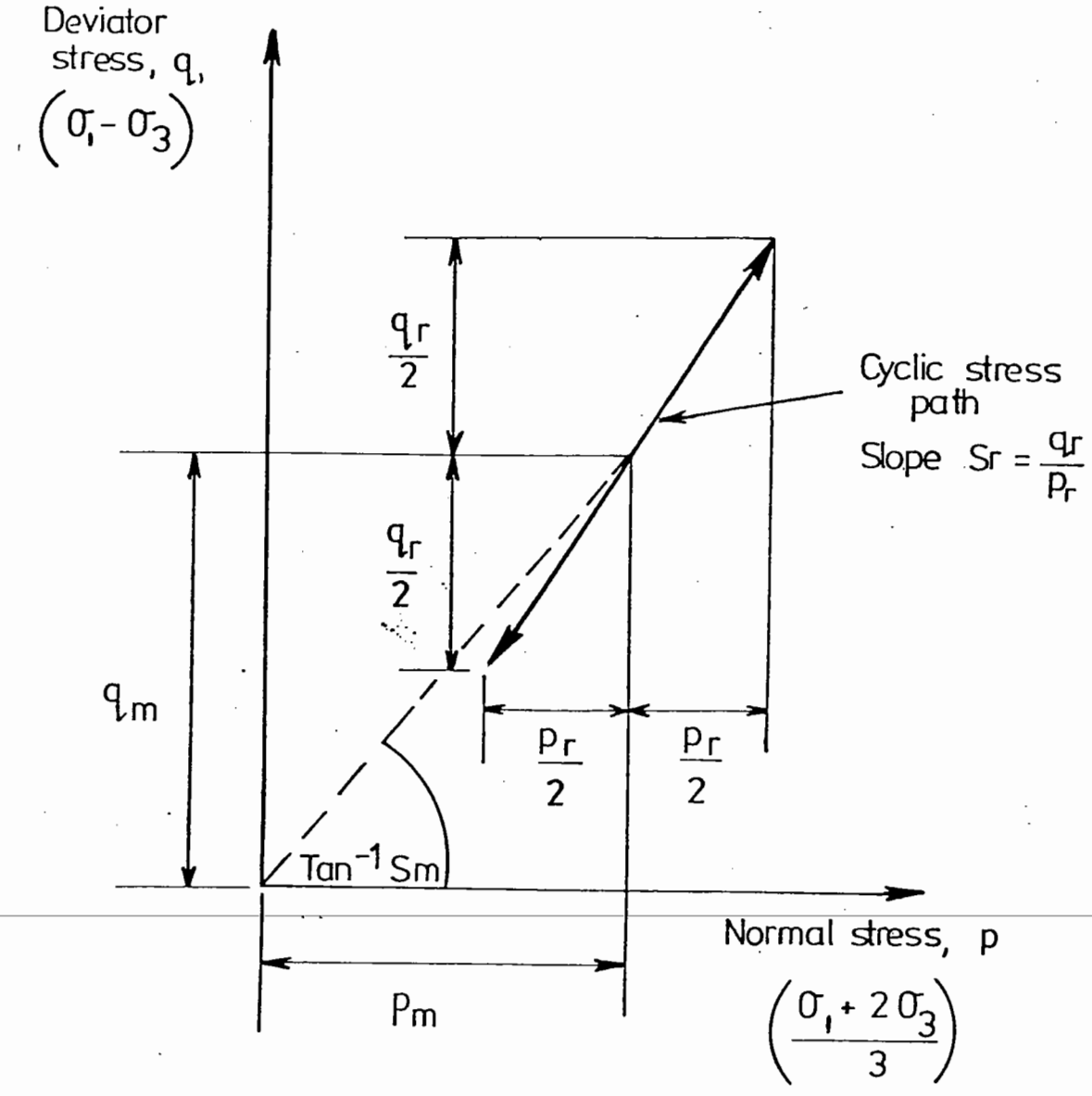

FIG. 4.2 COMPONENTS OF STRESS IN THE REPEATED LOAD TRIAXIAL TEST

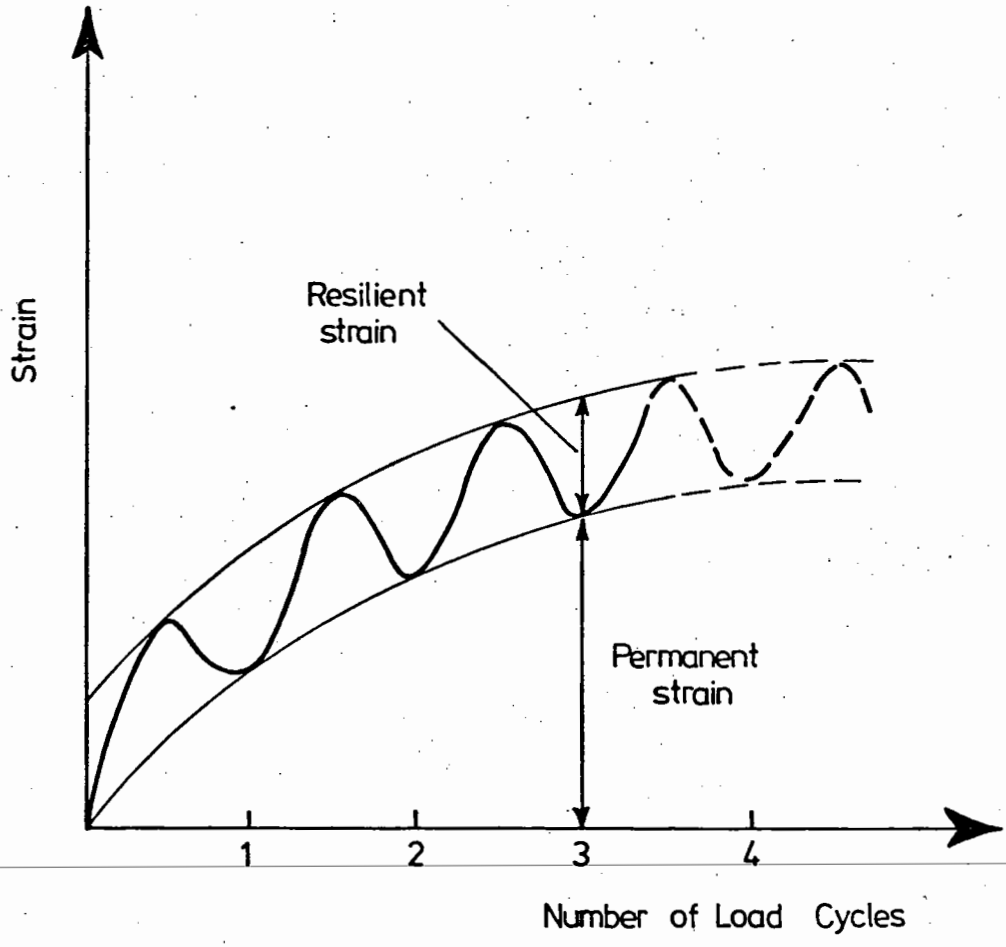

FIG. 4.3 COMPONENTS OF STRAIN IN THE REPEATED LOAD TRIAXIAL TEST

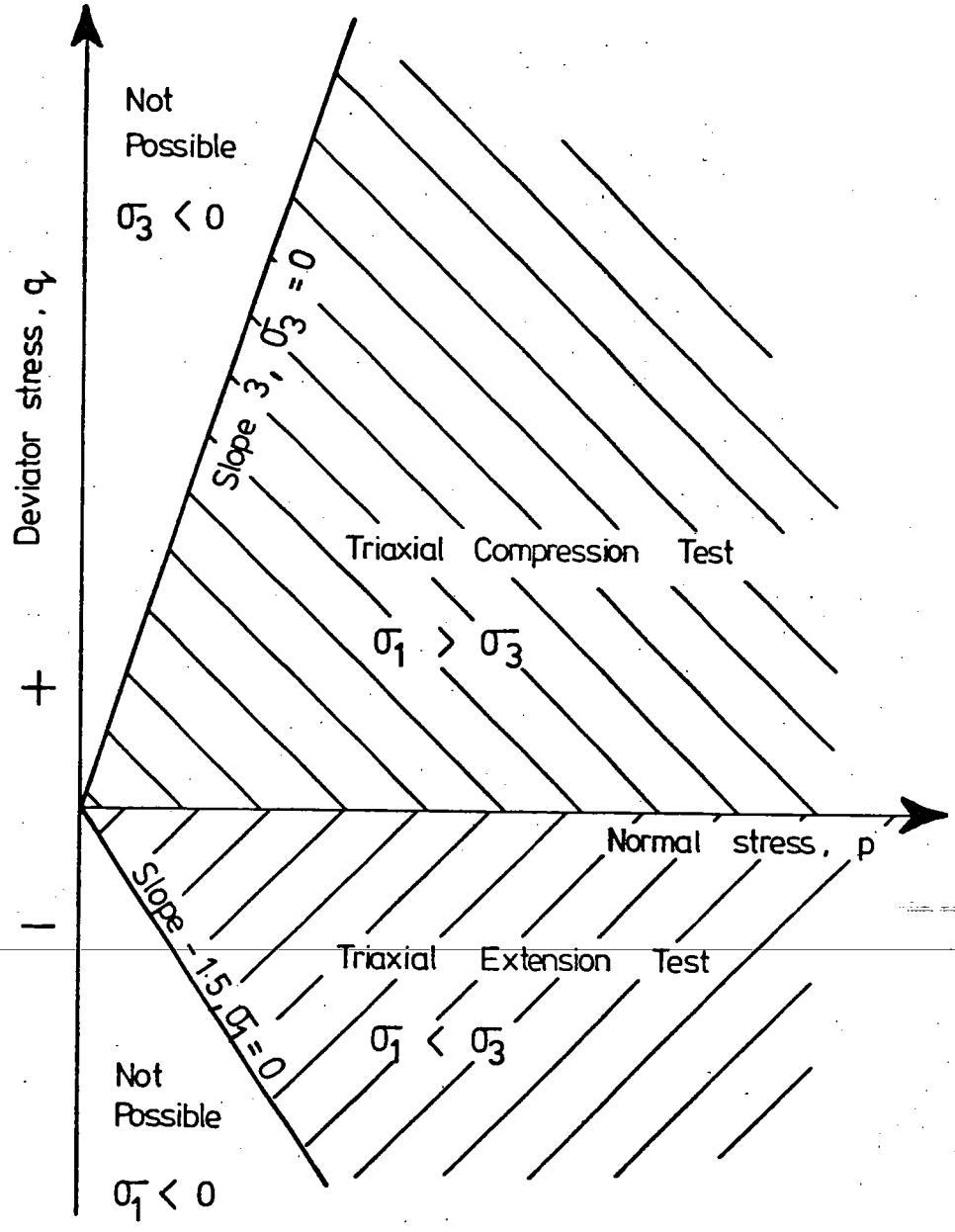

FIG. 4.4 RANGE OF STRESSES WHICH CAN BE APPLIED IN THE TRIAXIAL TEST TO UNBOUND MATERIAL

CHAPTER FIVE

THE MATERIAL

5.1 CHOICE OF MATERIAL

The following criteria were used in selecting a material for use in this project:

(1) That it should be an unbound granular base material commonly used for road construction in Britain.

(2) That it should be possible to produce consistent uniform samples of the material.

(3) That it should be possible to measure the effective stress in the material.

(4) That it should be a material which has been used for related work.

The material selected to meet these requirements was a crushed limestone conforming with the specification for wet-mix base material (Clause 808, DOE, 1969) supplied by Amalgamated Roadstone Corporation, Chipping Sodbury. To ensure consistency, the material was sieved and regraded to the optimum grading for high density as used in previous work at Birmingham (Kennedy, 1974). The grading curve, together with the specification limits for wet-mix base and type 1 sub-base, is shown in Fig. 5.1.

In order to measure effective stress (see Section 4.3.1), it was necessary that the material should be tested either dry or saturated. In the absence of detailed information, it is considered that the granular layer in a typical pavement is more likely to be dry, and the use of dry material also simplified sample preparation and obviated the need for pore pressure measurement.

Full details of the physical properties of this crushed limestone aggregate are given by Kennedy (1974). They are summarised in Table 5.1.

Table 5.1

Aggregate Properties

Property	Value	Size fraction
Specific gravity	2.71	All size fractions
Aggregate crushing value	19	$\frac{1}{2}$" - $\frac{3}{8}$" sieves
Aggregate abrasion value	7.4	
Angularity	10.1	
Elongation	26%	
Flakiness	21%	
Liquid limit	23%	passing 200 sieve
Plastic limit	20%	
Weighted moisture absorption	0.62%	Sample grading

5.2 COMPACTION

The most satisfactory method of compacting dry granular material is by vibration (see Sections 3.1 and 3.2). A vibrating table was chosen in preference to a vibrating hammer because there was less tendency for the samples to become layered, and because the material could be vibrated around studs set into the sides of the sample which became firmly embedded to make good location points for the strain transducers (see Section 6.2.1). The vibrating table, manufactured by Podmores Engineering Limited, was 300 mm square and was capable of

producing accelerations of 4 g on a mass of 30 kg. It was driven by an electro-magnet which enabled the amplitude of vibration to be continuously varied, but the frequency was fixed by that of the mains supply (50 Hz).

The samples were 150 mm diameter and 300 mm high, which was large enough to accommodate material with a maximum particle size of 38 mm (1½" BS sieve) without being too large for handling and testing. It was desirable to have a height to diameter ratio of at least two in order to reduce end effects, and to give a reasonable length of the sample away from the ends on which deformation measurements could be taken. The sample former, shown on top of the vibrating table in Plate 1, was made of aluminium in four pieces bolted together. The inner surface had a porous lining (300 μm bronze mesh) which was connected to a vacuum to hold the sample membrane firmly in place during compaction (see Fig. 5.2). Before describing the sample preparation method in detail, sample uniformity is discussed.

5.3 SAMPLE UNIFORMITY

Samples were initially made in six similar layers from individually graded batches of material, but it was found that the finer particles tended to migrate towards the bottom of the sample during compaction. Visual examination showed that the centre of the sample was fairly uniform and that there was an increased fines content in the bottom 50 mm and a reduced fines content in the top 50 mm. This indicated that all particles of any particular size moved by the same amount relative to the material as a whole, fine particles down and coarse particles up. If the completed sample was turned upside down and vibrated again, there was little change, suggesting that the problem was caused by the way in

which the material was placed. By dividing samples into upper and lower halves, and sieving each half, the relative movement was analysed. Typical results are shown in Fig. 5.3. It can be seen that the relative particle movement is roughly equal to the difference in particle size (mean diameter). Visual examination confirmed that after compaction of each layer, there was a single layer of coarse particles on top of the mass of uniformly compacted material, and that this layer of coarse particles appeared at the top of the sample as each layer was added and vibrated.

In order to make uniform samples, the relationship between particle size and movement was used to make adjustments to the batches of materials used for the top and bottom layers of the sample. All samples tested were made from a batch of coarse material placed at the bottom, then five batches graded according to the curve in Fig. 5.1 and a batch of fine material placed at the top. This correction to the first and last batches of material resulted in uniform samples, and details of the grading of each batch are given in Table 5.2. The effect of this correction on the grading of the top and bottom halves of the sample is given in Table 5.3.

An additional benefit of having a batch of fine material at the top was that the surface, on which the top platen rested, was much smoother. Such a correction would not be required for partially saturated material where the moisture provides sufficient cohesion to prevent the relative movement of different particle sizes. A few brief experiments indicated that there are difficulties in applying the method to an open graded, dry material where the fine particles can always find their way through the large voids between the coarse material.

Table 5.2

Gradings for Sample Preparation

BS sieve	Cumulative weight (grams) passing		
	first batch	five uniform batches	last batch
$1\frac{1}{2}$"	510	2180	610
$\frac{3}{4}$"	155	1500	610
$\frac{3}{8}$"	60	1135	520
$\frac{3}{16}$"	25	860	410
No. 7	10	635	315
No. 14	0	440	230
No. 25	0	330	170
No. 52	0	260	130
No. 100	0	200	100
No. 200	0	160	80

Table 5.3

Uniformity Achieved in Typical Dense Sample

BS sieve	Cumulative percentage passing		
	Design Grading	Grading achieved	
		Top half	Bottom half
$1\frac{1}{2}$"	100	100	100
$\frac{3}{4}$"	68.2	67.5 (65.5)	67.0 (72.0)
$\frac{3}{8}$"	51.6	50.6 (48.7)	51.6 (55.4)
$\frac{3}{16}$"	39.0	37.9 (36.4)	39.7 (42.2)
No. 7	28.9	27.9 (26.8)	29.5 (31.4)
No. 14	20.8	20.1 (18.5)	21.2 (22.0)
No. 25	15.0	14.3 (13.8)	15.2 (16.4)
No. 52	11.75	11.2 (10.9)	11.9 (12.9)
No. 100	9.2	8.6 (8.4)	9.0 (9.9)
No. 200	7.2	6.9 (6.7)	7.3 (7.9)

Note: Figures in brackets were for a sample without the correction layers.

5.4 DETAILS OF SAMPLE PREPARATION

Each sample was enclosed in two latex membranes. The inner one (0.3 mm thick) was held against the porous inner surface of the sample former by an applied vacuum during sample preparation and the outer one (0.5 mm thick) was added afterwards to cover any punctures produced in the inner one during compaction. Fig. 5.4 shows how the location studs were attached to the inner membrane, and how the outer membrane was sealed around the 6 BA rod protruding from each stud. The studs were attached to the inner membrane before it was placed inside the sample former and the 6 BA rods were screwed in after the outer membrane had been added. There were six studs on each sample 75 mm apart as shown in Fig. 5.2.

The procedure for preparing each sample was as follows. The bottom platen was placed on the vibrating table, and the sample former was clamped onto the table on top of the platen with the inner membrane held inside (see Fig. 5.2). After each batch of material was placed in the sample former, it was tamped by hand and then vibrated for 90 sec with a nominal surcharge placed on top to keep the surface level. Six consecutive periods of vibration were used of 15 seconds each, starting with the largest amplitude and decreasing to the smallest. A different proceedure was used for the last batch which consisted of finer material. Any large particles which projected up too high from the layer below were removed, before this batch was placed, and vibration was applied for a shorter time with a surcharge until a reasonable flat top surface was obtained.

The top platen was then placed in position and the voids of the sample were evacuated so that the sample former could be removed. The second membrane was placed over the sample and both membranes were sealed

by stretching 'O' rings over the platens. The density of each sample (see Appendix A) was calculated from the weight of material used and the external dimensions.

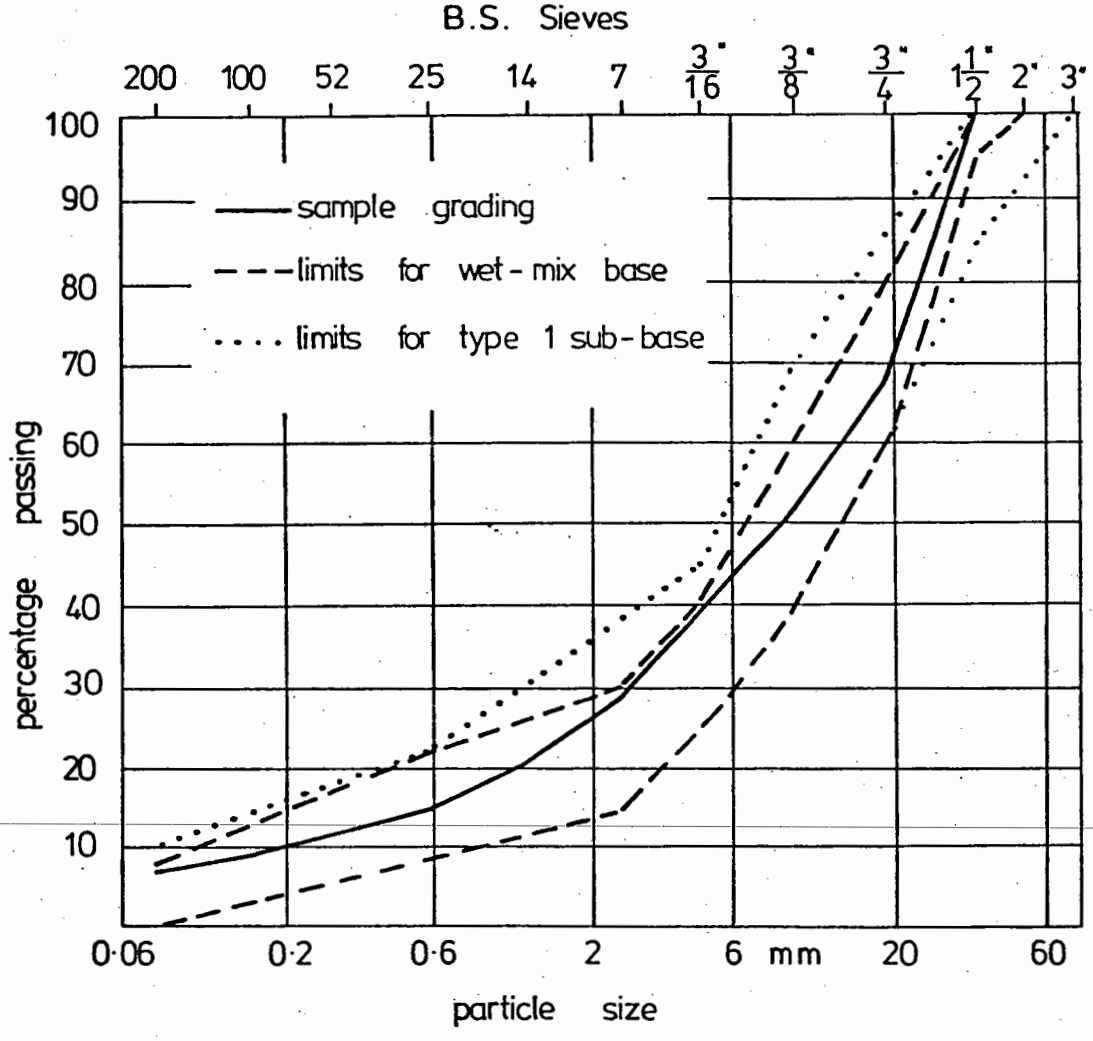

FIG. 5.1 GRADING CURVE FOR THE MATERIAL

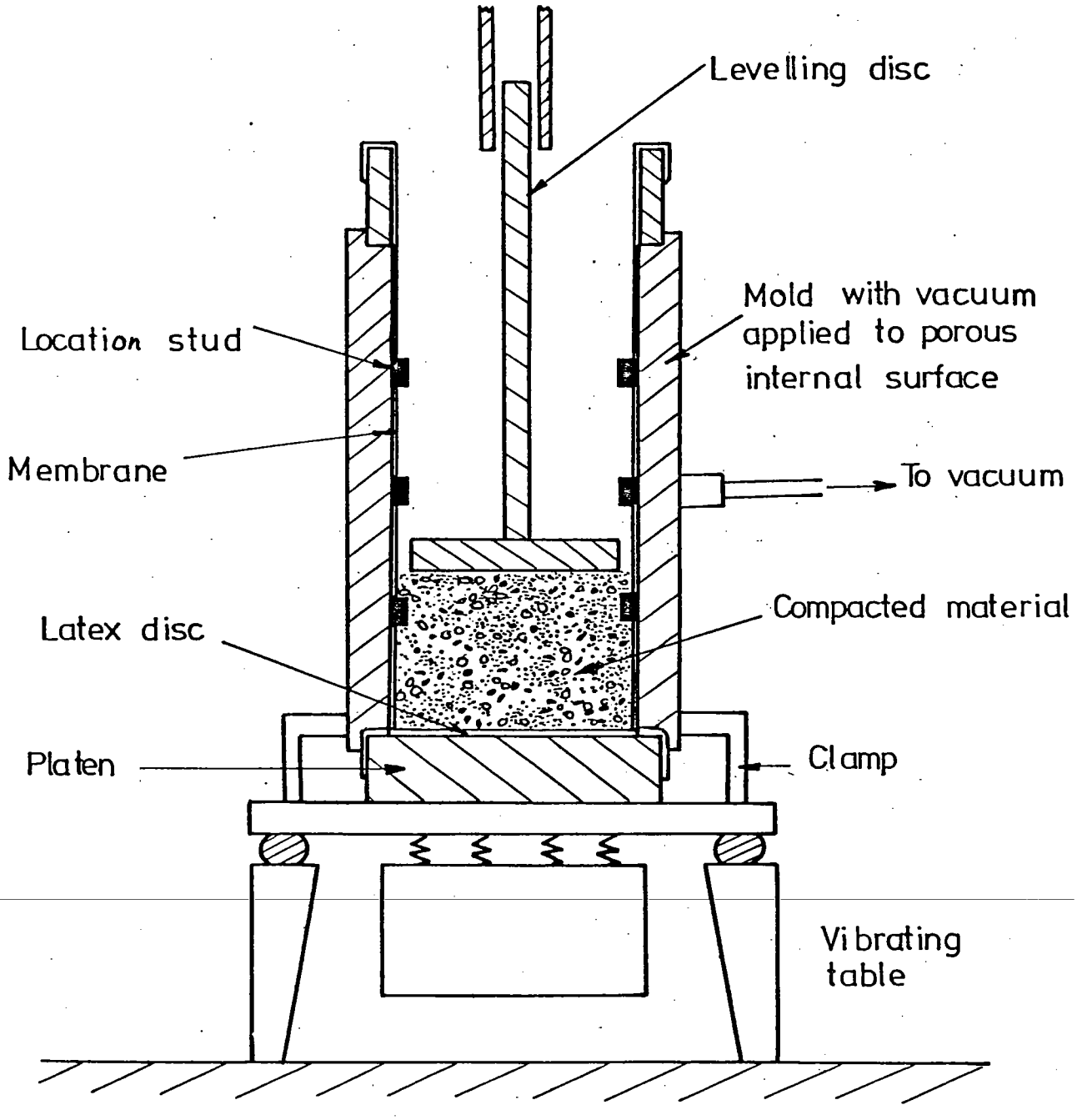

FIG. 5.2 SAMPLE PREPARATION

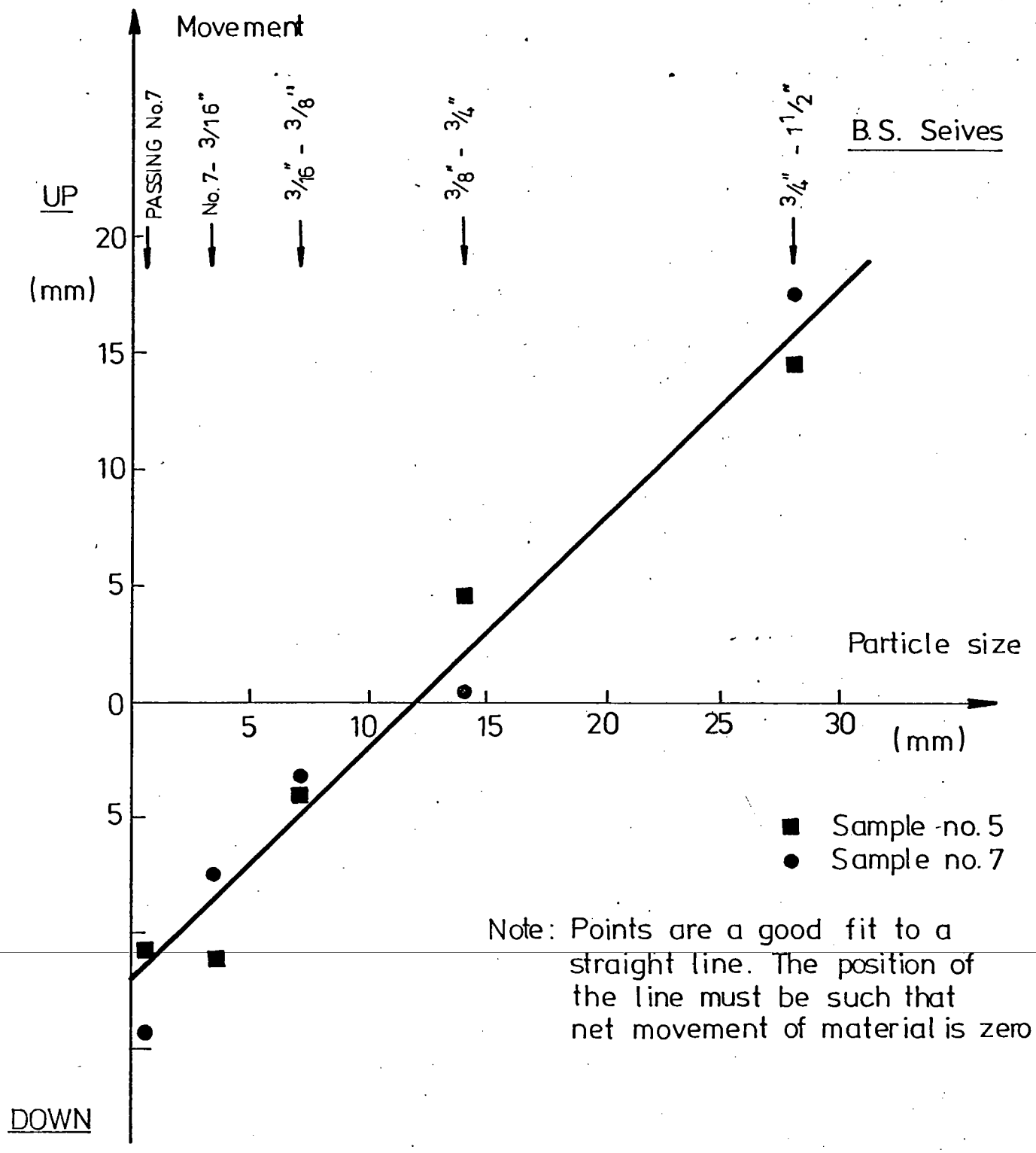

FIG. 5.3 RELATIVE MOVEMENT OF AGGREGATE PARTICLES DURING COMPACTION

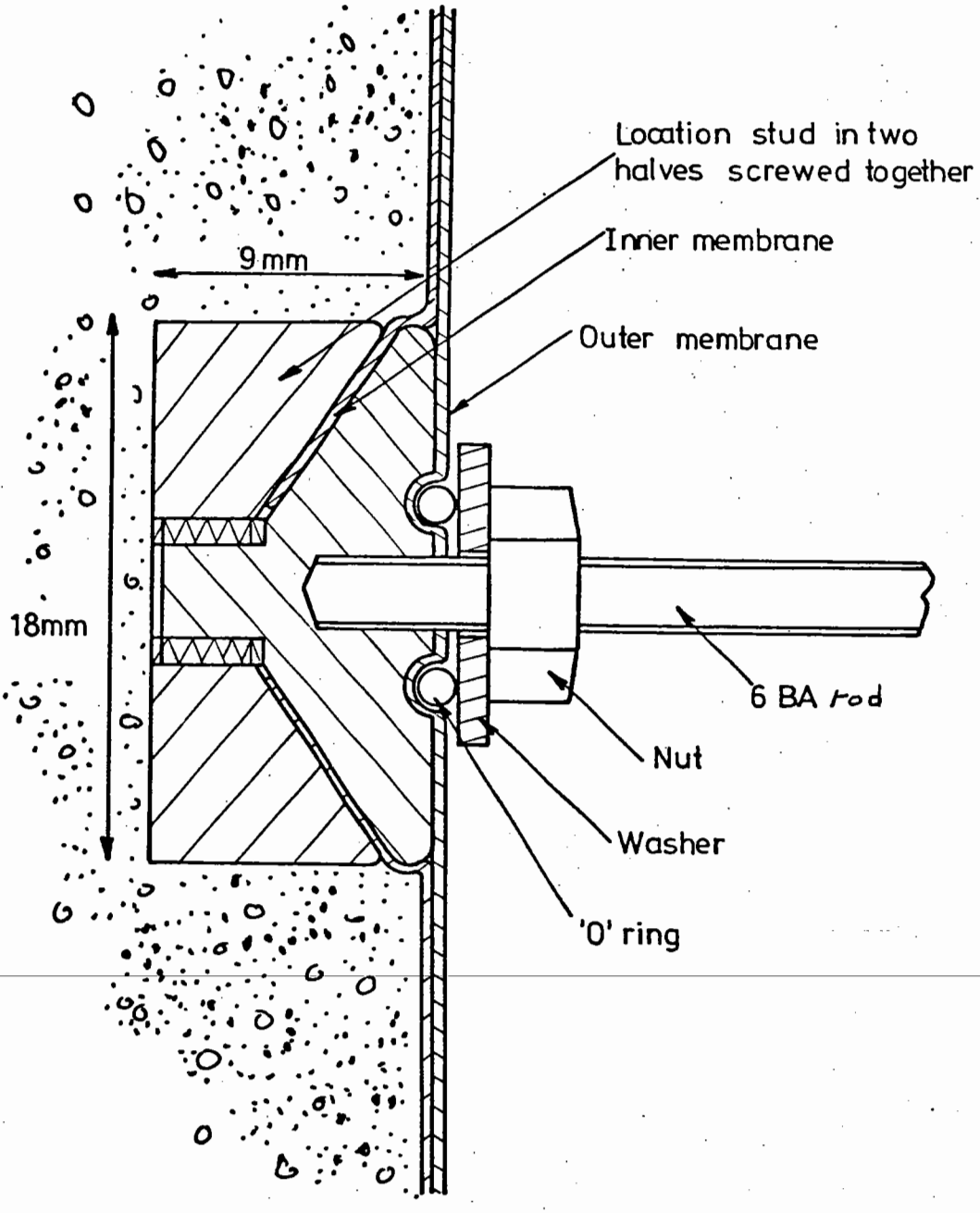

FIG. 5.4 LOCATION STUD

CHAPTER SIX

THE EQUIPMENT

6.1 LOADING EQUIPMENT

The loading equipment used in this project was based on servo-hydraulic equipment developed at Nottingham University over several years. The essential features of this type of equipment are described by Cullingford et al (1972) and full details of the design and control of an earlier version of the apparatus for testing 36 mm diameter soil samples are given by Parr (1972).

The principal components of the equipment are shown in Fig. 6.1. The axial load and the confining stress are applied to the samples in a triaxial cell by hydraulic actuators. The axial load is continuously monitored by a load cell, and the output from this load cell is compared with a load command signal by the electronic control system. An error signal is then applied to the servo-valve on the actuator so as to correct the load applied to that required. The confining stress is similarly controlled by the output of a pressure sensor in the cell fluid.

Plate 2 is a general view of the loading frame, and Plate 3 shows the electronic control system and associated monitoring equipment. The various mechanical components are described below, together with the facilities available on the electronic control system. The capabilities of the equipment are summarised in Table 6.1. The design and construction of the electronics was done entirely by the Applied Science Faculty Workshop and only general details are given here. Calibration of the load cell and pressure sensor is described in Appendix B and the design and performance of the loading equipment is discussed in Appendix C.

Table 6.1

Capabilities of the Equipment

Sample size	
Diameter	150 mm
Height	300 mm
Applied stresses	
Confining stress	0 - 400 kN/m^2
Deviator stress	0 - 1200 kN/m^2
Rate of loading	
Sine wave (confining stress	0 - 2 Hz
Sine wave (deviator stress	0 - 16 Hz
Ramp loading (constant rate of increase)	Zero to maximum in 100 - 10,000 sec
Rest periods	
Wave train	1, 2, 4, 8 .... 2^{15} pulses
Rest period	0 - 55 minutes
Strain measurement (both axial and radial strain)	
Resilient strain	0 - 5,000 με
Permanent strain	0 - 10%

6.1.1 Triaxial Cell

The triaxial cell was supplied by Leonard Farnell and Company Limited. The internal dimensions were 300 mm diameter and 550 mm high. The cell was made primarily from aluminium alloy to withstand a pressure of 1000 kN/m^2. A large port was provided in the top of the application of variable confining stress, and sealed outlets were incorporated in the base for 48 electrical terminals and 4 pressure/vacuum lines. During testing the cell rested on a mechanical jack, and at other times it could be lowered onto a trolley and pulled clear of the loading frame.

6.1.2 Axial Load

Axial load was applied by a 50.8 mm diameter hydraulic actuator supplied by Eland Engineering Limited and controlled by a Dowty servo-valve. The actuator could apply a deviator stress of 1200 kN/m^2 on a 150 mm diameter sample at frequencies up to 16 Hz (see Appendix C).

The original load cell supplied with the triaxial cell was a strain gauged cylinder, 136 mm diameter and 3 mm thick, mounted on the base of the triaxial cell (see Plate 4). This load cell was used for the preliminary tests and the main programme of resilient strain tests, but was then replaced because it could not measure negative deviator stresses. It was also susceptible to bedding errors and, as it was not very sensitive, semiconductor strain gauges were required to measure low stresses.

The opportunity was taken to design a completely new load cell consisting of foil strain gauges fixed to the lower portion of the loading rod, which was milled down to a 12 mm square section from the original 19.05 mm round. This load cell was more sensitive, more linear, and not susceptible to bedding errors. It was used for all the remaining tests, and can be seen above the sample on Plate 6.

It should be noted that it is important to have the load cell inside the triaxial cell so that friction between the loading rod and the triaxial cell top does not give a false reading, and it is therefore essential that the load cell is not affected by changes in cell pressure.

6.1.3 Application of Negative Deviator Stress

After carrying out the six resilient strain tests in the main test programme, it was decided to carry out three further tests which involved loading the sample in triaxial extension, i.e. applying negative (tensile) deviator stress. It was required that the axial stress should be less than the confining stress but it was not intended to apply tension to the sample as this would cause immediate failure of dry unbound material. The original loading arrangement and the modifications required to apply negative deviator stress are shown diagrammatically in Fig. 6.2. Joint 'A' was replaced by a tapered shear pin, clamps were provided to hold down the triaxial cell onto the jack, and joints 'B' and 'C' were replaced by sealed cavities. These cavities were open to the atmosphere, so that the cell pressure held the top cap on to the sample while tensile deviator stress was applied. This arrangement enabled the original platens to be retained, and simplified setting-up procedure. The top cavity, 140 mm diameter, was smaller than the sample so that the top cap would separate from the platen if the loading rod was pulled suddenly upward by the 'panic' circuits.

6.1.4 Loading Platens and Stress Conditions

The loading platens were made from aluminium alloy with polished steel faces. Two shallow grooves were cut around the circumference of

each one to enable the sample membrane to be sealed with 'O' rings and a "drainage" connection was taken to the outside edge from a sintered stainless steel disc in the centre. They were 180 mm diameter to allow for radial expansion of the sample, and "frictionless" contact was provided by a greased latex disc on the polished face.

These frictionless ends (similar to those recommended by Rowe and Barden, 1964) were not entirely successful because the large aggregate particles in the material pushed the grease to one side within two or three hours. However, all strain measurements were taken on the central part of the sample, and it has been shown theoretically (Dehlen, 1969) that end friction does not have a significant effect in this case if the height to diameter ratio is at least two. It can be noted in passing that barrelling occurred in two of the four single loading tests (see Section 7.3) and that in the resilient strain tests there was no significant difference between radial strain measured at the centre and the quarter points of the sample (see Appendix D).

6.1.5 Confining Stress

For tests with constant confining stress air was used as the confining medium, the pressure being controlled by a Norgen valve from a regulated air supply. For tests with variable confining stress silicone oil (Dow Corning Type 250/20 cs) was used. This oil has a relatively low viscosity, 20 centistrokes at 25^{o}C, is chemically inert and is an excellent electrical insulator. It was found to have no effect on latex membranes, strain gauged transducers or LVDT's. The pressure of the oil was controlled by a hydraulic actuator, 25.4 mm diameter, operating a pressure cylinder, 127 mm diameter. The pressurising cylinder was connected to the triaxial cell by a large

bore flexible tube which incorporated a baffle to eliminate surges of pressure. Cyclic cell pressures of 400 kN/m^2 could be applied at frequencies up to 2 Hz. Details of the control and stability are given in Appendix C.

The confining stress was measured by a pressure sensor placed inside the triaxial cell. This consisted of a strain gauged diaphragm, 22 mm diameter and 0.6 mm thick, made of stainless steel. The front face of the diaphragm was in contact with the cell fluid, and the rear face was enclosed by a sealed cavity which had a connection taken out to atmospheric pressure. The pressure sensor can be seen resting on the cell base in Plate 4.

6.1.6 Electronic Control System

In the usual mode of operation the axial load ram was controlled by the output of the load cell. The load cell output (with suitable amplification) was compared with a command signal and the difference used to determine the flow in the servo-valve controlling the hydraulic actuator. The confining stress was similarly controlled by the output of the pressure sensor. The two command signals were derived from the same waveform generator (Prosser Type A100) which had facilities for producing many different waveforms, and had two sinusoidal outputs with variable phase difference. This was necessary at frequencies greater than 1 Hz to compensate for delay in the mechanism applying the confining stress. Controls were provided on each servo-loop for the mean and the repeated amplitude of the command signal, and for the loop gain.

There were additional controls for the axial load. These enabled the command signal to be taken from a ramp generator and the feedback to be taken from axial strain measurements (see Section 6.2), so that single load tests could be performed at a constant rate of strain.

There was also a facility for increasing the command signal in the normal load controlled mode so that the axial load could be enhanced to take account of the change in cross-section of a sample during the course of a test.

The control cabinet had numerous monitoring points and housed a number of peripheral circuits:

(a) A stabilised voltage supply and amplifiers for the load cell, the pressure sensor and for a pore-pressure transducer if this should be required.

(b) A load cycle counter, and facilities for providing "rest periods" at intervals between "trains" of load pulses.

(c) Galvanometer matching circuits so that all relevant signals could be recorded on a u/v recorder (see Section 6.3) and timing circuits so that the recorder could be switched on and off at intervals during a long test.

(d) Dither oscillators for the servo-valves.

6.2 DEFORMATION MEASUREMENT

Various methods of strain measurement are discussed in the review of experimental techniques (Sections 3.4.3 - 3.4.5). The principal aim of this project was to determine the behaviour of a particular material under a range of different stress conditions. Therefore, strain measurements taken from points located on the sample were considered to be desirable to minimise end effects.

6.2.1 Location Studs

After trying several other methods, the location studs shown in Fig. 5.4 were developed. They take advantage of the fact that using

a vibrating table for compaction enabled the material to be compacted around the studs (see Fig. 5.2). Each stud can be considered as an aggregate particle with an extension protruding through the membrane. During compaction they were held in place by the inner membrane, the outer membrane being added afterwards to seal any punctures in the first one.

6.2.2 Axial Strain

Axial strain was measured by four small LVDT's operating over separate gauge lengths as shown in Fig. 6.3. LVDT's are well proven for the measurement of axial strain in the repeated load triaxial test. Those used here were type 357/0.2" supplied by S.E. Laboratories, which have a range of ±5 mm and a weight of about 10 g. The simple method of attachment shown in Plate 5 was found to cope quite adequately with the small degree of barrelling that often occurred during sample deformation. Tests on a dummy sample (a hollow aluminium cylinder) showed that their response was linear up to a frequency of 30 Hz.

6.2.3 Radial Strain

Various methods have been tried in the past for the measurement of radial deformation in the repeated load triaxial test and these are described in Section 3.4.4. It was at first thought that a development of the collar and LVDT used by Brown and Snaith (1974) on bituminous material would be satisfactory. However, this was rejected because it could not cope with large enough deformations. Attention was then turned to the possibility of using a flexible semicircle, strain gauged in the middle and pinned to opposite ends of a sample diameter, and a prototype was made from a strip of stainless steel 1.6 mm thick. It proved to be feasible, but suffered from practical problems of

attachment to the sample, and its tendency to be highly susceptible to external vibrations.

These problems were overcome by the flexible strain ring shown in Fig. 6.4. Its advantages were:

(1) Greater sensitivity than a semicircle of similar dimensions.

(2) Interference from external vibrations eliminated because of its symmetry.

(3) Easy attachment to the sample because it was not required to pivot at these points.

The ring was made narrower at the strain gauges to give a better deflected shape and increased sensitivity. Selection of a suitable material from which to make the ring did present some difficulty because it was important to use a material with a low elastic modulus to reduce the stiffness of the ring. Perspex was tried but it could not be machined to shape without damage. However, a cracked perspex ring was used to make a simple plasticine mould in which to cast a ring from araldite. This was successful, and after wiring with 600 Ω foil strain gauges, the ring was found to have a sensitivity of 0.88 mV/mm.

A steel mould was then made from which several araldite rings were cast. The araldite used was resin MY 778 with hardener HY 956, and the mould release agent was QZ 11B. This is a casting araldite with an elastic modulus of 4.0 kN/mm^2, and the rings weighed 27 g with a stiffness of 0.50 N/mm.

Polymerised materials are susceptible to creep and it was feared that this might lead to errors in permanent strain readings in tests lasting for several hours or days. To compat creep each ring was

cured for at least one month at 40°C and then cycled many times at a large amplitude (1000 cycles at ±15 mm). After this process two of the rings were found to have changed shape significantly and they were rejected. Of the remaining seven the four with fewest defects, such as air bubbles, were chosen to be strain gauged. All four rings had the same sensitivity (within 2%) and it was found that there was no significant creep in the output at deflections of less than 7.5 mm (5% strain on a 150 mm diameter) over a period of 24 hours.

At low levels of strain creep or stress relaxation is roughly proportional to the applied strain, and if stress relaxation occurred in a deflected ring on this basis there would be no change in its shape. Creep in a transducer being used to measure deflection is therefore not as significant as it would be in a transducer, such as a proving ring, being used to measure load.

Apart from the single loading tests, only one test (PC-1, see section 9) developed a radial strain of more than 5% and this test was relatively short being stopped after 12,000 cycles (3½ hours).

Frequency tests on a dummy sample showed that the response of the strain rings was linear up to 30 Hz if air was used as a confining fluid. However, when silicone oil was used, there was some modulation on the output at frequencies greater than 2 Hz especially when the cell pressure was pulsed at these frequencies. It was concluded that this was due to the viscosity of the oil affecting the deflection of the rings.

6.3 DATA COLLECTION

An ultra-violet chart recorder (S.E. Laboratories type 3000 D/L) was used for recording all measurements of stress and strain. Six channels were normally used:

(1) Deviator stress

(2) Cell pressure

(3) Axial strain

(4) Radial strain

(5) Resilient axial strain

(6) Resilient radial strain

Other information such as gain settings and number of load repetitions was marked on the paper by hand. The u/v recorder was found to be a very flexible method of data collection. The frequency response was well above that required (±5% at 200 Hz for the galvanometers used, type C300) and a continuous record was produced of all inputs which enabled spurious electrical signals to be clearly identified and eliminated. It provided a quick visual indication and at the same time a permanent record which could be referred to at a later date. The recording could be started and stopped by hand whenever required, or automatically during the course of a long test. Its disadvantages were that resolution (0.3% f.s.d.) and linearity (±2% f.s.d.) were rather poor, and all the data had to be transferred by hand to data sheets and computer cards before being processed.

A general purpose digital voltmeter and a dual beam oscilloscope were also available for routine monitoring and setting up procedures.

The load cell and the pressure sensor were calibrated in terms of volts output per unit of stress (100 kN/m^2). Before each test the galvanometers recording deviator stress and cell pressure were set on a suitable range for the stresses to be applied in that test. This was done by the galvanometer matching circuits and was necessary because of the poor resolution of the u/v recorder.

The LVDT's measuring axial strain and the strain rings measuring

radial strain were powered by a 3 kHz carrier system and this carrier system had suitable outputs for the galvanometers in the u/v recorder. Individual strain transducers were calibrated in terms of divisions on the recorder output for increments of strain at a variety of sensitivity settings on the carrier system. Normally, measurements were taken with all four LVDT's wired together on one channel of the carrier system, and the three strain rings wired together on another channel. When taking these "overall" readings the calibration constants were slightly different (see Appendix B).

For the resilient strain readings the strain signals were passed through a d.c. offset generator and then amplified (usually by a factor of 20 times). The offset generator ensured that the amplified strain signal remained on scale. Using this technique, resilient strains of 5 $\mu\varepsilon$ could be resolved even if superimposed on a large permanent strain.

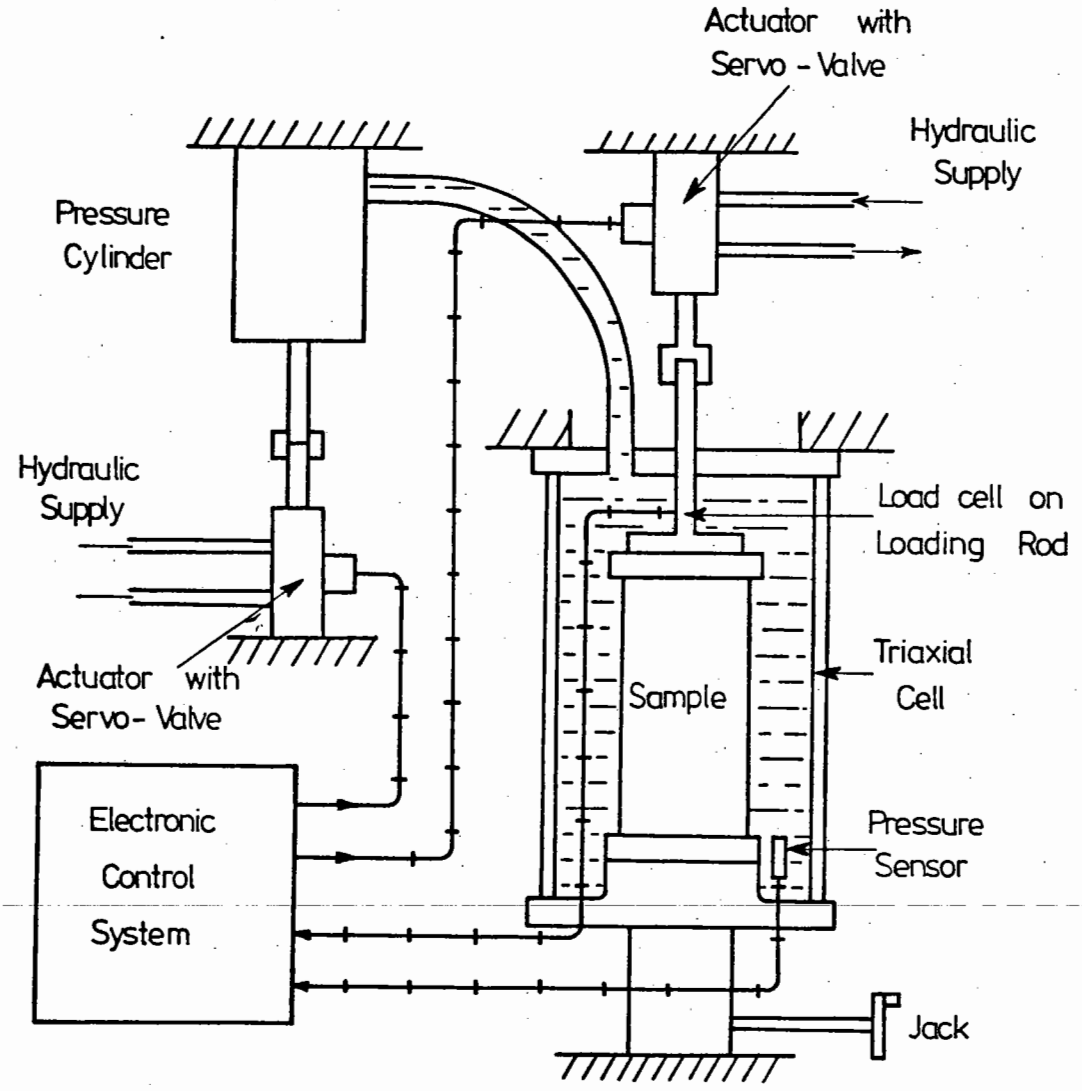

FIG. 6.1 DIAGRAM OF LOADING EQUIPMENT

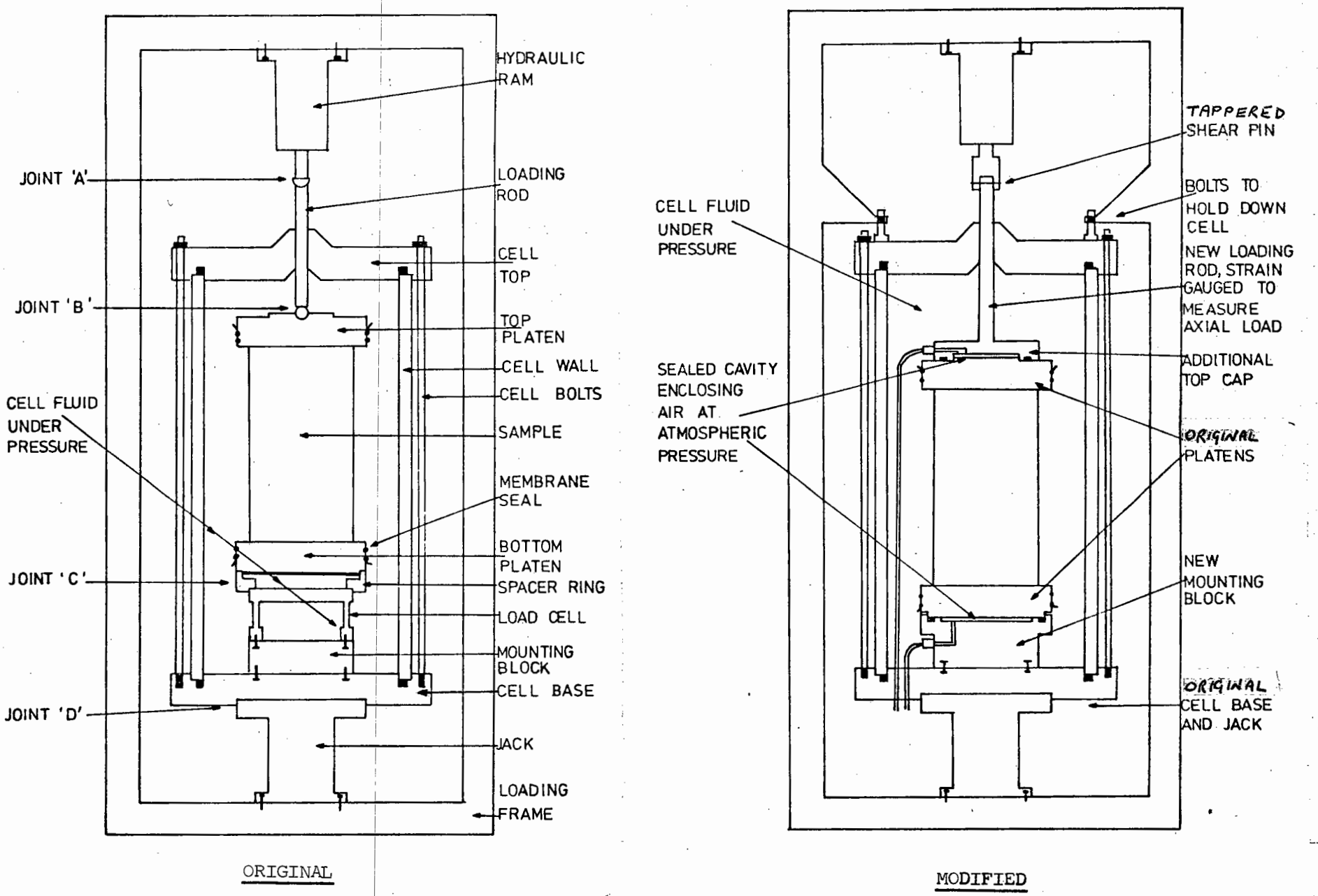

FIG. 6.2 MODIFICATIONS TO THE AXIAL LOADING ARRANGEMENT TO APPLY TENSILE DEVIATOR STRESS

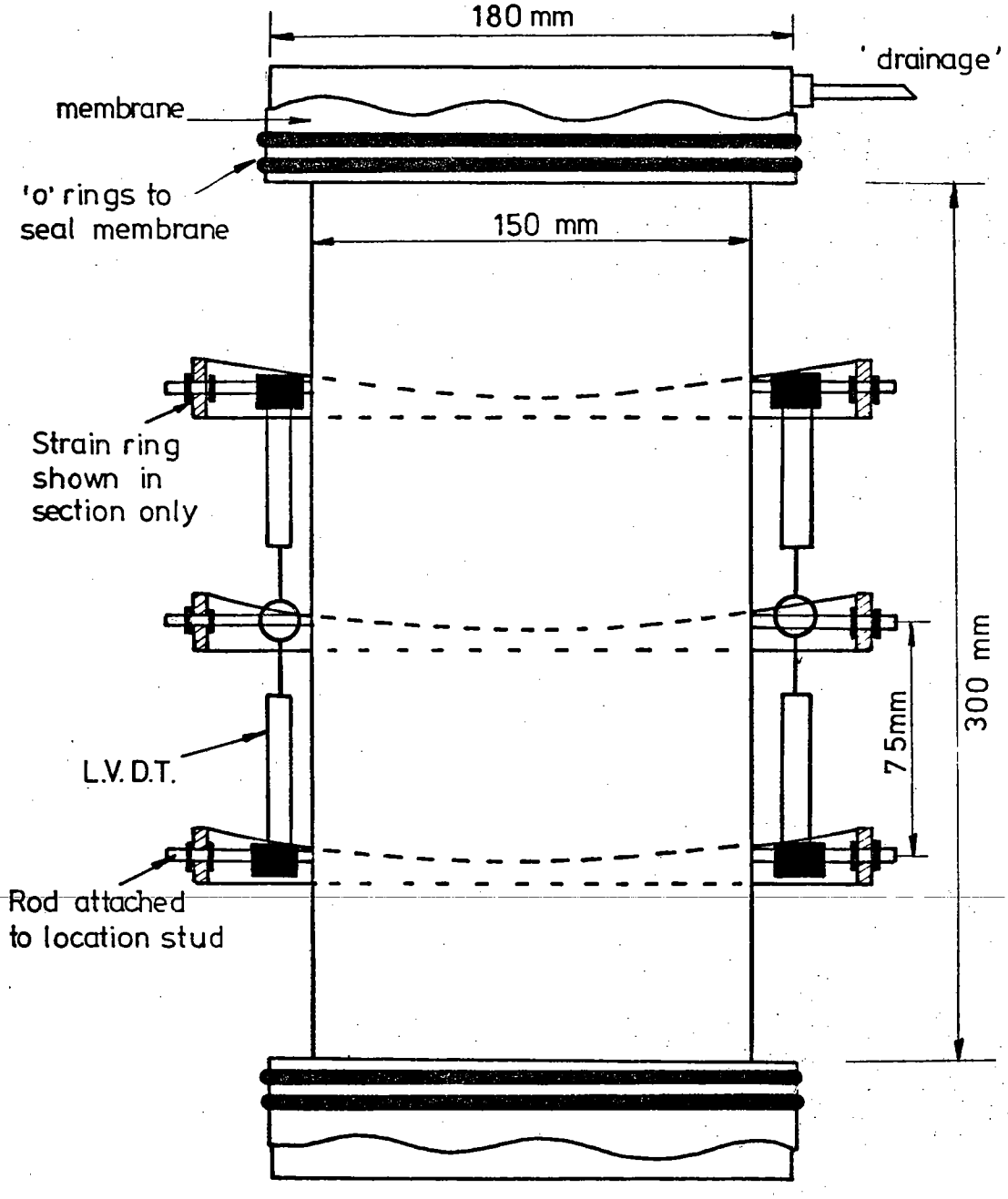

FIG. 6.3 POSITION OF STRAIN TRANSDUCERS

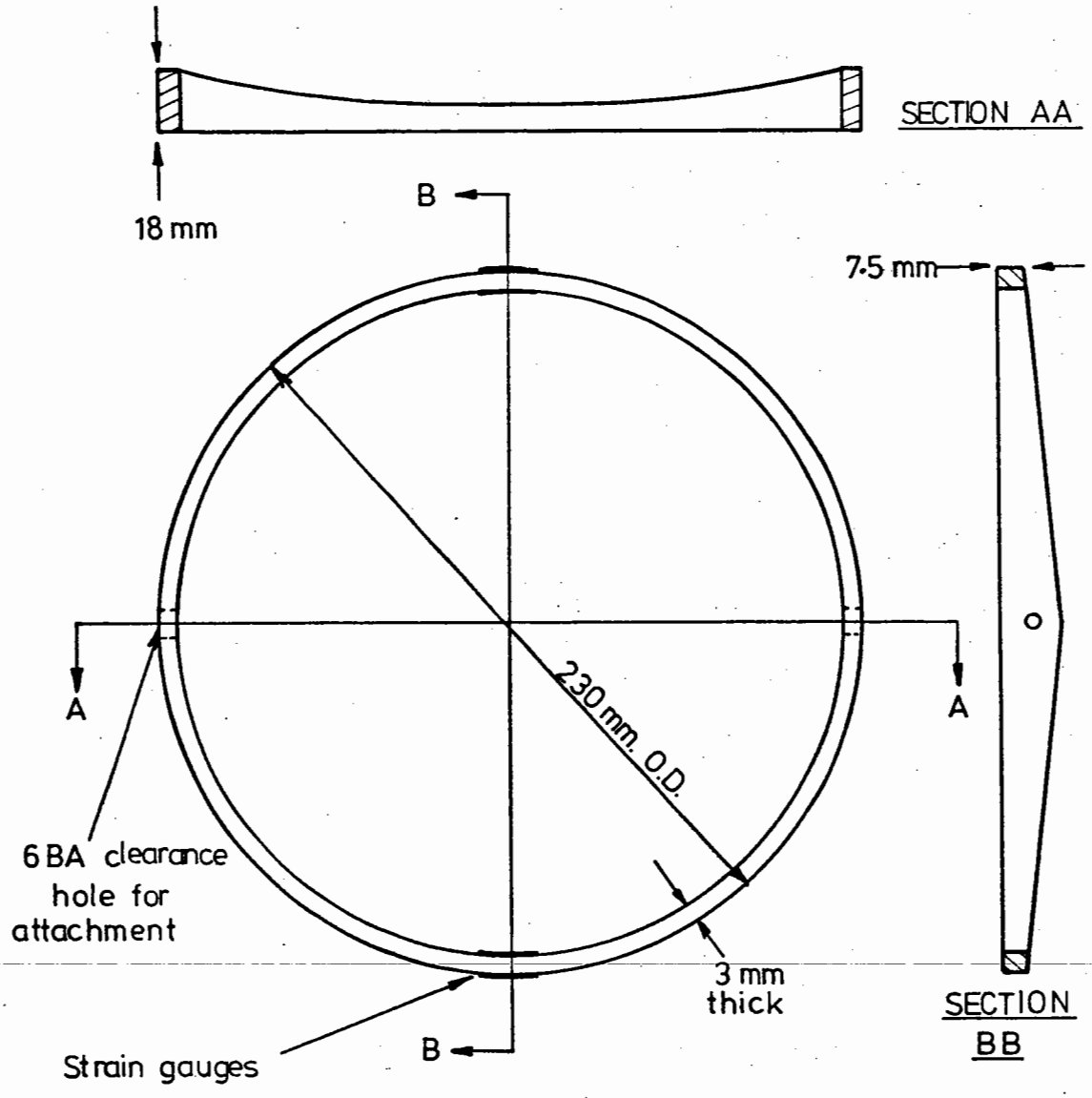

FIG. 6.4 ARALDITE STRAIN RING

CHAPTER SEVEN

PRELIMINARY TESTS

The purpose of these tests was to obtain some general data on the behaviour of the test material so that the main resilient and permanent strain tests could be carried out in the most useful way.

7.1 SINGLE LOAD TESTS

Four single load tests were performed at a constant rate of axial strain. Three tests were at constant confining stress, σ_3, and the fourth was at constant normal stress, p. A further test with p constant (OT-20) was abandoned because of difficulties in controlling the equipment at the very low cell pressures involved. The four successful tests are detailed in Table 7.1, and the results are shown in Figs. 7.1 to 7.4.

Table 7.1

Single Load Tests

Overall behaviour

Test	OS-160	OS-160A	OS-20	OT-160
Sample	102	104	103	106
Type of test	σ_3 constant (160 kN/m^2)	σ_3 constant (160 kN/m^2)	σ_3 constant (20 kN/m^2)	p constant (160 kN/m^2)
Rate of strain (%/min)	0.27	0.11	0.11	0.11
Max. stress ratio (σ_1/σ_3)	9.1	8.7	9.5	6.3
Shearing resistance (φ)	53.4°	52.6°	54.2°	46.6°
Overall strain at max. stress:				
Axial strain (ε_1) %	4.0	3.9	1.8	2.3
Radial strain (ε_3) %	2.7	2.8	2.5	2.6

It can be seen from Figs. 7.1 and 7.2 that the two tests at σ_3 = 160 kN/m^2 were very similar as regards maximum stress ratio and strain behaviour. In one of the tests (OS-160) there were three points, labelled A, B and C on Fig. 7.1, where a rapid increase in radial strain occurred. Detailed examination of the strain readings (see para. 7.1.1) showed that this rapid increase occurred at one strain ring only, but not the same one in each case.

Test OS-20 (σ_3 = 20 kN/m^2) reached about the same maximum stress ratio, but the strain behaviour was rather different, the sample dilating right from the start of the test. It appears that a lateral stress of 20 kN/m^2 is insufficient to maintain the material in a densely packed state.

Test OT-160 (normal stress, p = 160 kN/m^2) reached a lower maximum stress ratio than the tests with constant confining stress (6.3 compared with 9). It appears that the material is weaker when stressed in this way. The strain behaviour was intermediate between that of the other tests.

In general, these results agree with those reported by Kennedy (1974) for the same material, and follow the normal pattern for a densely packed sand under "drained" conditions.

7.1.1 Individual Strain Measurements

At intervals during these tests, readings were taken from individual LVDT's and strain rings. Those at maximum deviator stress and at the end of each test are given in Tables 7.2 and 7.3 respectively. The standard deviation between individual readings taken at the same time varied from 9% to 41%* These variations were fairly random, and it seems likely that they were due to the random particle distributions in the material. It should be noted that the gauge lengths over which

* Percentage of the strain at that time.

these readings were taken (75 mm for the LVDT's and 150 mm for the strain rings) are only a few times larger than the maximum particle size of 38 mm. However, when overall strain readings are plotted, as in Figs. 7.1 to 7.4, reasonably smooth curves result, except for the radial strain in Test OS-160 as noted above.

The final dimensions of samples after the single loading tests are given in Table 7.4. Barrelling occurred in Test OS-20 and to a certain extent in Test OT-160.

Table 7.2

Single Load Tests

Individual strain measurements at maximum deviator stress

Test		OS-160	OS-160A	OS-20	OT-160
LVDT	1	4.65%	3.79	0.98	2.60
	2	3.32	3.94	2.48	1.49
	3	3.07	4.70	2.34	1.88
	4	5.62	3.07	1.36	3.61
Standard deviation		1.19	0.67	0.73	0.93
Strain Ring	1	2.52	3.16	2.13	1.88
	2	3.25	2.76	2.65	2.95
	3	3.42	-	2.56	2.91
Standard deviation		0.48	0.28	0.28	0.61

Note: The readings for Test OS-160 were taken just after the maximum stress was reached.

Table 7.3

Single Load Tests

Individual strain measurements at the end of each test

Test		OS-160	OS-160A	OS-20	OT-160
LVDT	1	6.11%	5.32	4.97	5.82
	2	5.17	5.74	5.52	5.20
	3	4.28	6.51	4.65	3.47
	4	6.21	4.13	4.37	6.68
Standard deviation		0.91	0.99	0.49	1.36
Strain Ring	1	2.69	5.16	5.81	3.76
	2	4.23	4.47	7.48	7.35
	3	4.12	-	3.16	7.22
Standard deviation		0.86	0.49	2.18	2.04

Table 7.4

Single Load Tests

Final dimensions of samples

Test	OS-160	OS-160A	OS-20	OT-160
Final height of sample measured at the edge	275 - 280 mm	281 - 288 mm	271 - 280 mm	284 - 289 mm
Final diameter of sample				
Top (mm)	157	163	153	152
Strain Ring 1	155	161	159	154
Strain Ring 2 (middle)	156	158	163	158
Strain Ring 3	158	157	156	158
Bottom	158	154	152	153
Comment	Uniform	Tapered	Barrelled	Slightly Barrelled

Note

(1) Initially, all samples were 300 mm high and 150 mm diameter.

(2) The variation in the final height of a sample was due to tilting of the top platen.

7.2 STRESS HISTORY EFFECTS*

Three tests were performed to assess the effect of stress history on the resilient strain behaviour of the material. The results of these tests are described individually followed by an overall assessment of stress history effects. All the tests were performed at a frequency of 1 Hz and the majority were at constant confining stress. The stress parameters which describe the various cyclic stress paths applied during these tests are defined in Section 4.4.1.

7.2.1 Test RX

The stresses applied in this test are given in Table 7.5 and shown diagrammatically in Fig. 7.5. For each series of readings the confining stress, σ_3, was held constant and 100 cycles were applied at different repeated deviator stresses, q_r. 100 cycles was chosen because this was the number suggested by Hicks (1970) after tests on similar types of material.

Table 7.5

Test RX - Stresses Applied

Series	σ_3 (kN/m^2)	q_m	Stress ratio q_r/σ_3
1	40	$q_r/2$	1, 2, 3, 4, 5, 6, 5, 4, 3, 2, 1
2	160	$q_r/2$	As series 1
3	40	$q_r/2$	As series 1
4	160	$q_r/2$	10,000 cycles of $q_r/\sigma_3 = 6$

* In this context stress history refers to the effect of previous repeated stresses on the material, and should not be confused with consolidation which takes place in cohesive materials subject to a static stress under drained conditions.

The resilient strains measured during each series of readings are shown in Fig. 7.6. It can be seen that during each period of 100 cycles, the resilient strain changed, usually decreasing by 0 to 10%. There were also differences of up to 10% between strains in the increasing and decreasing stress sequencies of each series. Both of these effects were less marked in series three than in series one although the same stress paths were used in each case. From Fig. 7.5 it can be seen that very little permanent strain developed during series three.

Series four differed from the first three in that 10,000 cycles were applied at the same stress level, σ_3 = 160 kN/m^2 and q_r/σ_3 = 6. From Fig. 7.7 it can be seen that it was about 2000 cycles before the resilient strain reached a steady value. During this period, Fig. 7.5 shows that there was a rapid build up of permanent strain.

The test indicated that to define the resilient response of the material from the resilient strain occurring after 50 to 100 cycles on any stress path as was done by Hicks (1970) and Allen and Thompson (1973) might not be satisfactory.

7.2.2 Test RY

The purpose of this test was primarily to determine the number of stress cycles which were required for the resilient strain to reach a steady value for various stress paths. The figure of 2000 obtained in the previous test was from only one stress path.

The stresses applied to the sample are given in Table 7.6, and shown diagrammatically in Fig. 7.8. The mean normal stress, p_m, was held constant at 48 kN/m^2 throughout the test and several series of readings were taken at different values of mean deviator stress, q_m, and repeated deviator stress, q_r. The applied stress paths are shown in

Fig. 7.9. Cycling was continued on each stress path until two readings of resilient strain at an interval of 200 cycles were within 5 με. The permanent strain which developed during the test is shown in Fig. 7.8 and the resilient strain in Fig. 7.10.

Table 7.6

Test RY - Stresses Applied

Series	p_m (kN/m^2)	q_m/p_m	q_r/p_m
1	48	0.5	0.5, 1, 0.5
2	48	1.0	0.5, 1, 1.5, 2, 1.5, 1, 0.5
3	48	1.5	0.5, 1, 1.5, 2, 2.5, 3, 2.5, 2, 1.5, 1, 0.5
4	48	1.0	0.5, 1, 1.5, 2, 1.5, 1, 0.5
5	48	0.5	0.5, 1, 0.5

Within each series, σ_3 was kept constant, i.e. $p_r/q_r = 1/3$

The number of cycles taken for the resilient strain to reach a steady value varied between 200 and 1000, and there was a tendency for it to take longer to reach a steady value at higher stress ratios.

The strains shown in Fig. 7.10 were those measured at the end of each group of stress paths, and it can be seen that they are up to 10% higher during the decreasing stress sequences. The difference was smaller in Series 4 and 5 in which the mean deviator stress, q_m, was decreased and it will be noted from Fig. 7.8 that zero permanent strain accrued.

7.2.3 Test RZ

Tests RX and RY gave some indication that changes in the resilient

strain behaviour of the material occurred during the build up of permanent strain. Test RZ demonstrated this more clearly. The test was in two parts:

Part (a) (Sample 110) - A series of different stress paths* was applied to the sample and the resilient strains recorded. The sample was then given a permanent strain of about 2% by applying 100 load cycles at a high stress ratio ($q_r/p_m = 4$). Part of the original series of stress paths was then repeated.

Part (b) (Sample 111) - The permanent strain was applied first, followed by the same two series of resilient stress paths* as in Part (a).

Some of the resilient strains measured during this test are shown in Figs. 7.11 and 7.12. It can be seen that in Test RZ (a) there is a marked difference in resilient strain between the first and second series, but in Test RZ (b) very little difference. This was also the case for the other stresses which were applied.

7.2.4 Assessment of Stress History Effects

The tests described above indicated two distinct stress history effects:

(a) If the material is subject to a number of load cycles which do not cause any substantial permanent strain, the resilient strain will reach a steady value after 200-1000 cycles. During this period, the resilient strain usually decreases by an amount from 0-10%, as it approaches the steady value.

---

* The series of stress paths applied during this test were taken from the resilient strain test programme (Section 8.1). Only one level of mean normal stress was used (192 kN/m^2), and only four cycles were applied of each stress path to avoid any build up of permanent strain while resilient behaviour was being measured.

(b) If permanent strain occurs, the resilient strain caused by any applied stress path is affected; both the initial value and the steady value reached after a number of cycles. In these few tests, there was no clear pattern of the way in which permanent strain affected the resilient behaviour of the material; increases and decreases in resilient strain of up to 30%* were observed. This is discussed in more detail after the results of the permanent strain tests have been described (Section 9.4).

If the material is subjected to a number of cycles at high stress ratio, the permanent strain so caused will extend the time taken for the resilient strain to reach a steady value. This effect was observed in series four of Test RX (see Fig. 7.7).

These preliminary tests indicated that the material is subject to stress history effects. The magnitude of the effect is broadly in agreement with previous reports, but other workers have not distinguished between the two separate effects (Hicks, 1970; and Brown, 1974). Steps were taken to minimise these effects in the resilient strain tests although they could not be completely eliminated.

It was decided that for the resilient tests (Chapter 8) only a few cycles should be applied to obtain a reading from each stress path to prevent substantial permanent deformation occurring during the course of the test, and that the effect of large numbers of load cycles and permanent strain on resilient behaviour should be investigated in the permanent strain tests (Chapter 9). In previous studies, larger numbers of cycles have been used to investigate resilient behaviour (50-100 by Hicks, 1970; and about 10^4 by Brown, 1974) but on balance the preliminary tests showed that measurements taken after only a few cycles would be more useful.

---

* Percentage of the strain in the resilient strain tests.

The possibility of taking readings after about 1000 cycles of each stress path, when the resilient strain would have reached a steady value, was considered but rejected because it would lead to substantial permanent deformation developing during the course of the test, so that the resilient measurements taken on a particular sample would not be consistent. Therefore, four cycles were applied on each stress path, and the resilient strain was recorded as the peak to peak value in the last three of these four cycles.

7.3 EFFECT OF FREQUENCY

A brief test in three parts was performed on a single sample to determine whether the resilient strains observed were dependent on the frequency of testing:

Part (a) $\sigma_3 = 128$ kN/m^2 (constant)

$q = 0 - 384$ kN/m^2

2000 cycles were applied at 2 Hz so that the resilient strain reached a steady value, then 16 cycles were applied at 0.2, 0.5, 1, 2, 5, 10 and 20 Hz.

Part (b) $\sigma_3 = 128$ kN/m^2 (constant)

$q = 96 - 288$ kN/m^2

3000 cycles were applied at 20 Hz so that the resilient strain reached a steady value, then 16 cycles were applied at 20, 10, 5, 2, 1, 0.5 and 0.2 Hz each.

Part (c) $\sigma_3 = 120 - 264$ kN/m^2

$q = 0$

2000 cycles were applied at 2 Hz so that the resilient strain reached a steady value, then 16 cycles were applied at 2, 1, 0.5 and 0.2 Hz each.

The results, shown in Fig. 7.13, indicate that resilient strain is not dependent on frequency in the range 0.2 to 5 Hz. Increases in strain occurred at higher frequencies in Part (a) in which the deviator stress, q, was cycled from 0 - 384 kN/m^2, but detailed examination of the waveform of the results showed that the increase was caused by the impact loading which occurred as the load was re-applied after falling to zero. In general, this confirms previous findings that frequency of testing has little effect on granular material (Lashine et al, 1971).

As a result of this test, 1 Hz was chosen as a suitable frequency for the resilient strain tests (Chapter 8) and the permanent strain tests (Chapter 9). This was the fastest frequency at which the equipment could be operated reliably with variable confining stress (see Section 6.1.5) and radial strain measurements (see Section 6.2.3).

7.3.1 Hysterysis

In the description of these preliminary tests, the shape of the resilient strain pulse which resulted from each sinusoidal pulse of repeated stress was not considered. No detailed measurements were taken of the shape of the strain pulse, but some general comments might be useful at this stage.

The strain waveform generally lagged slightly behind the stress waveform in a manner indicating that there was a certain amount of energy absorption by the material during each load cycle. When the stress and strain waveforms were displayed on the X and Y axes respectively of an oscilloscope, the loop formed was typically 'banana' shaped as shown in Fig. 7.14. The shape of the loop was found to be virtually independent of the frequency of loading in the range 0.1 to 10 Hz, indicating that the energy absorption was due to hysterysis rather than viscous damping.

The loop was generally lop-sided as shown, reflecting the non-linear behaviour of the material, and the shape was highly dependent on the stress path applied and the strain measurement displayed (axial or radial).

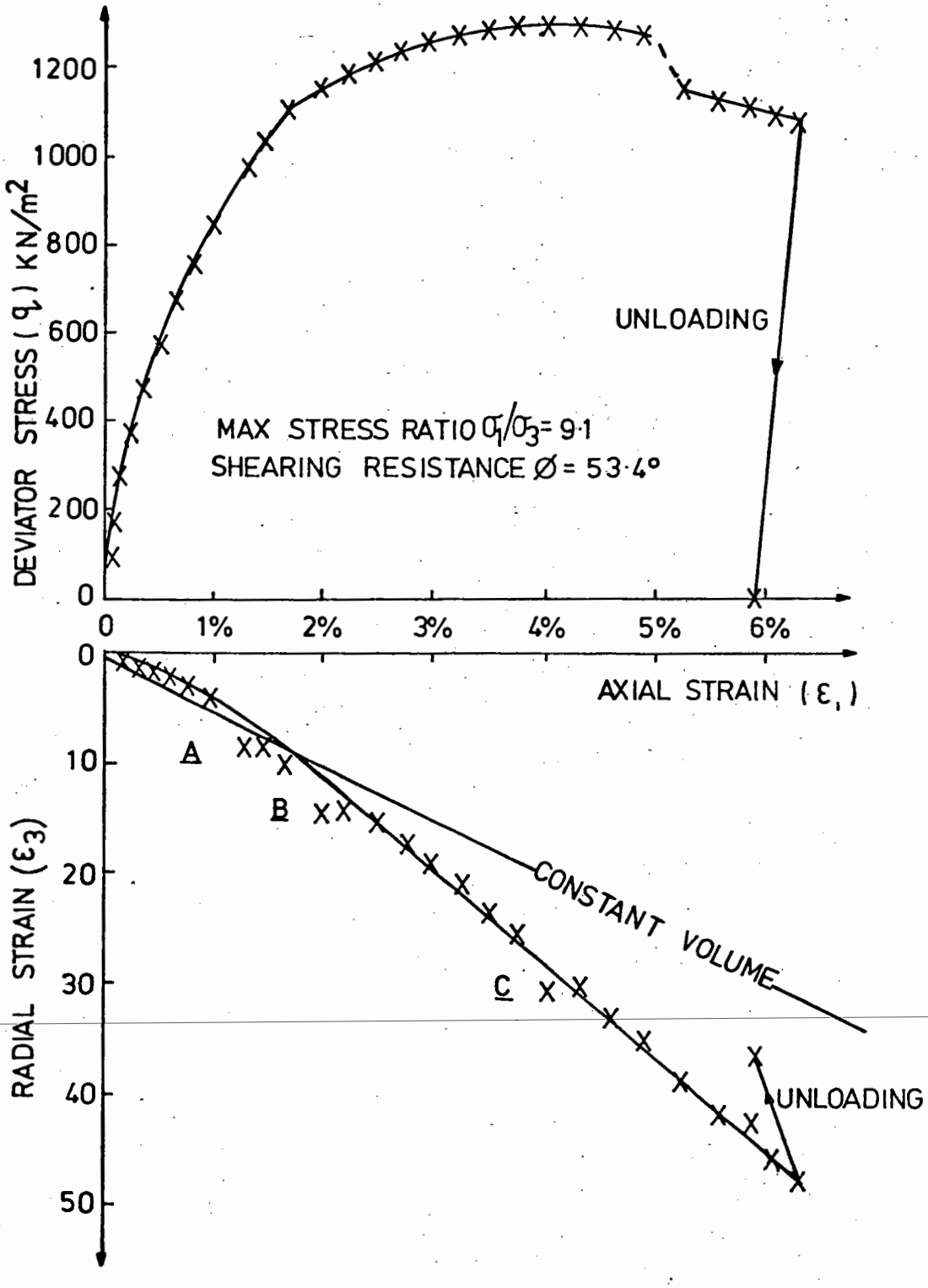

FIG. 7.1 SINGLE LOAD TEST, OS-160, AT CONSTANT CONFINING STRESS (160 kN/m²)

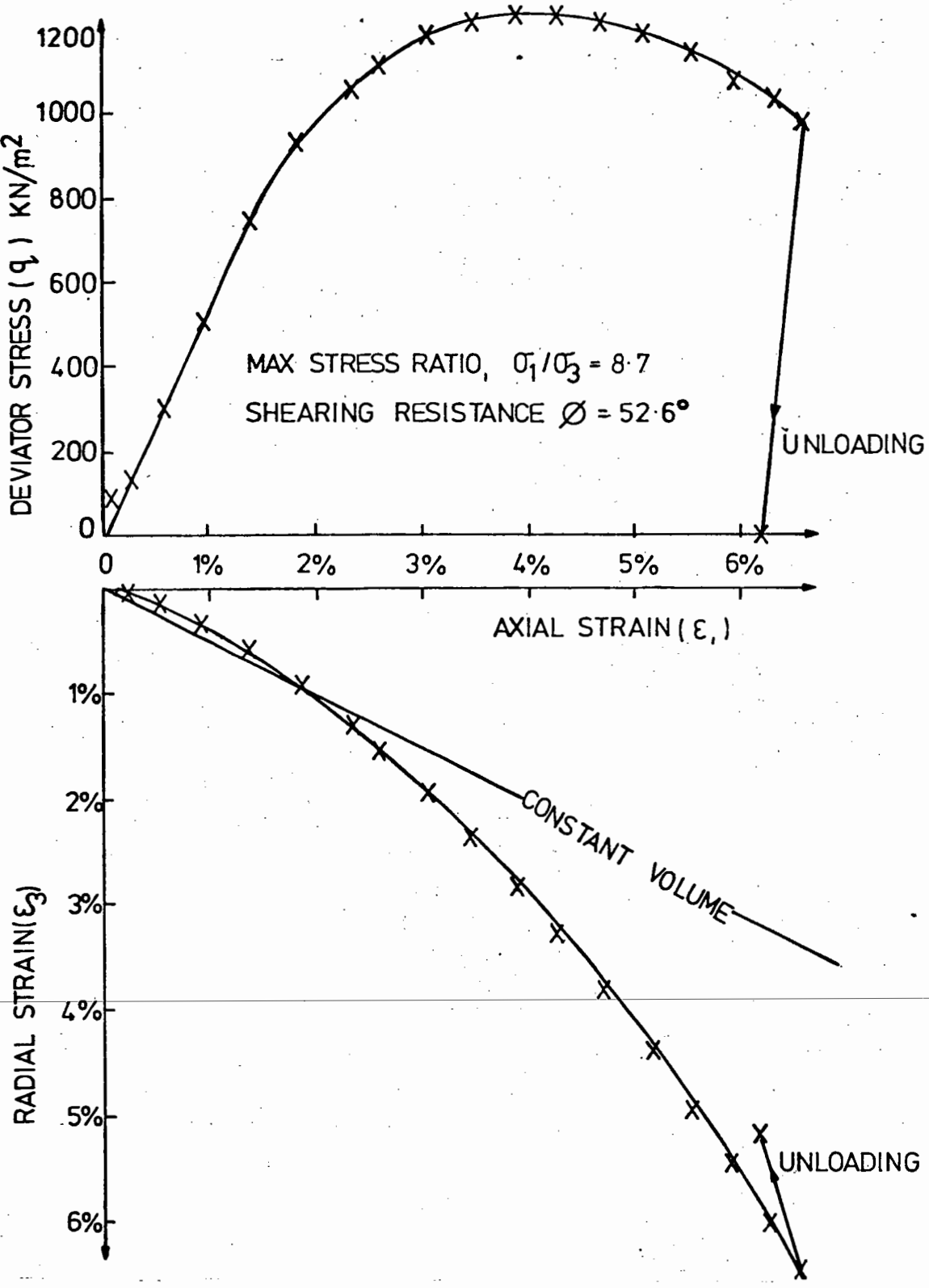

FIG. 7.2 SINGLE LOAD TEST, OS-160A, AT CONSTANT CONFINING STRESS (160 kN/m²)

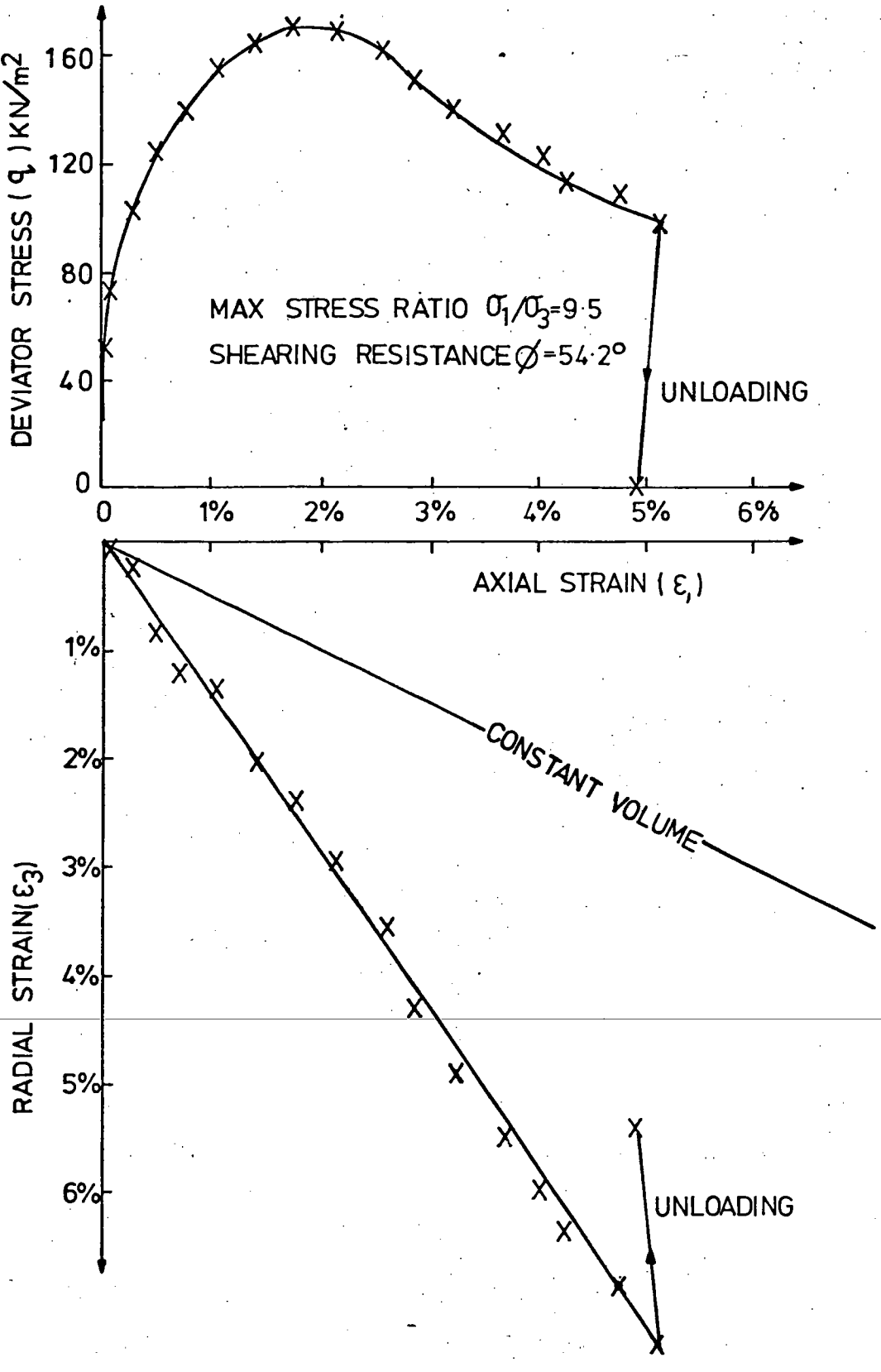

FIG. 7.3 SINGLE LOAD TEST, OS-20, AT CONSTANT CONFINING STRESS (20 kN/m^2)

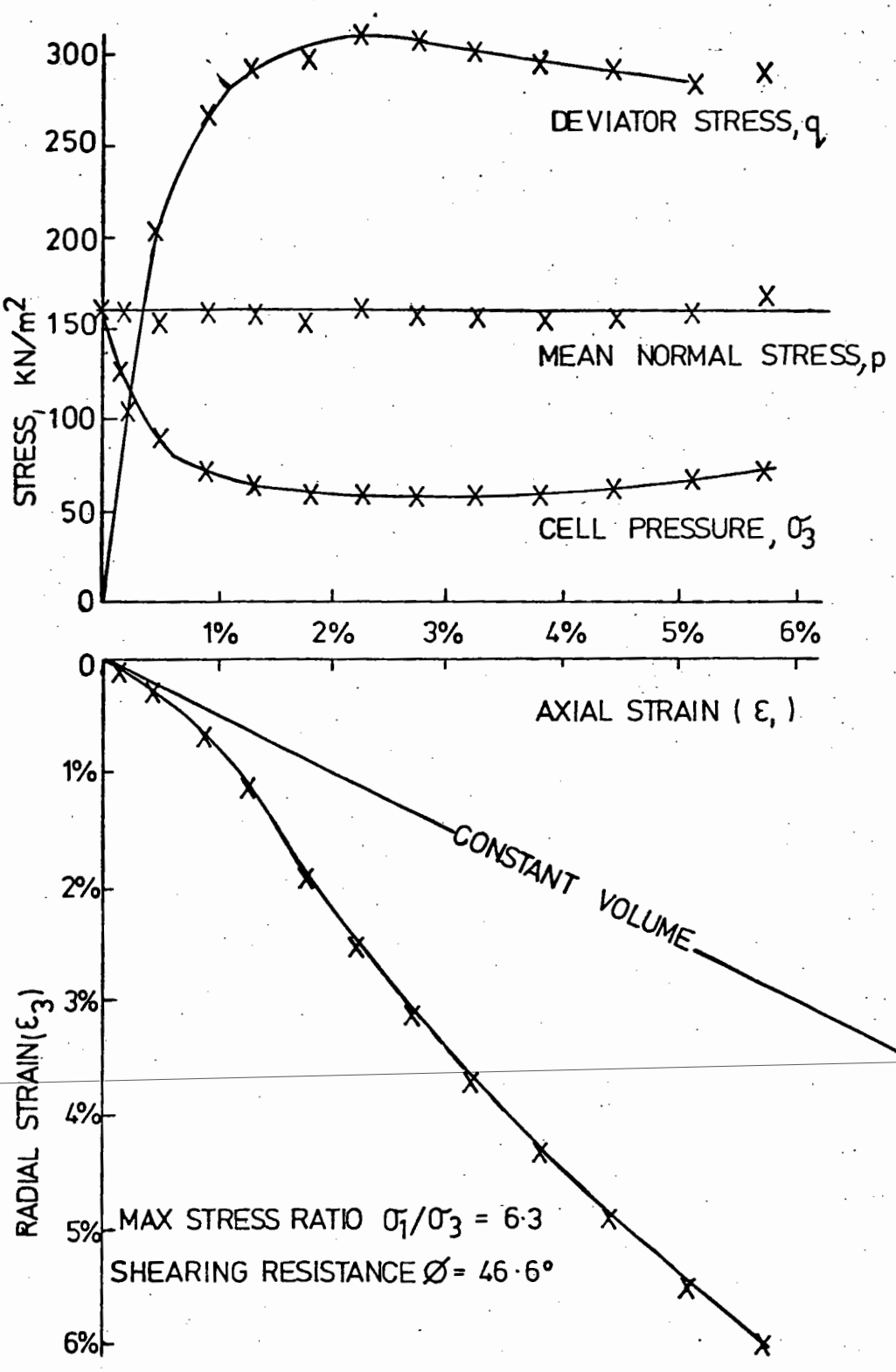

FIG. 7.4 SINGLE LOAD TEST, OT-160, AT CONSTANT NORMAL STRESS (160 kN/m^2)

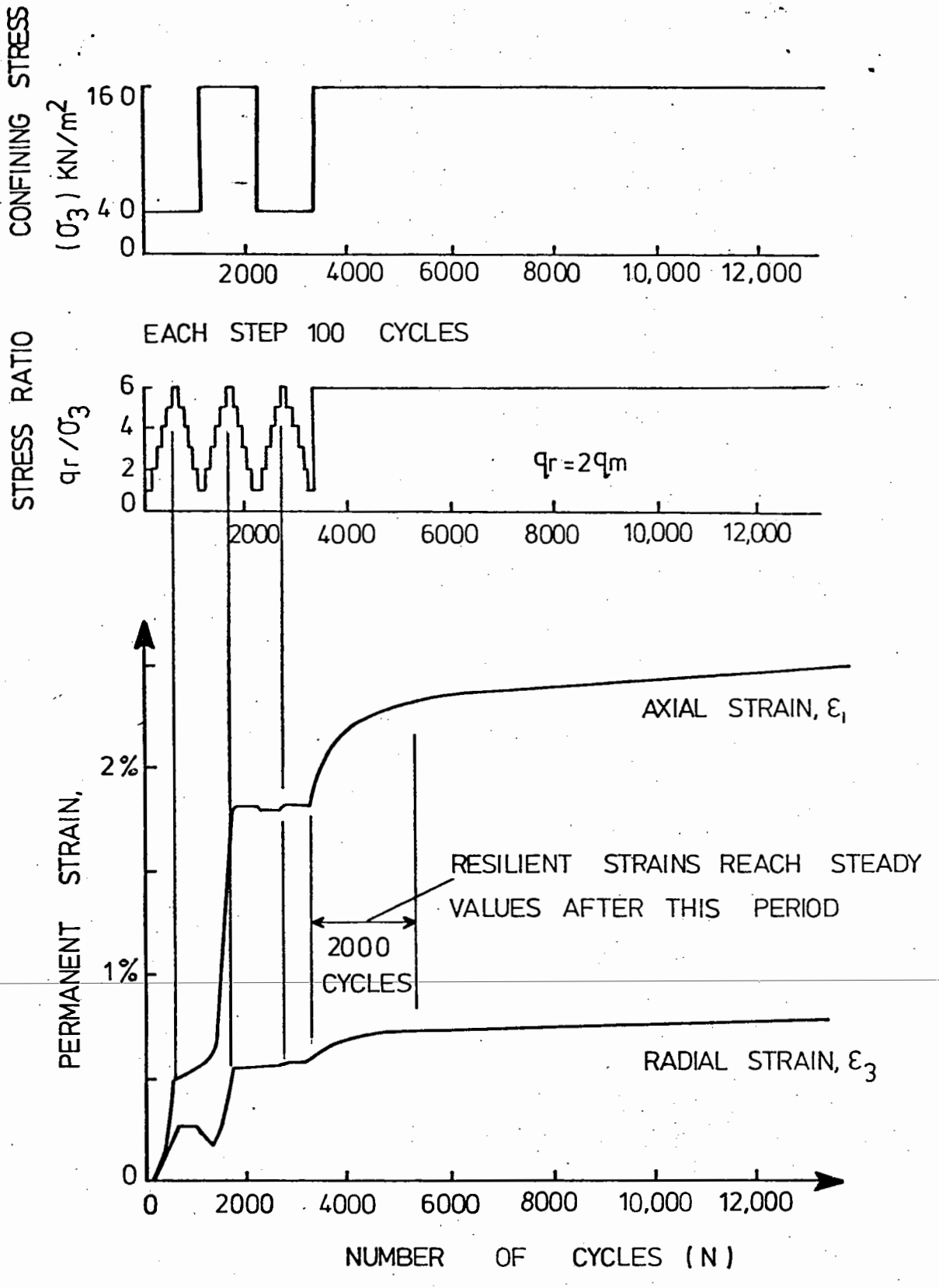

FIG. 7.5 TEST RX, STRESSES APPLIED AND PERMANENT STRAIN

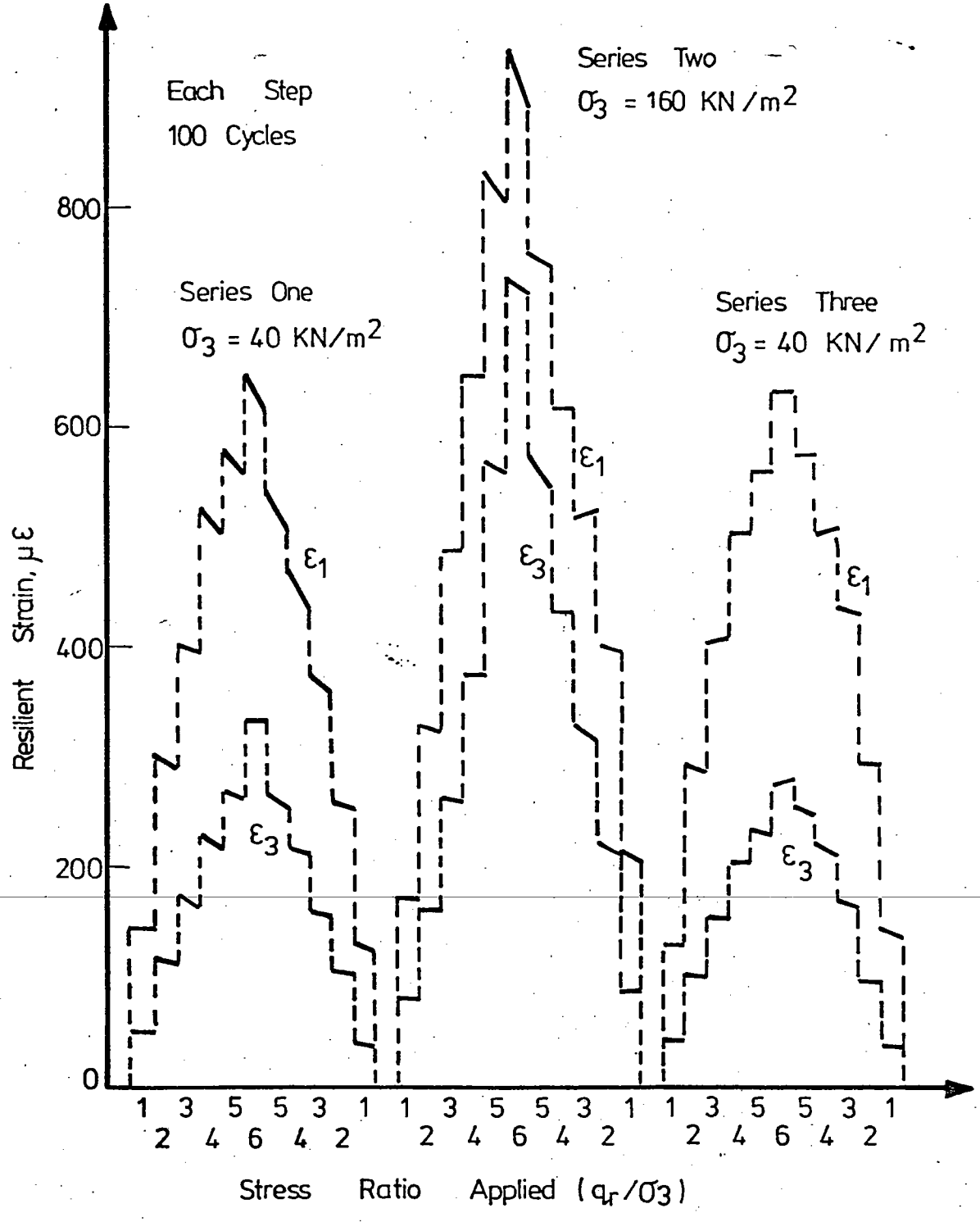

FIG. 7.6 TEST RX, RESILIENT STRAIN IN SERIES ONE, TWO AND THREE

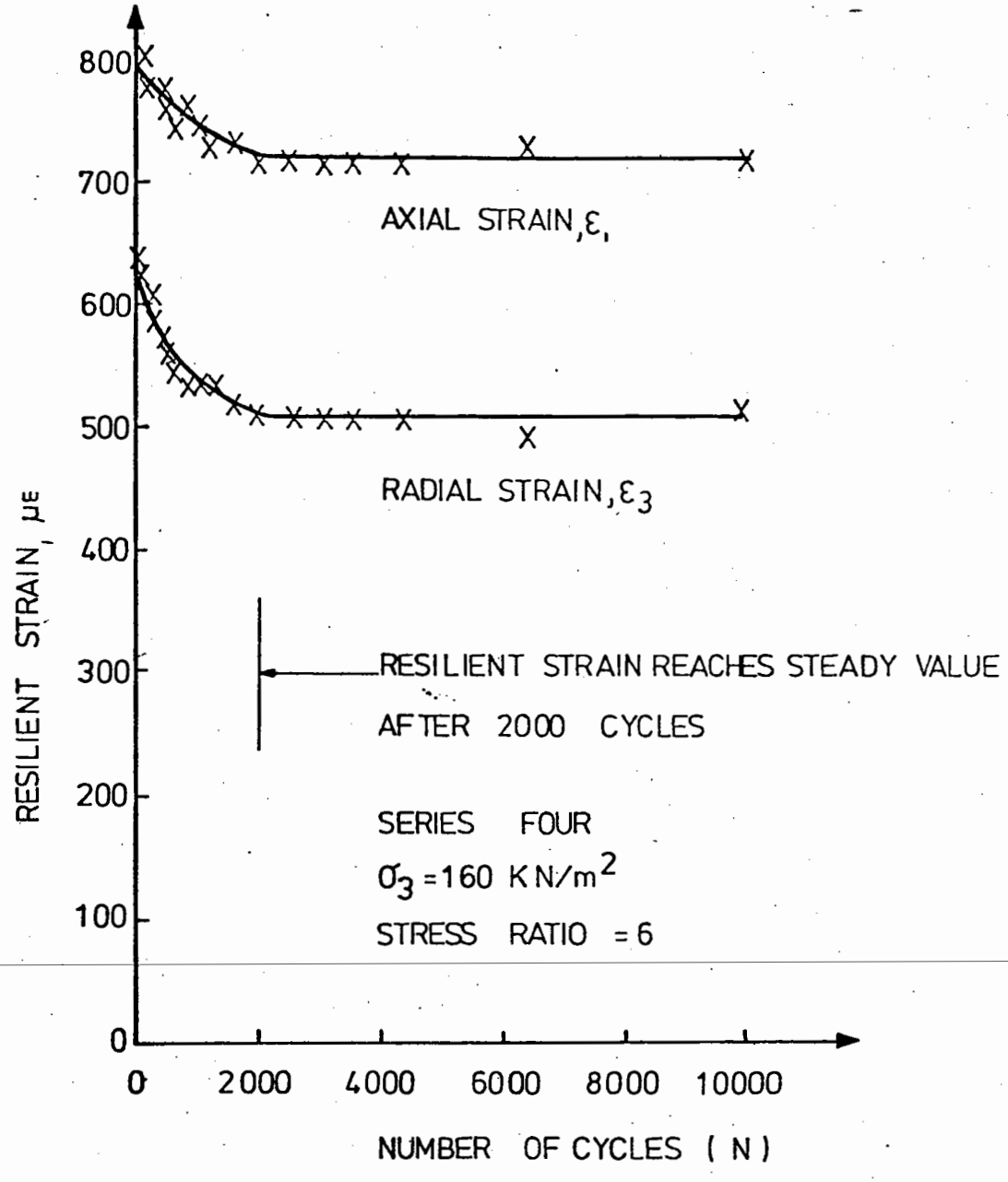

FIG. 7.7 TEXT RX, RESILIENT STRAIN IN SERIES FOUR

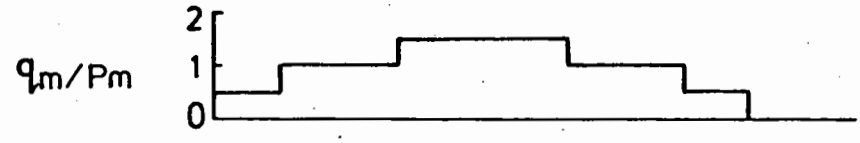

$P_m = 48\ KN/m^2$, $P_r = q_r/3$, ie CONSTANT CONFINING STRESS IN EACH SERIES OF STRESS CYCLES

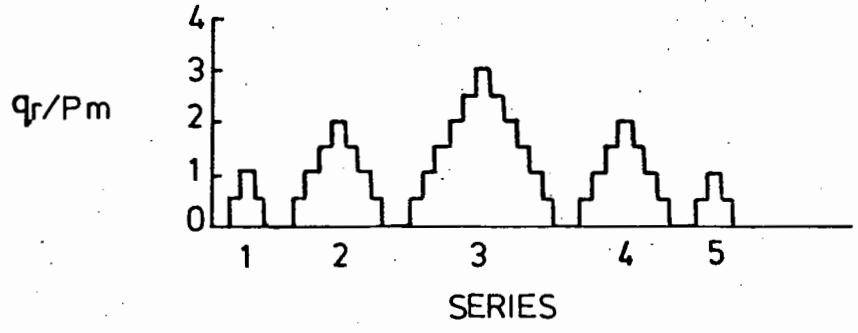

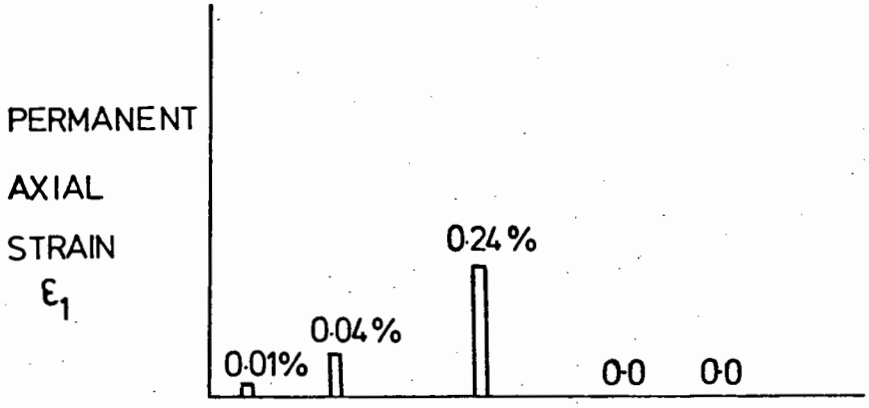

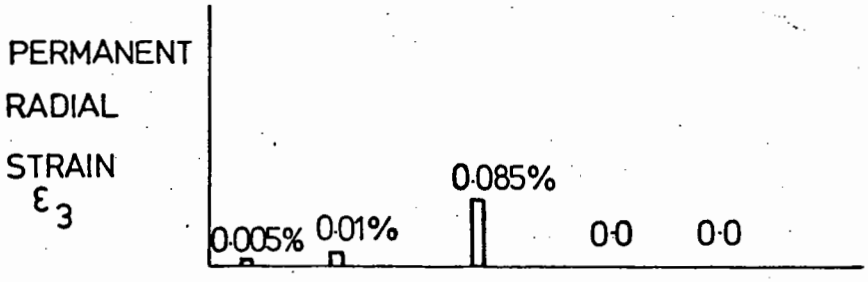

FIG. 7.8 TEST RY, STRESSES APPLIED AND PERMANENT STRAIN

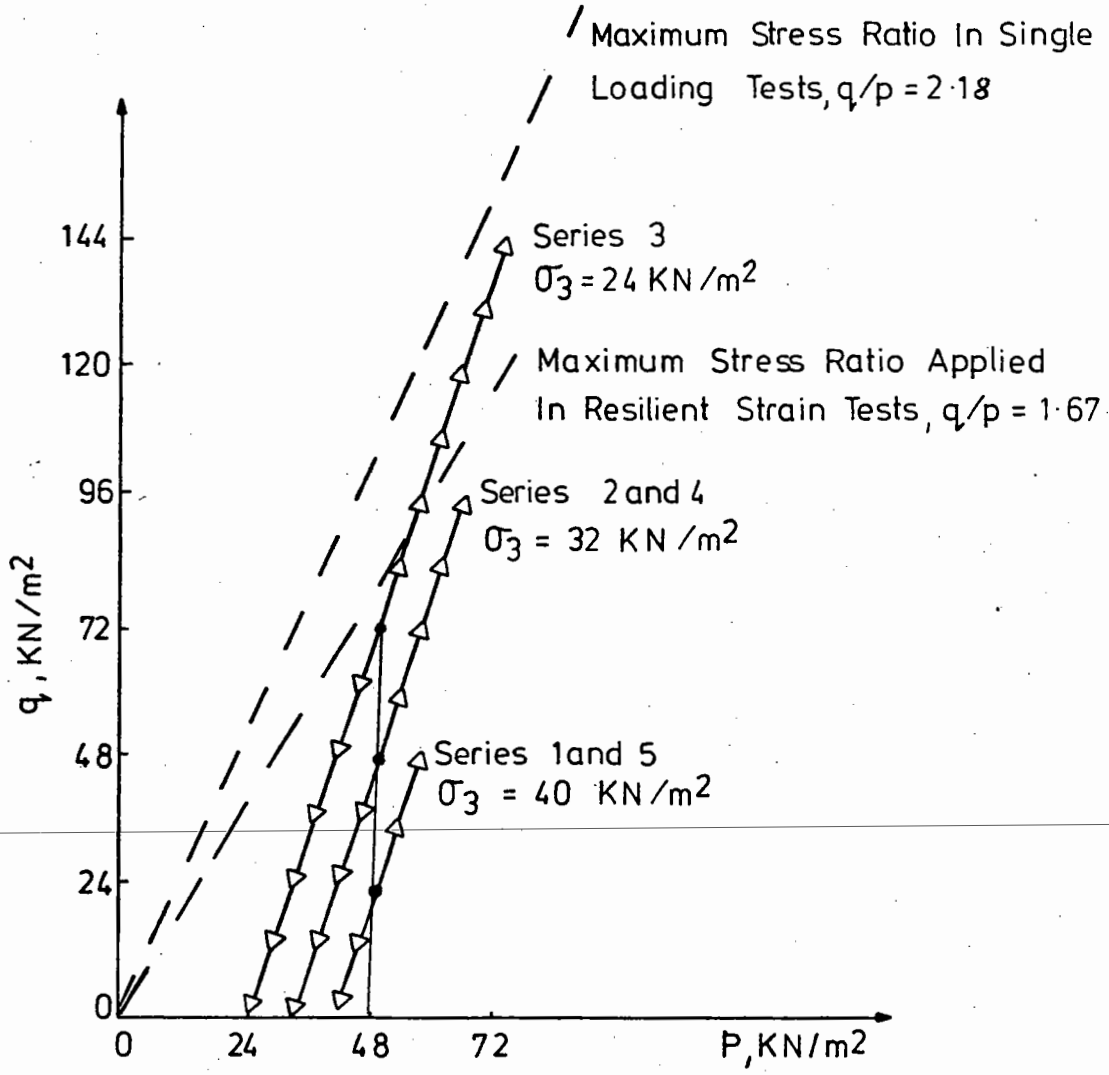

FIG. 7.9 TEST RY, APPLIED STRESS PATHS

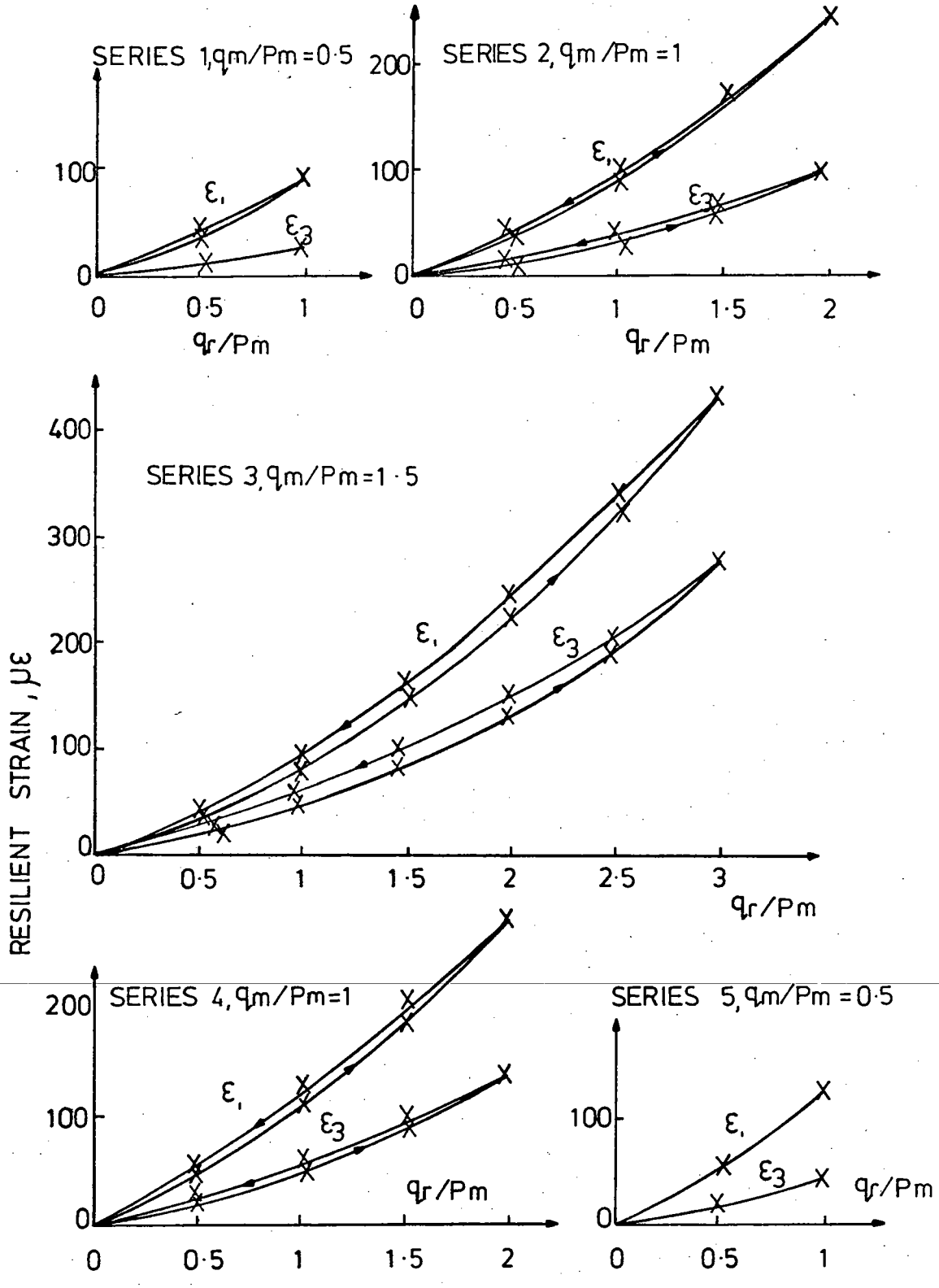

FIG. 7.10 TEST RY, RESILIENT STRAIN

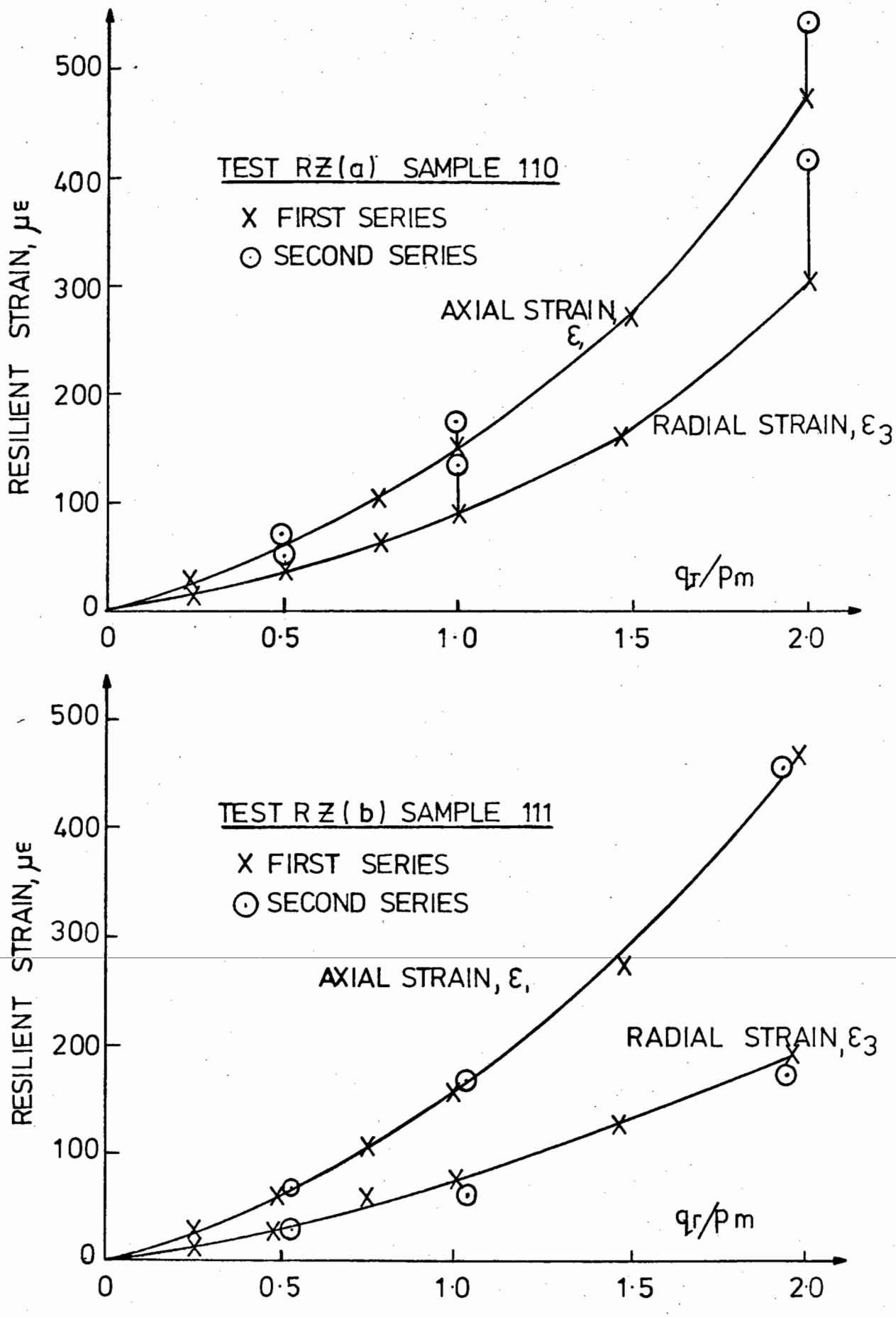

FIG. 7.11 TEST RZ, RESILIENT STRAIN FOR SOME STRESS PATHS WITH CONSTANT CONFINING STRESS (p_m = 192 kN/m^2, S_m = 1.0, S_r = 3)

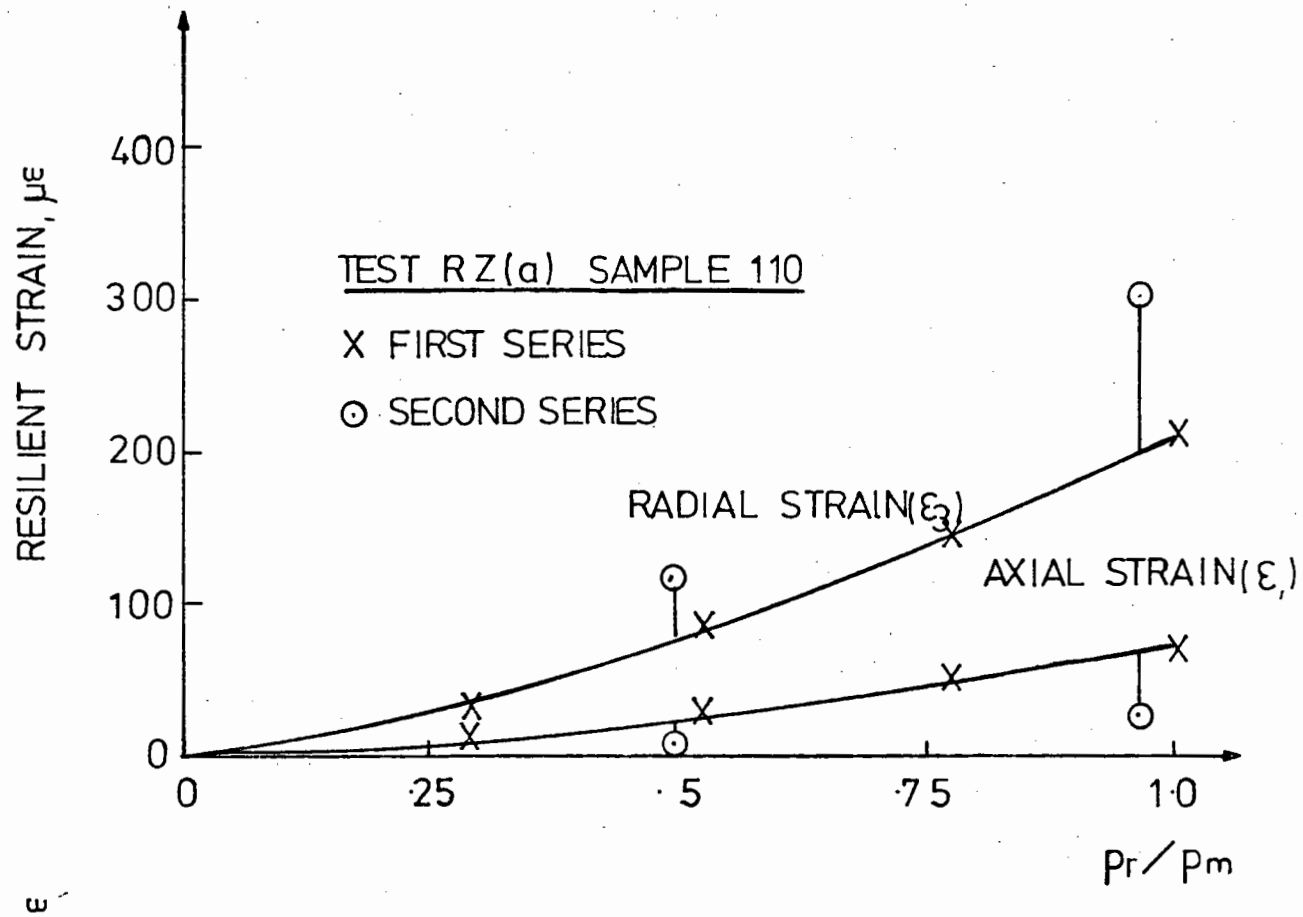

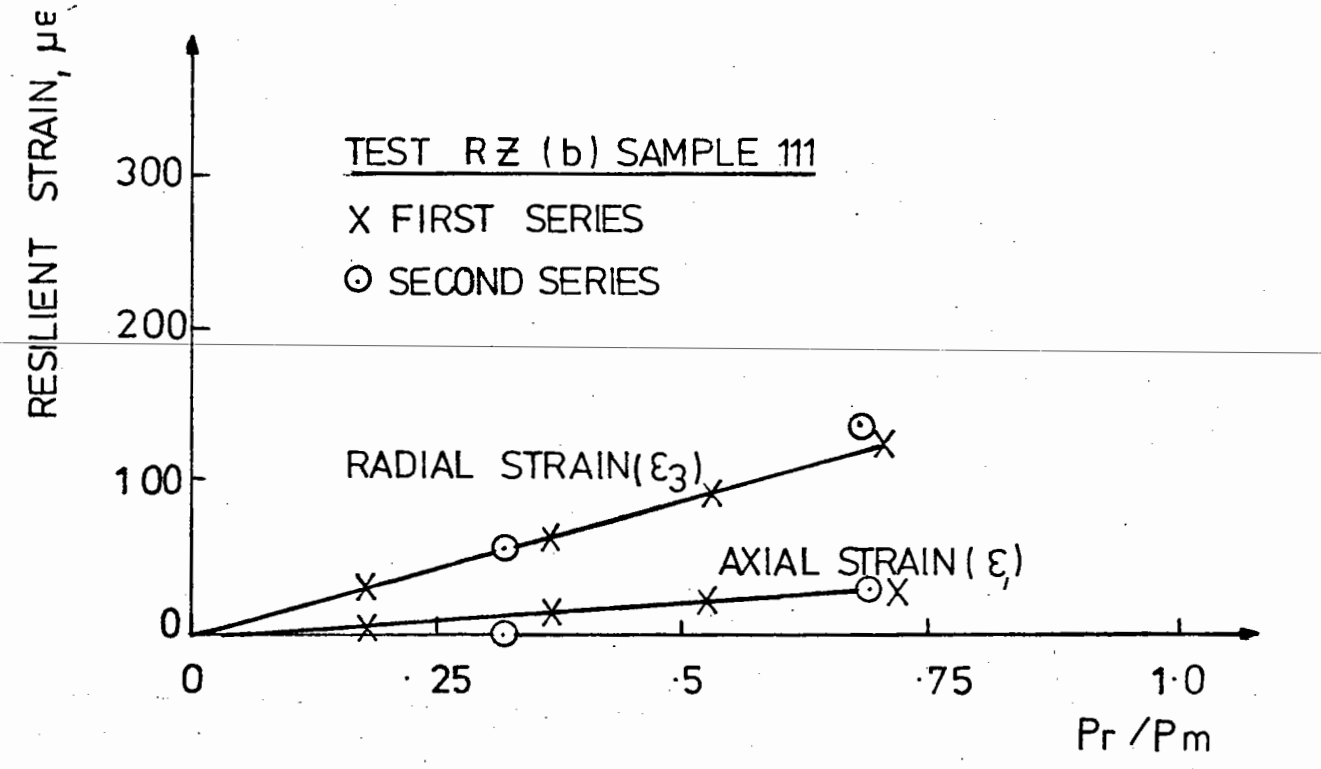

FIG. 7.12 TEST RZ, RESILIENT STRAINS FOR SOME STRESS PATHS WITH CONSTANT DEVIATOR STRESS (p_m = 192 kN/m^2, S_m = 0.5, S_r = 0)

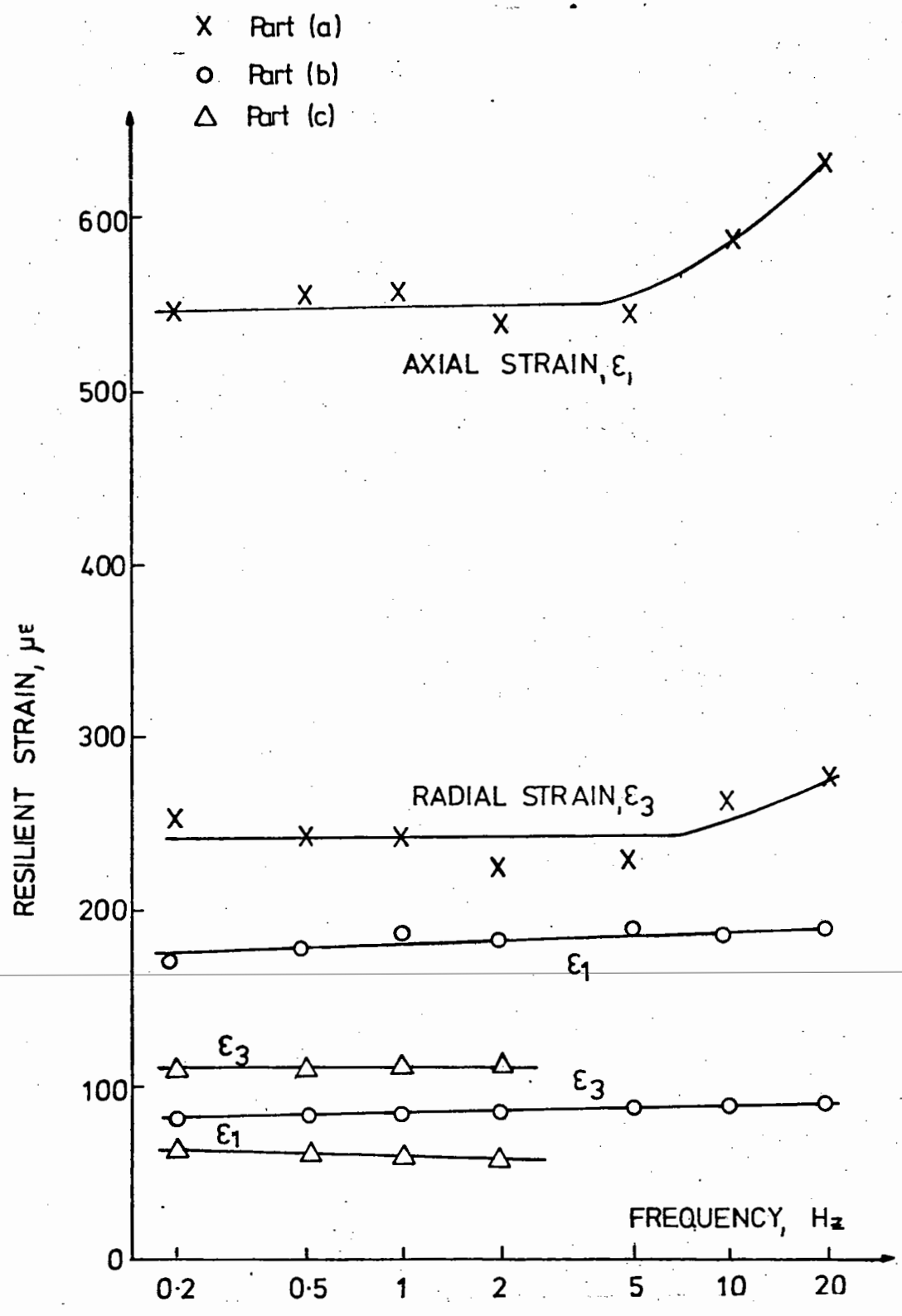

FIG. 7.13 EFFECT OF FREQUENCY ON RESILIENT STRAIN

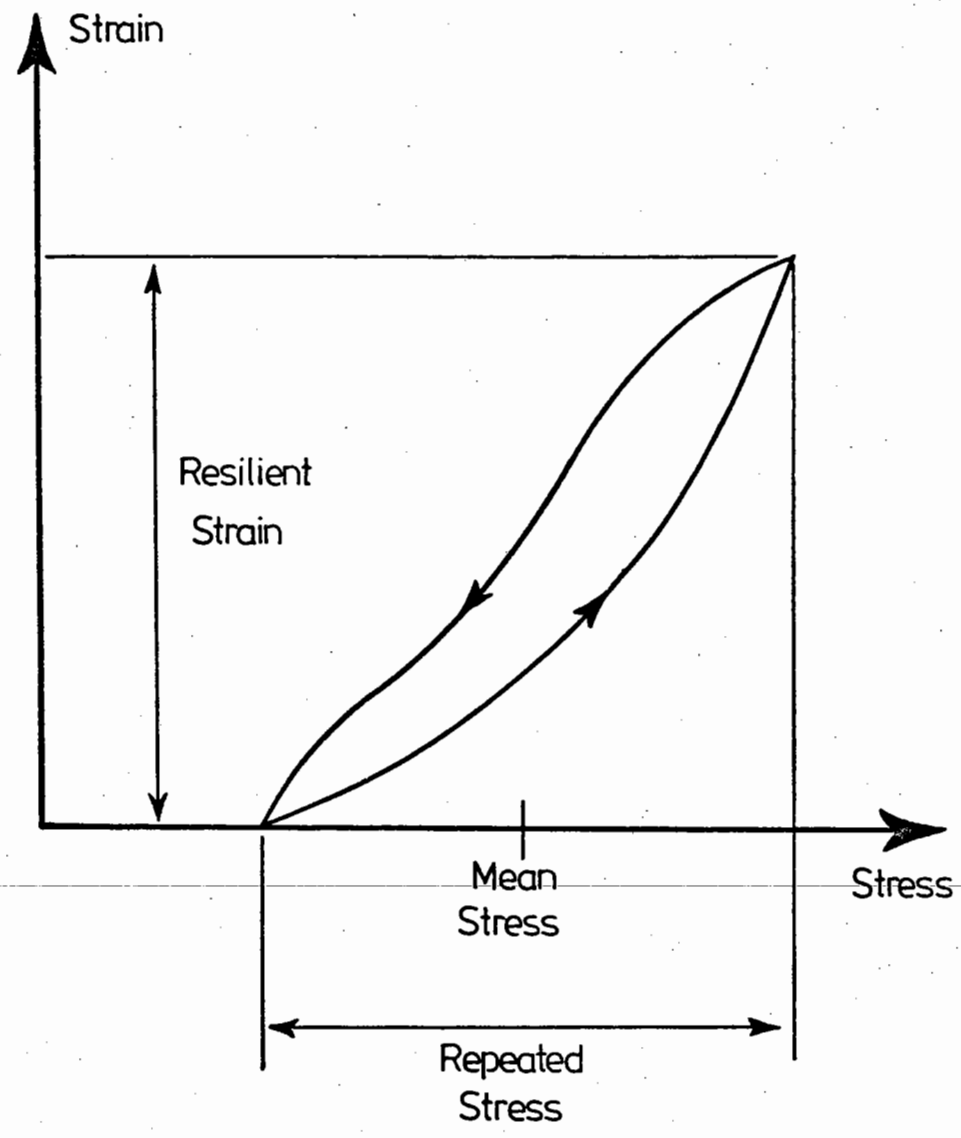

FIG. 7.14 TYPICAL HYSTERYSIS LOOP

CHAPTER EIGHT

RESILIENT STRAIN TESTS

In this chapter, the resilient strain tests are described and a model is developed from the results which predicts the resilient strain behaviour of the material. The results are also compared with previous work, and the significance of the resilient strain model is discussed.

8.1 RESILIENT STRAIN TEST PROGRAMME

Nine resilient strain tests were carried out in the repeated load triaxial apparatus. Each one involved the application of a wide range of different stress paths to a single sample. The parameters which define these stress paths are defined in Section 4.4.1. Four cycles were applied to take a reading of resilient strain on each stress path, and the reasons for this are explained in Section 7.2.4. As an example, Fig. 8.1 shows two stress paths applied in those tests involving constant confining stress. In this case, the repeated stress ratio (S_r) or the slope of the line in p, q space is 3. Under variable confining stress, the slope would be less than 3 if the confining stress was cycled in phase with the axial load.

In these resilient strain tests, stress paths of different amplitudes were applied in several stress directions in p, q space. Fig. 8.2 shows the stress paths applied at one particular value of mean stress. Similar sets of stress paths were applied with other values of mean stress which included several different values of mean normal stress (p_m), and mean deviator stress (q_m).

The value of the parameters which define each of the stress paths applied during these tests are set out in Table 8.1 in terms of the

Table 8.1

Resilient Strain Tests

Stress Parameter	Main Test Program (Six Samples)	Tests with Negative Deviator Stress (Three Samples)
Mean Normal Stress p_m (kN/m^2)	(12), (24), 48, (96), 192, (384)	48, 192
Mean Stress Ratio S_m (q_m/p_m)	(0), (0.25), 0.5, (0.75), 1.0 (1.25), (1.5)	-0.75, -0.5, -0.25, 0 0.25, 0.5, 0.75, 1.0, 1.25
Repeated Stress Ratio S_r (q_r/p_r)	0, (1.0), (1.5), 3.0, ∞, (-1.0)	0, 3.0, ∞
Repeated Stress Amplitude q_r/p_m ($q_r \neq 0$)	(0.25), 0.5, (0.75), 1.0, (1.5), $q_r = 2q_m$	0.5, 1.0, 1.5, 2.0
p_r/p_m ($q_r = 0$)	(0.17), 0.33, (0.5), 0.67	0.33, 0.67

Consider, as an example, a particular stress path from the main test program.

Mean normal stress, $p_m = 192$ kN/m^2

Mean stress ratio, $S_m = 0.5$

Therefore, since $S_m = q_m/p_m$, $q_m = 96$ kN/m^2

Repeated stress ratio, $S_r = 1.5$, and

Repeated stress amplitude, $q_r/p_m = 1.0$

Therefore since $S_r = q_r/p_r$ $p_r = 128$ kN/m^2

and $q_r = 192$ kN/m^2

Therefore the stresses applied are:

Normal stress, p, 128 - 256 kN/m^2

Deviator stress, q, 0 - 192 kN/m^2

Applying these stresses in a triaxial test where $p = \sigma_1/3 + 2\sigma_3/3$ and $q = \sigma_1 - \sigma_3$ indicates:

Deviator stress ($\sigma_1 - \sigma_3$), 0 - 192 kN/m^2

Cell pressure, σ_3, 64 - 128 kN/m^2

stress invariants. In the case of the three tests involving negative deviator stress, each sample was subjected to four cycles of stress at every combination of the values shown. When the main test programme of six samples was carried out, the equipment did not have the facility to apply negative deviator stress. For these tests, the number of stress parameters was too large to take a reading at every possible combination, and so the number of readings was reduced by excluding those combinations which involved a secondary value (in parentheses in Table 8.1) of more than one parameter. An example is given underneath Table 8.1 of how the stresses actually applied to the sample are calculated from the given stress parameters.

As an additional measure to avoid the development of permanent strain, stress paths which involved a stress ratio (q/p) of greater than 1.67 or less than -1 were excluded (see Fig. 8.2). Bearing this in mind, the main test programme involved about 200 different stress paths applied to each sample. All six samples were subjected to the same stress paths, but not all in the same order. The order in which these stress paths were applied is given in Table 8.2. For the short series of readings, stress paths which involved a secondary value of any of the parameters in Table 8.1 were excluded. The order in which readings were taken did not have any significant effect on the results.

8.2 RESULTS OF RESILIENT STRAIN TESTS

The results presented in this section were evaluated from readings repeated on several samples and the strains presented are average values. A full table of results is presented in Appendix D. In order to simplify the presentation initially, selected sets of readings will be considered; those in which the mean normal stress was 192 kN/m^2 and

Table 8.2

Order of Applying Stresses in Resilient Strain Tests

Tests R-1, R-2 and R-3

Mean Normal Stress p_m (kN/m^2)	Series of stress paths applied
12	Short (15 readings)
24	Short
48	Full (59 readings)
48	Short*
96	Short
192	Full
192	Short*
384	Short
48	Short

Tests R-4, R-5 and R-6

Mean Normal Stress p_m (kN/m^2)	Series of stress paths applied
384	Short
192	Full
192	Short*
96	Short
48	Full
48	Short*
24	Short
12	Short
192	Short

Note Readings were taken from individual strain transducers for those series of stress paths marked *.

the mean stress ratio (S_m) was -0.5, 0, +0.5 and +1.0. Some of the stress paths applied for these readings are shown in Fig. 8.3.

Resilient strain in a triaxial test has two components, resilient volumetric strain, v_r, and resilient shear strain, ϵ_r, defined as:

$$v_r = \epsilon_{1r} + 2\epsilon_{3r} \tag{8.1}$$

$$\epsilon_r = \tfrac{2}{3}(\epsilon_{1r} - \epsilon_{3r}) \tag{8.2}$$

where ϵ_{1r} and ϵ_{3r} are the resilient values of the axial and radial strain measured on the sample. Compressive strains are taken as positive.

For any cyclic stress path applied to the material, there will be a corresponding cyclic or resilient strain path. The important factors defining this strain path are its magnitude and its direction. In repeated load tests with constant cell pressure, these factors are conveniently described by the terms resilient modulus (E_r) and resilient Poisson's ratio (ν_r). However, for tests in which various directions of stress path are applied, it is necessary to consider the direction of resilient strain more carefully before going on to develop a model which will predict its magnitude.

Fig. 8.4 shows the directions of resilient strain for those sets of readings described above. The numbering of the points indicates the repeated stress amplitude; number 1 being as shown in Fig. 8.3, number 2 double that amplitude and so on. Considering first the case where the mean stress ratio is zero ($S_m = 0$), Fig. 8.4(b), the points to note in this case are:

(a) The line marked $S_r = 0$, i.e. cyclic normal stress and constant deviator stress, is along the volumetric strain axis with very low shear strain.

(b) The line marked $S_r = \infty$, i.e. cyclic deviator stress and constant normal stress is along the shear strain axis with very low volumetric strain.

(c) The line marked $S_r = 3$, i.e. constant cell pressure, shows both volumetric strain and shear strain.

Together, these points indicate that in this particular condition, the material is behaving isotropically. However, when other values of S_m are considered, the material is no longer isotropic. In the case where $S_m = -0.5$, Fig. 8.4(a), the two lines, $S_r = 0$ and $S_r = \infty$, converge in the first quadrant, and in the cases of positive mean stress ratios ($S_m = 0.5$ and 1.0, Figs. 8.4(c) and (d)), they diverge. In these last two cases, readings were taken for other stress directions, and the corresponding strain directions are spread out at intermediate positions.

Closer examination shows that there is one stress direction ($S_r = 1.5$) which gives the same strain direction in each case ($\epsilon_r/v_r = 1.0$). As the mean stress ratio (S_m) is reduced from +1.0 to -0.5, the lines for other stress directions tend to converge towards this strain direction. Conversely, as the mean stress ratio is increased they diverge and seem to be converging on a strain direction, ϵ_r/v_r, of about -0.5.

This relationship between the applied direction of repeated stress and the resulting direction of resilient strain is shown more clearly in Fig. 8.5. Each line represents one value of mean stress ratio (S_m). It can be seen that there are two particular directions of applied stress for which the resulting strain direction is independent of the mean stress level. In the following section these stress and strain directions are used to develop a model of the material behaviour.

8.3 MODEL OF RESILIENT STRAIN BEHAVIOUR

The mathematical model presented below was developed so that all the resilient strain data (over 200 readings on each sample) could be condensed into a single expression enabling resilient strain to be calculated for any applied stress path. The physical significance of the model is not considered here but, clearly, the change in stiffness of granular materials under different stress conditions is associated with the interlock between the aggregate particles and the stress and strain directions found above originate in the packing arrangement of the particles. These directions refer to the representation of stress (and strain) in principal stress space or the p-q plane and not to the physical orientation of the stress.

The stress state of a sample in the triaxial test has two components. The most commonly used components are the principal stresses, σ_1 and σ_3, or stress invariants such as p and q. This model for the resilient strain behaviour of the material is expressed in terms of stress components in the particular directions found in Fig. 8.5, that is, q/p = 1.5 (direction A) and q/p = -0.75 (direction B). Components of stress in these directions can then be defined as:

$$t_A = p + \frac{4}{3} q$$

$$t_B = p - \frac{2}{3} q \qquad (8.3)$$

Any stress path in the repeated load triaxial test can be defined by two mean stress components and two repeated stress components. Up to this point, p_m, q_m and p_r, q_r have been used for mean and repeated stress, but the stress path can also be defined by components in the A and B directions. These components, normalised with respect to p_m, are, for mean stress:

$$(T_m)_A = (p_m + \frac{4}{3} q_m)/p_m = 1 + \frac{4}{3} S_m$$
$$(T_m)_B = (p_m - \frac{2}{3} q_m)/p_m = 1 - \frac{2}{3} S_m \qquad (8.4)$$

and for repeated stress:

$$(T_r)_A = (p_r + \frac{4}{3} q_r)/p_m$$
$$(T_r)_B = (p_r - \frac{2}{3} q_r)/p_m \qquad (8.5)$$

Resilient strain can also be expressed by two components in the corresponding strain directions in Fig. 8.5 $\epsilon_r/v_r = 1.0$ and $\epsilon_r/v_r = -0.5$.

$$(W_r)_A = v_r + 2\epsilon_r$$
$$(W_r)_B = v_r - \epsilon_r \qquad (8.6)$$

It was shown above that a repeated stress in the direction $(T_r)_A$ or $(T_r)_B$ gave rise to a resilient strain in the direction $(W_r)_A$ and $(W_r)_B$ respectively at all values of mean stress.

In Fig. 8.6 the data shown in Fig. 8.4 is replotted to show the resilient strain components, W_r, as a function of the resilient stress components, T_r. It is apparent that for each value of mean stress ratio $(W_r)_A$ is a unique function of $(T_r)_A$, and $(W_r)_B$ a unique function of $(T_r)_B$. In the case of $S_m = 0$, the same relationship applies for both directions. As the stress ratio is increased, the material becomes stiffer in the A direction and less stiff in the B direction.

Closer examination shows that these relationships form a single family of curves related to the W_r axis. In Fig. 8.7, the family of curves is reduced to a single line by use of the stress function, $2T_r/(T_m + 1)$. The resilient behaviour of the material in those

readings for which p_m was 192 kN/m^2 can, therefore, be represented by an equation of the form:

$$W_r = f[2T_r/(T_m + 1)] * \quad (8.7)$$

The broken lines on Figs. 8.6 and 8.7 are in fact defined by the equation:

$$W_r = 300 \sinh[2T_r/(T_m + 1)] * \quad (8.8)$$

An alternative form of this equation would be:

$$W_r = 300\left[X + \frac{X^3}{6}\right] \quad (8.9)$$

where $X = 2T_r/(T_m + 1)$. These two forms differ by only about 3% within the range of the experimental data. The equation applies equally to the relationship of resilient strain in the A direction ($\epsilon_r/v_r = 1.0$) to stress in the A direction ($q/p = 1.5$) as to the relationship in the B directions ($\epsilon_r/v_r = -0.5$ and $q/p = -0.75$).

The detailed discussion and development of the model has so far considered results for $p_m = 192$ kN/m^2. However, a similar pattern was obtained at other values of p_m and full details are given in Appendix D. Fig. 8.8 shows the relationship between W_r and $2T_r/(T_m + 1)$ for readings in which p_m was 48 kN/m^2. The model prediction line in this case has the equation:

$$W_r = 190 \sinh[2T_r/(T_m + 1)] * \quad (8.10)$$

The behaviour of the material over the full range of mean normal stress is shown in Fig. 8.9. It is observed that at higher values of p_m, the relationship between the resilient strain parameter (W_r) and the mean normal stress (p_m) approaches a straight line on this log-log

---

* It may be significant that $(T_m)_A + 1 = 2\sigma_{1m}/p_m$ and $(T_m)_B + 1 = 2\sigma_{3m}/p_m$.

representation. The points in Fig. 8.9 are taken from the "best-fit" lines through the experimental points in Fig. 8.6 and from similar lines for other values of p_m (see Appendix D). An overall resilient stress-strain relationship for the material can therefore be expressed in the form:

$$W_r = (p_m/K)^n \sinh[2T_r/(T_m + 1)] \qquad (8.11)$$

where $K = 6.8 \times 10^{-6}$ kN/m^2, $n = 0.33$, and W_r has units of microstrain.

8.4 DISCUSSION OF RESILIENT STRAIN BEHAVIOUR

The model of material behaviour represented by Eqn. 8.11 was found to be the simplest way of reducing the undoubtedly complex behaviour of this material to a manageable form. Prior to discussing the model in detail, it is useful to compare the findings of this work with those of previous investigators.

8.4.1 Comparison with Previous Work

Several other workers have noted that frequency of loading and the number of load applications have little effect on the resilient behaviour of granular materials (Hicks, 1970; Morgan, 1966; and Brown, 1974). This was confirmed by the preliminary tests described in Chapter 7.

The most commonly used relationship representing the non-linear behaviour of granular materials (for example, Hicks and Monismith, 1971; and Shackel, 1973) has the form:

$$E_r = k_1(\theta)^{k_2} \qquad (8.12)$$

where E_r = resilient modulus of elasticity

θ = sum of the principal stresses

k_1, k_2 = constants which depend on the material and test conditions.

The resilient strain model developed in the previous section is in agreement with this relationship under certain restricted conditions; viz, when q_m, q_r and p_r are small compared with p_m. However, this represents a situation where the material is well away from failure, a qualification noted by other workers for the applicability of Eqn. 8.12. The significance of this restriction is discussed in more detail in Section 10.2.4.

Under these conditions, T_m is approximately equal to 1 and T_r is small. Eqn. 8.11 then becomes:

$$W_r \triangleq (p_m/K)^n . T_r \qquad (8.13)$$

If this equation is expanded in terms of the resilient strains, ϵ_{1r} and ϵ_{3r}, and the repeated stresses, σ_{1r} and σ_{3r}:

$$\epsilon_{1r} = \frac{\frac{7}{9}\sigma_{1r} - \frac{4}{9}\sigma_{3r}}{K^n (p_m)^{1-n}} \qquad (8.14)$$

$$\epsilon_{3r} = \frac{\frac{5}{9}\sigma_{3r} - \frac{2}{9}\sigma_{1r}}{K^n (p_m)^{1-n}} \qquad (8.14)$$

This shows that under these restricted conditions:

$$E_r = 1.29 \times 10^6 K^n . p_m^{1-n} \quad \text{and} \quad \nu_r = \frac{2}{7} \triangleq 0.29 \qquad (8.15)$$

Substituting values for K and n, and bearing in mind that p_m is equivalent to $\theta/3$, gives similar constants to those found by previous investigators.

$$E_r = 24{,}000\ p_m^{0.67} \qquad (8.16)$$

Other workers have found that the direction of resilient strain or Poisson's ratio was dependent on the applied stress ratio (Hicks, 1970)

and the type of confining stress - constant or variable - (Allen and Thompson, 1974; and Brown and Hyde, 1975). In this work, the application of a much wider range of stress paths than previously used has enabled a precise form to be put on the relationship (Eqn. 8.11). Brown (1974) defined a relationship between resilient strain and normalised stress parameters which has some similarities to Eqn. 8.11, but that work related to granular material subjected to a limited range of stress conditions.

The most comprehensive previous work on granular materials was that by Hicks (1970), although his tests were all with constant confining stress and the deviator stress was returned to zero after each load cycle. Typical results from one of his resilient strain tests on a dense dry crushed stone (Sample No. C(0)-3D) are reproduced in Fig. 8.10. The strains which are predicted by the resilient strain model developed here for the same stresses are shown in Fig. 8.11. The form of the results is very similar, but the strains measured by Hicks are somewhat larger. This is probably because he used a finer material, maximum particle size 19 mm compared with 38 mm in these tests.

It will be noted that the use of the terms resilient modulus (E_r) and resilient Poisson's ratio (ν_r) has been avoided in the analysis of the results. It is felt that these terms cannot accurately describe the complex non-linear behaviour of a granular material such as that which was tested in this investigation.

8.4.2 Anisotropy

Granular material shows two types of anisotropy in its stress-strain behaviour. The first is inherent in the structure of the material due to the method of sample preparation or to the loading history. The second is caused by the stresses being applied to the material. Eqn. 8.11

incorporates only the latter type of anisotropy indicating that $(W_r)_A$ decreases and $(W_r)_B$ increases with increasing mean stress ratio (S_m). Examination of Fig. 8.9 shows that, particularly at low values of mean normal stress, there is some difference in the behaviour of the material along the A and B directions which is not attributable to the level of mean stress ratio. This inherent anisotropy at low stress levels is probably due to the methods of sample preparation and testing. It is shown later (Section 9.4) that permanent strain increases the degree of inherent anisotropy in the material but does not affect the A and B directions used in development of the resilient strain model.

8.4.3 Variations in Results

The granular material which was tested consisted of relatively large particles in a more or less random arrangement. It is important to appreciate that this causes considerable variations in strain readings on a single sample and also in the strains measured on different samples compacted and tested in exactly the same way.

Each point on Figs. 8.4 and 8.6 represents the average values of measurements taken from several samples (from three to nine). The strains recorded on individual samples varied from this mean by amounts from ±10% to ±50% at different stress conditions. Furthermore, the strains measured on each sample were the mean from a number of transducers at different positions on the sample. The variation between different transducers on a single sample was as large as the variation between samples.

Details of these variations, between one sample and another, and on the same sample are included in Appendix D (Figs. D.1 to D.2 and Figs. D.15 to D.26).

Some of these variations are due to experimental error but the

majority are due to the nature of the material. In these tests, the sample diameter and the gauge lengths over which strain was measured were only 4 times the maximum particle size. The situation would no doubt be improved by scaling down the particle size distribution in the sample or by using much larger samples, but the alternative adopted in this investigation of averaging the results from several samples is the most realistic.

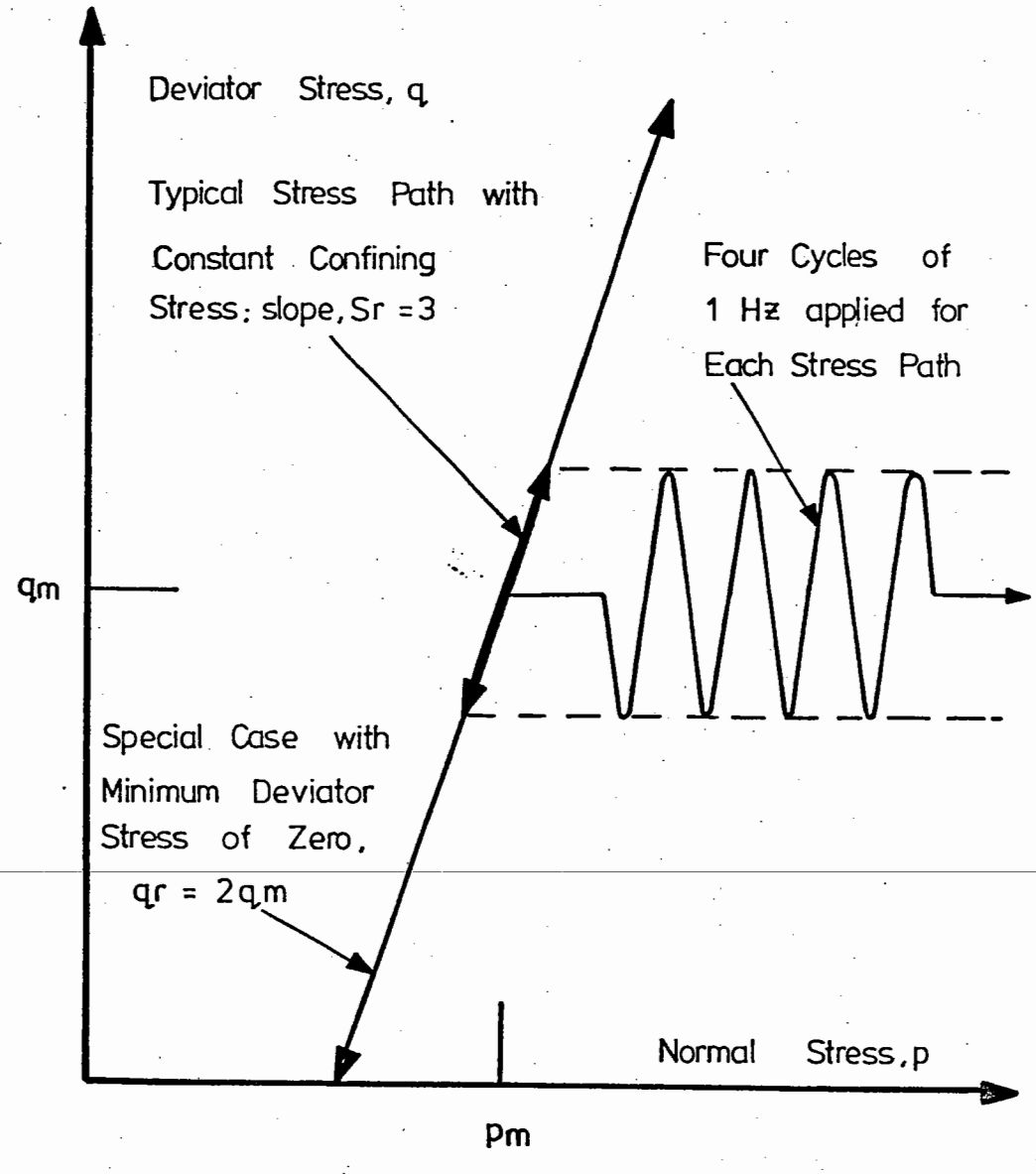

FIG. 8.1 TYPICAL STRESS PATHS WITH CONSTANT CONFINING STRESS

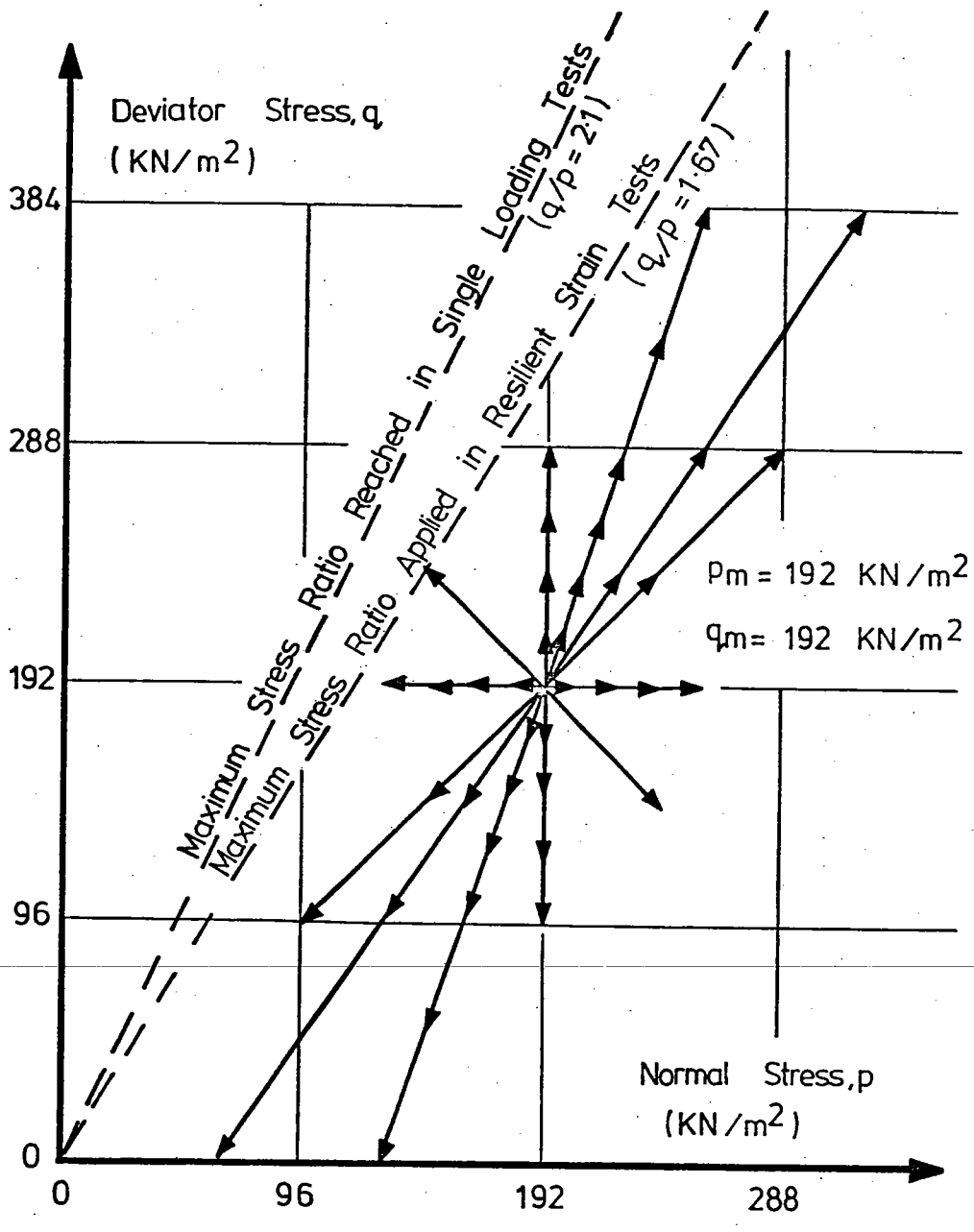

FIG. 8.2 STRESS PATHS APPLIED AT A TYPICAL VALUE OF MEAN STRESS

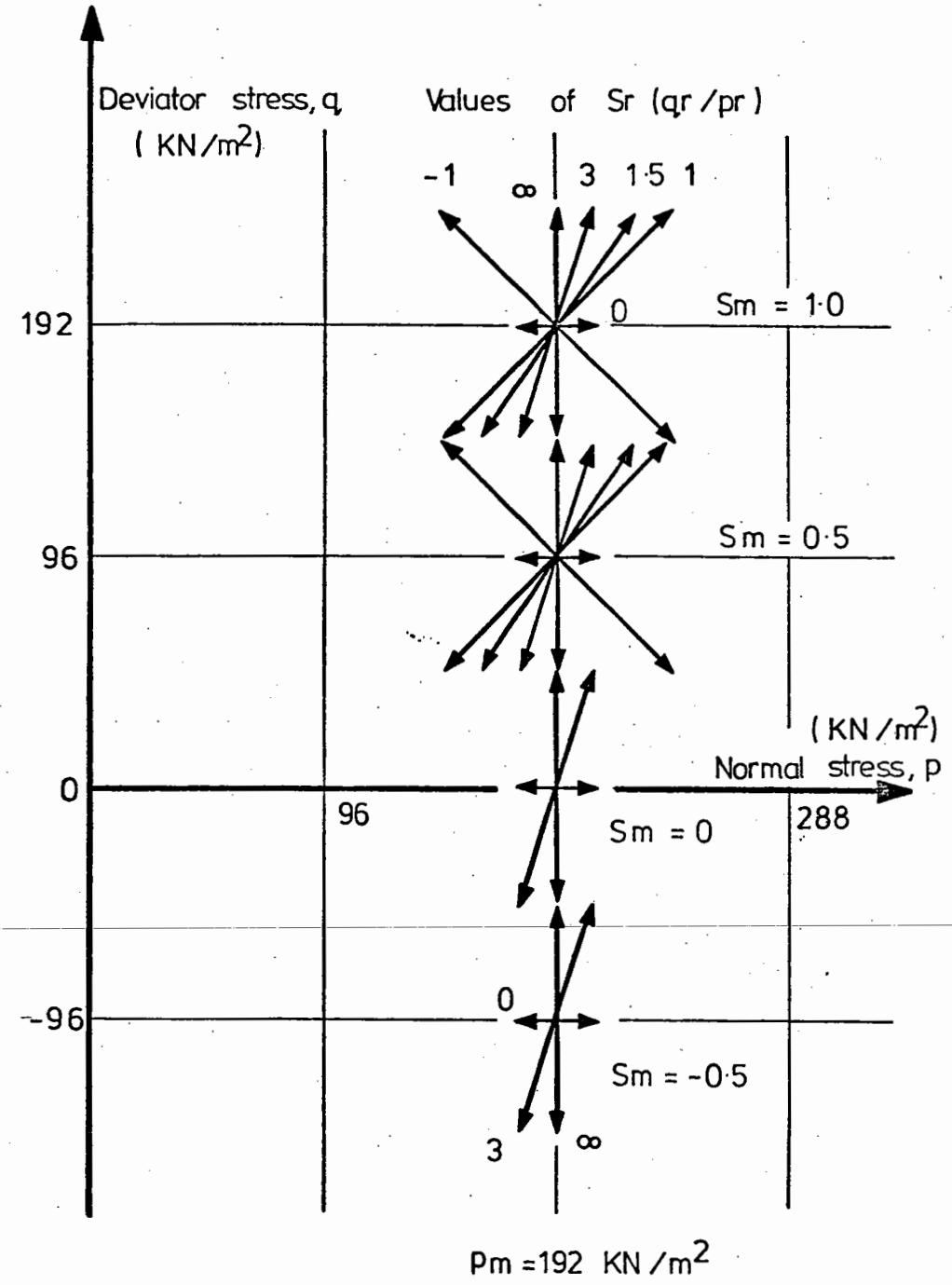

FIG. 8.3 SOME OF THE STRESS PATHS USED IN THE PRESENTATION OF THE RESULTS

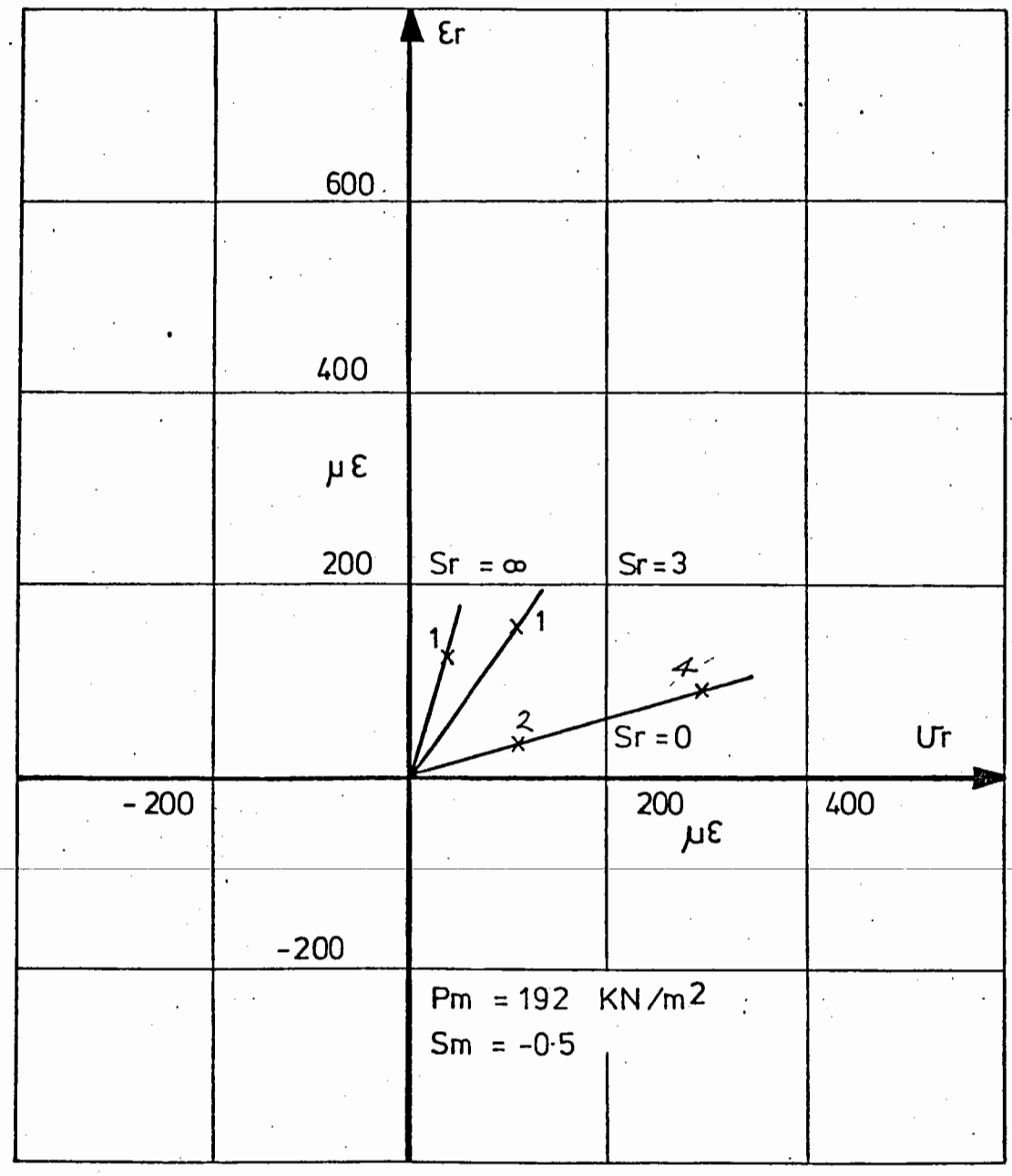

(a) $S_m = -0.5$

FIG. 8.4 RESILIENT STRAIN DIAGRAMS FOR p_m = 192 kN/m²

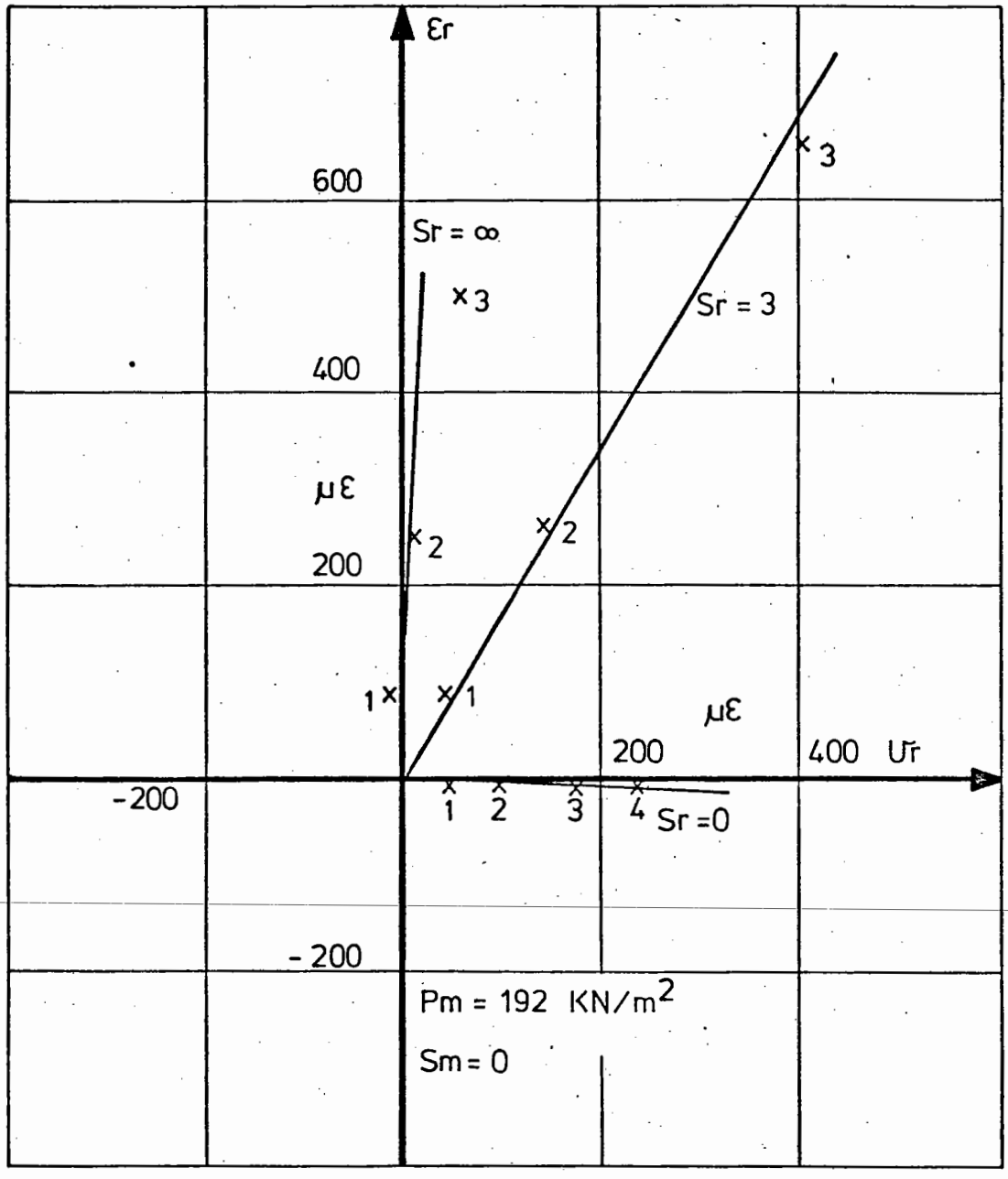

(b) $S_m = 0$

FIG. 8.4 RESILIENT STRAIN DIAGRAMS FOR p_m = 192 kN/m²

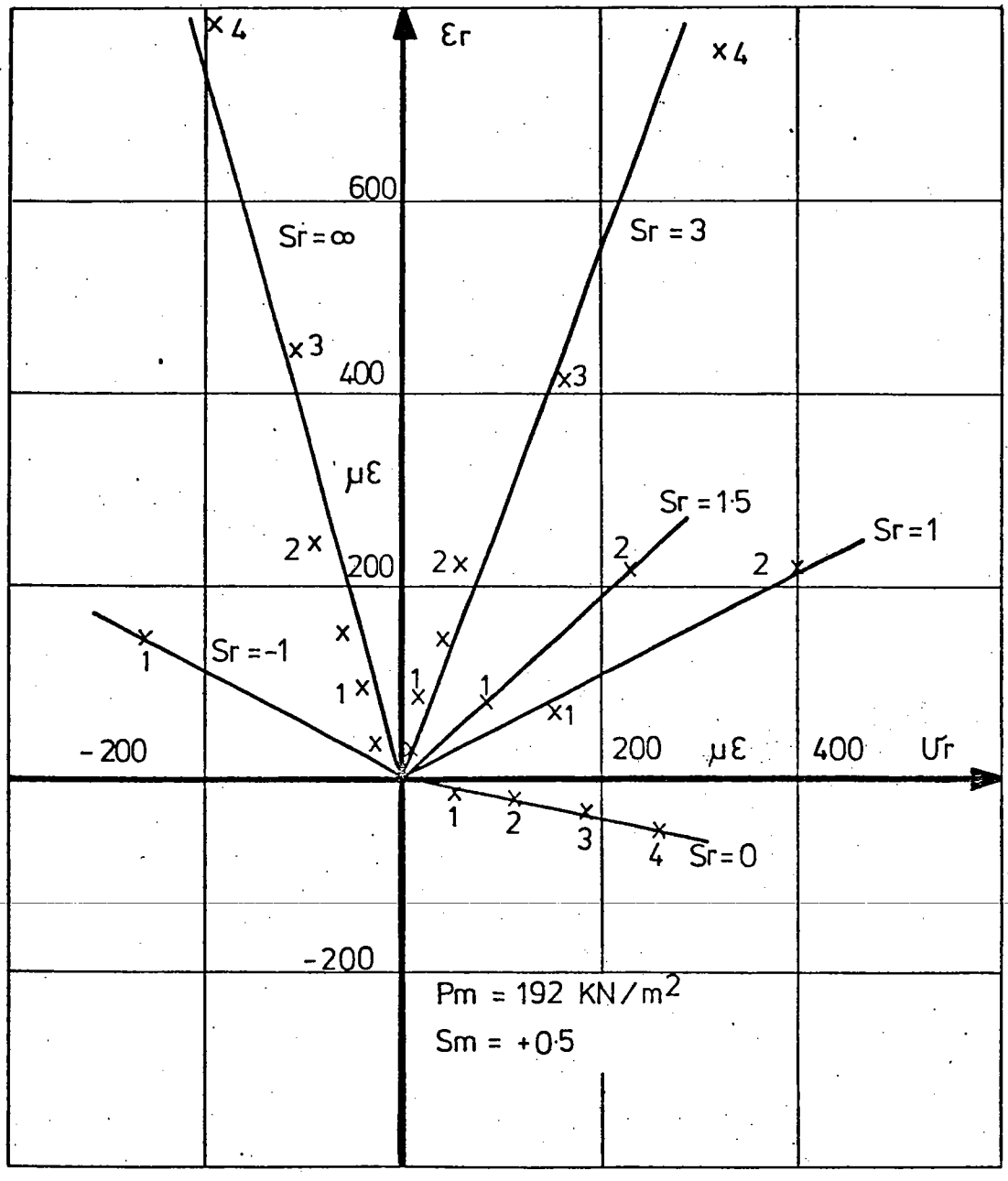

(c) $S_m = +0.5$

FIG. 8.4 RESILIENT STRAIN DIAGRAMS FOR p_m = 192 kN/m²

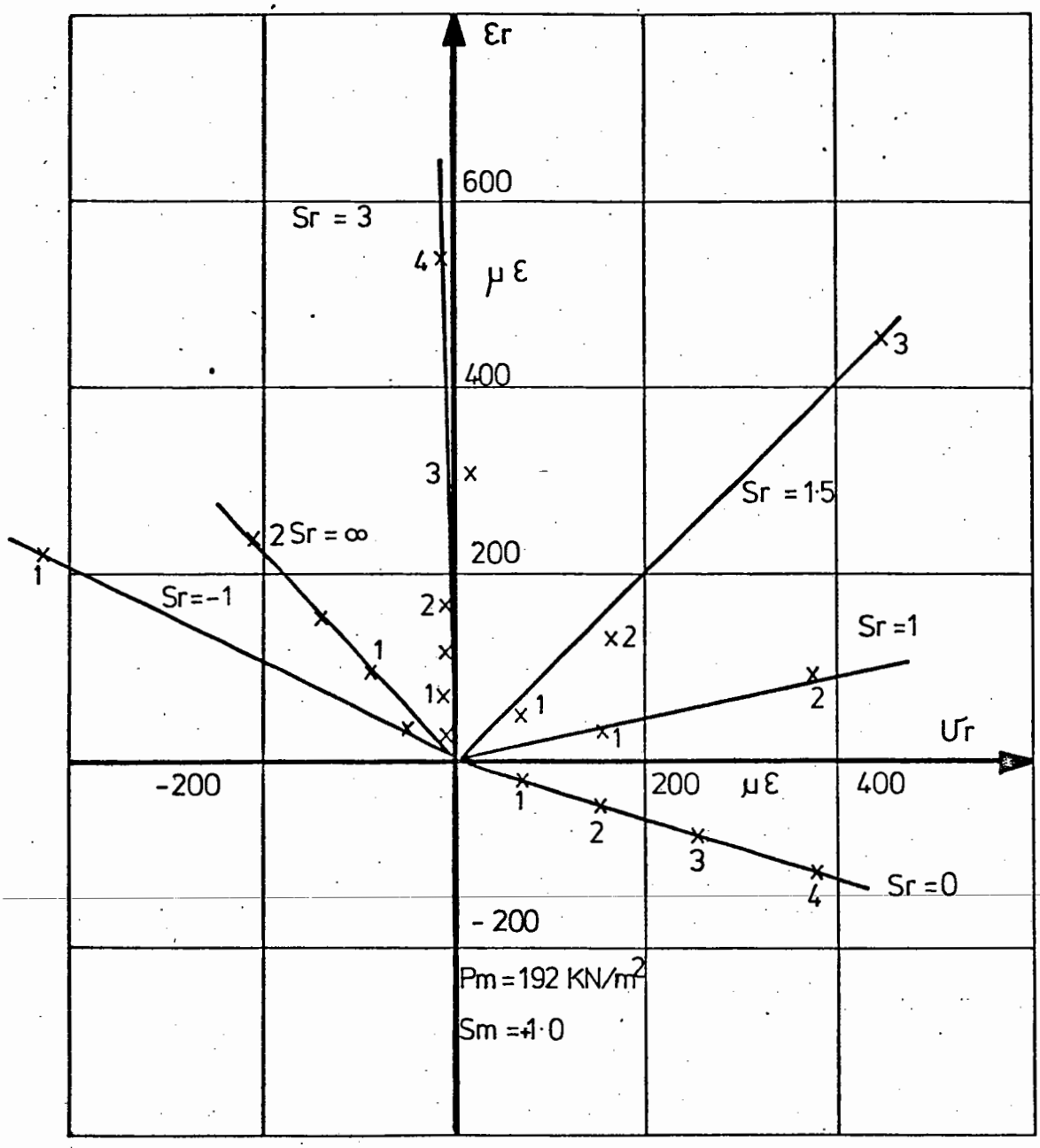

(d) $S_m = +1.0$

FIG. 8.4 RESILIENT STRAIN DIAGRAMS FOR p_m = 192 kN/m²

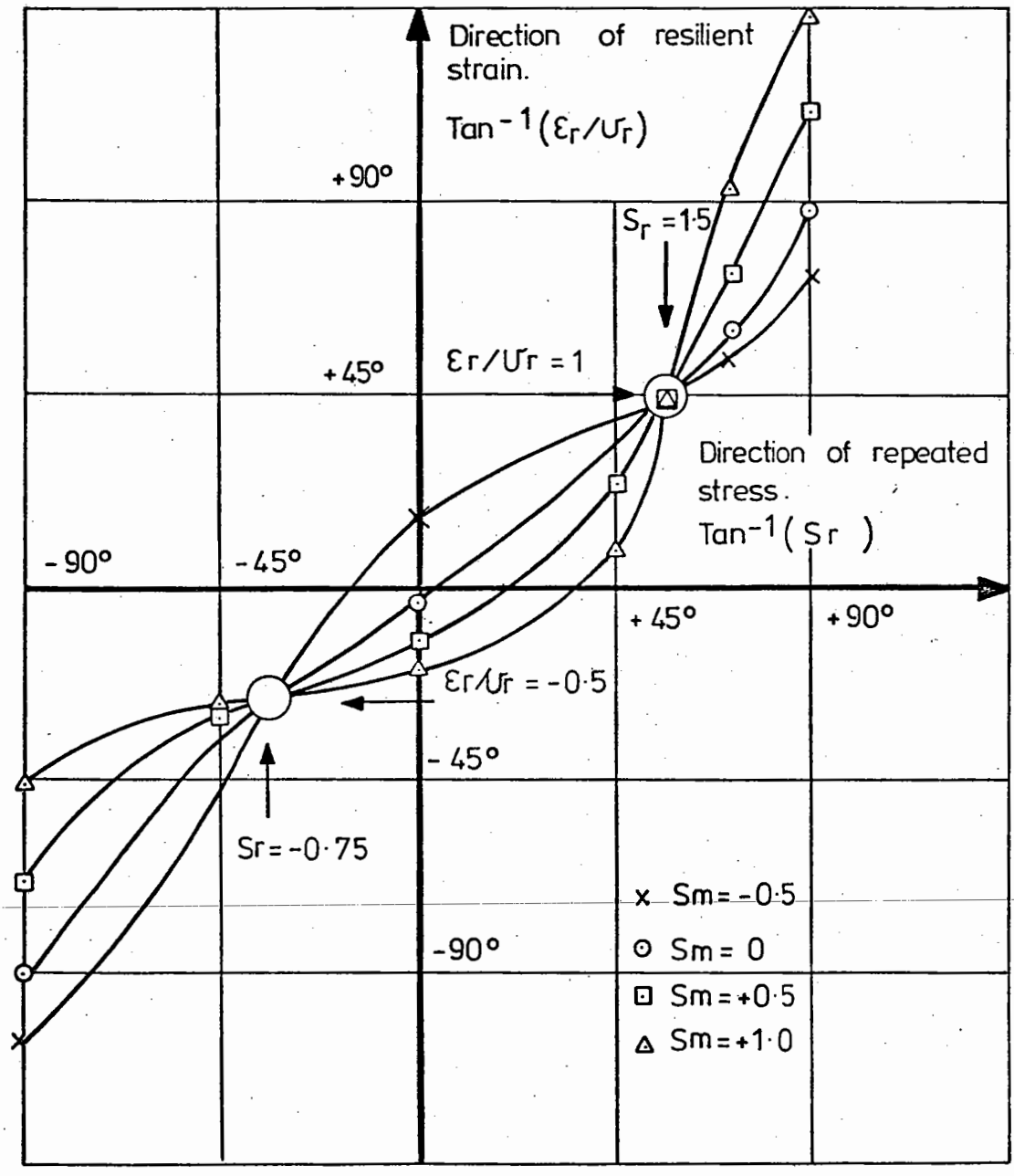

FIG. 8.5 RELATIONSHIP BETWEEN THE DIRECTION OF RESILIENT STRAIN AND THE DIRECTION OF REPEATED STRESS

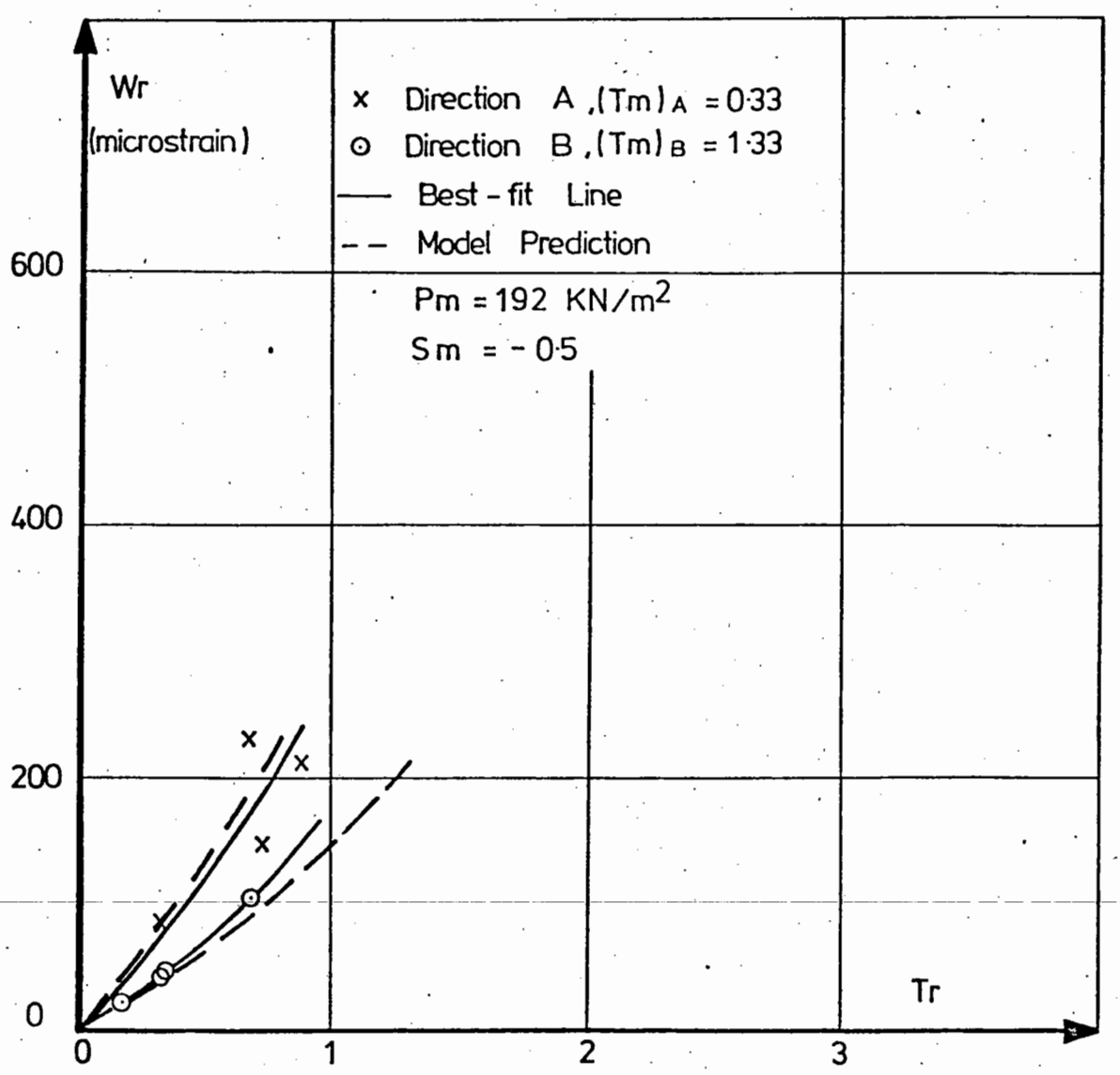

(a) $S_m = -0.5$

FIG. 8.6 RELATIONSHIP BETWEEN THE RESILIENT STRAIN PARAMETER, W_r, AND THE REPEATED STRESS PARAMETER, T_r

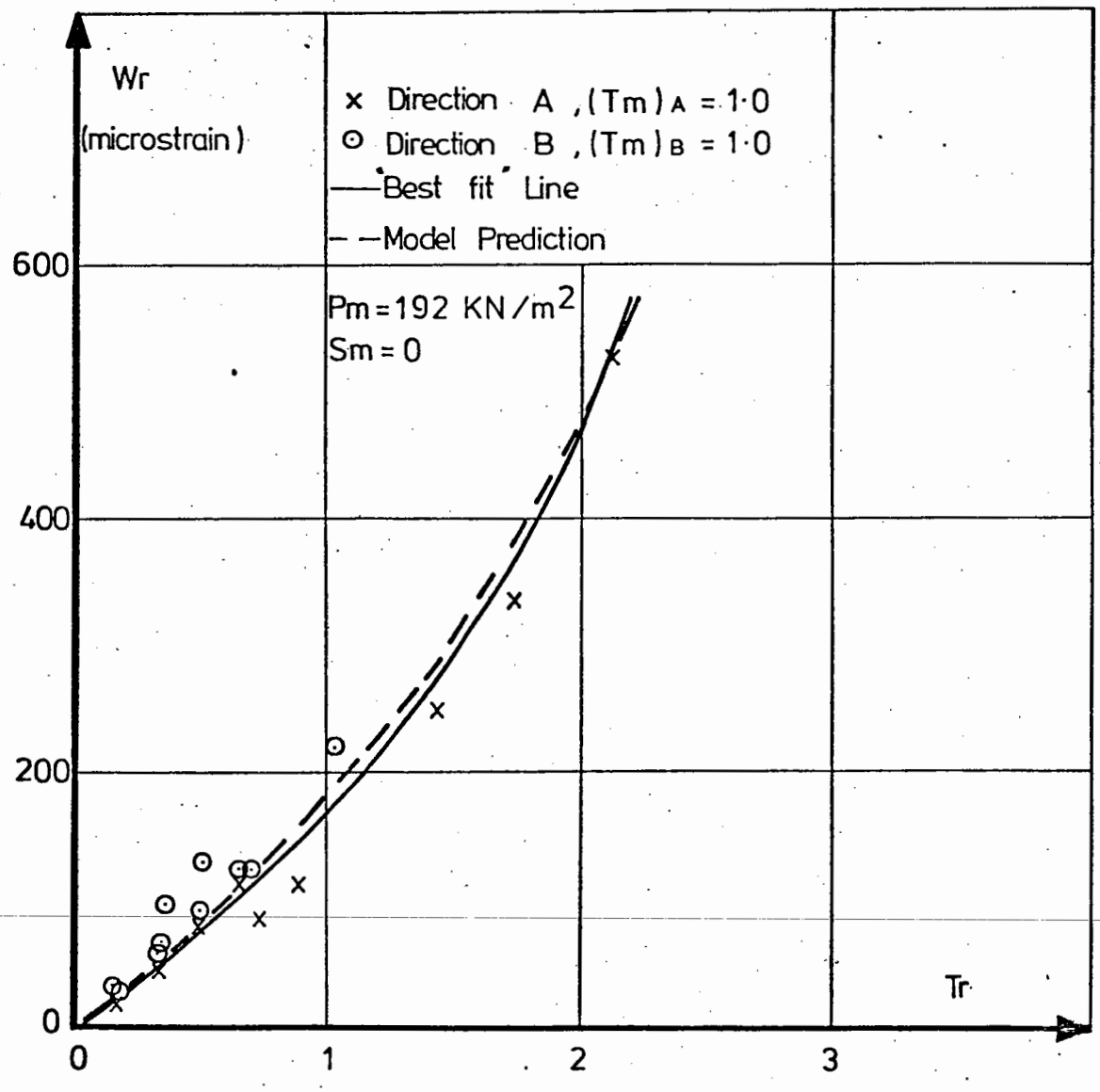

(b) $S_m = 0$

FIG. 8.6 RELATIONSHIP BETWEEN THE RESILIENT STRAIN PARAMETER, W_r, AND THE REPEATED STRESS PARAMETER, T_r

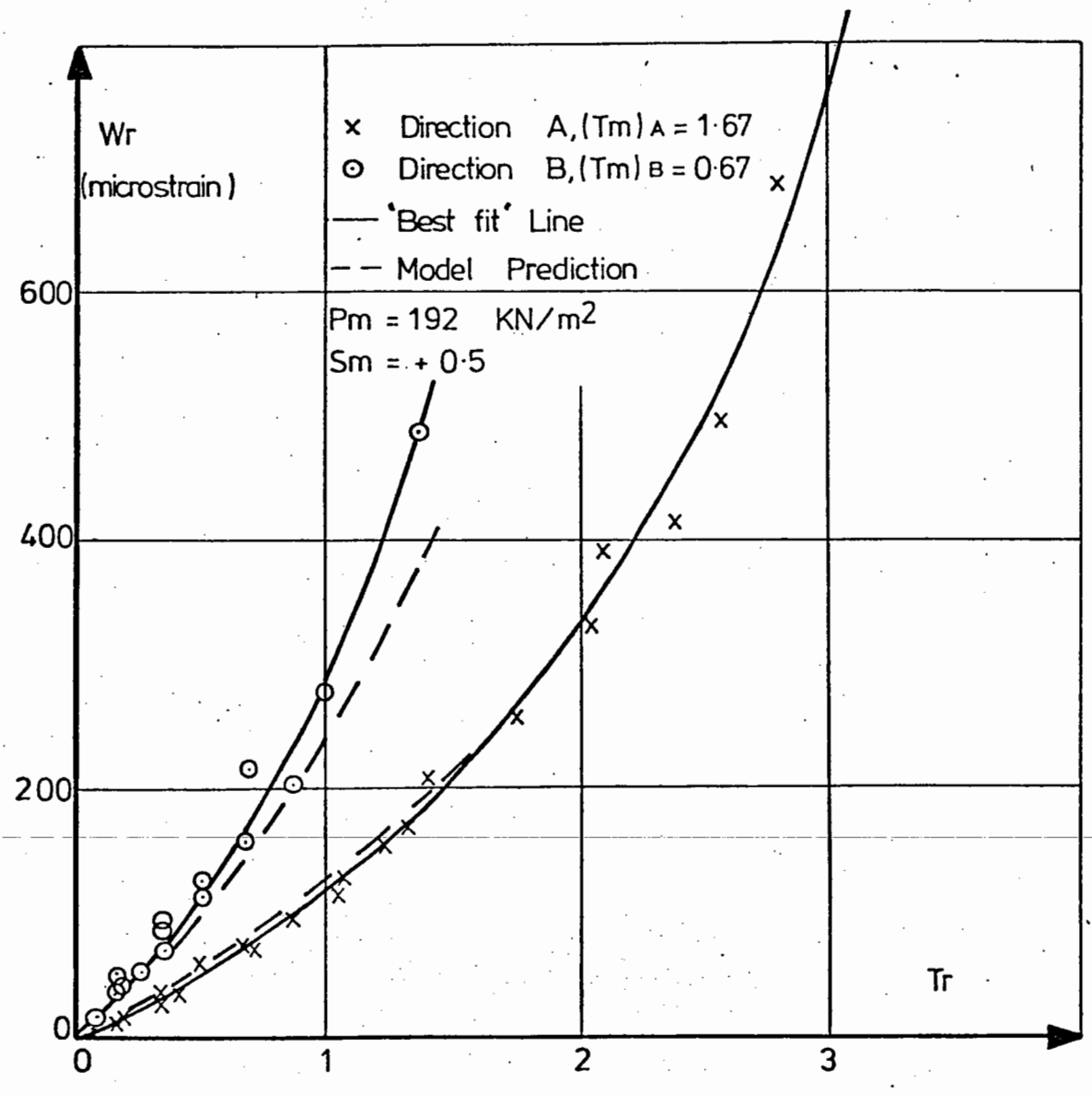

(c) $S_m = +0.5$

FIG. 8.6 RELATIONSHIP BETWEEN THE RESILIENT STRAIN PARAMETER, W_r, AND THE REPEATED STRESS PARAMETER, T_r

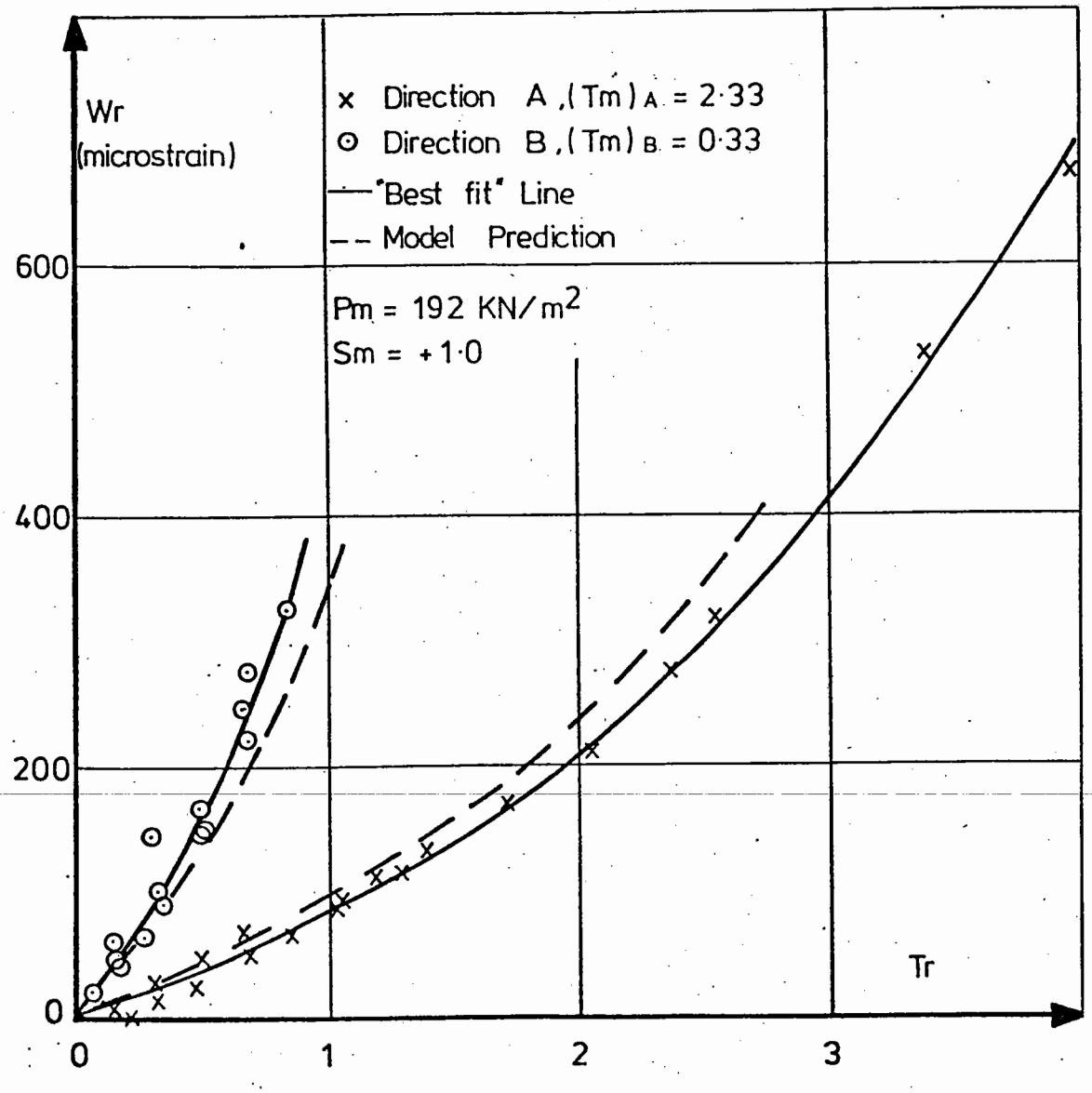

(d) $S_m = +1.0$

FIG. 8.6 RELATIONSHIP BETWEEN THE RESILIENT STRAIN PARAMETER, W_r, AND THE REPEATED STRESS PARAMETER, T_r

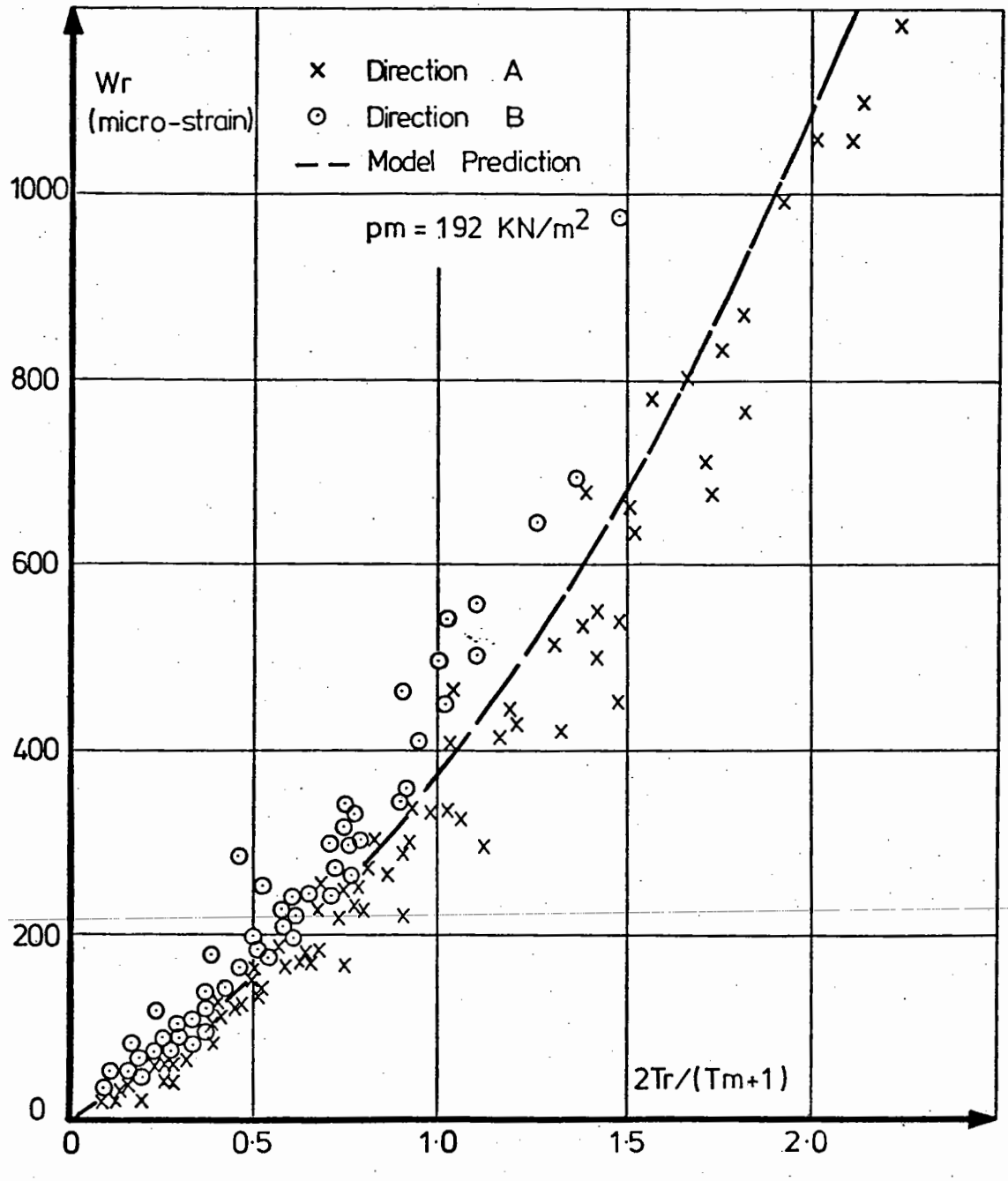

FIG. 8.7 RELATIONSHIP BETWEEN THE RESILIENT STRAIN PARAMETER, W_r, AND THE STRESS FUNCTION, $2T_r/(T_m + 1)$ FOR $p_m = 192$ kN/m^2

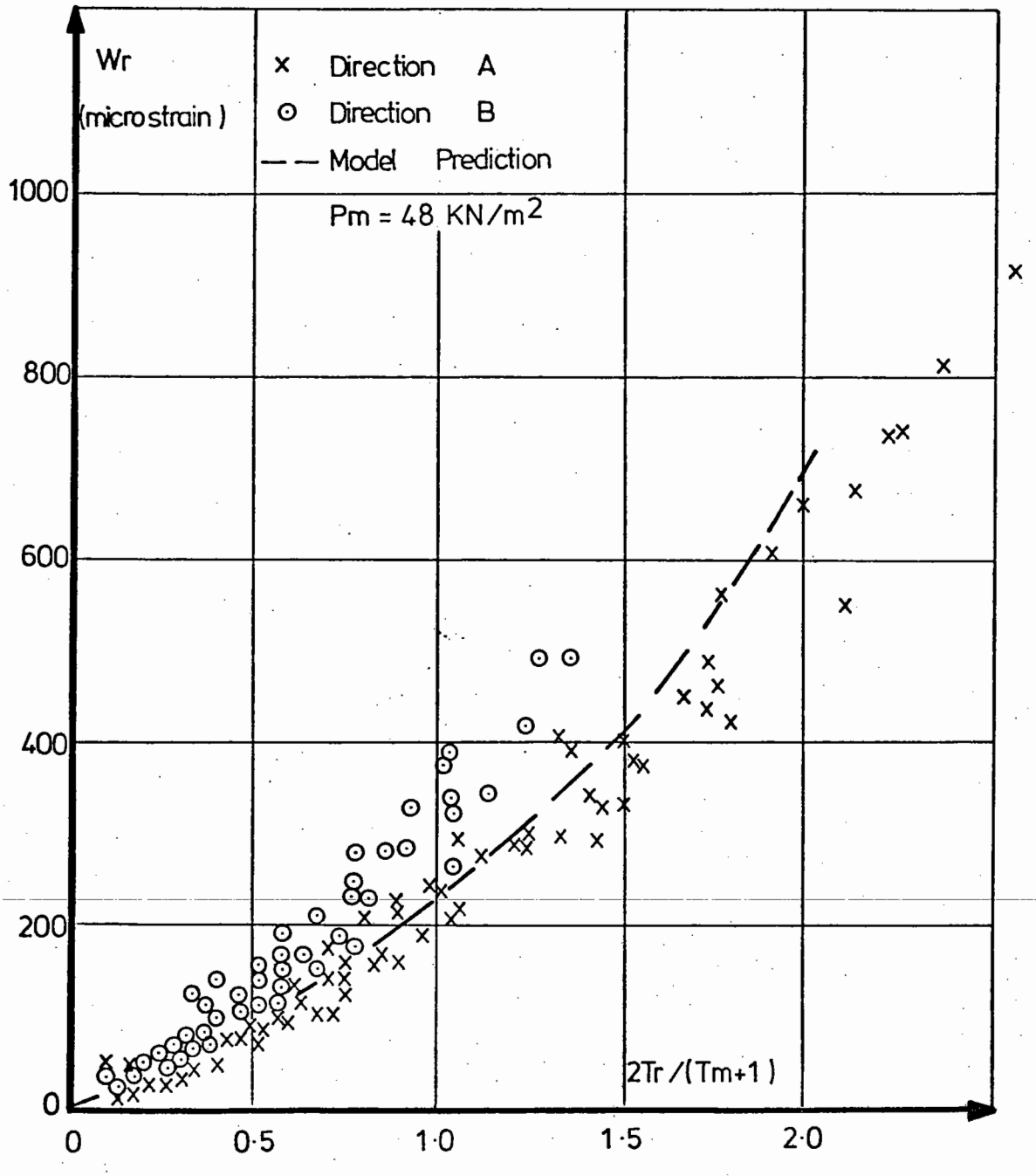

FIG. 8.8 RELATIONSHIP BETWEEN THE RESILIENT STRAIN PARAMETER, W_r, AND THE STRESS FUNCTION, $2T_r/(T_m + 1)$, FOR p_m = 48 kN/m^2

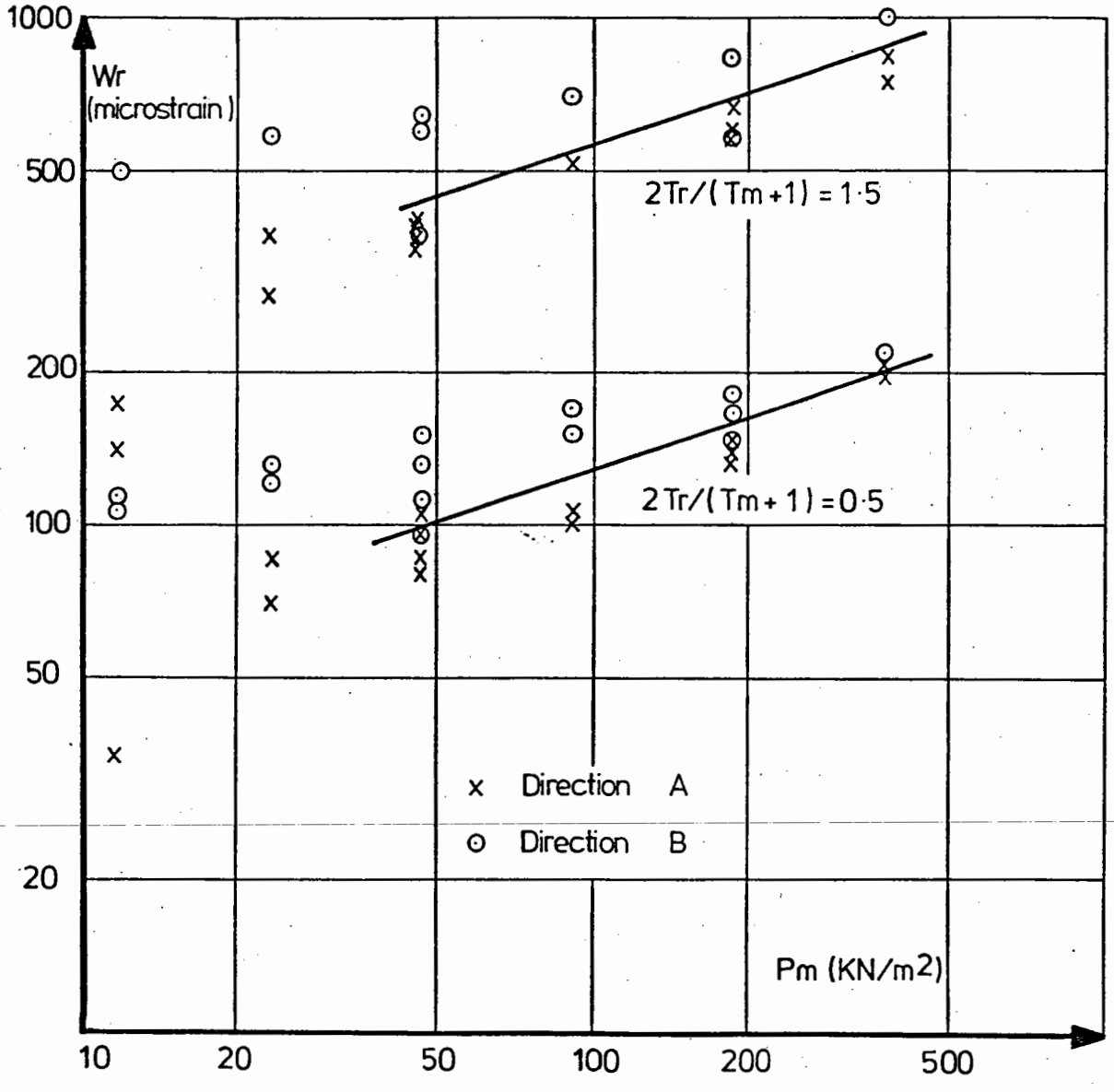

FIG. 8.9 RELATIONSHIP BETWEEN THE RESILIENT STRAIN PARAMETER, W_r, AND THE MEAN NORMAL STRESS, p_m

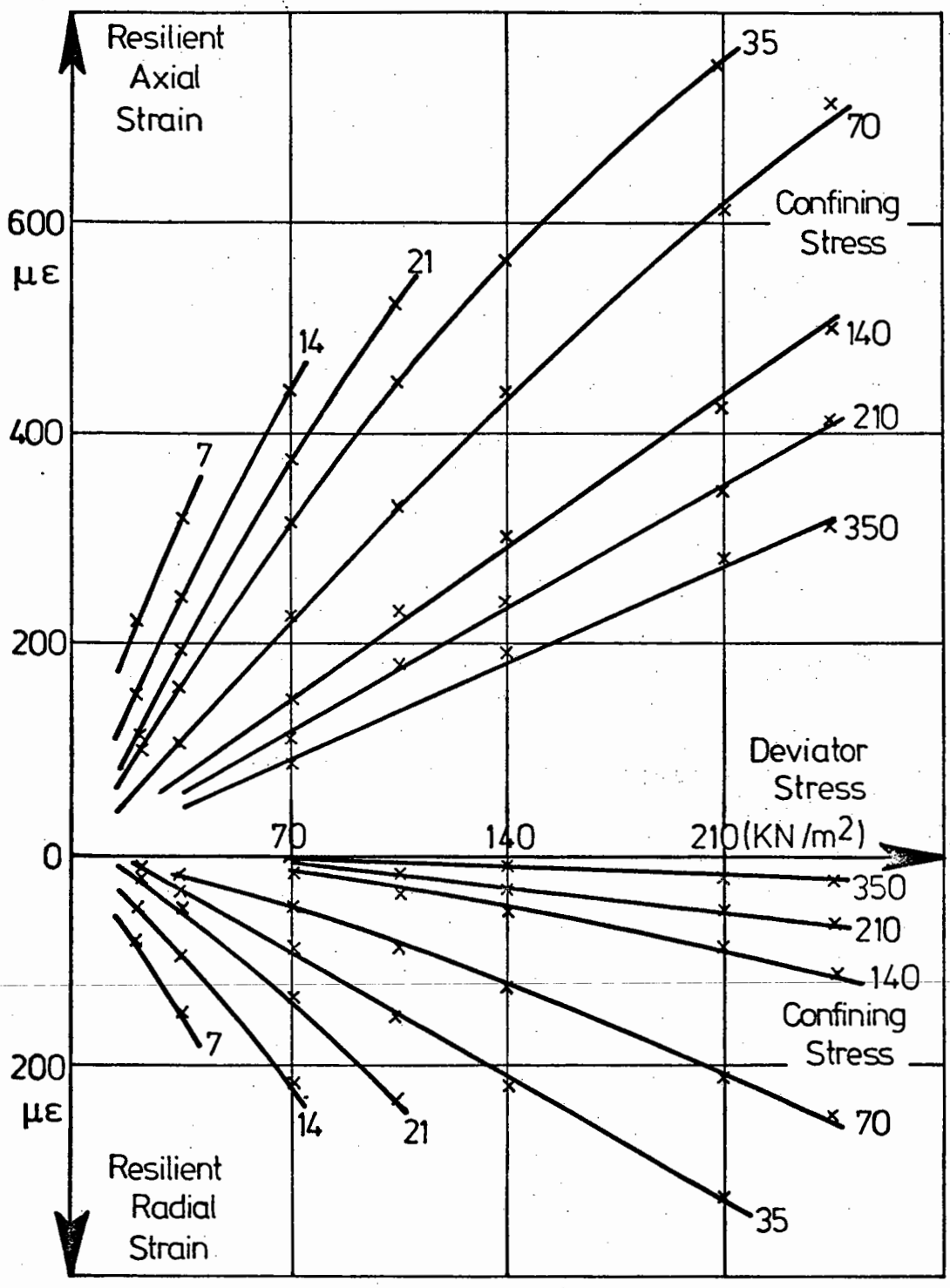

FIG. 8.10 RESILIENT BEHAVIOUR OF A DENSE DRY CRUSHED STONE (AFTER HICKS, 1970)

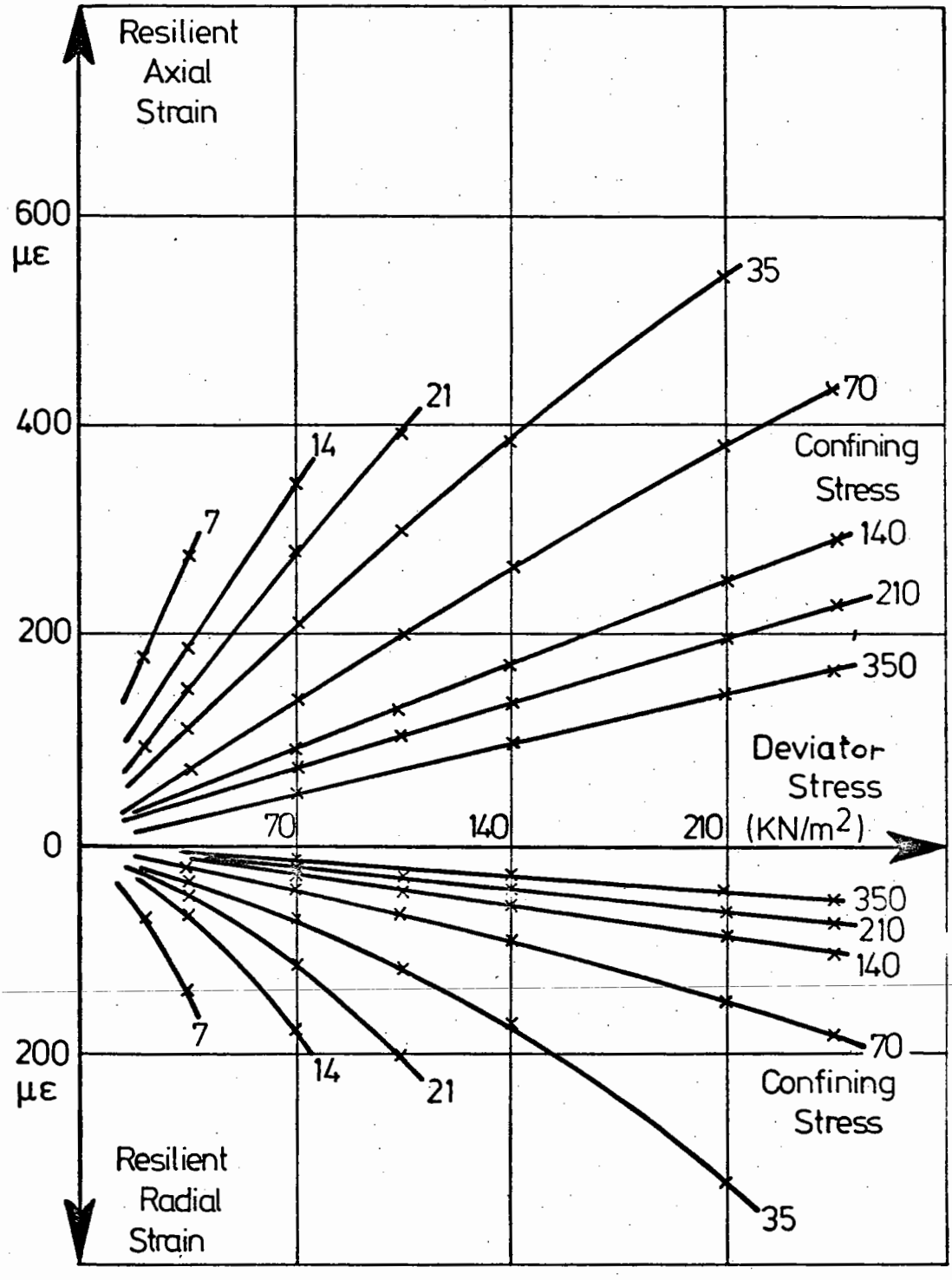

FIG. 8.11 BEHAVIOUR PREDICTED BY THE RESILIENT STRAIN MODEL FOR THE SAME STRESS CONDITIONS AS FIG. 8.10

CHAPTER NINE

PERMANENT STRAIN TESTS

A programme of 30 permanent strain tests was originally envisaged. It was possible to carry out 14 of these tests in the time available, and in this chapter, these tests are described and the results are discussed.

A comprehensive model of the resilient strain behaviour of the material was developed from the resilient tests, but no such model can be postulated for permanent strain. This is because far less data is available even though more tests were carried out. The reason for this situation is that while a resilient strain reading can be taken from only a few cycles, a permanent strain reading requires a complete test of, say, 100,000 cycles. The scatter in the results also makes it difficult to draw more definite conclusions.

9.1 PERMANENT STRAIN TEST PROGRAMME

The permanent strain test programme is presented in Table 9.1. The stress paths are described in terms of the parameters defined in Section 4.4.1 and used for the resilient strain tests. On the right-hand side of Table 9.1, the number of tests carried out on that stress path is shown with the codes used to identify them. They are also shown as stress paths on a p-q diagram in Fig. 9.1.

These tests each involved the application of a large number of stress cycles on the same stress path. About 100,000 cycles were applied in each case, except for test PC-1, when the sample failed after 12,000 cycles, and test PF-2, when a fault developed in the electronics after less than 10,000 cycles. Details are given in Table 9.2.

Table 9.1

Permanent Strain Test Programme

Stress parameters defining test				Tests carried out	
Mean normal stress, p_m (kN/m^2)	Mean stress ratio, S_r (q_m/p_m)	Repeated stress ratio, S_r (q_r/p_r)	Repeated stress amplitude (q_r/p_m)	Number	Identification codes
192	1.5	3	1.5	3	PA-1 PA-4 PA-5
192	1.5	3	5	2	PB-1 PB-2
192	2	3	2	2	PC-1 PC-2
192	1	3	1	1	PD-1
192	1.5	0	$\frac{p_r}{p_m} = 0.5$	2	PE-1 PE-2
192	1.5	∞	1.5	2	PF-1 PF-2
192	1.5	1.5	1.5	2	PG-1 PG-2

Table 9.2

Details of Each Permanent Strain Test

Test	No. of cycles applied	Resilient strain readings taken (stresses are in kN/m^2)			Comment
		After 1,000 cycles	After 10,000 cycles	At the end of the test	
PA-1	158,000	Short, σ_3 = 96	Short, σ_3 = 96	Short, p_m = 192	
PA-4	100,000	Short, σ_3 = 96	Short, σ_3 = 96	Full, p_m = 192	
PA-5	262,000	-	-	Full, p_m = 192 Short, p_m = 48	
PB-1	98,000	Short, σ_3 = 96	Short, σ_3 = 96	Full, p_m = 192	
PB-2	82,000	Short, σ_3 = 96	Short, σ_3 = 96	-	Friction, see note (1)
PC-1	12,000	Short, σ_3 = 64	-	-	Failed, see note (2)
PC-2	102,000	Short, σ_3 = 64	Short, σ_3 = 64	Full, p_m = 192 Short, p_m = 48	
PD-1	100,000	Short, σ_3 = 128	Short, σ_3 = 128	Full, p_m = 192 Short, p_m = 48	
PE-1	101,000	Short, p_m = 192	Short, p_m = 192	Full, p_m = 192 Short, p_m = 48	
PE-2	96,000	-	-	Full, p_m = 192 Short, p_m = 48	
PF-1	100,000	Short, p_m = 192	Short, p_m = 192	Full, p_m = 192 Short, p_m = 48	
PF-2	10,000	Short, p_m = 192	-	-	Test stopped early, see note (3)
PG-1	101,000	-	-	Full, p_m = 192 Short, p_m = 48	
PG-2	100,000	-	-	-	Poor control, see note (4)

Table 9.2 - Notes

(1) Test PB-1 was stopped after 82,000 cycles because considerable friction developed between the loading rod and the triaxial cell top due to poor lubrication. The problem was overcome by replacing the brass bush by a linear ball bushing.

(2) Large strains developed in test PC-2 so that after 10,000 cycles the LVDT's measuring axial strain were beyond their linear range, and after 12,000 cycles the sample had deformed so much that the strain transducers might have been damaged. The sample at the end of test PC-2 is shown in Plate 1. The axial strain was 10.5%.

(3) Test PF-2 was stopped after 10,000 cycles because a fault developed in the electronics so that cell pressure control was very poor.

(4) During test PG-2 pressure from the hydraulic power supply was not constant. Therefore, control was poor, and it was considered that the readings of resilient strain were unreliable.

After 1,000 cycles and 10,000 cycles, each test was interrupted to take a short series of resilient strain readings at stress ratios lower than were applied in the rest of the test. For tests in which the confining stress was constant (PA to PD) air was used as the cell fluid, and the resilient strain readings used the same constant confining stress. Otherwise a short series of readings from the resilient strain test programme was used at the same mean normal stress at the rest of the test. In the case of three tests (PA-5, PF-2 and PG-1) these resilient strain readings were omitted to check that the interrpution of a test was not influencing the permanent strain behaviour of the sample.

Usually, at the end of each test, a full series of resilient strain readings was taken at a mean normal stress of 192 kN/m^2, and in some cases also a short series at 48 kN/m^2. Details of the resilient strain readings which were taken during the various tests are given in Table 9.2.

9.2 RESULTS OF PERMANENT STRAIN TESTS

The results of the permanent strain tests are shown in Figs. 9.2 to 9.8 in terms of the permanent shear strain, $\epsilon_p = \frac{2}{3}(\epsilon_{1p} - \epsilon_{3p})$, and permanent volumetric strain, $v_p = \epsilon_{1p} + 2\epsilon_{3p}$, which developed as the test progressed. The number of load cycles, N, taken to reach a particular point is given at intervals along the curves. These diagrams are largely self explanatory, but some description is required to bring out the important features. It should be noted that they have been plotted on several different scales because of the wide range of the results.

9.2.1 Tests in which the Permanent Strain Reached a Constant Level

With the exception of tests PC and PF which are described in the next section, all tests followed a similar pattern involving three phases:

(a) A large initial strain occurred in the first few cycles, the majority of this being in the first cycle.

(b) Between about 10 and 1,000 cycles, the development of permanent strain was approximately proportional to the logarithm of the number of cycles.

(c) After 1,000 cycles the permanent strain gradually stabilised so that by 100,000 cycles it was almost constant at a terminal value of two or three times the strain which occurred in the first few cycles.

In these tests the shear strain, which was generally less than 2%, was accompanied by a small volumetric contraction (generally less than 1%). Most of the curves decrease in slope towards the end of the test, indicating that the shear strain tended to stabilise before the volumetric strain.

It can be seen from Figs. 9.2 to 9.8 that there is considerable scatter between replicate tests, and this scatter makes it impossible to establish any firm relationship between the applied stress path and the permanent strain. However, there is some correlation between permanent shear strain and the applied stress ratio (q_{max}/p_m) as shown in Fig. 9.9.

9.2.2 Tests Leading to Failure

The maximum stress ratio applied in tests PC and PF was very high ($q/p = 2.25$ in both cases compared with the maximum stress ratio reached

in the single loading tests of q/p = 2.18) and the permanent shear strains which developed were much greater than in the tests described above.

There was a marked difference in behaviour between tests PC-1 and PF-1 on the one hand and tests PC-2 and PF-2 on the other. Tests PC-2 and PF-2 showed very little volumetric strain and the shear strain did appear to stabilise towards the end of the test. However, tests PC-1 and PF-1 showed considerable dilation from the first few cycles and the permanent strain continued to increase right up to the end of the test. Test PC-1 was stopped after 12,000 cycles when the shear strain had reached 12.3% and the volumetric strain -5.5% (the negative sign indicating dilation). The appearance of the sample at the end of the test is shown in Plate 6.

9.3 DISCUSSION OF PERMANENT STRAIN BEHAVIOUR

Because of the scatter in results between replicate samples it is not possible to develop a permanent strain model. The complexity of the behaviour suggests that there is probably more than one factor which determines how much permanent strain occurs when the material is subjected to large numbers of load applications.

9.3.1 A Possible Mechanism of Permanent Strain in Granular Material

For cohesive soils and for bituminous materials, permanent deformation under repeated loading has been linked with creep behaviour under single loading (Hyde, 1974; and Snaith, 1973). However, there is no evidence to show any time dependent strain in granular materials and it is therefore postulated that the mechanism of permanent strain is essentially one of "shakedown" with the possibility of "incremental collapse" at higher stresses. This is supported by the fact that in the

majority of tests the permament strain stabilised after relatively little deformation had occurred.

Similar phenomena of shakedown and incremental collapse have been observed in plastic (ductile) structures subject to two or more independently varying load systems (Heyman, 1964). Shakedown in a plastic structure is accompanied by a redistribution of internal stresses in the structure and shakedown in granular material would also be accompanied by a rearrangement of inter-particle contacts. The non-linear behaviour of the material and the random arrangements of the particles might allow shakedown to occur under only one load system. If the particles in their new positions were packed at a slightly higher density, the material would become stronger and eventually be able to resist the applied stresses without further rearrangements. However, if the first few load applications caused a severe rearrangement, together with dilation, the material would become weaker and might eventually fail in a manner similar to incremental collapse.

If this is the case, the results of tests PC-1 and PF-1 indicate that a repeated stress ratio at least as high as that which can be sustained in single loading must be applied to cause incremental collapse*.

In those tests which reached a stable condition, the permanent shear strain was always less than 2% and it is significant that in the single loading tests, described in Section 7.1, dilation commenced when the shear strain had reached about 2%. Tests PC-2 and PF-2 represent an intermediate type of behaviour.

---

* It should be appreciated that in a repeated loading test it is unlikely that the equipment will be able to apply the full maximum load in the first one or two cycles if very rapid permanent strain is occurring. The material might then be strengthened sufficiently to sustain a stress ratio somewhat greater than that which is possible in single loading.

9.3.2 Comparison with Previous Work

Previous investigations into the permanent strain behaviour of granular materials using the repeated load triaxial test generally employed a constant confining stress and measured strain in the axial direction only. Therefore, to make a comparison, the results of this study need to be expressed in a compatible form. Figs. 9.10 to 9.13 show the permanent axial strain, ϵ_{1p}, and the permanent radial strain, ϵ_{3p}, plotted against the number of load cycles applied. As noted above, there was a large initial strain in the first few cycles and the permanent strain stabilised towards the end of each test except for tests PC-1 and PF-1.

Fig. 9.14 shows the permanent axial strain after 100,000 cycles as a function of the stress ratio $q_{max}/\sigma_{3\,mean}$. It can be seen that there is an approximately straight line relationship with the axial strain on a logarithmic scale. Also shown in Fig. 9.14 are results from one of the granular bases tested by Barksdale (1972). This material was a crushed granite compacted and tested at optimum moisture content and the results are not incompatible with those from this work on a dry crushed limestone.

Brown and Hyde (1975) reported the results of repeated loading tests on Breedon gravel (a well graded crushed stone) and they found that the permanent axial strain stabilised after about 10,000 cycles and that the final value was directly proportional to the stress ratio q_{max}/σ_3. They also reported some tests with a variable confining stress and found that these obeyed the same relationship when the stress ratio was expressed in the form $q_{max}/\sigma_{3\,mean}$ as in Fig. 9.14. Therefore, it appears that the behaviour of the Breedon gravel is dependent on the same factors even though they produce a different relationship between permanent strain and stress ratio.

Shenton (1974) carried out repeated load tests on railway ballast, a uniform granular material. He observed a similar relationship between permanent strain and the number of load cycles to that described above, except that in all cases the permanent strain continued to increase up to the end of the test and was accompanied by dilation. This may indicate that the particles of a uniform material are unable to repack to a higher density under repeated loading, and hence the test does not reach a stable situation. He found that the permanent strain, ϵ_{1p}, after any number of load cycles, N, was related to the permanent strain developed in the first load cycle, ϵ_I, by the equation:

$$\epsilon_{1p} = \epsilon_I(1 + 0.2 \log_{10}N) \qquad (9.1)$$

The way in which permanent strain developed in the tests described here was similar but the relationship was not so well defined.

9.4 EFFECT OF PERMANENT STRAIN ON RESILIENT BEHAVIOUR

As mentioned in the permanent strain test programme, Section 9.1, measurements of resilient strain behaviour were taken during and at the end of the permanent strain tests. The purpose of these measurements was to assess whether permanent strain and/or large numbers of load cycles altered the resilient strain behaviour of the material significantly from that observed in the resilient strain tests. Each group of resilient strain readings taken in the permanent strain tests was plotted on a separate diagram showing the resilient strain parameter, W_r, as a function of stress parameter, $2T_r/(T_m + 1)$. These diagrams (which are all presented in Appendix D) were then compared with the equivalent diagrams drawn from the resilient strain test data (Figs. 8.7 and 8.8).

In almost all cases, there was a good correlation between $(W_r)_A$ and $2(T_r)_A/((T_m)_A + 1)$ and between $(W_r)_B$ and $2(T_r)_B/((T_m)_B + 1)$, indicating that the significant directions of stress and strain found in the resilient strain tests were still applicable. There was generally more scatter in the experimental points, but this is to be expected when data from a single sample is compared with the average from several samples. In some of the permanent strain tests, the relationship between W_r and $2T_r/(T_m + 1)$ was exactly the same as that from the resilient strain tests. In other cases, $(W_r)_A$ was somewhat lower and $(W_r)_B$ was somewhat higher. The changes which were observed from the results of resilient strain readings taken at the end of each test are shown in Table 9.3. It can be seen that the effect of permanent strain is to introduce some degree of inherent anisotropy into the resilient strain behaviour of the material. This anisotropy is always biased in the same sense, making the material stiffer in the A direction and less stiff in the B direction, and the degree of anisotropy varies from nothing to 40%.

Fig. 9.15 shows the values of the resilient strain parameters $(W_r)_A$ and $(W_r)_B$ at selected values of the stress parameter, $2T_r/(T_m + 1)$ plotted against the permanent shear strain which developed during the test. There is no correlation between permanent strain and the degree of anisotropy, and it is concluded that the random arrangement of particles within each sample may be masking any such effect. The reason that the anisotropy is always biased in the same sense may be that all the permanent strain tests and the majority of the resilient strain tests were carried out in axial compression or it may originate from the sample preparation method.

It is of interest to know at what point during the test this

Table 9.3

Effect of Permanent Strain on the Resilient Strain Parameter, W_r

The figures given in this table indicate approximately the difference in the resilient strain parameters at the end of each test from the values $(W_r)_A$ and $(W_r)_B$, indicated by the resilient strain tests. Full details can be found in Appendix D.

Test	p_m = 192 kN/m^2		p_m = 48 kN/m^2	
	$(W_r)_A$	$(W_r)_B$	$(W_r)_A$	$(W_r)_B$
PA-1	0	0	-	-
PA-4	0	0	-	-
PA-5	0	+20%	0%	+20%
PB-1	0	0	-	-
PB-2	-	-	-	-
PC-1	-	-	-	-
PC-2	0	+50%	very scattered	
PD-1	0	0	0	0
PE-1	-40%	+30%	-50%	+30%
PE-2	0	+10%	0	+30%
PF-1	-20%	+40%	-20%	+60%
PF-2	-	-	-	-
PG-1	-20%	+10%	-40%	+20%
PG-2	-	-	-	-

anisotropy develops. From the resilient strain readings taken during some of the tests (see Appendix D), it can be said that samples which exhibited significant anisotropy at the end of the test showed a similar amount after 1,000 cycles and after 10,000 cycles. Anisotropy can therefore develop quite early in the test and it is not surprising that the resilient strain tests showed a small measure of anisotropic behaviour even though only four load cycles were applied on each stress path and the permanent strain which developed was small (0.2% on average). Points representing the average degree of anisotropy recorded in the resilient strain tests are labelled 'R' on Fig. 9.15.

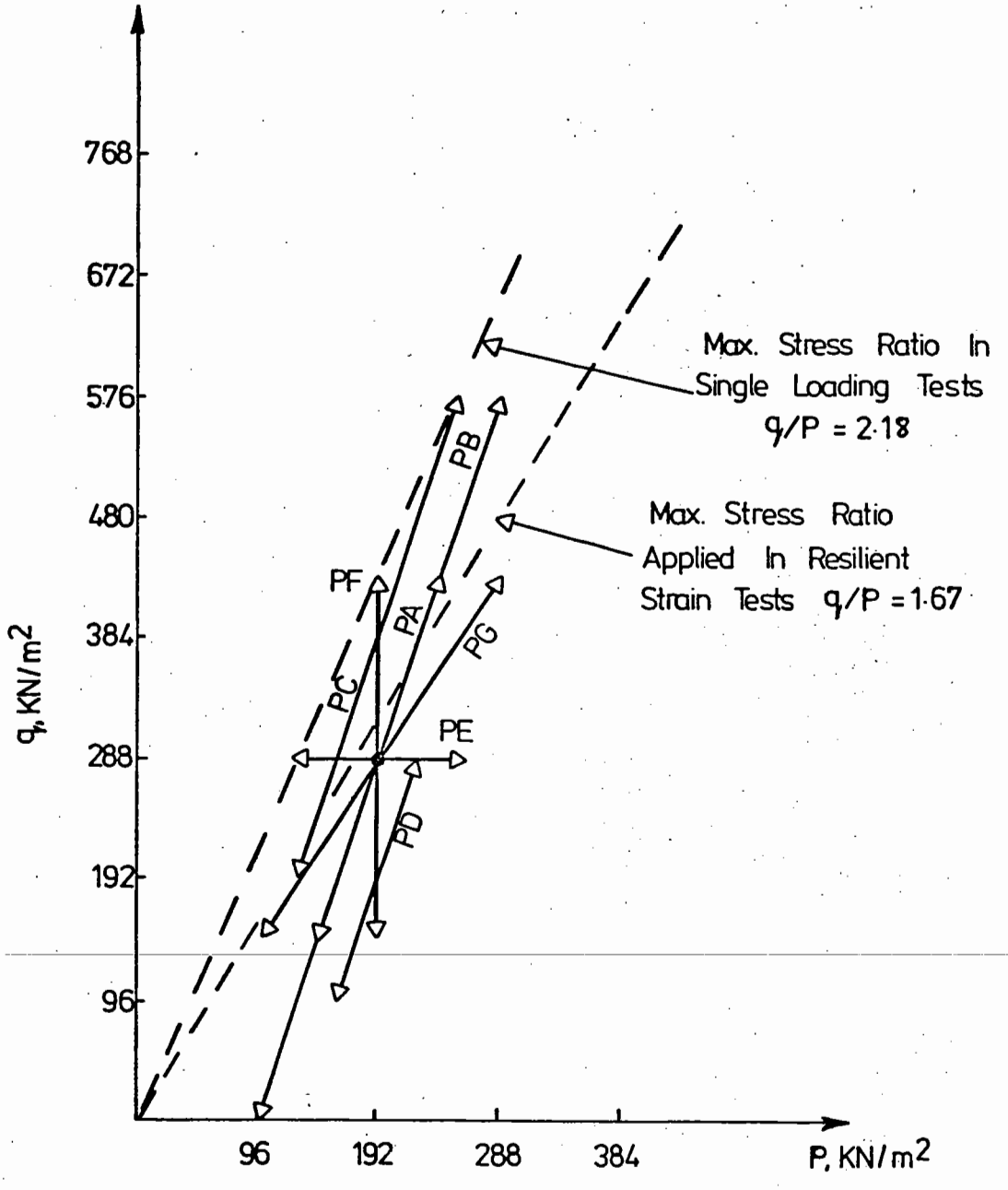

FIG. 9.1 STRESS PATHS APPLIED IN PERMANENT STRAIN TESTS

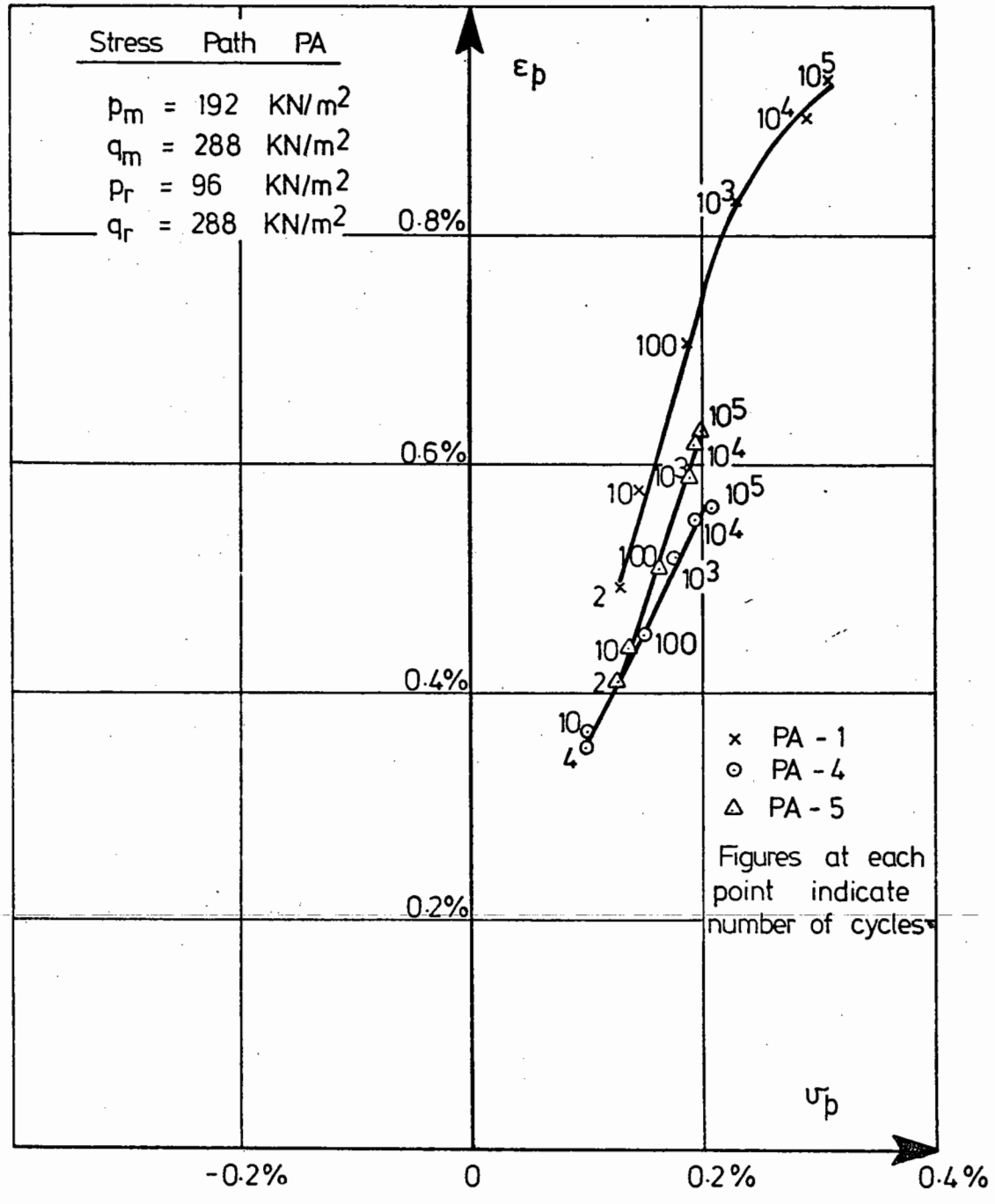

FIG. 9.2 PERMANENT STRAIN DIAGRAM FOR TESTS PA-1, PA-4 AND PA-5

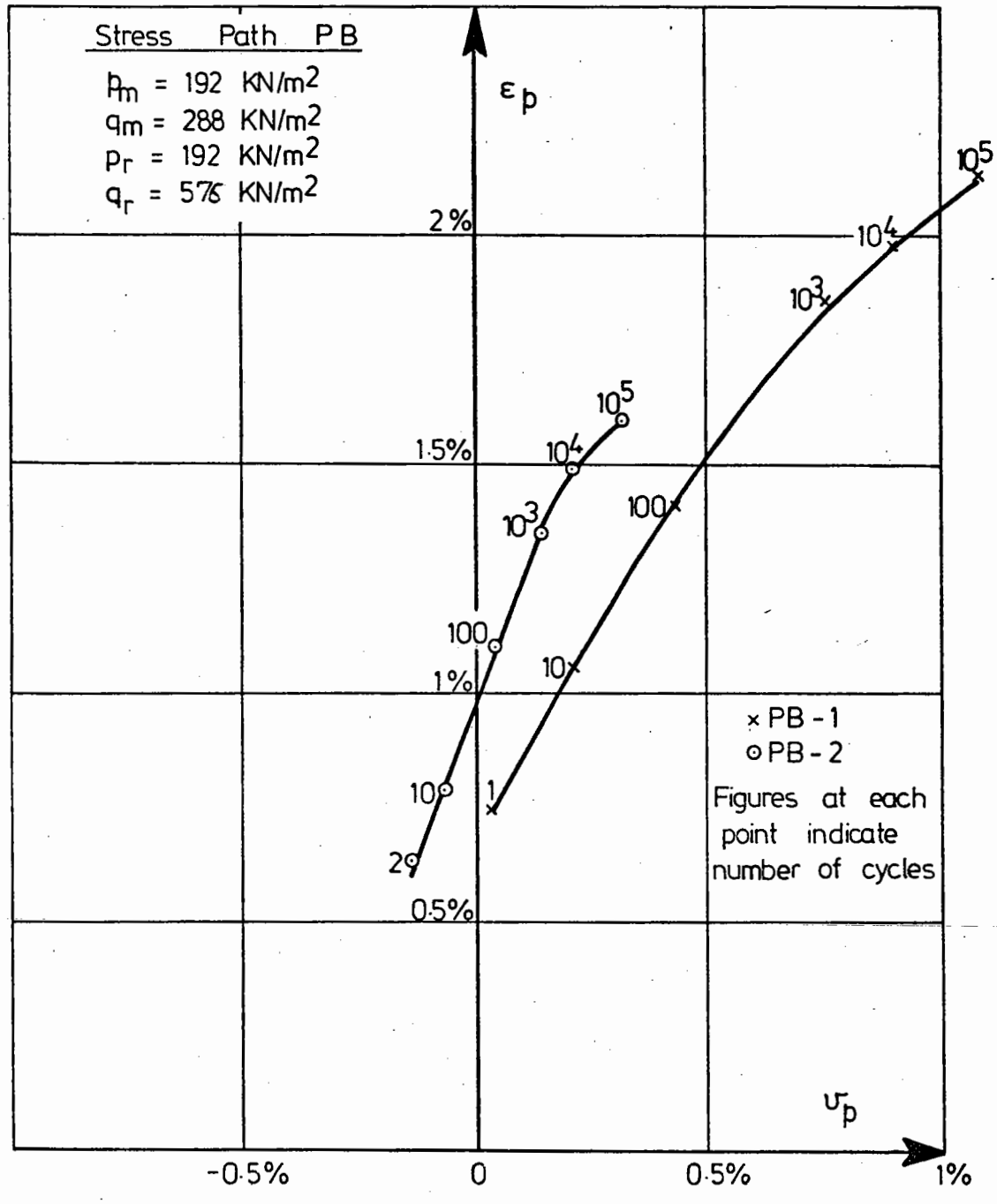

FIG. 9.3 PERMANENT STRAIN DIAGRAM FOR TESTS PB-1 AND PB-2

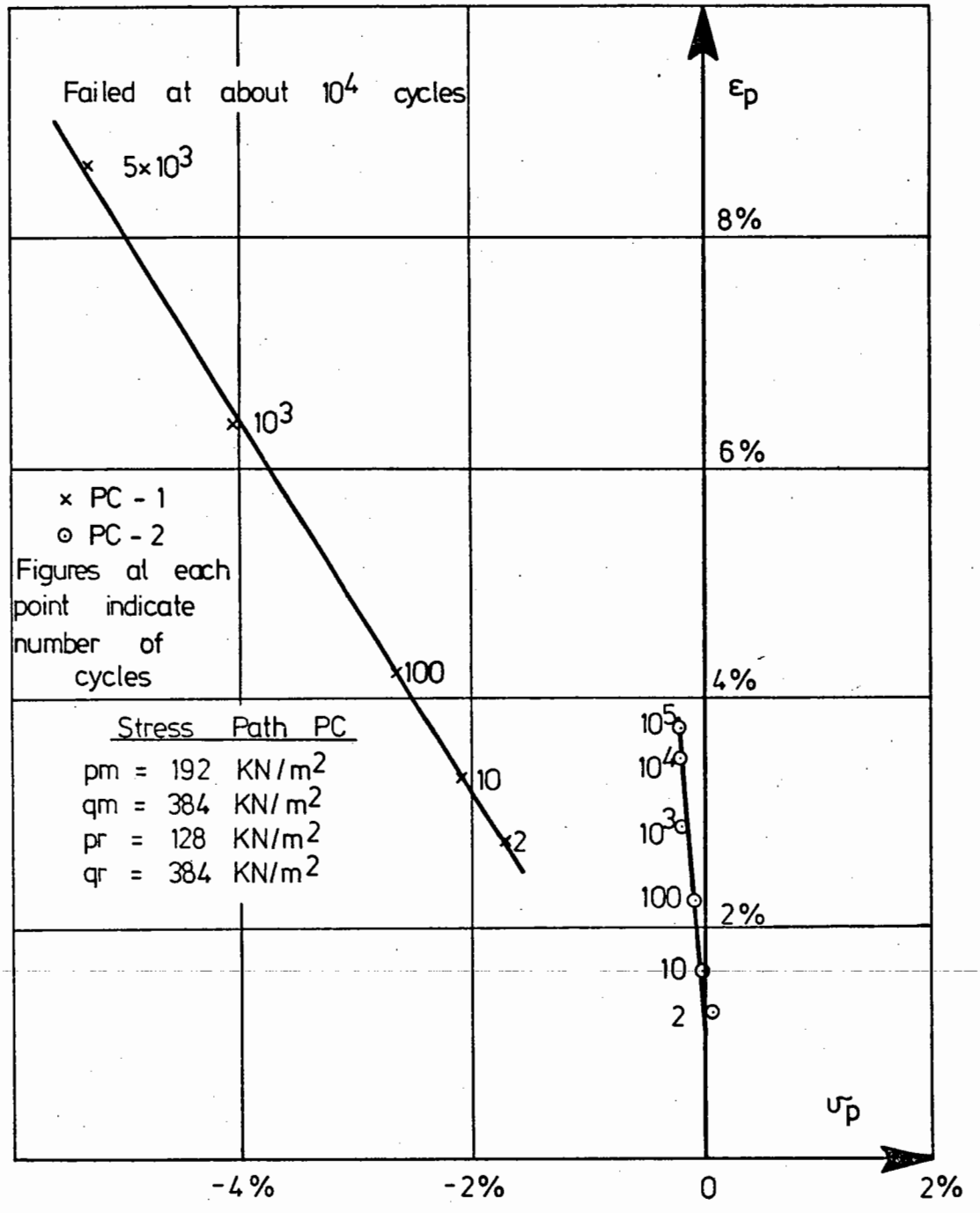

FIG. 9.4 PERMANENT STRAIN DIAGRAM FOR TESTS PC-1 AND PC-2

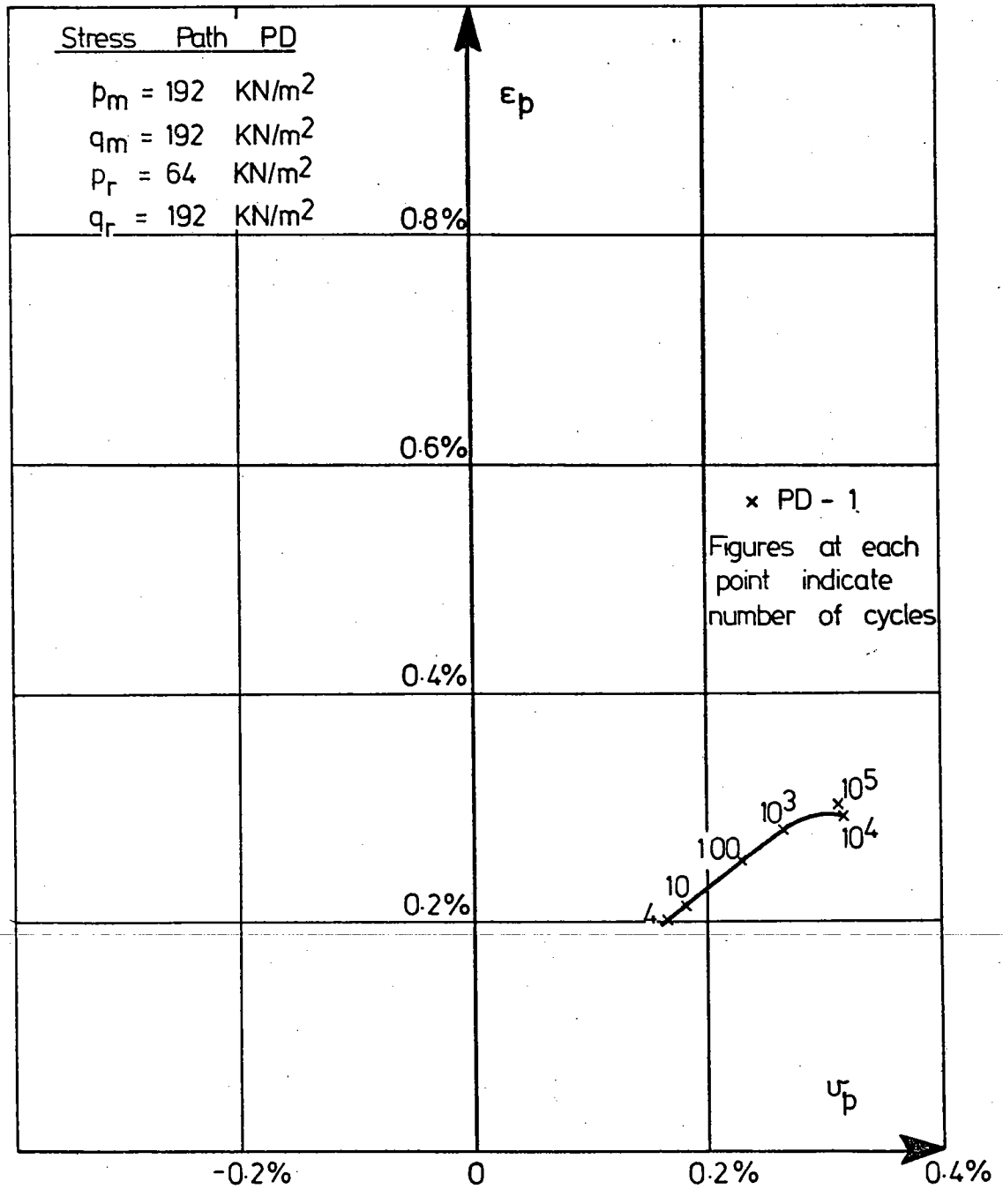

FIG. 9.5 PERMANENT STRAIN DIAGRAM FOR TEST PD-1

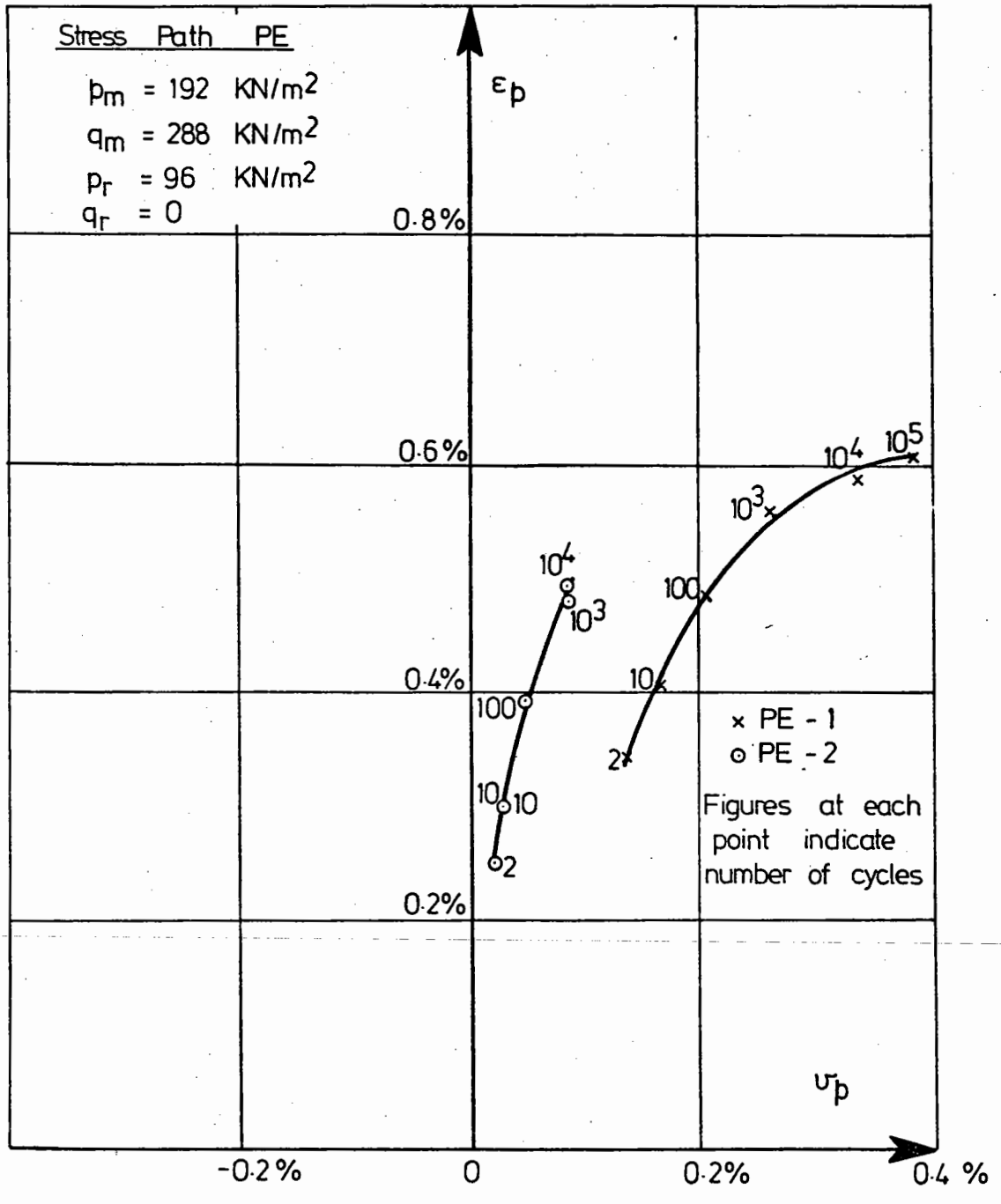

FIG. 9.6 PERMANENT STRAIN DIAGRAM FOR TESTS PE-1 AND PE-2

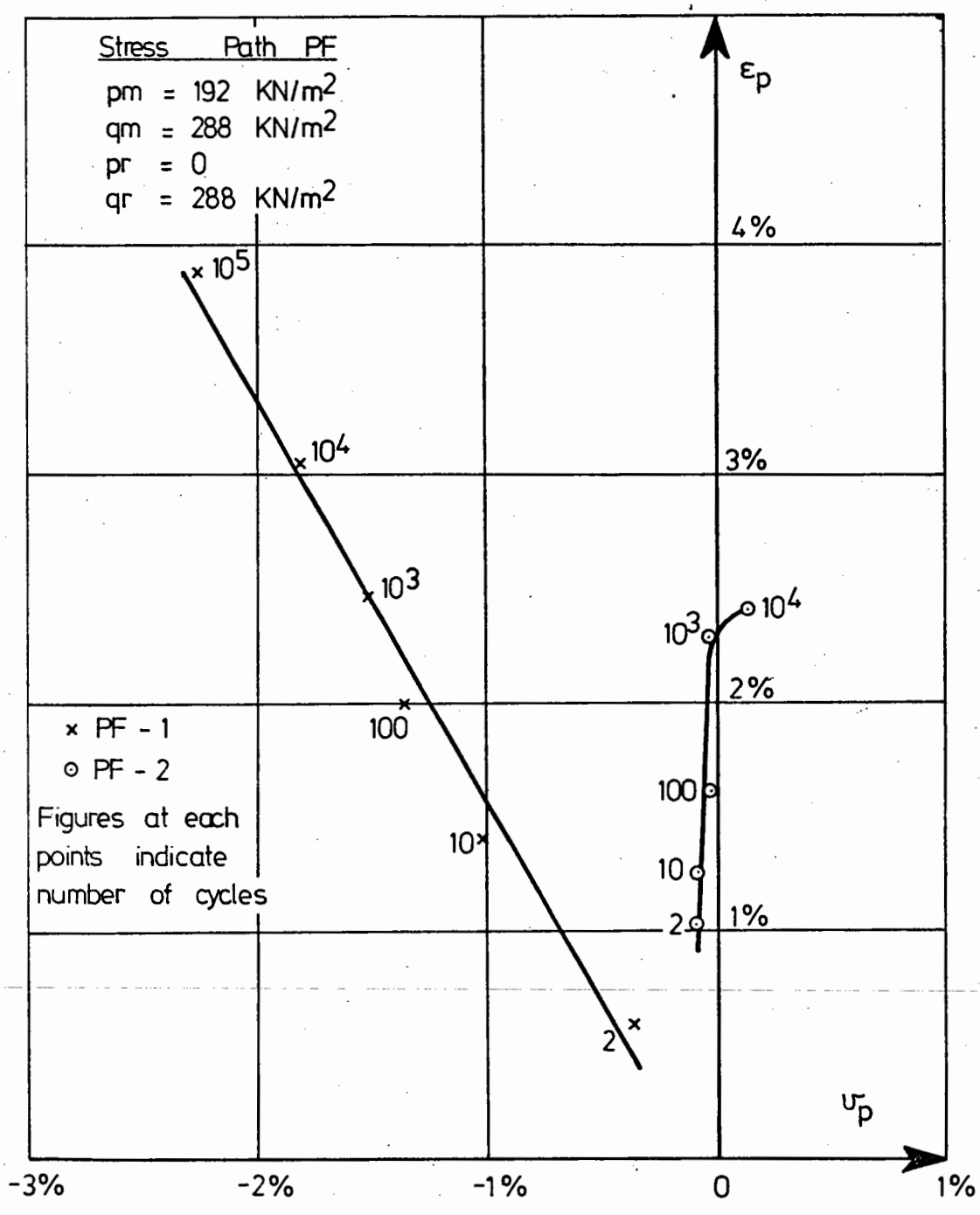

FIG. 9.7 PERMANENT STRAIN DIAGRAM FOR TESTS PF-1 AND PF-2

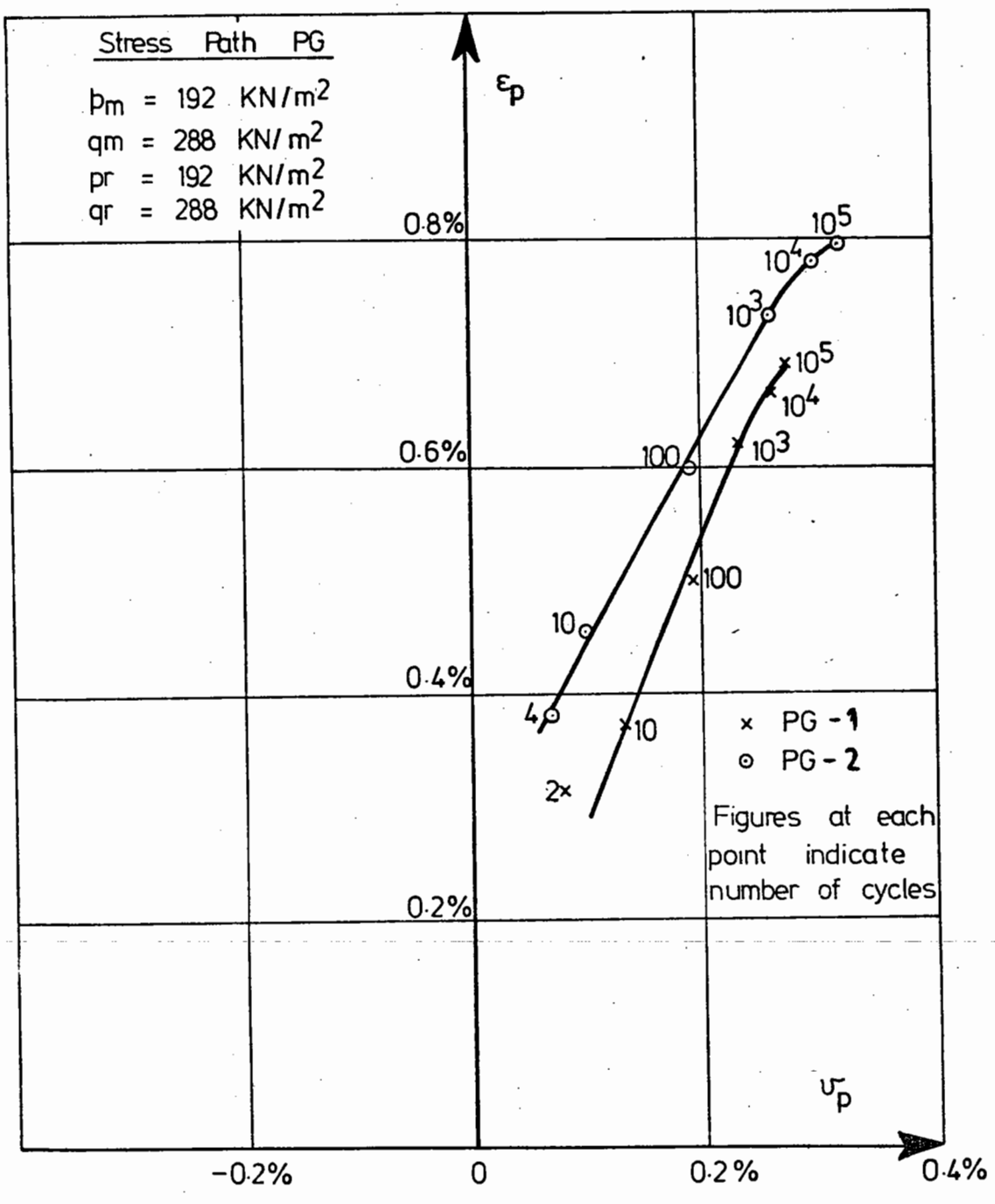

FIG. 9.8 PERMANENT STRAIN DIAGRAM FOR TESTS PG-1 AND PG-2

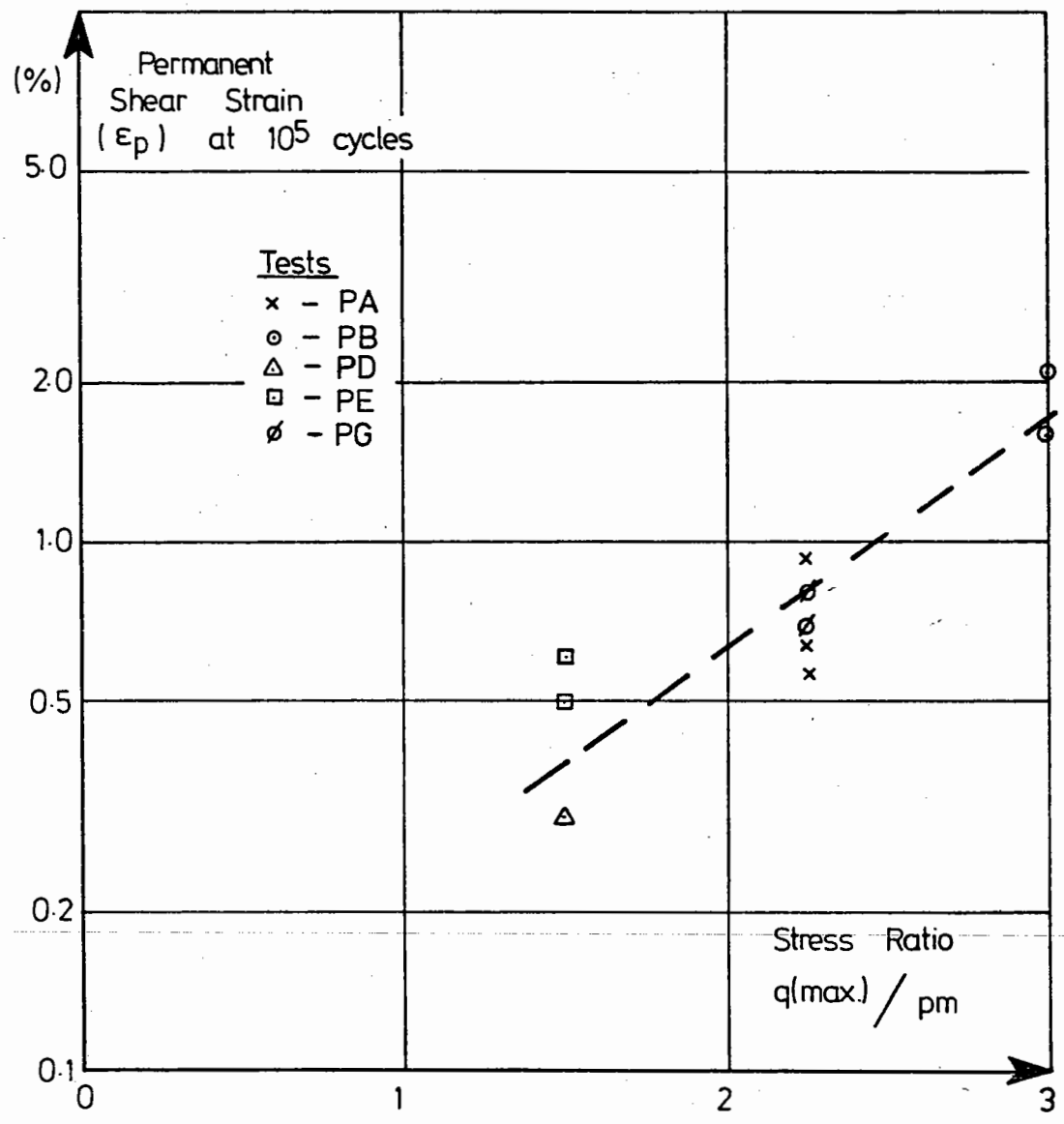

FIG. 9.9 RELATIONSHIP BETWEEN PERMANENT SHEAR STRAIN AND THE APPLIED STRESS RATIO, q_{max}/p_m

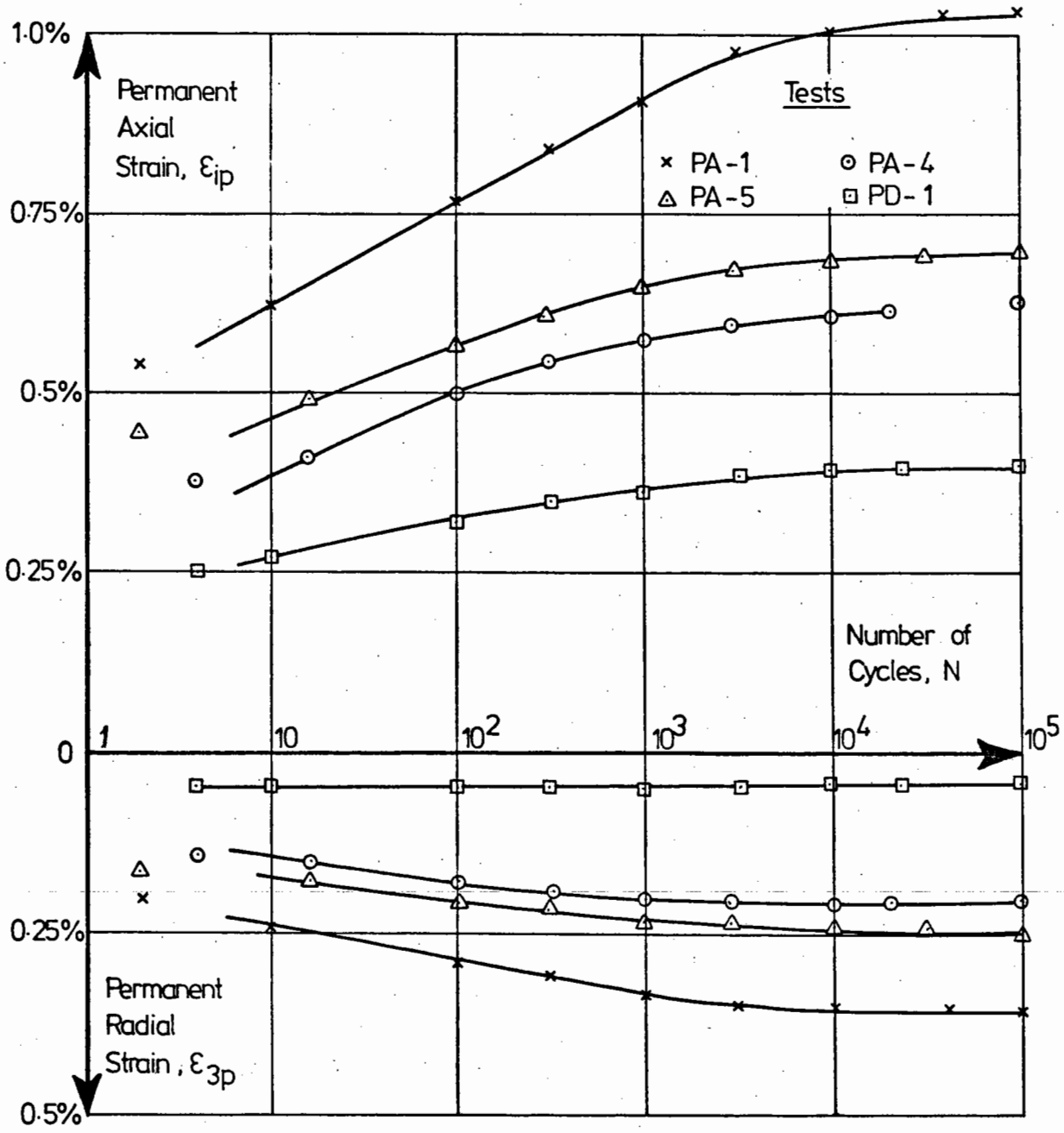

FIG. 9.10 RELATIONSHIP BETWEEN PERMANENT STRAIN AND NUMBER OF LOAD CYCLES FOR TESTS PA-1, PA-4, PA-5 AND PD-1

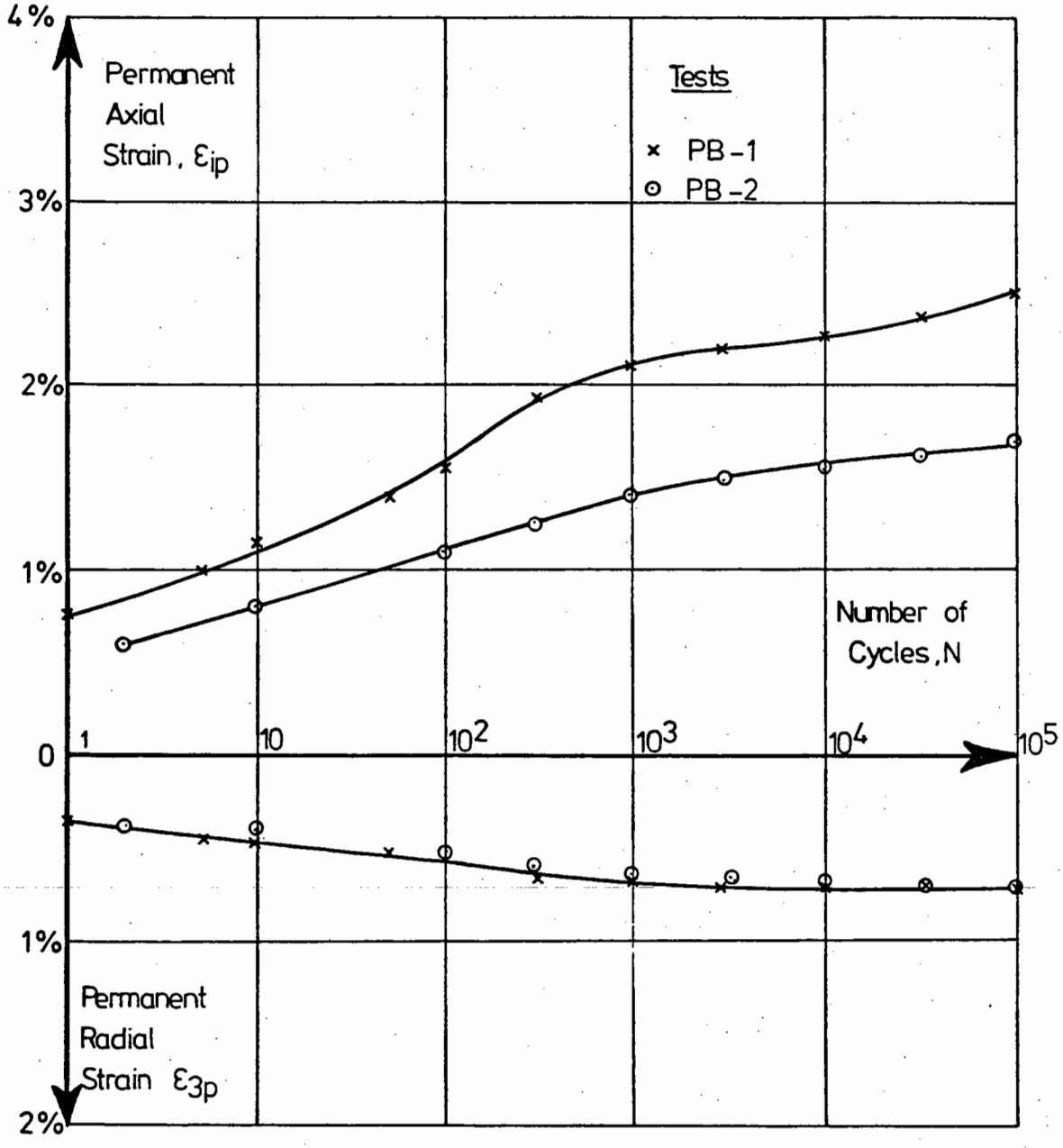

FIG. 9.11 RELATIONSHIP BETWEEN PERMANENT STRAIN AND NUMBER OF LOAD CYCLES FOR TESTS PB-1 AND PB-2

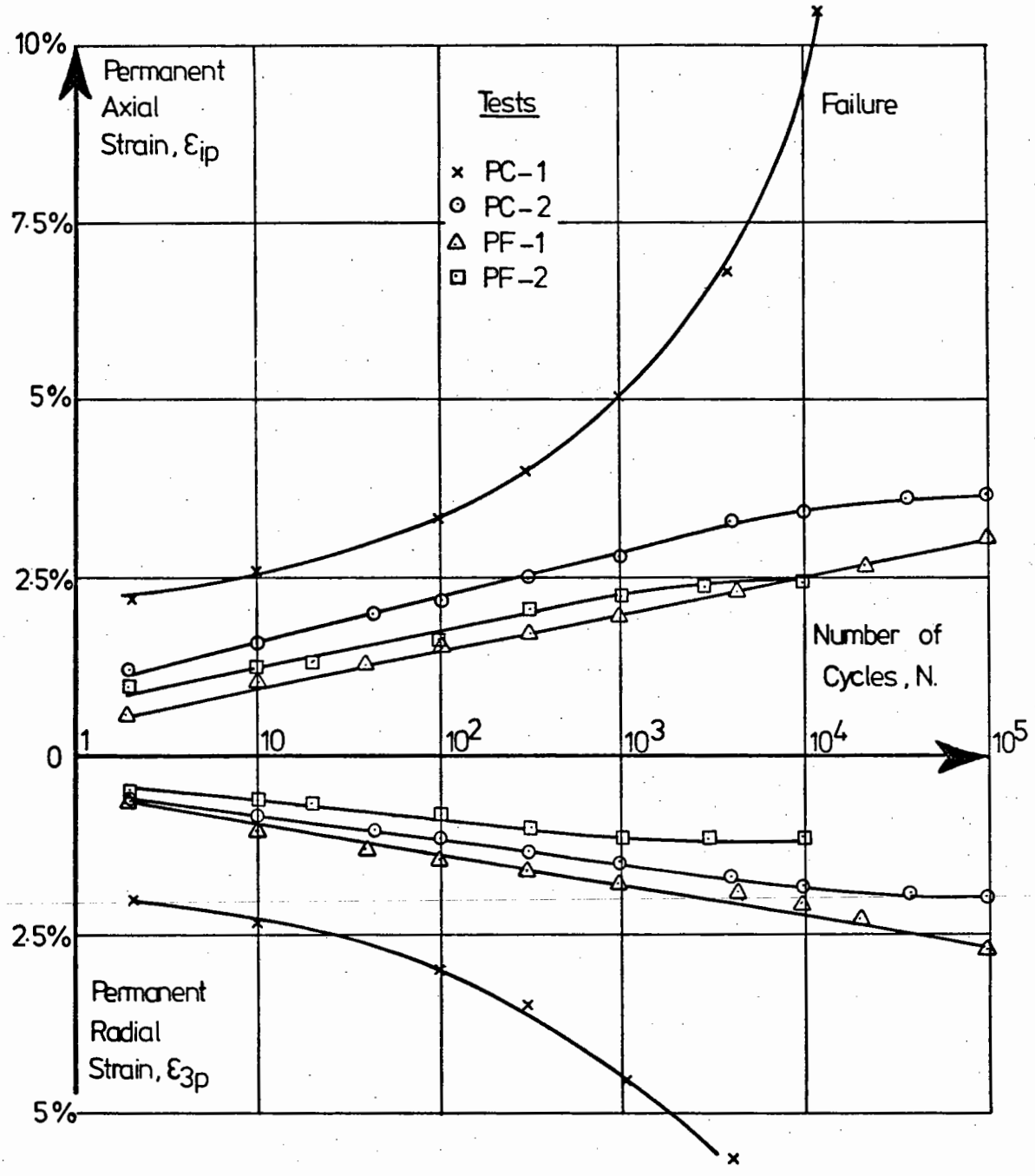

FIG. 9.12 RELATIONSHIP BETWEEN PERMANENT STRAIN AND NUMBER OF LOAD CYCLES FOR TESTS PC-1, PC-2, PF-1 AND PF-2

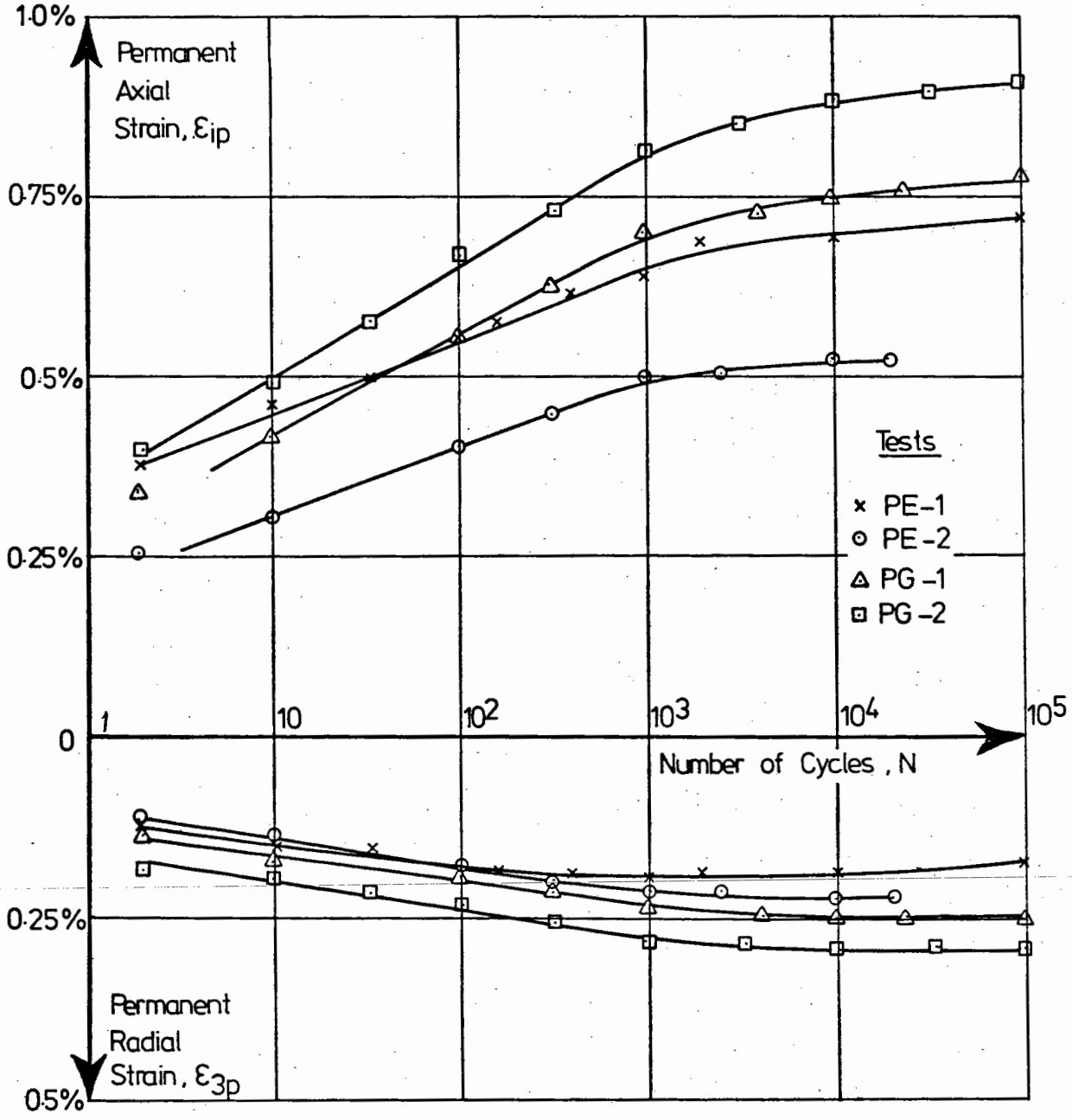

FIG. 9.13 RELATIONSHIP BETWEEN PERMANENT STRAIN AND NUMBER OF LOAD CYCLES FOR TESTS PE-1, PE-2, PG-1 AND PG-2

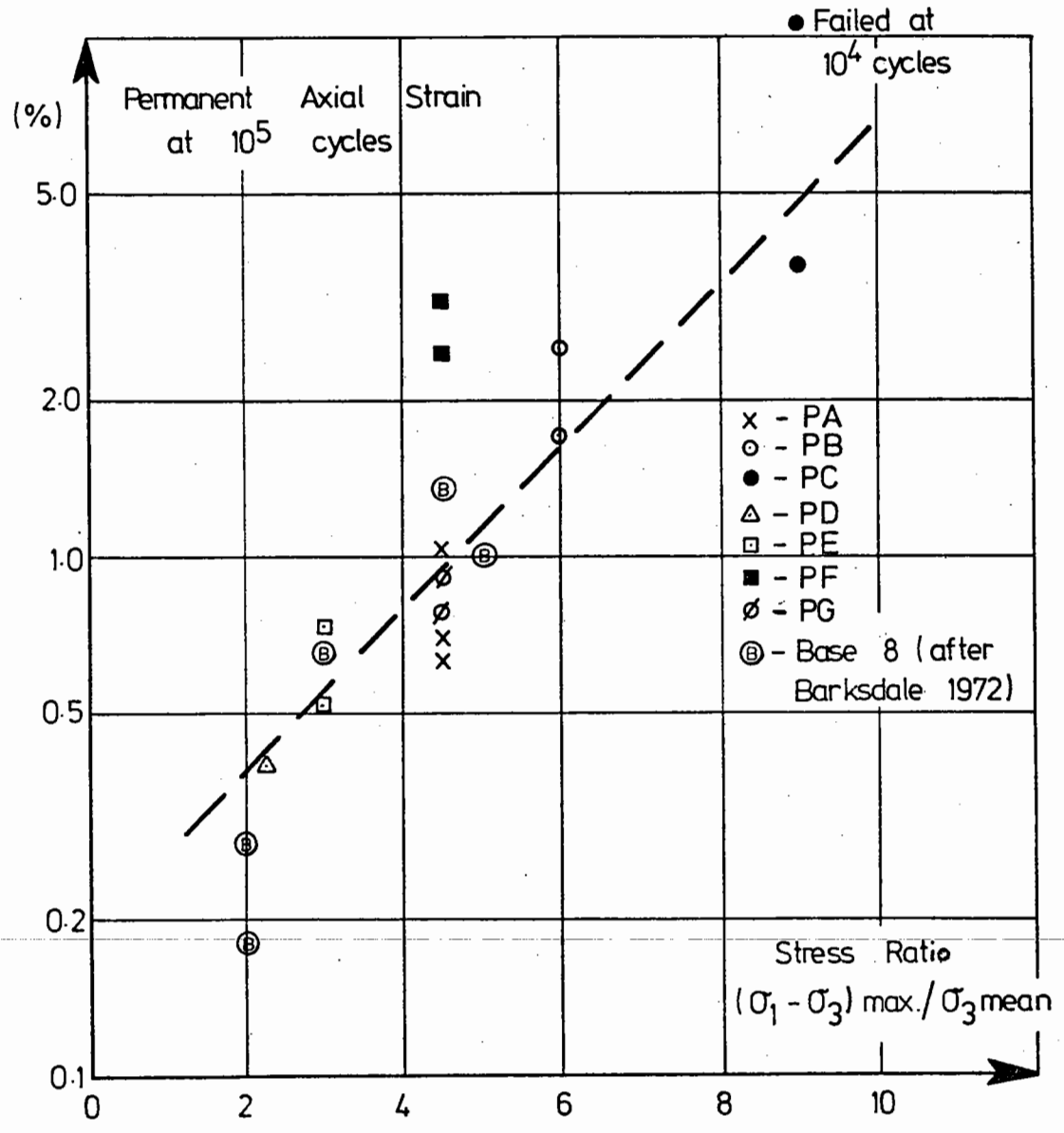

FIG. 9.14 RELATIONSHIP BETWEEN PERMANENT AXIAL STRAIN AND THE APPLIED STRESS RATIO, $(\sigma_1 - \sigma_3)_{max}/\sigma_{3mean}$

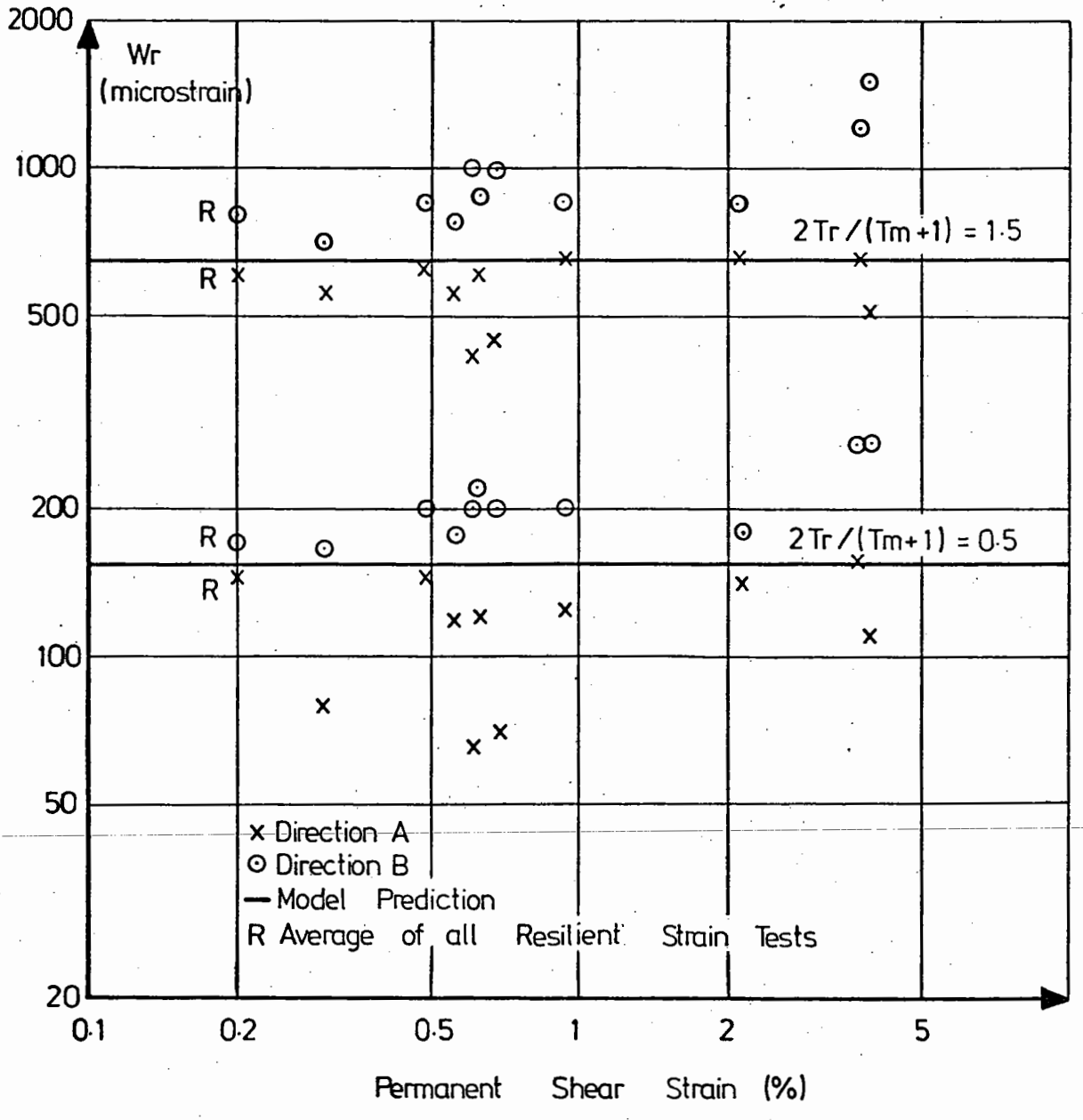

FIG. 9.15 EFFECT OF PERMANENT STRAIN ON THE RESILIENT STRAIN PARAMETER, W_r

CHAPTER TEN

APPLICATION OF RESULTS TO PAVEMENT DESIGN

10.1 EXISTING METHODS FOR THE STRUCTURAL ANALYSIS OF PAVEMENTS CONTAINING A GRANULAR LAYER

Generally speaking, a flexible pavement can be considered as a semi-infinite structure consisting of 3 or 4 layers of different materials. Analysis of the stresses and strains which occur in this structure as the result of a superimposed wheel load requires that the resilient behaviour of the materials in each layer is specified. The computed stresses and strains can then be compared with certain design criteria which are related to the design life of the pavement. The most commonly used criteria are:

(1) Tensile strain in the bituminous layer (related to fatigue life).

(2) Tensile stress in the granular layer.

(3) Vertical compressive stress in the subgrade (related to permanent deformation in that layer).

Discussion here deals primarily with the second criterion, tensile stress in the granular layer. Unbound granular material cannot sustain tension, and therefore if the tensile stress produced by a passing wheel load is greater than the initial compressive stress in the material, it will 'fail'. This initial compressive stress comes from the weight of overlying material and possibly from suction forces if moisture is present. However, the stiffness of the granular layer will have a considerable influence on the tensile strain at the bottom of the bituminous layer and on the vertical stress in the subgrade. If a particular layer is very stiff, it will sustain the applied loads without

imposing large stresses and strains on the adjacent layers, but if its stiffness is low, the adjacent layers may easily become overstressed.

Two methods are available for analysing the stress distribution in a pavement structure, the integral transform method (Peutz et al, 1968; Thrower, 1968; and Warren and Dieckman, 1963) and finite element methods (Duncan et al, 1968; and Dehlen, 1969).

10.1.1 Integral Transform Method

In this method, the pavement is divided horizontally into a number of layers, and each layer is assumed to be linear elastic with uniform behaviour throughout the layer. The elastic properties are normally specified by assigning to each layer values of the resilient modulus, E_r, and resilient Poisson's ratio, ν_r. In a granular layer, for which the stiffness is highly stress dependent, this is a substantial simplification, and choosing suitable values for E_r and ν_r is difficult.

In Chapter 2, it was shown that E_r is largely dependent on the mean normal stress, p_m, and that under certain restricted conditions:

$$E_r = K_1 p_m^{K_2} \qquad (10.1)$$

where K_1 and K_2 are constants.

In a typical pavement, the mean normal stress in the granular layer might vary from 5 to 200 kN/m^2 and hence the resilient modulus might vary by a factor of 10 or more (assuming $K_2 = 0.67$).

In pavement analyses based on this method, the problem has been avoided in one of two different ways. The first method is to assume an arbitrary value for the stiffness of the granular layer of $2\frac{1}{2}$ times that of the underlying subgrade (Brown and Pell, 1972). The justification for this is that it agrees with stiffness measurements made on pavement structures by Heukelom and Klomp (1962) and with a theoretical model,

involving decompaction of the material under tensile stress, which they put forward to explain their stiffness measurements. These stiffness measurements were made by a wave propagation technique which does not produce stresses in the material comparable with those produced by a wheel load, and their theoretical model does not take into account the non-linearity of granular materials or their observed behaviour in the laboratory.

It has been observed that granular materials cannot be compacted to their maximum density on a weak subgrade and hence the subgrade stiffness may have some effect on the stiffness of the granular layer above. However, laboratory studies (Hicks, 1970) have indicated that the stiffness of the material is influenced to a greater degree by the applied stress level than by the density.

The use of this modular ratio between the subgrade and the granular base layer in a pavement analysis will invariably predict a certain amount of tensile lateral stress at the bottom of the granular layer. Brown and Pell (1972) postulated as a design criterion that the material will sustain a tensile lateral stress of half the compressive vertical stress plus the horizontal overburden pressure. This is unrealistic as samples of the material in the laboratory fail when both the vertical stress and the lateral stress are compressive if sufficiently high stress ratios are reached, and the material certainly cannot sustain tension under any conditions.

The second method involves an iterative process (Hicks and Monismith, 1972). After determining an initial stress distribution in the pavement, the modulus of the granular layer is calculated from a relationship such as equation 10.1, using a representative value of stress, for example that at the centre of the layer directly under the wheel load. The

structure is then re-analysed and further adjustments made if necessary. This method may give a good indication of the influence of the granular layer on the adjacent layers in the pavement. However, the stresses and strains indicated in the granular layer itself will not be accurate and will not allow any assessment to be made of whether the stress ratios in the layer are high enough to cause failure or large permanent deformations.

The use of the integral transform method may be quite satisfactory for the overall analysis of a pavement structure but it cannot be used to assess the behaviour of the granular layer in detail.

10.1.2 Finite Element Method

In this method, the structure is divided into elements both horizontally and vertically. For pavement structures, an axisymmetrical arrangement of elements is normally used. Each element is assigned appropriate stiffness coefficients, and then with suitable boundary conditions the structure can be solved to find the stress and strain distributions due to an applied load. The method is well described by Taylor (1971). To incorporate non-linear materials, an incremental or iterative procedure is used in which the element stiffnesses are adjusted after each stage of the calculation to take account of the state of stress existing in the element. Relaxation techniques can also be employed to eliminate regions of tension or high stress ratio by redistribution of the stresses (Kirwan and Snaith, 1975; Barker, 1976).

The finite element method requires rather more computing time than the integral transform method, but the results give a much better indication of the stress distribution in the granular layer when appropriate non-linear stress-strain relationships are specified (Dehlen, 1969; Barksdale and Hicks, 1975). Existing finite element

programs require input data for non-linear materials in the form of a relationship between the elastic constants (E and ν, or G and K) and the stress in the material. The modifications which would be required to use the resilient strain model developed in Chapter 8 in a finite element program are discussed in the next section.

10.2 USE OF THE RESILIENT STRAIN MODEL

The resilient strain model developed in Chapter 8 enables the resilient strain in the material to be calculated for any applied axisymmetric stresses and a simple numerical example is given below. Before the model can be incorporated into a finite element calculation, it must be extended to cover three-dimensional stress systems.

10.2.1 Simple Numerical Example

From the results of the resilient strain tests, it was found that the relationship between the resilient strain parameters, $(W_r)_A$ and $(W_r)_B$, and the stress parameters, T_A and T_B was:

$$W_r = \left(\frac{p_m}{K}\right)^n \sinh(2T_r/(T_m + 1)) \qquad (10.2)$$

for both the A and B directions.

The stress components (T) and the strain components (W) were developed from triaxial tests in which the material was subjected to a normal stress (p) and a deviator stress (q). If the definitions of T and W are rewritten in terms of principal stress and principal strain, they become:

$$T_A = \left(\frac{5}{3}\sigma_1 - \frac{2}{3}\sigma_3\right)/p_m$$

$$T_B = \left(-\frac{1}{3}\sigma_1 + \frac{4}{3}\sigma_3\right)/p_m \qquad (10.3)$$

and
$$W_A = \frac{7}{3}\epsilon_1 + \frac{2}{3}\epsilon_3$$
$$W_B = \frac{1}{3}\epsilon_1 + \frac{8}{3}\epsilon_3 \qquad (10.4)$$

Consider a point in the granular base layer of a flexible pavement directly below a passing wheel load. Assume that the stresses at this point have been estimated as a vertical stress (σ_1) of 150 kN/m^2 and a horizontal stress ($\sigma_2 = \sigma_3$) of 50 kN/m^2 due to the wheel load. If there is 200 mm of overlying material in the road, with a density of 2,500 kg/m^3, there will be a vertical overburden pressure of 5 kN/m^2, and if the coefficient of lateral pressure (K_o) is taken as one, the horizontal stress due to this overburden will also be 5 kN/m^2.

The principal stresses at this point then have mean and repeated components as follows (in kN/m^2):

$$\sigma_{1m} = 80 , \quad \sigma_{1r} = 150$$

and $$\sigma_{2m} = \sigma_{3m} = 30 , \quad \sigma_{2r} = \sigma_{3r} = 50$$

Therefore, the mean normal stress, p_m, = 46.7 kN/m^2. These values can then be substituted in equation 10.3 to find the stress parameters:

$$(T_m)_A = 2.40 , \quad (T_r)_A = 4.62$$

$$(T_m)_B = 0.28 \text{ and } (T_r)_B = 0.36$$

The values of $(T_m)_A$ and $(T_r)_A$ can now be inserted in equation 10.2 with the values of the constants K and n which were found in the resilient strain tests to give the strain parameters:

$$(W_r)_A = 1393\ \mu\epsilon$$

and inserting the values of $(T_m)_B$ and $(T_r)_B$:

$$(W_r)_B = 111\ \mu\varepsilon$$

Equation 10.4 can now be solved to give the principal strains:

$$\varepsilon_{1r} = 607\ \mu\varepsilon \quad \text{and} \quad \varepsilon_{3r} = -34\ \mu\varepsilon$$

This indicates that at the point under consideration the wheel load would produce a compressive vertical strain of 607 microstrain and a tensile radial strain of 34 microstrain. If some anisotropy was assumed so that $(W_r)_A$ was 20% less and $(W_r)_B$ was 20% greater, the same stresses would produce a compressive vertical strain of 481 microstrain and a tensile radial strain of 10 microstrain. Results from a variety of other applied stresses are given in Section 10.2.4.

10.2.2 Extension of the Model to Three Dimensions

At first sight, the A and B directions to which the resilient behaviour of the material is related appear to be independent. However, if the B direction is split into two directions (B and C) on opposite sides of the p-q plane, the three directions are found to be symmetrical in principal stress space. The stress components in three dimensions can then be defined as:

$$\begin{aligned} T_A &= \left(\tfrac{5}{3}\sigma_1 - \tfrac{1}{3}\sigma_2 - \tfrac{1}{3}\sigma_3\right)/p_m \\ T_B &= \left(-\tfrac{1}{3}\sigma_1 + \tfrac{5}{3}\sigma_2 - \tfrac{1}{3}\sigma_3\right)/p_m \\ T_C &= \left(-\tfrac{1}{3}\sigma_1 - \tfrac{1}{3}\sigma_2 + \tfrac{5}{3}\sigma_3\right)/p_m \end{aligned} \qquad (10.5)$$

and the strain components as:

$$W_A = \tfrac{7}{3}\varepsilon_1 + \tfrac{1}{3}\varepsilon_2 + \tfrac{1}{3}\varepsilon_3$$

$$W_B = \frac{1}{3}\epsilon_1 + \frac{7}{3}\epsilon_2 + \frac{1}{3}\epsilon_3 \qquad (10.6)$$

$$W_C = \frac{1}{3}\epsilon_1 + \frac{1}{3}\epsilon_2 + \frac{7}{3}\epsilon_3$$

The symmetry of the directions can be seen from these definitions, and it will be observed that if $\sigma_2 = \sigma_3$, equations 10.5 and 10.6 revert to equations 10.3 and 10.4. Therefore, to extend the resilient strain model to three dimensions, the basic stress-strain relationships (equation 10.2) remain unaltered if the components of stress and strain are redefined.

These relationships can be expressed more conveniently in matrix form:

$$[T] = \frac{[M]}{p_m} \cdot [\sigma] \qquad (10.7)$$

$$[W] = [N] \cdot [\epsilon] \qquad (10.8)$$

$$[W_r] = \left(\frac{p_m}{K}\right)^n \cdot [L_r] \cdot [T_r] \qquad (10.9)$$

where $[M]$ and $[N]$ are change of reference matrices defined by equations 10.5 and 10.6 and $[L_r]$ is a flexibility matrix of the form:

$$\begin{bmatrix} (L_r)_A & 0 & 0 \\ 0 & (L_r)_B & 0 \\ 0 & 0 & (L_r)_C \end{bmatrix}$$

where $$L_r = \sinh(2T_r/(T_m + 1))/T_r \qquad (10.10)$$

Equations 10.7 to 10.9 can be combined to give a complete stress-strain equation for the material:

$$[\epsilon_r] = \frac{[N]^{-1} \cdot [L_r] \cdot [M]}{K^n \cdot p_m^{(1-n)}} \cdot [\sigma_r] \qquad (10.11)$$

10.2.3 Use of the Model in Finite Element Calculations

In theory, there is no reason why equation 10.11 should not be used as the basis for defining the flexibility of an element in a finite element array. To do so would require some rewriting of the program and could not be done by using the facilities for a stress dependent modulus available in existing finite element programs.

The principal stresses $[\sigma]$, together with their orientation $[\alpha]$ can be related to the direct and shear stresses $[S]$ acting on each element in the x, y and z directions.

$$[\sigma_r] = [R_\alpha].[S_r] \qquad (10.12)$$

$$[\sigma_m] = [R_\alpha].[S_m] \qquad (10.13)$$

Similarly, the principal strain matrix is related to the direct and shear strains $[U_r]$:

$$[\epsilon_r] = [R_\alpha].[U_r] \qquad (10.14)$$

It will be observed that the same orientation matrix $[R_\alpha]$ has been used in each case, assuming that the principal repeated stresses, the principal mean stresses and the principal resilient strains all have the same spatial orientation. In fact, the assumption is implicit in the resilient strain model and could not be otherwise in a model derived from triaxial tests where no rotation of the principal stresses is possible. This assumption may not hold for an element in a pavement structure, and it is suggested that the matrix $[R_\alpha]$ should be based on the orientation of the principal repeated stresses in which case the matrix $[\sigma_m]$ will represent mean stresses in the same direction although these may not be principal mean stresses. The principal resilient strains will be in the same direction as the principal resilient stresses.

The flexibility of the material in an element can now be defined by the matrix:

$$\frac{[R_\alpha]^{-1}.[N]^{-1}.[L_r].[M].[R_\alpha]}{K^n.p_m^{(1-n)}}$$

It is normally assumed in finite element programs that the flexibility and stiffness matrices will be symmetrical, and this significantly reduces the storage requirements and the computing time. This condition is only fulfilled by the matrix above if

either $$(L_r)_A = (L_r)_B = (L_r)_C \qquad (10.15)$$

or $$[N]^{-1} = k[M] \qquad (10.16)$$

where k is a scalar.

The first alternative only applies close to the space diagonal in principal stress space, and it is an essential feature of the model that the material becomes progressively more anisotropic away from the space diagonal.

The other alternative specifies a relationship between the stress directions (A, B and C) and the corresponding strain directions. This relationship does not hold for the model. From equations 10.5 and 10.6:

$$[M] = \frac{1}{3}\begin{bmatrix} 5 & -1 & -1 \\ -1 & 5 & -1 \\ -1 & -1 & 5 \end{bmatrix} \qquad (10.17)$$

$$[N] = \frac{1}{3}\begin{bmatrix} 7 & 1 & 1 \\ 1 & 7 & 1 \\ 1 & 1 & 7 \end{bmatrix} \qquad (10.18)$$

Therefore:

$$[N]^{-1} = \frac{1}{18}\begin{bmatrix} 8 & -1 & -1 \\ -1 & 8 & -1 \\ -1 & -1 & 8 \end{bmatrix} \qquad (10.19)$$

and it can be seen that $[N]^{-1}$ is not a scalar multiple of $[M]$.

However, if the A, B and C directions are redefined so that:

$$[M'] = \frac{1}{4}\begin{bmatrix} 6 & -1 & -1 \\ -1 & 6 & -1 \\ -1 & -1 & 6 \end{bmatrix} \qquad (10.20)$$

$$\text{and} \qquad [N'] = \frac{3}{7}\begin{bmatrix} 5 & 1 & 1 \\ 1 & 5 & 1 \\ 1 & 1 & 5 \end{bmatrix} \qquad (10.21)$$

$$\text{then} \qquad [N']^{-1} = \frac{1}{12}\begin{bmatrix} 6 & -1 & -1 \\ -1 & 6 & -1 \\ -1 & -1 & 6 \end{bmatrix} \qquad (10.22)$$

and $[N']^{-1}$ is a scalar multiple of $[M]$, then the flexibility matrix of the element will be symmetrical, and the essential features of the resilient strain model are preserved. It is shown in Appendix E that the resilient strain test data will fit a model incorporating this adjustment as well as the original model, and that the change will make a difference of about 2-3% in the calculation of resilient strain.

To make allowance in the calculation for material with some inherent anisotropy would be possible by making suitable adjustments to the element flexibility matrix. However, it is probably not justified until some evidence can be obtained of what types of anisotropy are inherent in site compacted material.

10.2.4 Comparison between Three Theoretical Models

To determine if the proposed resilient strain model indicates substantially different stress distributions in the granular layer of a pavement to those indicated by existing methods would require this model to be incorporated in a finite element analysis as described in the previous section. No such analysis is available at the present time and so a simpler method of comparison has been adopted.

Three different theoretical models were used to calculate the strain in a layer of granular material subject to various stresses that might be caused directly below a passing wheel load. The stress-strain relationship used in these calculations is given in Eqn. 10.11, different coefficients being used in the flexibility matrix, L_r, for each calculation. In all cases, K was taken as 6.8×10^{-6} kN/m^2 and n as 0.33. Because of the symmetry, $\sigma_2 = \sigma_3$ (lateral stress), and $(L_r)_B = (L_r)_C$.

(1) Simple Model, $(L_r)_A = (L_r)_B = 1$

This model is similar to that found by previous investigators (see Section 8.4.1) and can be rewritten as:

$$E_r = 1.29 \times 10^6 . K^n . p_m^{(1-n)} ; \quad \nu_r = 0.29$$

(2) Isotropic Model, $L_r = \sinh(2T_r/(T_m + 1))/T_r$

This is the model developed from the resilient strain test data.*

(3) Anisotropic model, similar to (2) except that $(L_r)_A$ was reduced by 20% and $(L_r)_B$ was increased by 25%. This model would be typical of the resilient behaviour observed in the permanent strain tests after large numbers of load cycles.

* This model allows for stress induced anisotropy but not anisotropy inherent in the material.

The imposed stresses chosen for these calculations cover a wide range and are about the right order of magnitude for the stresses in the granular layer of a road pavement. They are shown as stress paths in a p-q diagram in Fig. 10.1. Initially, the material is assumed to be under a small effective normal stress of 20 kN/m^2. This might be 5 kN/m^2 caused by a 200 mm of overlying material (density 2,500 kg/m^2, and a coefficient of lateral pressure (K_o) of 1) plus 15 kN/m^2 suction due to the presence of moisture.

Table 10.1 shows the vertical stress and lateral stress applied and the resilient strain as calculated by each model. The equivalent values of resilient modulus, E_r, and resilient Poisson's ratio, ν_r, which would give the same strain are also shown. It can be seen that there is a considerable region (represented by stress paths E, F, G, H, J, K, L and M) for which there is good agreement between the simple model and the isotropic model. For these stress paths the resilient Poisson's ratio is 0.29 and in fact the isotropic model indicates somewhat smaller variation in the resilient modulus than the simple model. However, when higher stress ratios are applied (stress paths B, D and P) there is considerable divergence between the two models with the simple model underpredicting strain largely because of the constant value of Poisson's ratio which it employs. As one would expect, the anisotropic model predicts strains up to 25% greater or smaller than the isotropic model depending on the ratio of the applied stresses.

In the region of agreement between the simple model and this isotropic model, the equivalent values of Poisson's ratio, ν_r, are virtually constant at 0.29 and the equivalent values of resilient modulus, E_r, range between 226 and 296 MN/m^2. This is not a large range and at

Table 10.1

Comparison Between Three Resilient Strain Models

(1) Simple Model, (2) Isotropic Model, (3) Anisotropic Model.

	Vertical stress (kN/m^2)	Lateral stress (kN/m^2)	Model	Vertical strain ($\mu\varepsilon$)	Lateral strain ($\mu\varepsilon$)	Equivalent Values	
						E_r (MN/m^2)	ν_r
A	20	-10	(1)	142	-71	181	0.29
			(2)	139	-111	-	-
			(3)	124	-133	-	-
B	40	-20	(1)	284	-142	181	0.29
			(2)	655	-1518	-	-
			(3)	715	-1885	-	-
C	50	0	(1)	219	-63	228	0.29
			(2)	237	-85	211	0.36
			(3)	197	-94	254	0.48
D	100	0	(1)	368	-105	271	0.29
			(2)	463	-224	216	0.48
			(3)	363	-257	255	0.65
E	50	12.5	(1)	171	-21	250	0.29
			(2)	189	-24	226	0.29
			(3)	152	-19	283	0.29
F	100	25	(1)	275	-34	311	0.29
			(2)	347	-43	247	0.29
			(3)	278	-35	309	0.29
G	50	25	(1)	132	13	271	0.29
			(2)	151	16	238	0.29
			(3)	116	29	345	0.20
H	100	50	(1)	205	20	349	0.29
			(2)	269	26	265	0.29
			(3)	207	49	381	0.21
J	50	50	(1)	69	69	311	0.29
			(2)	84	84	256	0.29
			(3)	55	111	-	-
K	100	100	(1)	103	102	418	0.29
			(2)	141	141	296	0.29
			(3)	92	187	-	-
L	20	50	(1)	-30	104	288	0.29
			(2)	-35	123	244	0.29
			(3)	-44	153	196	0.29
M	40	100	(1)	-45	159	377	0.29
			(2)	-61	214	281	0.29
			(3)	-76	267	225	0.29
N	0	25	(1)	-63	78	228	0.29
			(2)	-88	84	196	0.34
			(3)	-80	101	178	0.28
P	0	50	(1)	-105	132	271	0.29
			(2)	-237	166	176	0.42
			(3)	-208	196	167	0.35

first sight it might seem to justify the use of linear elastic methods of analysis. However, the range of applied stress ratios covered by this region is limited:

$$-0.75 < q/p < +1.5$$
$$0.4 < \sigma_1/\sigma_3 < 4.0 \qquad (10.23)$$

Pavement analyses (including those using the integral transform method) generally indicate a considerable region underneath the wheel load where these limits are exceeded (Stock, 1976). The finite element technique proposed by Barker (1976) of using the simple model together with relaxation techniques to eliminate regions of high stress ratio may produce good agreement over a wider range of behaviour. However, the model used here avoids the discontinuous change in behaviour which this Elasto-Plastic analysis employs.

10.3 PERMANENT DEFORMATION

In the majority of the permanent strain tests, the permanent axial strain stabilised towards the end of the test at a value of less than 2.5%. If this amount of deformation occurred throughout a layer of granular material 200 mm thick, it would make a contribution of less than 5 mm to the permanent deformation at the surface. Surface deformation does not become serious until it reaches about 20 mm and therefore a contribution of less than 5 mm from the granular layer does not seem unreasonable.

In those tests where the permanent strain reached more than 2.5%, the applied stress ratio was quite high ($q/p = 2.25$, that is, $\sigma_1/\sigma_3 = 10$) and therefore to predict when granular material will be subject to high stress ratios is an important factor in determining permanent deformation.

In the previous section it was shown that the simple resilient strain model ($E_r = k_1 p_m^{k_2}$) predicted the resilient behaviour quite well except at high stress ratios ($q/p > 1.5$, that is, $\sigma_1/\sigma_3 > 4$). Therefore, the use of this simple model in analysis may not give a true picture of which regions in the layer are subject to stress ratios high enough to produce substantial permanent strain.

10.4 COMPARISON BETWEEN LABORATORY AND FULL SCALE CONDITIONS

When using the results of laboratory tests to analyse the behaviour of full scale pavement structure, it is important that the differences between the two situations are fully appreciated. Some of the work which is required to explore the effect of these differences is mentioned in Chapter 12. They do not invalidate the work done in the laboratory but indicate that caution must be exercised when applying the results.

The first point to make is that all the work described in Chapters 8 and 9 was concerned with the behaviour of a single material, a crushed limestone aggregate of a particular grading and density. Other work in this field (Hicks, 1970; Barksdale, 1972; and Kennedy, 1974) has compared several granular materials without investigating their behaviour under different stress conditions in as much detail. The behaviour of granular materials in a pavement structure must be considered in the context of both the detailed work described here on one material and the comparison found by other workers between materials of different aggregate types, gradings and densities.

Moisture content does have an effect on granular materials (Hicks, 1970) and there is some evidence that this can be dealt with by the theory of effective stress. Drainage conditions must be considered carefully in this context.

When compacting small samples of material in the laboratory, it is impossible to reproduce the methods used in road construction. In the absence of any evidence to the contrary, it must be assumed that site compacted material behaves in a similar way to material compacted in the laboratory to the same grading and density. There was some evidence from the laboratory tests that the large numbers of load cycles applied in the permanent strain tests caused some inherent anisotropy in the material. It would be reasonable to assume that some degree of anisotropy also develops in the granular layers of a road. However, the type of anisotropy may well be affected by the shear reversal that takes place during traffic loading, and by the methods used in compacting the material.

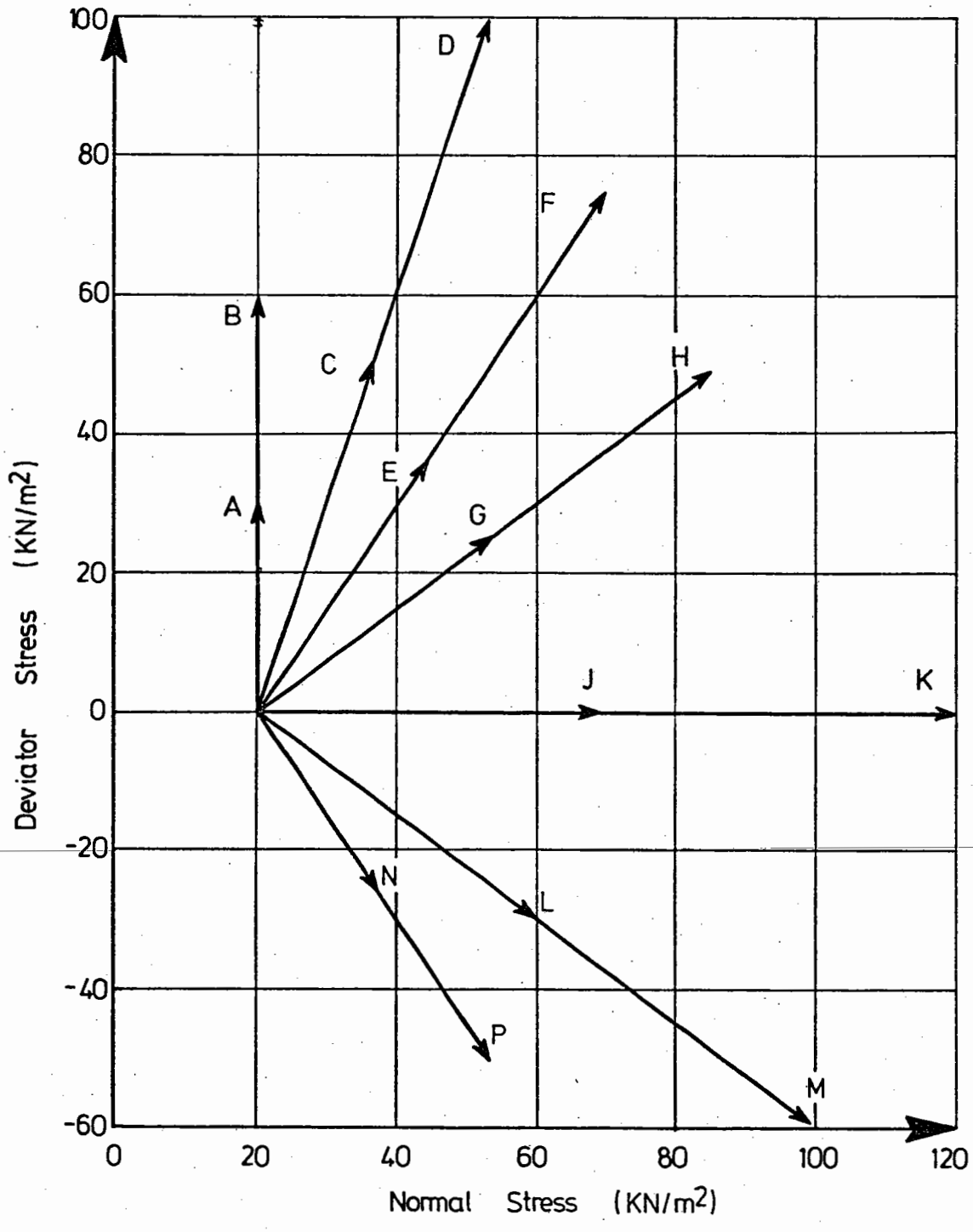

FIG. 10.1 STRESS PATHS USED IN THE COMPARISON BETWEEN THE THREE RESILIENT STRAIN MODELS

CHAPTER ELEVEN

CONCLUSIONS

After carrying out a large number of triaxial tests on samples of a well-graded crushed limestone (maximum particle size 38 mm), all compacted to the same density in a dry state, the following conclusions have been reached.

11.1 SINGLE LOADING

From the single loading tests described in Section 7.1, the material was found to have no cohesion and an angle of shear resistance, φ', of 53°.

11.2 RESILIENT BEHAVIOUR UNDER REPEATED LOADING

From the preliminary tests described in Chapter 7 it was found that:

(a) Frequency of loading in the range 0.1 to 20 Hz has little effect on the behaviour of the material.

(b) The material is subject to stress history effects, but these can be reduced by using only a few load cycles and by avoiding high stress ratios.

From the resilient strain tests, described in Chapter 8, it was found that:

(c) There are two particular directions of repeated stress which can be applied in the p, q plane for which the resulting strain directions in the v, ϵ plane are independent of the mean stress conditions of the material.

(d) The resilient stress-strain relationship for the material can be expressed in the form:

$$(W_r)_A = (p_m/K_A)^n \sinh[2(T_r)_A/((T_m)_A + 1)]$$
$$(W_r)_B = (p_m/K_B)^n \sinh[2(T_r)_B/((T_m)_B + 1)] \qquad (11.1)$$

where $K_A = K_B = 6.8 \times 10^{-6}$ kN/m^2, $n = 0.33$

and W_r has units of microstrain.

W_r, T_r and T_m are components of resilient strain, repeated stress and mean stress respectively in the directions referred to in conclusion (c). They are defined in Chapter 8.

(e) Under restricted conditions, when q_m, q_r and p_r are small compared with p_m, the material behaves isotropically with a resilient modulus given by the equation:

$$E_r = 24{,}000\ p_m^{0.67} \text{ kN/m}^2 \qquad (11.2)$$

and a resilient Poisson's ratio of 0.29.

From the permanent strain tests, described in Chapter 9, it was found that:

(f) After a large number of load cycles some inherent anisotropy develops which influences the resilient behaviour of the material. This can be incorporated in the stress-strain relationship (Eqn. 11.1) by increasing K_A and reducing K_B.

11.3 PERMANENT STRAIN UNDER REPEATED LOADING

From the permanent strain tests, described in Chapter 9, in which 100,000 load cycles were applied along the same stress path, it was found that:

(a) Except for tests in which a high stress ratio was applied, the permanent strain stabilised towards the end of the test.

(b) For tests in which a high stress ratio was applied, $(q/p)_{max} = 2.25$, the permanent strain was much larger and continued to increase up to the end of the test. Deformation in these tests was accompanied by dilation.

11.4 GENERAL CONCLUSIONS

(a) When testing this material, substantial variations in strain measurement occurred from one sample to another because of the relatively large aggregate particles present. Such variations must be taken into account when considering the results of tests on this type of material.

(b) The analysis of pavement structures containing a layer of granular material must take into account the non-linear behaviour of that material, if a realistic assessment is required of the stresses and strains within the granular layer.

(c) Theoretical concepts can be used to extend the stress-strain relationship (Eqn. 11.1) to a three-dimensional form, making it suitable for characterising the material in a finite element analysis.

CHAPTER TWELVE

RECOMMENDATIONS FOR FURTHER WORK

In Section 10.4 a comparison was made between conditions in laboratory tests and those in the granular layer of a flexible pavement. Most of the work recommended below is designed to assess the significance of the differences between these two situations. The aim is to provide a sound theoretical framework within which the behaviour of granular materials can be described, and which encompasses the full range of conditions from those possible in laboratory tests to those appertaining to a full scale pavement under traffic.

These recommendations are restricted to the stress-strain behaviour of granular materials but some data is lacking in the basic properties of granular materials, especially permeability. Also, a theoretical mechanism of the interaction between aggregate particles would be useful to explain the observed stress-strain behaviour and the related phenomenon of compaction.

12.1 FURTHER WORK ON THE SAME MATERIAL

The work done under this contract has enabled the resilient behaviour of a particular material in its dry state to be fully characterised within the limits of the triaxial test. Some useful data has also been obtained on permanent strain behaviour, but this aspect requires further study so that a relationship between permanent strain and the applied stress path can be established. However, tests in which large numbers of load repetitions are applied on the same stress path may not be the best way of proceeding because of the limited amount of information which can be gained from each sample. It may be

more fruitful to first establish the role of dilation and compaction during permanent strain and the effect of preloading to various stress levels at the start of a test.

Further information can be obtained on the effect of permanent strain on resilient strain behaviour as further permanent strain tests are carried out. It would be interesting to know whether the anisotropy caused by permanent strain is biased in the opposite direction by permanent strain tests in axial extension.

12.2 EFFECT OF MOISTURE CONTENT ON THE MATERIAL

The most important question here is whether the behaviour of saturated material can be accounted for from the characteristics of the dry material and the theory of effective stress. This could be established by carrying out saturated drained tests, preferably with a pore pressure probe in the centre of the sample to check that there is no appreciable transient pore pressure away from the drainage connections. Undrained tests could then be carried out, and pore pressure measurements (mean and transient) used to compute the effective stress in the material.

Partially saturated material presents a more difficult problem, but it may be possible to infer an equivalent value of suction or pore pressure from the stress-strain behaviour if direct measurements cannot be made.

12.3 PROPERTIES OF OTHER GRANULAR MATERIALS UNDER REPEATED LOADING

Previous work (for instance, Hicks, 1970) has shown that frequency of loading and loading history do not have a significant influence on the behaviour of a wide range of granular materials.

With regard to the effect of applied stress on resilient behaviour, conclusion (c) was that, "there are two particular directions of repeated

stress which can be applied in the p, q plane for which the resulting strain directions in the v, ϵ plane are independent of the mean stress condition of the material". It can only be established if similar directions apply to other types of granular material (i.e. different density, grading or aggregate types) by conducting repeated load triaxial tests with the facility for variable confining stress. If so and the resilient strain model is valid for other types of granular material, the constants K and n in the stress-strain relationship (equation 8.13) could be found by a much simpler test such as the Resonance Test described by Robinson (1974) or the "Static Triaxial Creep Test" suggested by Kalcheff and Hicks (1973). The latter test is essentially a procedure for using the convention triaxial apparatus for conducting slow repeated load tests.

Permanent deformation in granular materials under repeated loading is a complex phenomenon, and there are indications that sample preparation and the strain occurring in the first few load cycles may be important factors. The overall aim should be to link permanent deformation with the behaviour of the same material under single loading, and a useful first step in this process would be to establish a criterion for permanent strain in a particular material with some degree of confidence.

12.4 APPLICATION OF THE TEST RESULTS TO PAVEMENT DESIGN

Finite element programs (Kirwan and Snaith, 1975; Taylor, 1971) are available for the analysis of pavement structures in which one or more layers have stress dependent characteristics. In Section 10.2.3 it was shown that the resilient strain model developed in Chapter 8 could in theory be incorporated into a finite element program. However, to do so would require those parts of the program which set up the

element stiffness matrices to be rewritten. This should be done so that the stress distributions in a pavement structure based on the resilient strain model can be compared with those predicted by other methods.

The principal drawback of the repeated load triaxial test as a means of characterising materials for pavement design is that it cannot reproduce the rotation of principal stresses which occurs under traffic loading. The results of current work using a repeated load simple shear apparatus (Ansell and Brown, 1975) may help to provide an insight into this problem.

REFERENCES

ALLEN, J.J. and THOMPSON, M.R. (1974), "Resilient response of granular materials subjected to time-dependent lateral stresses", Trans. Research Record 510, pp. 1-13.

*

ANSELL, P. and BROWN, S.F. (1975), "The effect of cyclic shear stresses on granular material", Research Report submitted to British Rail and TRRL, Univ. of Nottingham.

BARKER, E.S. (1959), "Subsurface drainage of highways and airports", Committee on Subsurface Drainage, Highway Research Board Bulletin 209.

BARKER, W.R. (1976), "Elasto-plastic analysis of a typical flexible airport pavement", Unpublished Report, W.E.S.

BARKSDALE, R.D. (1972), "Laboratory evaluation of rutting in base course materials", Proc. 3rd Int. Conf. on the Struct. Design of Asphalt Pavements, London, pp. 161-174.

BARKSDALE, R.D. and HICKS, R.G. (1973), "Material characterization and layered theory for use in fatigue analyses", Highway Research Board Special Report 140, pp. 20-48.

BEAVIS, H.M. (1969), "Selection and construction of base course materials in roads", Australian Road Research Board, Bulletin No. 5.

BIAREZ, J. (1962), "Contribution a l'etude des properties mecaniques des sols et des materiau pulerulents", D.Sci. Thesis, Univ. of Grenoble.

BROWN, S.F. (1974), "Repeated load testing of a granular material", Journ. Geot. Eng. Div., ASCE, July.

* Allen, J.J. and Thompson, M.R. (1973), "The effects of non-constant lateral pressures on the resilient response of granular materials", Highway Research Laboratory, Univ. of Illinois.

BROWN, S.F. (1975), Discussion of "Significance of variably confined triaxial testing" by J.J. Allen and M.R. Thompson, Trans. Eng. Journ., ASCE, Vol. 101, No. TE4, November, pp. 832-834.

BROWN, S.F. and BRODRICK, B.V. (1973), "The performance of stress and strain transducers for use in pavement research", Research Report, Univ. of Nottingham.

BROWN, S.F. and BUSH, D.I. (1972), "Dynamic response of model pavement structures", Transportation Engineering Journal, ASCE, Vol. 98, No. TE4, pp. 1005-1022.

BROWN, S.F. and HYDE, A.F.L. (1975), "Significance of cyclic confining stress in repeated load triaxial testing of granular material", Transportation Research Record No. 537, pp. 49-58.

BROWN, S.F. and PELL, P.S. (1972), "A fundamental structural design procedure for flexible pavements", Proc. 3rd Int. Conf. on the Struct. Design of Asphalt Pavements, London, pp. 369-381.

BROWN, S.F. and SNAITH, M.S. (1974), "The measurement of recoverable and irrecoverable deformations in the repeated load triaxial test", Geotechnique, Technical Note, June, pp. 255-259.

BS 1377 (1975), "Methods of testing soils for civil engineering purposes", British Standards Institution.

CHADDOCK, B. (1974), Private Communication.

COFFMAN, B.S., KRAFT, D.G. and TAMAYO, J. (1964), "A comparison of calculated and measured deflections for the AASHO test road", Proc. AAPT, p. 54.

COOPER, S.W. (1973), Private Communication.

CULLINGFORD, G, LASHINE, A.K.F. and PARR, G.B. (1972), "Servo controlled equipment for dynamic triaxial testing of soils", Geotechnique, Vol. 22, No. 3, Technical Note.

DEHLEN, G.L. (1969), "The effect of non-linear material response on the behaviour of pavements subjected to traffic loads", Ph.D. Thesis, Univ. of California.

DEPARTMENT OF THE ENVIRONMENT (1969), "Specification for road and bridge works", HMSO.

DUNCAN, J.M., MONISMITH, C.L. and WILSON, E.L. (1968), "Finite element analysis of pavements", Highway Research Record 228, pp. 18-32.

DUNLAP, W.A. (1963), "A report on a mathematical model describing the deformation characteristics of granular materials", Technical Report No. 1, Project 2-8-62-27, Texas Transportation Institute.

DUNN, C.S. (1966), "The stability of aggregates used in road sub-bases", Roads and Road Construction, Vol. 44, pp. 77-81 and 102-108.

GLYNN, T.E. and KIRWAN (1969), "A stress-strain relationship for clays subjected to repeated loading", Proc. 7th Int. Conf. on Soil Mechs. and Found. Eng., Vol. 1, pp. 159-163.

HARDIN, B.O. and BLACK, W.L. (1966), "Sand stiffness under various triaxial stresses", Journ. Soil Mechs. and Found. Div., ASCE, March.

HAYNES, J.H. and YODER, E.J. (1963), "Effects of repeated loading on the gravel and crushed stone base course materials used in the AASHO Road Test", Highway Research Record No. 39, Highway Research Board.

HEUKELOM, W. and KLOMP, A.J.G. (1962), "Dynamic testing as a means of controlling pavements during and after construction", Proc. Int. Conf. on the Struct. Design of Asphalt Pavements, Ann Arbor, Michigan, pp. 667-679.

HEYMAN, J. (1964), "Beams and framed structures", Pergamon Press.

HICKS, R.G. (1970), "Factors influencing the resilient response of granular materials", Ph.D. Thesis, Univ. of California.

HICKS, R.G. and MONISMITH, C.L. (1971), "Factors influencing the resilient response of granular materials", Highway Research Board, No. 345, pp. 15-31.

HICKS, R.G. and MONISMITH, C.L. (1972), "Prediction of the resilient response of pavements containing granular layers using non-linear elastic theory", Proc. 3rd Int. Conf. on the Struct. Design of Asphalt Pavements, London, pp. 410-429.

HYDE, A.F.L. (1974), "Repeated load triaxial testing of soils", Ph.D. Thesis, Univ. of Nottingham.

KALCHEFF, I.V. and HICKS, R.G. (1973), "A test procedure for determining the resilient properties of granular materials", Journ. Testing and Evaluation, JTEVA, Vol. 1, No. 6, Nov., pp. 472-479.

KENNEDY, C.K. (1971), "Assessment, choice and proposed techniques for apparatus suitable for repeated loading of granular unbound materials", Department Publication No. 39, Dept. of Transportation and Environmental Planning, Univ. of Birmingham.

KENNEDY, C.K. (1974), "An experimental investigation of the behaviour of wet-mix road base material", Ph.D. Thesis, Univ. of Birmingham.

KIRWAN, R.W. and SNAITH, M.S. (1975), "Further investigations towards a rational method of design for flexible pavements, Part II", Final Technical Report, submitted to U.S. Army European Research Office by Trinity College Dublin.

KOLBUSZEWSKI, J. and ALYANAK, I. (1964), "Effect of vibrations on the shear strength and porosite of sands", The Surveyor, Vol. 123, pp. 23-27 (May 30) and pp. 31-34 (June 6).

KRIZAK, R.J. (1971), "Rheological behaviour of cohesionless soils subjected to dynamic loads", Trans. of the Society of Rheology, Vol. 15, No. 3, pp. 491-540.

LASHINE, A.K., BROWN, S.F. and PELL, P.S. (1971), "Dynamic properties of soils", Report No. 2, Dept. of Civil Engineering, Univ. of Nottingham.

LAU, J.S.O. (1975), "Repeated loading triaxial tests on sand", M.Sc. Thesis, Queen's University, Kingston, Ontario, Canada, April.

LEE, I.K. and MORGAN, J.R. (1966), "Stress and deflection measurements in subgrade materials", Proc. 3rd Conf., Australian Road Research Board, Vol. 3, Part 2, pp. 1168-1177.

LEES, G. (1968), "Design of aggregate gradings", Ph.D. Thesis, Univ. of Birmingham.

MOORE, W.M. and MILLBERGER, L.J. (1968), "Evaluation of TTI gyratory compactor", Research Report No. 99-3, Texas Transportation Institute.

MOORE, W.M., SWIFT, G. and MILLBERGER, L.J. (1969), "Deformation measuring system for repetitively loaded large diameter specimens of granular material", Research Report No. 99-4 , Texas Transportation Institute.

MOORE, W.M., SYLVESTER, C.B. and SCRIVNER, F.H. (1970), "A laboratory study of the relationship of stress to strain for a crushed limestone material", Research Report No. 99-5F, Texas Transportation Institute.

MORGAN, J.R. (1966), "The response of granular materials to repeated loading", Proc. 3rd Conf. Australian Road Research Board, Vol. 3, Part 2, pp. 1178-1192.

MURAYAMA, S. and SHIBATA, T. (1961), "Rheological properties of clays", Proc. 5th Int. Conf. on Soil Mechs. and Found Eng., Vol. 1.

OLOWOKERE, D.O. (1975), "Strength and deformation of railway ballast subject to triaxial loading", M.Sc. Thesis, Queen's University, Kingston, Ontario, Canada.

PARR, G.B. (1972), "Some aspects of the behaviour of London clay under repeated loading", Ph.D. Thesis, Univ. of Nottingham.

PELL, P.S. (1962), "Fatigue characteristics of bitumen and bituminous mixes", Proc. Int. Conf. on the Struct. Design of Asphalt Pavements, Ann Arbor, Michigan, pp. 310-323.

PEUTZ, M.G.F., VAN KEMPEN, H.P.M. and JONES, A. (1968), "Layered systems under normal surface loads", Highway Research Record 228, pp. 34-45.

PIKE, D.C. (1972), "Compactability of graded aggregates (1) Standard laboratory tests", TRRL Report LR 447.

ROBINSON, R.G. (1974), "Measurement of the elastic properties of granular materials using a resonance method", TRRL Supplementary Report 111UC.

ROWE, P.W. and BARDEN, L. (1964), "Importance of free ends in triaxial testing", ASCE, Vol. 90, SM1.

SCHOFIELD, A.N. and WROTH, C.P. (1968), "Critical state soil mechanics", McGraw-Hill, London.

SCOTT, R.F. (1963), "Principles of soil mechanics", Addison-Wesley.

SEED, H.G. and FEAD, J.W.N. (1959), "Apparatus for repeated loading tests on soils", Special Testing Publication 254, ASTM.

SHACKEL, B. (1973), "Repeated loading of soils - a review", Journ. Aust. Road Research Board, 5:3, pp. 22-49.

SHENTON, M.J. (1974), "Deformation of railway ballast under repeated loading (triaxial tests)", Report RP5, British Railways Research Dept.

SILVER, M.L. and PARK, T.K. (1975), "Testing procedure effects on dynamic soil behaviour", Proc. ASCE, Vol. 101, No. GT10, October.

SNAITH, M.S. (1973), "Deformation characteristics of dense bitumen macadam subjected to dynamic loading", Ph.D. Thesis, Univ. of Nottingham.

SNAITH, M.S. and BROWN, S.F. (1972), "Electro-hydraulic servo-controlled equipment for the dynamic testing of bituminous materials", RILEM Int. Symp. on the Deformation and the Rupture of Solids subjected to Multiaxial Stresses, III, Cannes, pp. 139-154.

STOCK, A.F. (1976), Private Communication.

TAYLOR, K.L. (1971), "Finite element analysis of layered road pavements", Ph.D. Thesis, Univ. of Nottingham.

TERREL, R.L. (1967), "Factors influencing the resilient characteristics of asphalt treated aggregates", Ph.D. Thesis, Univ. of California.

TERZAGHI, K. (1943), "Theoretical soil mechanics", Wiley.

THOMPSON, O.O. (1969), "Evaluation of flexible pavement behaviour with emphasis on the behaviour of granular layers", Ph.D. Thesis, Univ. of Illinois.

THROWER, E.N. (1968), "Calculations of stresses and displacements in a layered elastic structure", RRL Report LR 160.

TROLLOPE, E.H., LEE, I.K. and MORRIS, J. (1962), "Stresses and deformations in two-layer pavement structures under slow repeated loading", Proc. Australian Road Research Board, Vol. 1, p. 693.

WARREN, H. and DIECKMANN, W.L. (1963), "Numerical computation of stresses and strains in a multiple-layer asphalt pavement system", Unpublished internal report, Chevron Research Corporation, USA.

WILLIAMS, G.T. (1963), "Stress/strain relationships of granular soils", Thornton Report R 1297, "Shell" Research Limited.

APPENDIX A

LIST OF SAMPLES

Table A.1 gives a complete list of samples made by the normal method described in Section 5.4. Various other samples were made prior to these in order to establish the method of sample preparation and to investigate different methods of locating the strain transducers.

In all, 39 samples were made by this method between June 1974 and February 1976. Of these, two were not tested, two were used to check the performance of the equipment, ten were used for preliminary tests (Chapter 7), nine were used for resilient strain tests (Chapter 8) and sixteen for permanent strain tests (Chapter 9). The average sample density was 2233 kg/m^3 with a standard deviation of ± 10 kg/m^3.

Table A.1 Sample List

Sample No.	Date	Density kg/m^3	Test	
101	20.6.74	2245	Preliminary checks	
102	19.7.74	2241	OS-160	Preliminary Tests
103	25.7.74	2242	OS-20	
104	30.7.74	2238	OS-160A	
105	20.8.74	2238	Not tested	
106	29.8.74	2225	OT-160	
107	3.9.74	2240	OT-20	
108	25.9.74	2244	RX	
109	30.9.74	2235	RY	
110	10.10.74	2215	RZ(a)	
111	22.10.74	2212	RZ(b)	
112	17.11.74	2221	RF	
113	27.11.74	2228	R-1	Resilient Strain Tests R - main test programme S - tests with negative deviator stress
114	3.12.74	2211	R-2	
115	11.12.74	2239	R-3	
116	18.12.74	2231	R-4	
117	15.1.75	2227	R-5	
118	24.1.75	2224	R-6	
119	8.4.75	2231	Not tested	
120	9.4.75	2241	Push-pull trial	
121	11.6.75	2229	S-1	
122	23.6.75	2215	S-2	
124	11.8.75	2233	S-3	

/contd.

Table A.1 (contd.)

Sample No.	Date	Density kg/m^3	Test	
123	7.7.75	2238	PA-1	Permanent Strain Tests
125	15.8.75	2230	PA-2*	
126	28.8.75	2239	PA-3*	
127	2.10.75	2229	PA-4	
128	8.10.75	2227	PB-1	
129	12.10.75	2236	PB-2	
130	27.10.75	2238	PC-1	
131	3.11.75	2251	PC-2	
132	7.11.75	2239	PD-1	
133	27.11.75	2250	PA-5	
134	6.12.75	2234	PE-1	
135	11.12.75	2232	PF-1	
136	21.1.76	2237	PG-1	
137	4.2.76	2248	PF-2	
138	10.2.76	2229	PE-2	
139	14.2.76	2227	PG-2	

* Tests PA-2 and PA-3 are not presented in the results because they were stopped after only about 200 cycles when the axial load servo-valve became stuck. The problem was traced to an inadequate warming up period for the hydraulic power supply and did not occur again.

APPENDIX B

CALIBRATION OF TRANSDUCERS

Brief details are given of the methods used in calibrating each transducer followed by a summary of the calibration data used in computing the results.

Load Cell

The original load cell mounted on the triaxial cell base was calibrated as follows. The bottom platen was positioned on the load cell, and the load was applied from the axial loading ram through a standard proving ring. The voltage supplied to the strain gauges on the load cell was set at 10.00 volts. Readings were taken of the load cell output (with 1000 x amplification) and the deflection of the proving ring. The maximum loads used were equivalent to 250 kN/m^2 for the semi-conductor gauges and 1000 kN/m^2 for the foil gauges. The readings were plotted, and the sensitivity taken as the best straight line drawn through the points. Linearity was within about $\pm 2\%$ of the full scale reading.

In April 1975, a new load cell was incorporated into the bottom of the loading rod so that the equipment could apply negative deviator stress. This load cell was also used for the permanent strain tests.

The new load cell was calibrated in compression by loading through a standard proving ring as described above and in tension by using a hanger and weights. The sensitivity was the same in each case. The new load cell was not susceptible to the bedding errors which affected the original load cell, had better linearity ($\pm 0.5\%$), and was more sensitive so that the semiconductor strain-gauges were not required.

Pressure Sensor

With the triaxial cell assembled and filled with silicone oil, pressure was applied through an air regulator to the oil and to a column of mercury. The sensitivity was found by plotting readings in the same way as for the load cell. Linearity was within about ±1% of the full scale reading.

LVDTs

The LVDTs were attached to a calibration bench which allowed all four to be adjusted simultaneously by a micrometer thimble. The gain setting of the carrier system was set to an appropriate value (-54 dB) for a full scale deflection of 5% strain. Readings were taken from the u/v recorder for strains between 0 and 5% for each individual transducer and for the overall value from all four. Sensitivity was taken as the difference between the appropriate readings divided by the applied strain (displacement/gauge length). The sensitivity of the individual transducers was the same within about ±2% but the overall sensitivity of all four LVDTs together was 15% lower. Linearity was within the limits of the u/v recorder (±1%). Checks were also carried out to ensure that the different gain settings of the carrier system, and of the offset generator for resilient strain gave the correct scaling factors when sensitivities were compared.

Strain Rings

Calibration of the strain rings was very similar to that of the LVDTs. The normal gain setting of the carrier system was -36 dB, linearity was good, and the overall sensitivity of the three rings together was about 3% higher than individual rings.

Calibration Data

Table B.1 gives a summary of calibration data obtained by the methods described above. Changes which occurred in calibration due to alterations made to the equipment are noted in the comment column. The calibration used for a particular test was an average of the values found before and after that test.

Table B.1 Summary of Calibration Data

Date	Load Cell		Pressure sensor	LVDTs		Strain Rings		Comment
	Foil Gauges	Semiconductor Gauges		Individual	Overall	Individual	Overall	
	Volts per 100 kN/m^2			Divisions (u/v recorder) per 1% strain				
18.7.74	.195	-	1.27	20.2	17.6	23.4	24.4	Load cell mounting changed
7.9.74	.210*	1.72	1.255	19.9	17.4	23.4	24.6	u/v recorder serviced
9.10.74	.203	1.87	1.25	20.1	17.4	23.2	23.8	Carrier system readjusted
27.11.74	.205	2.16*	1.27	19.4	16.5	22.6	23.2	Resilient strain tests, main test programme
31.1.75	.206	2.17	1.31	19.65	16.6	22.6	23.3	New load cell
11.6.75	.478	-	1.28	-	-	21.5	21.8	Resilient strain tests with negative deviator stress
18.8.75	.473	-	1.29	19.35	16.6	21.5	22.1	Permanent strain tests
6.1.76	.472	-	1.29	19.1	16.4	21.6	22.1	

* Strain gauges replaced

APPENDIX C

PERFORMANCE OF LOADING SYSTEM

C.1 THEORY

Consider the design of each component in the simple servo-hydraulic loading system shown in Fig. C.1. The system is designed to apply a maximum load, L_o, to a sample, stiffness S. The output of the load cell is amplified so that at the maximum load the output voltage, V_ℓ, equals the maximum available, V_o (normally two-thirds of the supply voltage). The actuator is designed to apply the same maximum load with two-thirds of the hydraulic supply pressure, P_o, the remainder covering flow losses. The piston area of the actuator, A, is then given by:

$$A = 1.5\, L_o/P_o \qquad (C.1)$$

The servo-valve is the most critical component in the system, and its selection must be considered in more detail. If the rated flow of the servo-valve is Q_o, the flow into the actuator, Q, is given by:

$$Q = \frac{Q_o \cdot V_q}{V_o} \qquad (C.2)$$

where V_o is the rated voltage and V_q is the input voltage to the servo-valve.

It can be shown that the response time, T_r, of this system to a change in command voltage, V_c, is given by:

$$T_r = T_o + \frac{L_o A}{G\, Q_o S} \qquad (C.3)$$

If the delay in the loading mechanism, T_o, is greater than the response time of the control system $L_o A/G\, Q_o S$, the system will oscillate. The electrical gain, G, which can be used is, therefore, limited to:

$$G \leq L_o A / T_o Q_o S \qquad (C.4)$$

Hence the response time of the system is limited to:

$$T_r \geq 2T_o \qquad (C.5)$$

and the maximum frequency of loading, f_o, which can be accurately reproduced is:

$$f_o = 1/4\pi T_o \qquad (C.6)$$

Therefore, it can be seen that the delay in the loading mechanism determines the maximum frequency at which the system can operate.

The peak flow, Q_p, of the servo-valve when operating at a frequency, f, and a load, L, is given by:

$$Q_p = \frac{\pi f L A}{S} \qquad (C.7)$$

Therefore, if it is assumed that the maximum frequency of operation will be as given by equation C.6 at the maximum load, L_o, the servo-valve selected should have a rated flow, Q_o, given by:

$$Q_o = \frac{L_o A}{4T_o S} \qquad (C.8)$$

C.2 STABILITY

Experience with servo-hydraulic equipment at the University of Nottingham has shown that the most important factor affecting stability of the system is the null voltage of the servo-valve. Changes in the null voltage can be caused by a wide variety of environmental changes including air temperature, oil temperature, oil pressure and electrical noise. A change in the null voltage, ΔV, will produce a change in load, ΔL, given by:

$$\frac{\Delta L}{L_o} = \frac{1}{G} \cdot \frac{\Delta V}{V_o} \qquad (C.9)$$

If the highest possible gain is used, equation C.9 can be rewritten (using equations C.4 to C.7) as:

$$\frac{\Delta L}{L} = \frac{1}{4} \cdot \frac{Q_o}{Q_p} \cdot \frac{f}{f_o} \cdot \frac{\Delta V}{V_o} \qquad (C.10)$$

Therefore, stability can be improved by using frequencies of loading much lower than the maximum possible, and by using a servo-valve which is not over-designed for the load and frequency being applied. The use of lower frequencies will not in itself improve stability, except that it will allow the use of a servo-valve with a smaller flow rating. When operating at low loads, Q_p may be considerably smaller than Q_o, resulting in poor stability. This can be partly overcome by using a lower supply pressure, P_o, as this will reduce the flow rating of the servo-valve and allow a higher gain to be used.

It is possible to improve stability by compensating electrically for changes in null voltage (Chaddock, 1974) but this can lead to control problems when switching between open-loop and closed-loop operation.

C.3 CONTROL

Control of the system is said to be good if the load cell output, V_ℓ, accurately follows the command signal, V_c. The phase difference, θ, between the two signals will be approximately given by:

$$\theta = 2\pi f.T_r \qquad (C.11)$$

There will be a substantial phase lag if the system is operated near its maximum frequency. Control problems are made much worse by friction in the loading system, although this can be overcome by the use

of suitable dither signals. Dither is especially useful to overcome threshold limits in the servo-valve which essentially have the same effect as friction. These problems are generally only significant at low loads, and it is important not to use equipment designed for much higher loads than those being applied.

C.4 PERFORMANCE

The equipment was designed according to the theory above to meet the specification in Table C.1. The maximum pressure of the available hydraulic supply was 20,000 kN/m^2. Axial load was applied by a single ended hydraulic actuator, 50.8 mm diameter, with a servo-valve rated at 40 litres/min. The confining stress could be applied from a regulated air supply or by a 127 mm diameter pressurising cyclinder connected to the triaxial cell by a large bore flexible tube. The pressurising cylinder was operated by a hydraulic actuator also with a servo-valve rated at 40 litres/min.

The axial load system worked well, and the effective delay time (T_o in Fig. C.1) was found to be about 0.005 sec. The system responded fully to command signals at frequencies up to 16 Hz and would operate up to 30 Hz at reduced loads and with some phase lag.

The confining stress system was found to have a much larger delay time, about 0.04 sec, which is not surprising as the pressure is applied indirectly. This meant that the maximum frequency at which the system would fully respond to command signals was about 2 Hz. The fact that the specification of 20 Hz could not be achieved was not serious, because the behaviour of the material was found to be unaffected by frequency (see Chapter 7). A frequency of 1 Hz was used for almost all tests, because at this frequency there was no appreciable phase lag between the

deviator stress and the confining stress (see equation C.11).

Because the servo-valve was selected to deal with the flow demand expected at a frequency of 20 Hz and the maximum operating frequency of the confining stress system was 2 Hz, stability of the system was poor (see equation C.10). Changes of up to 20% in comfining stress occurred during some of the permanent strain tests due to changes in oil temperature during the course of the test. The behaviour of the servo-valves also appeared to be somewhat erratic during the course of the last few permanent strain tests, and it is thought that this is due to excessive wear developing.

C.5 DITHER

The approximate frequency of dither signals applied to the servo-loops was:

Axial load	200 Hz
Confining stress	800 Hz and 50 Hz

It was found necessary to use two dither signals in the confining stress system to overcome thresholds in the servo-valve response and "stiction" in the pressurising cylinder respectively. Dither was also important in reducing the interaction between the two servo-systems operating on the same sample, and for this reason, widely different frequencies were used. The amplitude of dither signals used was generally chosen to be barely detectable in the load cell and pressure sensor outputs.

C.6 SUGGESTED IMPROVEMENTS

As mentioned above, 1 Hz was found to be the most convenient frequency for testing. The existing servo-valves have a flow rating

much too high for the system to operate at this frequency with the best control and stability characteristics. It is recommended that they both be replaced by servo-valves with a rating of 4 litres/min. This would provide ample capacity for operating under full load at up to 2 Hz (the maximum possible for the confining stress system) and would enable the axial load system to be operated at higher frequencies and reduced load if required. This measure should improve stability by a factor of ten and probably improve control somewhat.

Further improvements in stability could possibly be made by improving the hydraulic supply. Better pressure control and the addition of temperature control might well improve stability further at low loads. The need for these improvements can only be gauged after some experience of operating the system with smaller servo-valves.

To significantly improve the frequency range of the confining stress system would require fundamental changes. A more direct system of pressure application would be required to reduce the effective delay time, T_o. One possibility would be a supply of pressurised cell fluid fed directly in and out of the triaxial cell by a high flow, low pressure servo-valve.

Table C.1 Specification of Equipment

Sample size	
Diameter	150 mm
Height	300 mm
Applied stresses	
Confining stress	0 - 400 kN/m^2
Deviator stress	0 - 1200 kN/m^2
Rate of loading	
Sine wave	0.1 Hz - 20 Hz
Ramp loading (constant rate of increase)	Zero to maximum in 100 - 10,000 sec
Rest periods	
Wave train	1, 2, 4, 8 .... 2^{15} pulses
Rest period	0 - 55 minutes
Strain measurement (both axial and radial strain)	
Resilient strain	0 - 5,000 $\mu\varepsilon$
Permanent strain	0 - 100,000 $\mu\varepsilon$

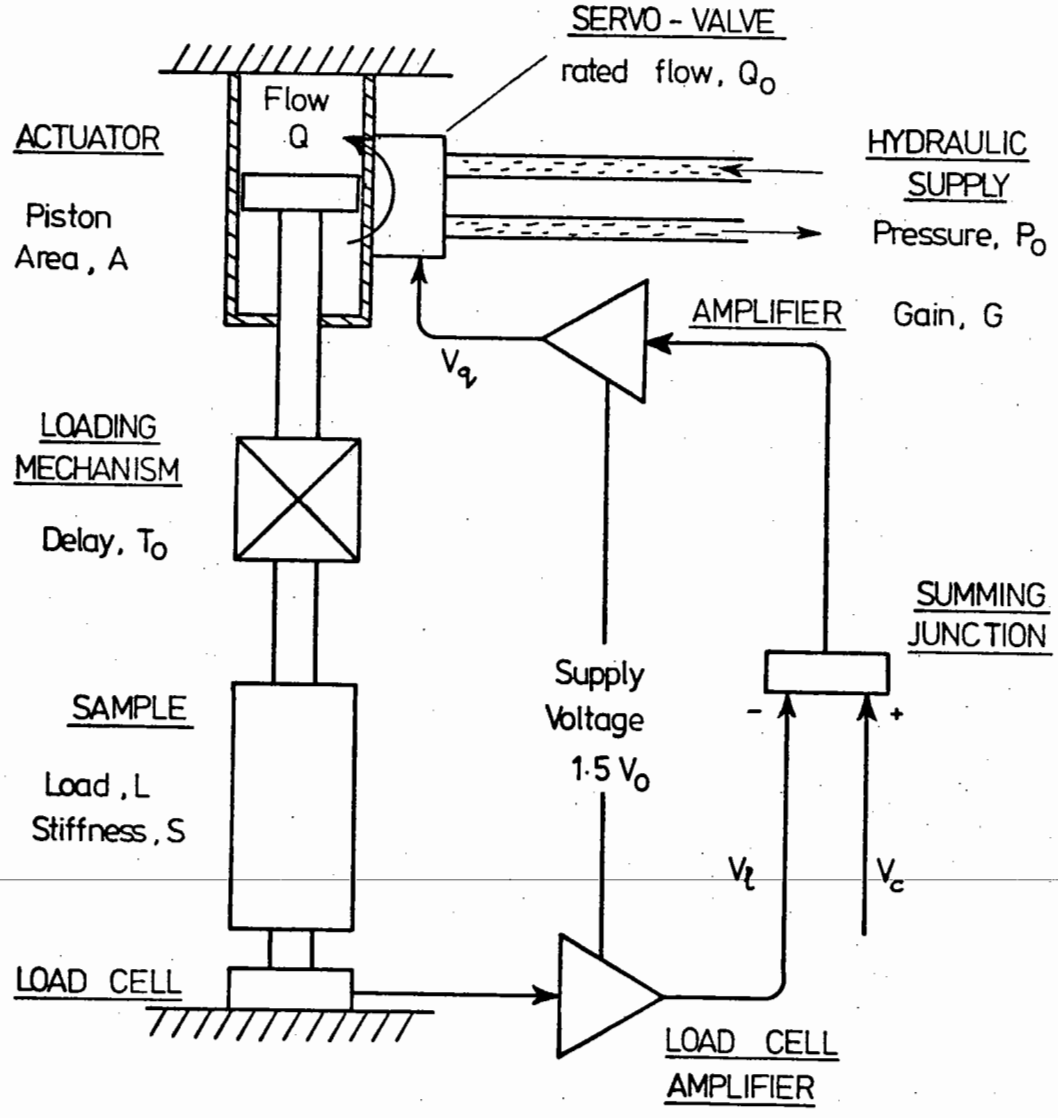

FIG. C.1 SCHEMATIC DIAGRAM OF SIMPLE SERVO-HYDRAULIC LOADING SYSTEM

APPENDIX D

COMPLETE RESILIENT STRAIN RESULTS

In Chapter 8, sufficient data was presented to give an overall impression of the resilient strain behaviour of the material and to trace the development of the resilient strain model. The reader is advised to study Chapter 8 before attempting to interpret the results given here, and to find definitions of the symbols used.

D.1 AVERAGE DATA FROM RESILIENT STRAIN TESTS

The basic data from the resilient strain tests is presented in Tables D.1 to D.6. Each line of these tables represents a particular stress path from the test programme (see Table 8.1). The values given are the average results of applying that stress path to the number of samples shown in column (1). This would normally be six for stress paths in the main test programme, three for those with negative deviator stress, and nine for those applied in both cases. In some cases, the number of samples was less than this because readings in which the stresses applied were not within 5% of those required in the programme have been excluded.

The parameters which define the stress path applied to take each reading are given in columns (2) to (5), and the resulting resilient strains are given in columns (6) and (7). In each case, the average resilient strain is followed by the standard deviation (in parentheses) between the different samples tested. The repeated stress parameters, $(T_r)_A$ and $(T_r)_B$, are given in columns (8) and (9), and the resilient strain parameters, $(W_r)_A$ and $(W_r)_B$, are given in columns (10) and (11).

Figs. D.1 and D.2 show the resilient strain diagrams (similar to

Fig. 8.4) for certain values of p_m (48 and 192 kN/m^2) and certain values of S_m (-0.5, 0, +0.5 and +1.0). Circles have been drawn on these diagrams to represent the standard deviation found in the strain for each stress path.

Figs. D.3 to D.8 show the resilient strain parameter, W_r, plotted against the resilient stress parameter, T_r, for all values of mean normal stress. It can be seen that the relationship between W_r and T_r is similar at all values of mean normal stress to that presented in Chapter 8 for p_m = 192 kN/m^2.

Figs. D.9 to D.14 show the resilient strain parameter, W_r, plotted against $2T_r/(T_m + 1)$ for all values of mean normal stress. These diagrams have been summarised in Fig. 8.9 to show the effect of mean normal stress on resilient strain behaviour. It can be seen that the material becomes progressively more anisotropic as the mean normal stress is reduced.

D.2 DATA FROM INDIVIDUAL TRANSDUCERS

Readings of strain from individual transducers were taken for certain stress paths in tests R-1 to R-6. (These were stress paths involving only primary values of the parameters in Table 8.1). Figs. D.15 to D.20 show the axial strain measured on the left and right hand side of the sample compared with that predicted by the resilient strain model for that stress path. Figs. D.21 to D.26 show the radial strain measured by each strain ring compared with that predicted. The strain predicted by the resilient strain model is used as the independent variable for these diagrams so that the scatter in individual readings can be seen without considering stress-strain relationships. The model was developed from the overall readings of strain on several samples, and the distance of the points from the line of 45° slope through the

origin gives a measure of the variation in individual readings from the average of these overall readings. Several points are worth noting from these diagrams:

(a) Axial strain was, in fact, measured by four LVDTs on a sample each operating over a gauge length of 75 mm. The readings have been combined in pairs to indicate the strain over gauge lengths of 150 mm on either side of the sample. The scatter from individual readings was much greater than that shown, and it is therefore apparent that 150 mm is the minimum gauge length for which worthwhile readings of strain can be taken on this material. The strain rings measured radial strain over a sample diameter of 150 mm and the scatter in axial and radial strain is broadly similar when compared on this basis.

(b) The overall readings of strain were often slightly less than the arithmetic mean of the individual readings allowing for the different calibration coefficients in each case. This was due to the fact that the individual strain waveforms were not exactly in phase, so that the electrical average taken for the overall reading might be slightly less than the arithmetic mean.

(c) It can be seen from Figs. D.21 to D.26 that the radial strain at values greater than 100 $\mu\varepsilon$ is generally under-predicted. This is largely due to the fact that the material is exhibiting some inherent anisotropy, which is not indicated by the resilient strain model used in the prediction. This anisotropy would also be expected to cause over-prediction of the axial strain, but this is not apparent in Figs. D.15 to D.20 and has probably been masked by the effect noted in item (b).

(d) There is some indication from Figs. D.15 to D.20 that the LVDTs are not registering properly at resilient strains less than about 25 με. This is probably due to mechanical 'backlash' between the moving parts. 25 με represents a relative movement of less than 2 μm between the core and the body of an LVDT on the sample (25.4 μm equals 1 thou).

D.3 RESILIENT STRAIN MEASUREMENTS TAKEN DURING PERMANENT STRAIN TESTS

Table 9.2 gives details of the resilient strain readings taken at intervals during the permanent strain tests. The measurements are presented in Figs. D.27 to D.39 in the form of diagrams showing the resilient strain parameter, W_r, plotted against the stress parameter, $2T_r/(T_m + 1)$. They should be compared with the equivalent diagrams drawn from the resilient strain test data, Figs. D.11 and D.13. The change in resilient strain behaviour brought about by permanent strain is summarised in Table 9.3.

Table D.1 Resilient Strain Tests, Average Data, p_m approx. 12 kN/m^2

No. of samples (1)	p_m, (kN/m^2) (2)	S_m (3)	p_r/p_m (4)	q_r/p_m (5)	v_r (με) (6)	ϵ_r (με) (7)	$(T_r)_A$ (8)	$(T_r)_B$ (9)	$(W_r)_A$ (με) (10)	$(W_r)_B$ (με) (11)
4	11.6	0.00	0.35	0.00	61 (7)	-20 (7)	0.35	0.35	22	81
6	11.7	0.00	0.67	0.00	121 (39)	-36 (22)	0.67	0.67	49	157
6	11.6	0.51	0.17	0.51	-15 (17)	23 (8)	0.85	-0.17	32	-38
6	11.7	0.53	0.33	0.99	-19 (31)	59 (20)	1.65	-0.33	99	-78
4	11.7	0.51	0.00	0.54	-50 (34)	39 (7)	0.72	-0.36	28	-89
6	11.7	0.54	-0.02	0.99	-85 (48)	88 (23)	1.30	-0.68	91	-174
5	11.7	0.51	0.33	0.00	68 (16)	-26 (8)	0.33	0.33	17	94
6	11.8	0.51	0.66	0.00	159 (48)	-62 (28)	0.66	0.66	35	220
6	11.7	1.02	0.17	0.51	-23 (16)	24 (6)	0.84	-0.17	25	-47
6	11.7	1.02	0.34	1.03	-37 (33)	63 (16)	1.72	-0.34	90	-100
5	11.9	1.05	0.65	1.96	-46 (26)	153 (30)	3.27	-0.65	261	-199
3	11.7	1.03	-0.03	0.51	-87 (31)	52 (6)	0.66	-0.37	16	-138
6	11.8	1.02	-0.01	1.04	-138 (69)	111 (21)	1.38	-0.71	85	-249
5	11.7	1.03	0.33	0.00	86 (22)	-38 (14)	0.33	0.33	9	124
6	11.7	1.02	0.67	0.00	236 (81)	-106 (40)	0.67	0.67	25	342

Table D.2 Resilient Strain Tests, Average Data, p_m approx. 24 kN/m^2

No. of Samples (1)	p_m, (kN/m^2) (2)	S_m (3)	p_r/p_m (4)	q_r/p_m (5)	v_r ($\mu\varepsilon$) (6)	ε_r ($\mu\varepsilon$) (7)	$(T_r)_A$ (8)	$(T_r)_B$ (8)	$(W_r)_A$ ($\mu\varepsilon$) (10)	$(W_r)_B$ ($\mu\varepsilon$) (11)
4	23.2	0.00	0.34	0.00	55 (13)	-13 (4)	0.34	0.34	30	68
6	23.1	0.00	0.70	0.00	130 (39)	-28 (20)	0.70	0.70	75	158
6	23.3	0.52	0.17	0.51	-7 (21)	35 (7)	0.85	-0.17	62	-42
6	23.4	0.53	0.33	1.00	-4 (38)	86 (17)	1.66	-0.33	167	-90
6	23.3	0.51	0.00	0.51	-42 (10)	45 (10)	0.68	-0.35	48	-86
5	23.4	0.53	0.00	0.99	-80 (68)	106 (24)	1.32	-0.65	132	-186
6	23.3	0.52	0.34	0.00	68 (19)	-21 (5)	0.34	0.34	25	89
5	23.2	0.52	0.67	0.00	183 (64)	-60 (20)	0.67	0.67	64	243
6	23.4	1.03	0.17	0.51	-19 (21)	35 (8)	0.85	-0.17	50	-54
6	23.3	1.03	0.34	1.02	-35 (47)	89 (18)	1.70	-0.34	143	-124
6	23.6	1.03	0.66	1.97	-62 (75)	231 (45)	3.28	-0.66	400	-293
6	23.4	1.03	0.00	0.51	-67 (38)	52 (10)	0.69	-0.34	37	-119
6	23.4	1.02	0.01	1.02	-149 (78)	136 (28)	1.36	-0.67	124	-285
6	23.3	1.03	0.35	0.00	101 (22)	-38 (10)	0.35	0.35	25	140
5	23.3	1.03	0.68	0.00	290 (70)	-100 (33)	0.68	0.68	90	390

Table D.3 Resilient Strain Tests, Average Data, p_m approx. 48 kN/m^2

No. of Samples (1)	p_m, (kN/m^2) (2)	S_m (3)	p_r/p_m (4)	q_r/q_m (5)	v_r (με) (6)	ϵ_r (με) (7)	$(T_r)_A$ (8)	$(T_r)_B$ (9)	$(W_r)_A$ (με) (10)	$(W_r)_B$ (με) (11)
3	46.1	-0.79	0.17	0.52	122 (6)	149 (13)	0.87	-0.17	420	-27
3	46.2	-0.78	0.00	0.53	65 (5)	115 (12)	0.70	-0.36	295	-50
2	46.0	-0.79	0.35	0.00	101 (23)	40 (16)	0.35	0.35	181	61
3	46.2	-0.53	0.18	0.53	79 (4)	109 (10)	0.88	-0.18	297	-30
2	46.1	-0.53	-0.01	0.53	29 (5)	96 (11)	0.69	-0.37	221	-66
2	45.9	-0.53	0.69	0.00	189 (2)	54 (6)	0.69	0.69	297	135
3	46.5	-0.26	0.17	0.52	48 (11)	82 (5)	0.86	-0.17	212	-34
3	46.5	-0.25	0.35	1.05	103 (32)	224 (26)	1.75	-0.35	551	-122
3	46.2	-0.26	0.01	0.52	7 (2)	75 (4)	0.70	-0.34	157	-68
3	46.7	-0.26	0.02	1.06	50 (12)	220 (35)	1.43	-0.69	490	-170
2	46.4	-0.26	0.33	0.00	52 (4)	-2 (1)	0.33	0.33	47	54
3	46.6	0.00	0.17	0.52	35 (16)	65 (8)	0.87	-0.17	165	-30
3	46.7	0.01	0.35	1.06	108 (32)	180 (19)	1.77	-0.35	468	-72
3	46.7	0.01	0.52	1.56	235 (34)	358 (46)	2.59	-0.52	915	-155

/contd.

Table D.3 (contd.)

No. of Samples (1)	p_m' (kN/m²) (2)	S_m (3)	p_r/p_m (4)	q_r/q_m (5)	v_r (με) (6)	ε_r (με) (7)	$(T_r)_A$ (8)	$(T_r)_B$ (9)	$(W_r)_A$ (με) (10)	$(W_r)_B$ (με) (11)
2	46.2	0.00	0.00	0.53	8 (15)	68 (3)	0.71	-0.35	144	-60
3	46.4	0.00	0.02	1.07	10 (10)	160 (30)	1.45	-0.70	330	-150
3	46.4	0.00	0.02	1.59	48 (13)	315 (58)	2.14	-1.04	678	-267
5	46.3	0.00	0.16	0.00	23 (5)	-6 (2)	0.16	0.16	12	29
8	46.3	0.00	0.34	0.00	56 (10)	8 (3)	0.34	0.34	40	65
4	45.9	0.00	0.52	0.00	100 (21)	-14 (4)	0.52	0.52	71	114
7	46.2	0.00	0.68	0.00	136 (21)	-19 (8)	0.68	0.68	99	155
9	46.7	0.27	0.17	0.51	10 (4)	49 (6)	0.85	-0.17	108	-40
3	46.7	0.26	0.36	1.07	67 (25)	156 (13)	1.78	-0.36	379	-89
2	46.7	0.26	0.52	1.57	171 (62)	286 (6)	2.62	-0.52	743	-115
9	46.7	0.27	0.00	0.51	-18 (34)	54 (6)	0.68	-0.34	90	-72
3	46.4	0.25	0.01	1.08	-21 (18)	159 (17)	1.45	-0.71	297	-180
2	46.7	0.25	0.00	1.56	-44 (24)	303 (48)	2.08	-1.04	561	-347
8	46.3	0.26	0.34	0.00	67 (6)	-13 (4)	0.34	0.34	41	80
8	46.2	0.27	0.68	0.00	160 (26)	-30 (8)	0.68	0.68	99	190
6	46.5	0.52	0.09	0.26	-6 (9)	20 (3)	0.43	-0.09	34	-26
9	46.7	0.51	0.17	0.52	7 (8)	53 (6)	0.87	-0.17	113	-46

/contd.

Table D.3 (contd.)

No. of Samples (1)	p_m, (kN/m²) (2)	S_m (3)	p_r/p_m (4)	q_r/q_m (5)	v_r (με) (6)	ϵ_r (με) (7)	$(T_r)_A$ (8)	$(T_r)_B$ (9)	$(W_r)_A$ (με) (10)	$(W_r)_B$ (με) (11)
6	46.7	0.51	0.26	0.77	11 (7)	90 (5)	1.28	-0.26	192	-79
9	46.8	0.52	0.34	1.01	25 (15)	131 (15)	1.68	-0.34	287	-106
3	46.9	0.51	0.51	1.54	94 (67)	256 (22)	2.59	-0.51	606	-162
4	46.6	0.51	0.00	0.26	-22 (14)	24 (2)	0.34	-0.17	27	-46
9	46.6	0.52	0.00	0.52	-34 (23)	60 (7)	0.70	-0.34	86	-94
6	46.6	0.51	0.01	0.77	-60 (39)	102 (10)	1.03	-0.50	145	-162
9	46.6	0.52	0.00	1.01	-65 (44)	154 (20)	1.35	-0.68	243	-219
2	46.4	0.52	0.00	1.56	-153 (5)	264 (84)	2.08	-1.03	374	-417
6	46.5	0.52	0.17	0.00	33 (4)	-11 (2)	0.17	0.17	11	44
9	46.4	0.52	0.34	0.00	74 (1)	-21 (3)	0.34	0.34	33	95
6	46.2	0.52	0.53	0.00	130 (16)	-34 (4)	0.53	0.53	63	163
9	46.3	0.52	0.68	0.00	181 (30)	-47 (5)	0.68	0.68	87	228
6	46.5	0.51	0.34	0.51	42 (13)	44 (6)	1.03	0.00	131	-2
6	46.6	0.52	0.68	1.00	103 (28)	115 (16)	2.01	0.01	333	-11
6	46.5	0.51	0.52	0.51	92 (10)	34 (5)	1.20	0.17	159	58
5	46.4	0.53	1.01	1.01	244 (40)	97 (29)	2.35	0.34	438	147
5	46.1	0.52	-0.51	0.52	-210 (61)	115 (11)	0.19	-0.86	19	-325

/contd.

Table D.3 (contd.)

No. of Samples (1)	p_m, (kN/m^2) (2)	S_m (3)	p_r/p_m (4)	q_r/q_m (5)	v_r (με) (6)	ϵ_r (με) (7)	$(T_r)_A$ (8)	$(T_r)_B$ (9)	$(W_r)_A$ (με) (10)	$(W_r)_B$ (με) (11)
9	46.9	0.77	0.17	0.52	-1 (20)	52 (7)	0.86	-0.17	103	-53
9	46.8	0.77	0.34	1.03	9 (13)	133 (16)	1.71	-0.34	275	-124
9	46.9	0.78	0.51	1.52	9 (16)	220 (34)	2.54	-0.51	450	-211
3	47.1	0.77	0.69	2.06	31 (15)	359 (46)	3.43	-0.69	748	-327
9	46.8	0.77	0.00	0.52	-51 (28)	65 (10)	0.69	-0.35	78	-116
9	46.7	0.77	0.00	1.04	-110 (57)	166 (26)	1.38	-0.69	222	-277
9	46.9	0.77	-0.01	152	-194 (91)	299 (48)	2.02	-1.02	404	-493
9	46.6	0.78	0.34	0.00	90 (13)	-28 (3)	0.34	0.34	23	107
9	46.7	0.77	0.69	0.00	213 (38)	-68 (16)	0.69	0.69	77	281
6	46.9	1.02	0.09	0.26	-13 (12)	21 (3)	0.43	-0.09	28	-34
9	47.0	1.02	0.17	0.51	-12 (20)	51 (7)	0.85	-0.17	91	-63
6	46.9	1.02	0.25	0.76	-22 (33)	91 (12)	1.27	-0.25	160	-113
9	46.9	1.02	0.34	1.02	-20 (37)	128 (20)	1.71	-0.34	236	-147
9	47.0	1.01	0.51	1.52	-23 (54)	212 (32)	2.53	-0.51	401	-235
9	46.9	1.02	0.67	2.02	-34 (84)	346 (44)	3.37	-0.67	657	-379
4	46.9	1.02	0.08	0.26	-38 (24)	29 (5)	0.34	-0.17	20	-66
9	46.8	1.03	0.00	0.51	-70 (33)	71 (12)	0.69	-0.34	73	-141
6	47.0	1.02	0.00	0.76	-122 (64)	128 (21)	1.02	-0.51	134	-250

/contd.

Table D.3 (contd.)

No. of Samples (1)	p_m, (kN/m²) (2)	S_m (3)	p_r/p_m (4)	q_r/q_m (5)	v_r (με) (6)	ϵ_r (με) (7)	$(T_r)_A$ (8)	$(T_r)_B$ (9)	$(W_r)_A$ (με) (10)	$(W_r)_B$ (με) (11)
9	46.8	1.02	0.00	1.03	-151 (71)	182 (31)	1.37	-0.68	213	-333
6	46.7	1.03	0.17	0.00	51 (12)	-17 (4)	0.17	0.17	17	68
9	47.8	1.03	0.34	0.00	114 (22)	-39 (7)	0.34	0.34	37	153
6	46.7	1.03	0.52	0.00	207 (50)	-72 (12)	0.52	0.52	64	279
9	46.6	1.03	0.67	0.00	287 (65)	-106 (20)	0.67	0.67	75	393
6	46.9	1.02	0.34	0.51	38 (17)	34 (2)	1.02	0.00	107	4
6	46.7	1.02	0.68	1.02	100 (27)	93 (16)	2.04	0.00	286	6
6	46.6	1.02	1.33	1.99	284 (96)	265 (69)	3.99	0.00	815	18
8	47.1	1.02	0.53	0.53	111 (27)	13 (3)	1.24	0.18	136	98
5	46.5	1.02	1.02	1.02	279 (57)	31 (16)	2.38	0.34	341	248
6	46.5	1.03	-0.51	0.52	-310(108)	180 (37)	0.18	-0.85	50	-491
9	47.1	1.28	0.17	0.51	-18 (16)	47 (7)	0.85	0.17	77	-65
6	47.0	1.27	0.34	1.01	-36 (32)	127 (19)	1.68	-0.34	218	-164
6	46.9	1.26	0.50	1.50	-56 (62)	224 (30)	2.51	-0.50	393	-280
9	47.0	1.28	0.00	0.51	-84 (32)	72 (13)	0.69	-0.34	60	-157
9	46.9	1.28	0.34	0.00	142 (32)	-51 (9)	0.34	0.34	41	193
6	47.2	1.53	0.17	0.50	-24 (16)	48 (6)	0.84	0.17	71	-72

Table D.4 Resilient Strain Tests, Average Data, p_m approx. 96 kN/m^2

No. of Samples (1)	p_m, (kN/m^2) (2)	S_m (3)	p_r/p_m (4)	q_r/q_m (5)	v_r ($\mu\varepsilon$) (6)	ε_r ($\mu\varepsilon$) (7)	$(T_r)_A$ (8)	$(T_r)_B$ (9)	$(W_r)_A$ ($\mu\varepsilon$) (10)	$(W_r)_B$ ($\mu\varepsilon$) (11)
6	91.9	0.00	0.34	0.00	69 (8)	-5 (4)	0.34	0.34	60	74
2	91.9	0.00	0.67	0.00	153 (26)	-11 (10)	0.67	0.67	130	164
6	92.8	0.51	0.18	0.53	7 (11)	64 (16)	0.88	-0.18	136	-58
6	92.9	0.52	0.34	1.06	37 (11)	190 (43)	1.77	-0.35	416	-152
6	92.4	0.51	0.00	0.54	-45 (27)	75 (15)	0.72	-0.35	105	-120
6	92.4	0.52	0.02	1.07	-80 (27)	208 (42)	1.45	-0.70	337	-288
4	92.5	0.52	0.34	0.00	88 (8)	-24 (3)	0.34	0.34	41	111
6	92.1	0.52	0.67	0.00	208 (29)	-49 (5)	0.67	0.67	111	257
6	93.6	1.03	0.17	0.52	-9 (20)	53 (9)	0.87	-0.17	97	-62
6	93.3	1.02	0.35	1.05	-13 (41)	142 (19)	1.75	-0.35	217	-155
6	93.4	1.02	0.69	2.07	-10 (84)	432 (58)	3.45	-0.69	854	-443
6	93.4	1.02	0.01	0.52	-77 (26)	74 (13)	0.70	-0.34	71	-151
5	93.1	1.02	0.02	1.06	-182 (67)	207 (36)	1.42	-0.69	232	-389
6	93.4	1.03	0.33	0.00	132 (25)	-42 (8)	0.33	0.33	48	174
6	93.2	1.03	0.65	0.00	321 (58)	-102 (14)	0.65	0.65	116	423

Table D.5 Resilient Strain Tests, Average Data, p_m approx. 192 kN/m^2

No. of Samples (1)	p_m, (kN/m^2) (2)	S_m (3)	p_r/p_m (4)	q_r/q_m (5)	v_r (με) (6)	ε_r (με) (7)	$(T_r)_A$ (8)	$(T_r)_B$ (9)	$(W_r)_A$ (με) (10)	$(W_r)_B$ (με) (11)
3	185.8	-0.77	0.18	0.53	223 (77)	272 (74)	0.88	-0.17	767	-50
3	186.6	-0.77	0.00	0.54	99 (47)	179 (39)	0.72	-0.36	454	-79
3	185.0	-0.78	0.33	0.00	140 (30)	56 (21)	0.33	0.33	253	84
3	186.1	-0.52	0.18	0.53	111 (36)	156 (34)	0.88	-0.17	423	-46
3	185.5	-0.52	0.01	0.54	39 (28)	127 (23)	0.73	-0.35	294	-88
3	185.6	-0.52	0.34	0.00	109 (25)	30 (12)	0.34	0.34	170	79
3	184.9	-0.52	0.68	0.00	291 (34)	87 (32)	0.68	0.68	466	204
3	186.5	-0.26	0.17	0.52	70 (20)	127 (20)	0.87	-0.18	325	-57
3	186.3	-0.26	0.35	1.06	272 (18)	414 (53)	1.76	-0.35	1100	-142
3	186.9	-0.26	0.01	0.53	24 (8)	121 (18)	0.71	-0.34	267	-97
3	186.2	-0.26	0.01	1.06	70 (19)	321 (36)	1.42	-0.70	711	-251
3	188.1	-0.26	0.34	0.00	110 (11)	10 (3)	0.34	0.34	130	101
3	185.4	-0.26	0.67	0.00	247 (14)	28 (16)	0.67	0.67	303	219
3	186.9	0.00	0.18	0.55	43 (18)	87 (14)	0.91	-0.19	218	-44
3	186.9	0.00	0.35	1.05	146 (32)	264 (57)	1.74	-0.35	674	-117

/contd.

Table D.5 (contd.)

No. of Samples (1)	p_m, (kN/m^2) (2)	S_m (3)	p_r/p_m (4)	q_r/q_m (5)	v_r (με) (6)	ϵ_r (με) (7)	$(T_r)_A$ (8)	$(T_r)_B$ (9)	$(W_r)_A$ (με) (10)	$(W_r)_B$ (με) (11)
3	187.1	0.00	0.51	1.54	403 (75)	659(174)	2.57	-0.52	1721	-256
3	186.1	0.00	0.01	0.55	-9 (11)	86 (10)	0.75	-0.36	163	-93
3	186.1	-0.01	0.01	1.06	7 (28)	247 (52)	1.43	-0.70	501	-240
3	185.8	-0.01	0.02	1.58	58 (53)	503 (11)	2.12	-1.03	1064	-444
6	186.3	0.00	0.17	0.00	45 (9)	-4 (2)	0.17	0.17	37	50
9	185.8	0.00	0.34	0.00	101 (12)	-4 (3)	0.34	0.34	92	105
5	185.9	0.00	0.51	0.00	174 (17)	-7 (8)	0.51	0.51	160	180
9	185.8	0.00	0.67	0.00	235 (20)	-5 (9)	0.67	0.67	225	240
8	187.1	0.26	0.18	0.53	45 (16)	101 (17)	0.87	-0.17	248	-56
3	187.3	0.25	0.35	1.04	86 (27)	225 (17)	1.73	-0.34	536	-138
3	186.9	0.25	0.52	1.57	237 (45)	473 (87)	2.62	-0.53	1183	-236
6	186.3	0.26	0.01	0.53	-19 (11)	99 (12)	0.72	-0.34	179	-118
3	185.8	0.26	0.01	1.05	-31 (21)	235 (35)	1.41	-0.69	439	-265
3	186.0	0.25	0.02	1.59	-47 (42)	458 (68)	2.14	-1.01	869	-505
7	186.2	0.26	0.33	0.00	100 (7)	-12 (7)	0.33	0.33	64	120
6	186.1	0.26	0.66	0.00	244 (24)	-27 (4)	0.66	0.66	189	271

/contd.

Table D.5 (contd.)

No. of Samples (1)	p_m, (kN/m^2) (2)	S_m (3)	p_r/p_m (4)	q_r/q_m (5)	v_r (με) (6)	ϵ_r (με) (7)	$(T_r)_A$ (8)	$(T_r)_B$ (9)	$(W_r)_A$ (με) (10)	$(W_r)_B$ (με) (11)
6	187.4	0.51	0.09	0.26	2 (12)	31 (7)	0.43	-0.08	64	-29
9	187.1	0.51	0.18	0.53	14 (20)	83 (8)	0.89	-0.17	181	-69
6	187.1	0.51	0.26	0.79	41 (25)	145 (13)	1.31	-0.27	332	-104
9	187.5	0.51	0.35	1.04	59 (34)	228 (21)	1.74	-0.34	515	-169
3	188.1	0.51	0.51	1.54	163 (16)	415 (49)	2.57	-0.52	993	-251
3	188.2	0.52	0.68	2.05	326 (16)	759 (73)	3.41	-0.69	1844	-433
6	187.0	0.51	0.00	0.26	-25 (13)	36 (7)	0.35	-0.17	47	-61
9	187.2	0.51	0.01	0.53	-44 (18)	93 (8)	0.72	-0.34	142	-137
6	186.7	0.51	0.01	0.79	-62 (33)	158 (12)	1.06	-0.52	254	-220
9	187.4	0.51	0.01	1.05	-91 (46)	248 (21)	1.40	-0.69	406	-339
3	187.1	0.52	0.02	1.55	-111 (9)	446 (54)	2.09	-1.01	781	-557
3	186.6	0.52	0.02	2.07	-190 (38)	783 (84)	2.78	-1.34	1375	-973
6	187.9	0.51	0.18	0.00	57 (7)	-16 (2)	0.18	0.18	25	73
9	187.5	0.51	0.35	0.00	113 (8)	-25 (3)	0.35	0.35	63	138
6	186.6	0.52	0.52	0.00	187 (11)	-37 (3)	0.52	0.52	113	225
9	186.6	0.52	0.68	0.00	259 (26)	-56 (7)	0.68	0.68	147	315
6	187.4	0.51	0.35	0.53	85 (16)	75 (10)	1.05	0.00	235	10
6	188.4	0.51	0.66	1.02	227 (40)	218 (29)	2.03	-0.02	662	9
6	186.9	0.51	0.52	0.52	153 (15)	72 (10)	1.23	0.17	297	82

/contd.

Table D.5 (contd.)

No. of Samples (1)	p_m, (kN/m^2) (2)	S_m (3)	p_r/p_m (4)	q_r/q_m (5)	v_r (με) (6)	ϵ_r (με) (7)	$(T_r)_A$ (8)	$(T_r)_B$ (9)	$(W_r)_A$ (με) (10)	$(W_r)_B$ (με) (11)
5	186.1	0.52	1.02	1.02	397 (33)	217 (32)	2.38	0.34	832	180
5	187.0	0.51	-0.51	0.53	-262 (24)	147 (8)	0.20	-0.86	32	-409
9	188.1	0.77	0.17	0.52	7 (20)	83 (29)	0.87	-0.18	172	-76
9	187.9	0.76	0.34	1.03	28 (29)	192 (16)	1.72	-0.35	413	-164
9	188.0	0.77	0.51	1.54	69 (44)	266 (35)	2.52	-0.52	802	-297
3	188.3	0.77	0.68	2.03	172 (29)	638 (78)	3.38	-0.67	1448	-466
9	187.6	0.77	0.00	0.52	-57 (28)	90 (9)	0.70	-0.35	123	-148
9	187.6	0.77	0.01	1.03	-124 (46)	233 (20)	1.39	-0.68	342	-356
8	187.3	0.77	0.02	1.55	-236 (74)	458 (40)	2.08	-1.01	681	-694
9	187.3	0.77	0.34	0.00	125 (8)	-32 (4)	0.34	0.34	60	158
9	187.3	0.77	0.67	0.00	293 (27)	-81 (12)	0.67	0.67	130	374
6	188.4	1.02	0.09	0.26	-10 (10)	25 (4)	0.48	-0.08	41	-35
9	188.3	1.02	0.17	0.52	-9 (16)	68 (7)	0.87	-0.18	127	-76
6	188.2	1.02	0.26	0.78	-9 (23)	117 (8)	1.30	-0.28	226	-126
9	188.2	1.02	0.34	1.03	-6 (30)	170 (11)	1.72	-0.35	334	-176
9	187.5	1.02	0.51	1.54	14 (40)	312 (25)	2.56	-0.52	638	-297
9	188.1	1.02	0.68	2.04	-9(132)	536 (45)	3.40	-0.68	1062	-544
5	187.9	1.02	0.00	0.26	-47 (10)	33 (4)	0.35	-0.17	19	-80
9	188.3	1.02	0.01	0.52	-84 (25)	93 (10)	0.70	-0.34	101	-177

/contd.

Table D.5 (contd.)

No. of Samples (1)	p_m, (kN/m^2) (2)	S_m (3)	p_r/p_m (4)	q_r/q_m (5)	v_r (με) (6)	ϵ_r (με) (7)	$(T_r)_A$ (8)	$(T_r)_B$ (9)	$(W_r)_A$ (με) (10)	$(W_r)_B$ (με) (11)
6	187.4	1.02	0.01	0.78	-137 (38)	157 (7)	1.06	-0.51	177	-294
9	188.0	1.02	0.01	1.03	-205 (50)	238 (18)	1.39	-0.68	271	-443
6	188.5	1.02	0.17	0.00	67 (4)	-22 (1)	0.17	0.17	22	90
9	188.3	1.02	0.33	0.00	150 (11)	-47 (4)	0.33	0.33	55	198
6	188.7	1.02	0.50	0.00	253 (19)	-79 (5)	0.50	0.50	96	332
9	188.6	1.02	0.66	0.00	376 (34)	-118 (10)	0.66	0.66	139	494
6	188.1	1.02	0.34	0.52	74 (13)	47 (5)	1.04	-0.01	168	26
6	187.7	1.02	0.68	1.03	164 (21)	134 (13)	2.06	-0.01	431	30
5	188.5	1.02	1.32	2.00	443 (40)	456 (36)	3.98	-0.02	1355	-12
8	188.2	1.02	0.51	0.52	153 (44)	33 (13)	1.20	0.16	219	119
6	187.7	1.02	1.00	1.03	377 (19)	87 (12)	2.38	0.31	551	290
6	188.0	1.02	-0.48	0.52	-433 (83)	215 (20)	0.22	-0.83	-3	-648
9	189.4	1.27	0.17	0.51	-10 (15)	65 (8)	0.85	-0.17	119	-75
6	188.7	1.27	0.34	1.02	-23 (31)	157 (12)	1.69	-0.34	291	-180
6	188.6	1.27	0.51	1.54	-51 (48)	292 (21)	2.56	-0.52	533	-343
8	189.4	1.27	0.00	0.51	-102 (26)	96 (10)	0.69	-0.34	90	-199
9	188.7	1.28	0.34	0.00	180 (17)	-59 (17)	0.34	0.34	62	239
5	189.3	1.52	0.17	0.52	-19 (11)	65 (5)	0.86	-0.17	110	-84

Table D.6 Resilient Strain Tests, Average Data, p_m approx. 384 kN/m^2

No. of Samples (1)	p_m, (kN/m^2) (2)	S_m (3)	p_r/p_m (4)	q_r/q_m (5)	v_r (με) (6)	ϵ_r (με) (7)	$(T_r)_A$ (8)	$(T_r)_B$ (9)	$(W_r)_A$ (με) (10)	$(W_r)_B$ (με) (11)
2	373.6	0.00	0.15	0.00	54 (6)	-5 (1)	0.15	0.15	44	58
5	373.6	0.00	0.32	0.00	135 (23)	-1 (5)	0.32	0.32	133	136
5	378.3	0.50	0.17	0.51	36 (18)	98 (6)	0.85	-0.17	233	-62
5	378.6	0.51	0.34	1.01	101 (35)	255 (9)	1.68	-0.34	611	-153
5	377.9	0.51	0.00	0.51	-48 (21)	104 (13)	0.68	-0.34	161	-153
4	377.7	0.51	0.01	1.01	-101 (52)	266 (14)	1.35	-0.67	431	-367
5	377.2	0.51	0.35	0.00	161 (16)	-22 (8)	0.35	0.35	116	183
4	371.7	0.51	0.66	0.00	378 (36)	-48 (20)	0.66	0.66	283	426
5	380.1	1.01	0.17	0.50	15 (17)	85 (7)	0.83	-0.17	185	-70
5	379.1	1.01	0.33	1.00	30 (33)	222 (6)	1.66	-0.33	475	-192
5	378.6	1.00	0.66	1.99	62(162)	594(153)	3.31	-0.66	1250	-532
5	378.7	1.01	-0.01	0.50	-103 (27)	112 (11)	0.65	-0.35	121	-215
5	377.9	1.01	-0.00	1.00	-265 (80)	302 (7)	1.33	-0.67	339	-567
5	376.7	1.02	0.35	0.00	225 (20)	-57 (9)	0.35	0.35	111	281
3	371.4	1.04	0.69	0.00	535 (32)	-142 (16)	0.69	0.69	251	677

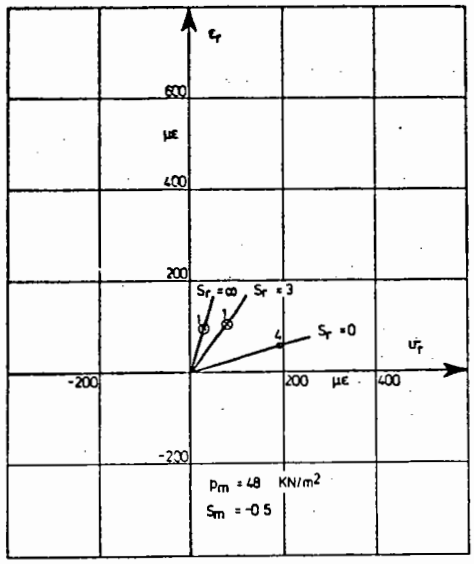

(a) $S_m = -0.5$

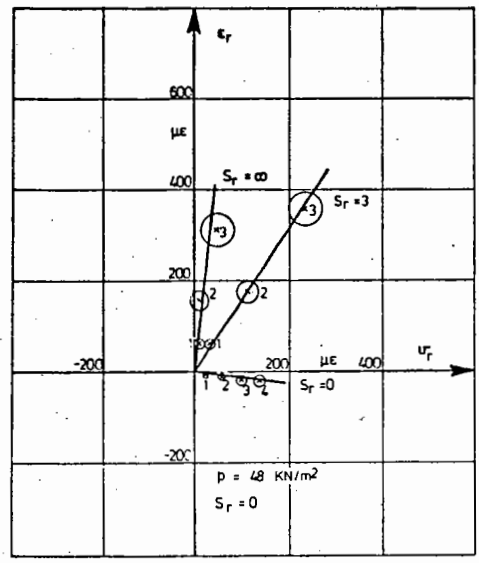

(b) $S_m = 0$

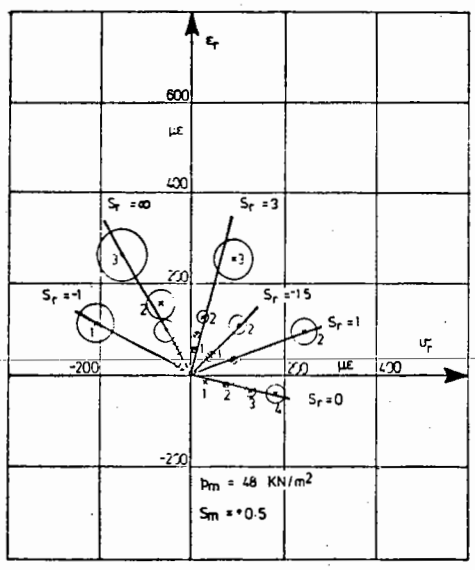

(c) $S_m = +0.5$

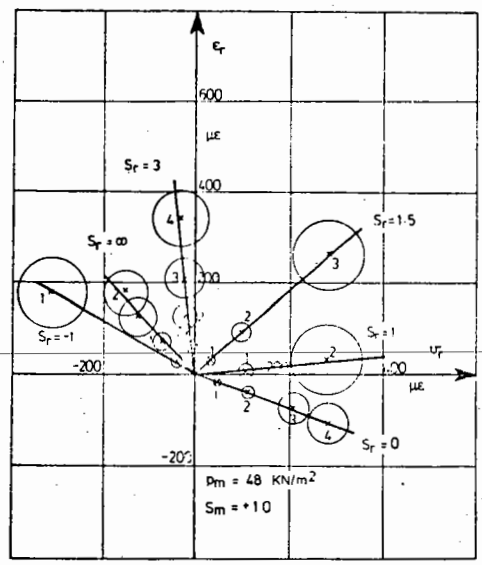

(d) $S_m = +1.0$

FIG. D.1 RESILIENT STRAIN DIAGRAMS FOR p_m = 48 kN/m² SHOWING DEGREE OF VARIATION BETWEEN SAMPLES

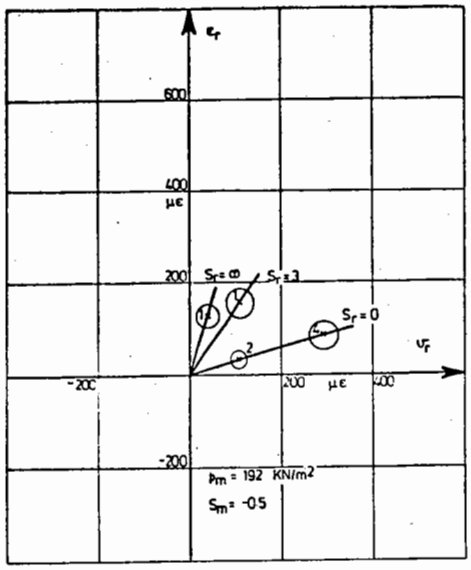

(a) $S_m = -0.5$

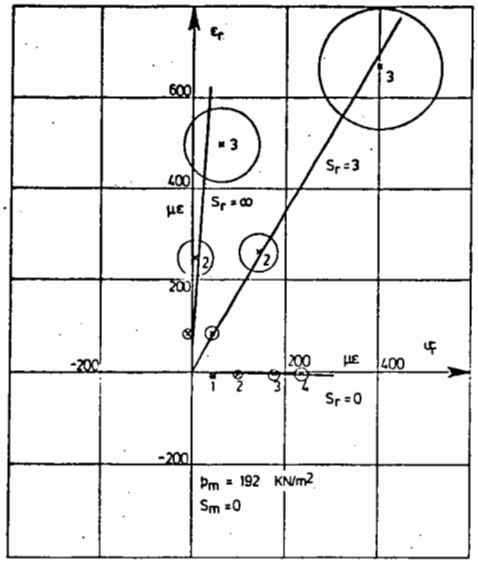

(b) $S_m = 0$

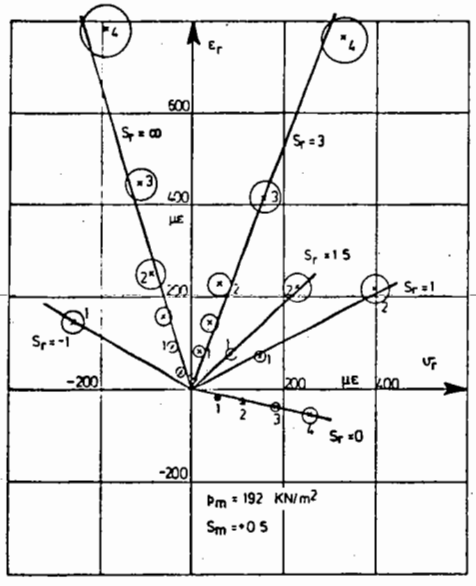

(c) $S_m = +0.5$

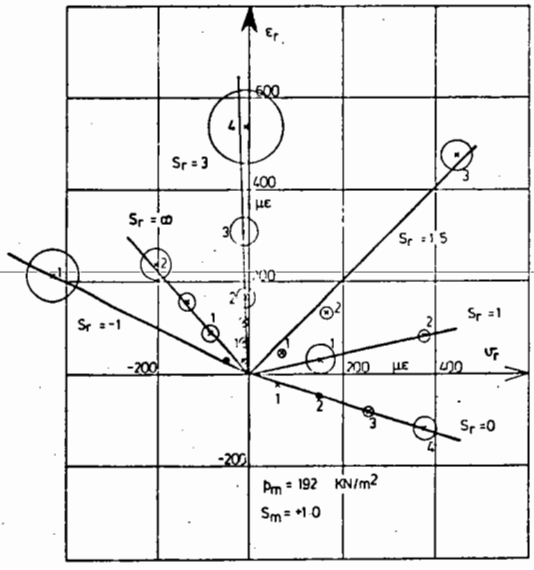

(d) $S_m = +1.0$

FIG. D.2 RESILIENT STRAIN DIAGRAMS FOR p_m = 192 kN/m^2 SHOWING DEGREE OF VARIATION BETWEEN SAMPLES

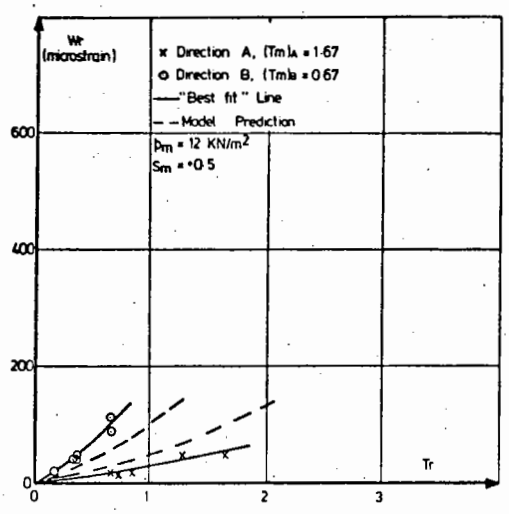

(a) $S_m = +0.5$

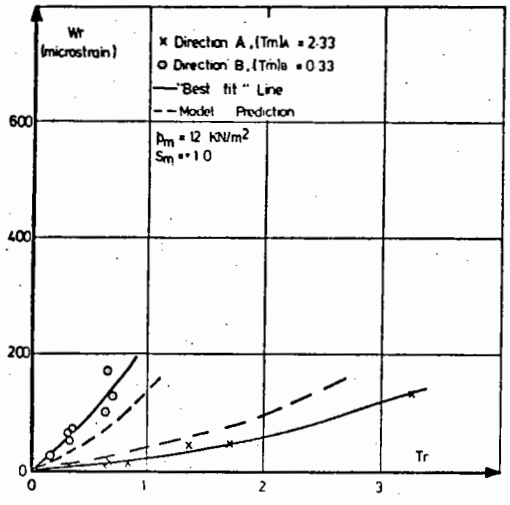

(b) $S_m = -0.5$

FIG. D.3 RELATIONSHIP BETWEEN THE RESILIENT STRAIN PARAMETER, W_r, AND THE REPEATED STRESS PARAMETER, T_r, FOR p_m = 12 kN/m^2

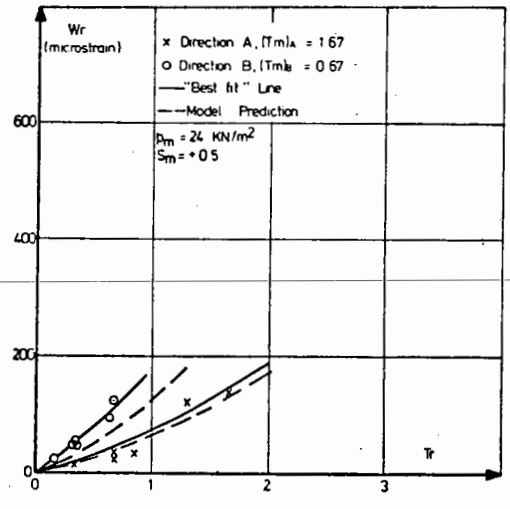

(a) $S_m = +0.5$

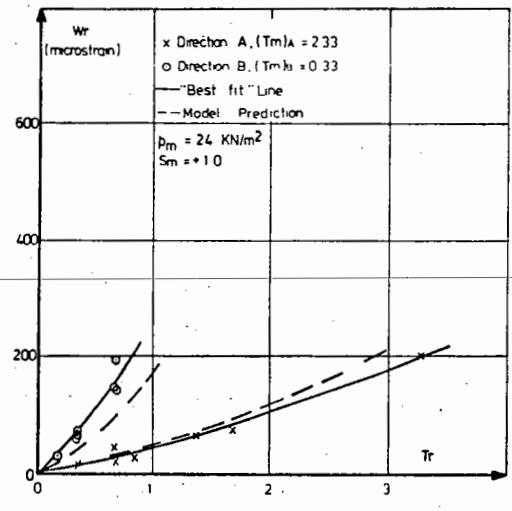

(b) $S_m = -0.5$

FIG. D.4 RELATIONSHIP BETWEEN THE RESILIENT STRAIN PARAMETER, W_r, AND THE REPEATED STRESS PARAMETER, T_r, FOR p_m = 24 kN/m^2

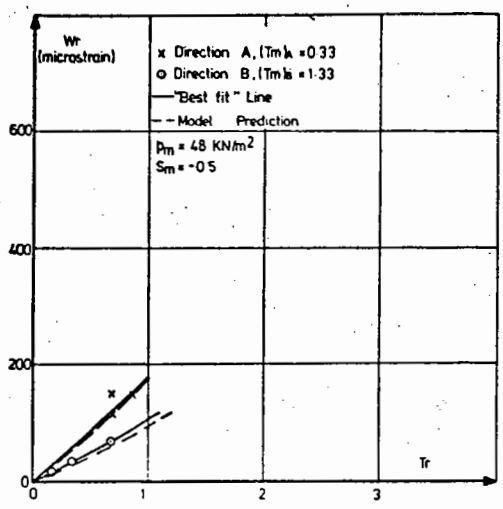

(a) $S_m = -0.5$

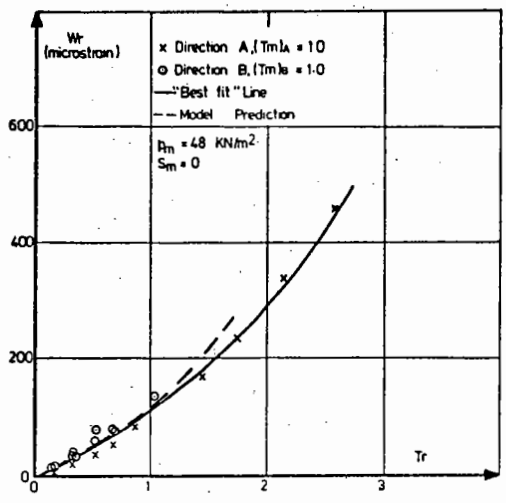

(b) $S_m = 0$

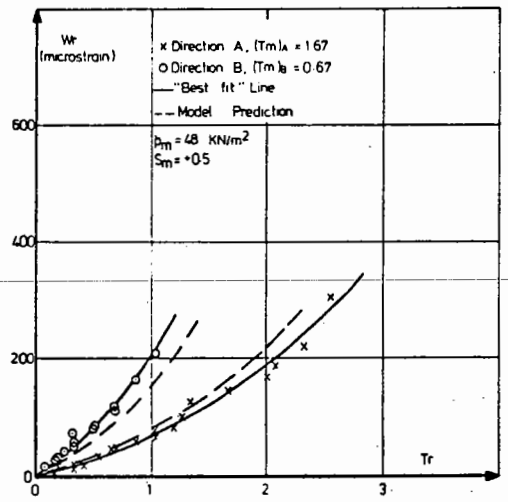

(c) $S_m = +0.5$

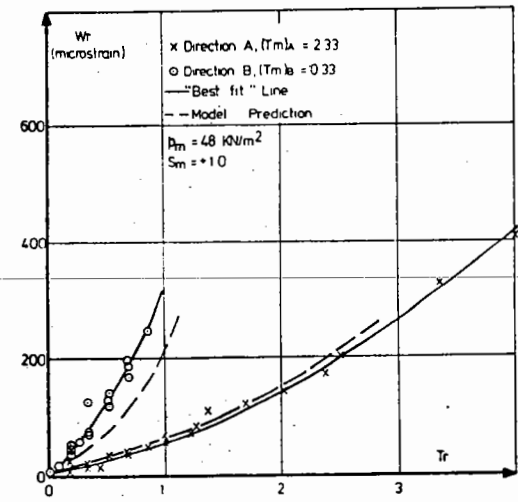

(d) $S_m = +1.0$

FIG. D.5 RELATIONSHIP BETWEEN THE RESILIENT STRAIN PARAMETER, W_r, AND THE REPEATED STRESS PARAMETER, T_r, FOR p_m = 48 kN/m^2

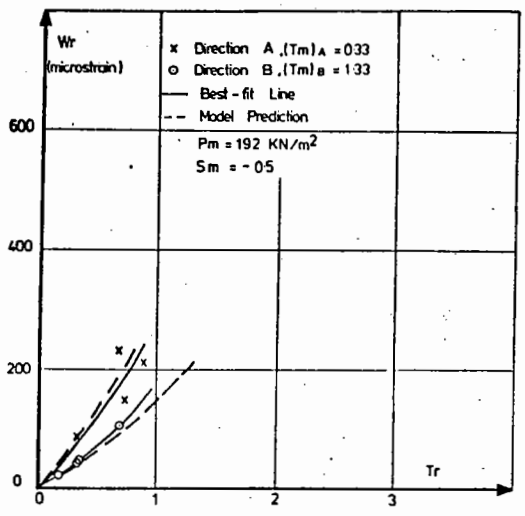

(a) $S_m = -0.5$

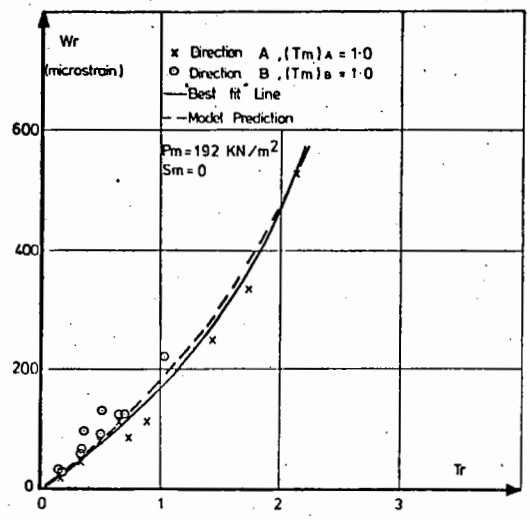

(b) $S_m = 0$

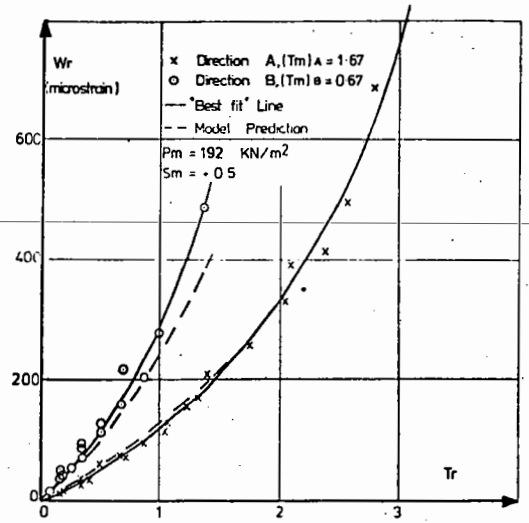

(c) $S_m = +0.5$

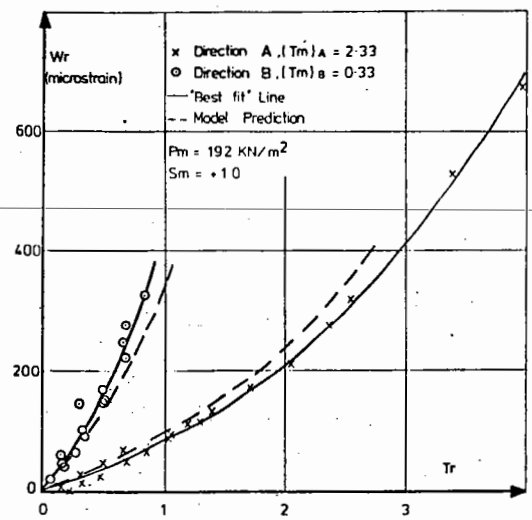

(d) $S_m = +1.0$

FIG. D.7 RELATIONSHIP BETWEEN THE RESILIENT STRAIN PARAMETER, W_r, AND THE REPEATED STRESS PARAMETER, T_r, FOR p_m = 192 kN/m^2

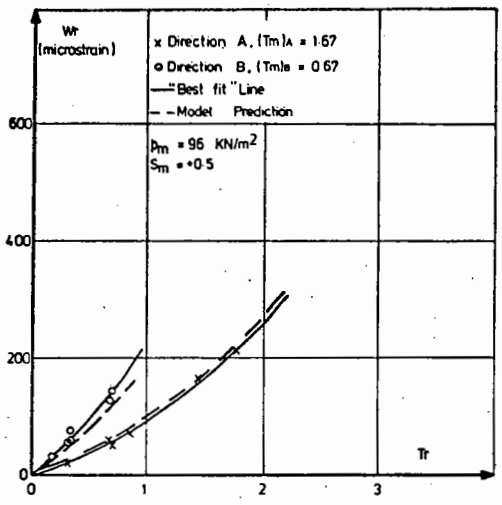

(a) $S_m = +0.5$

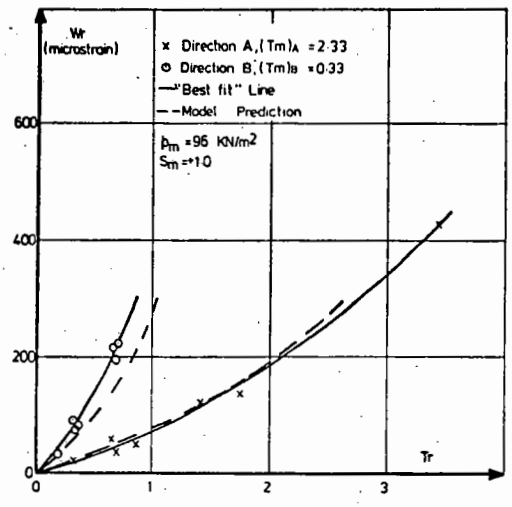

(b) $S_n = +1.0$

FIG. D.6 RELATIONSHIP BETWEEN THE RESILIENT STRAIN PARAMETER, W_r, AND THE REPEATED STRESS PARAMETER, T_r, FOR p_m = 96 kN/m^2

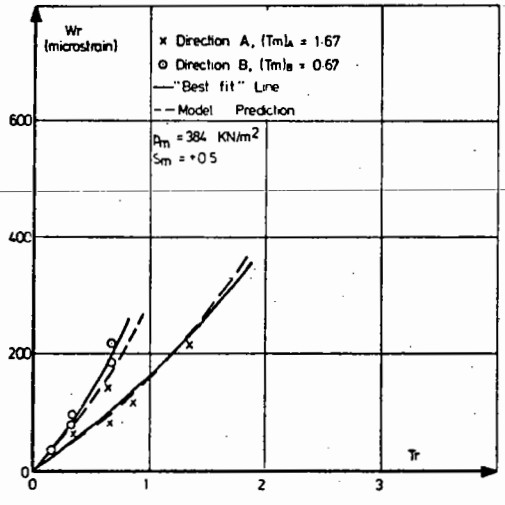

(a) $S_m = +0.5$

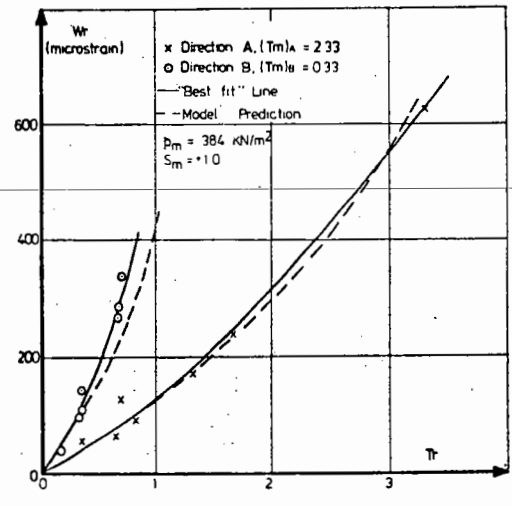

(b) $S_m = +1.0$

FIG. D.8 RELATIONSHIP BETWEEN THE RESILIENT STRAIN PARAMETER, W_r, AND THE REPEATED STRESS PARAMETER, T_r, FOR p_m = 384 kN/m^2

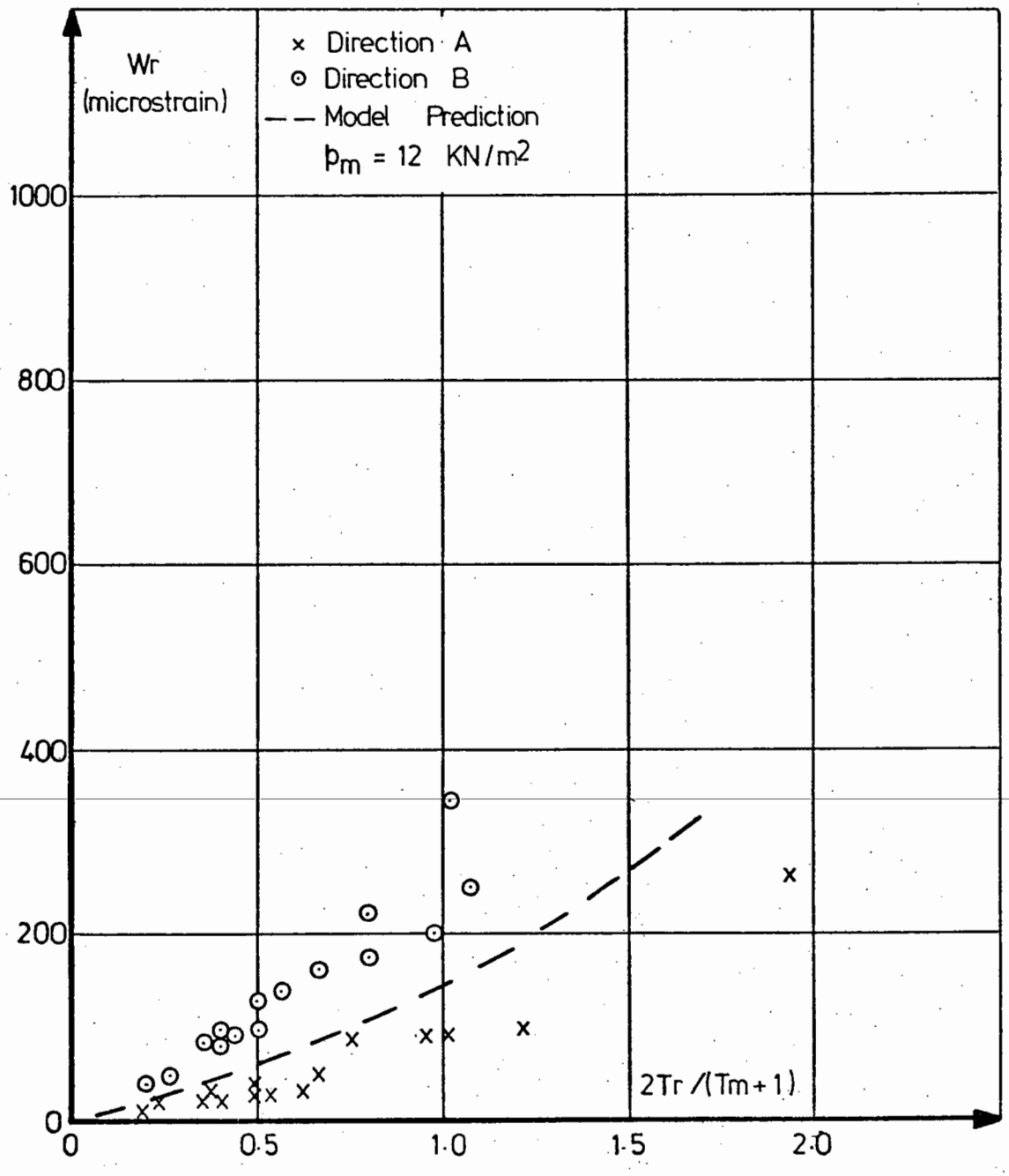

FIG. D.9 RELATIONSHIP BETWEEN THE RESILIENT STRAIN PARAMETER, W_r, AND THE STRESS FUNCTION, $2T_r/(T_m + 1)$, FOR p_m = 12 kN/m²

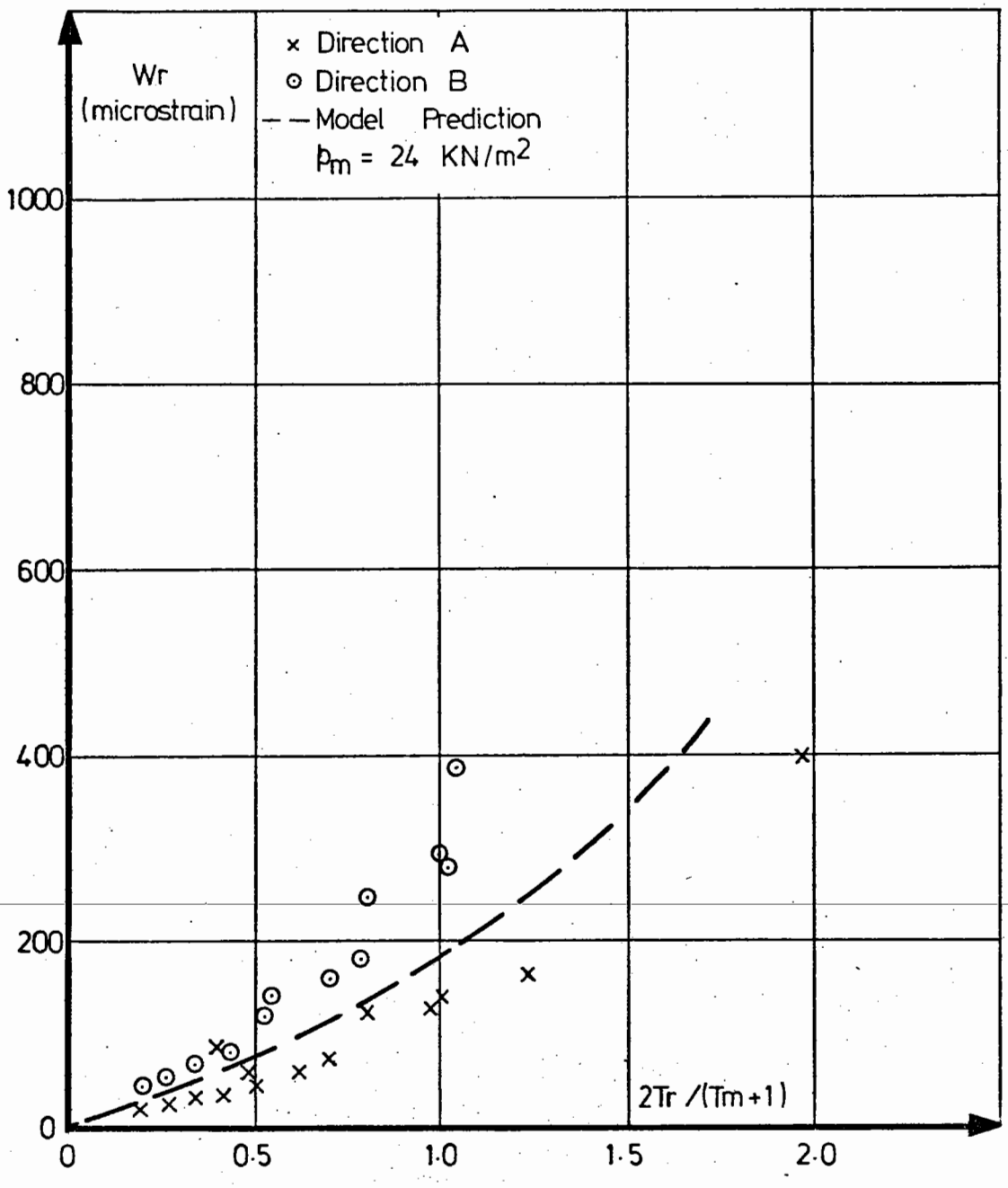

FIG. D.10 RELATIONSHIP BETWEEN THE RESILIENT STRAIN PARAMETER, W_r, AND THE STRESS FUNCTION, $2T_r/(T_m + 1)$, FOR p_m = 24 kN/m²

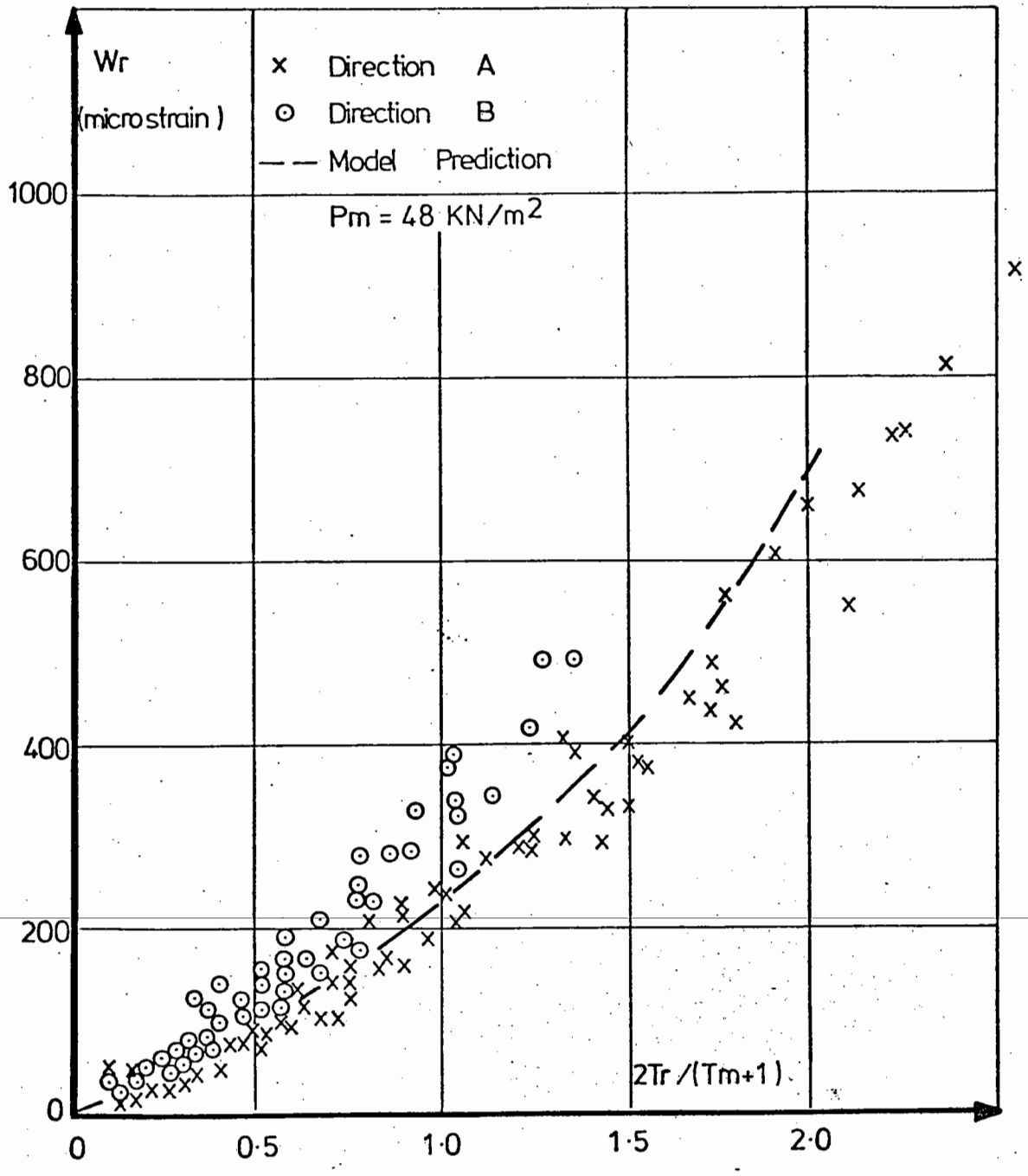

FIG. D.11 RELATIONSHIP BETWEEN THE RESILIENT STRAIN PARAMETER, W_r, AND THE STRESS FUNCTION, $2T_r/(T_m + 1)$, FOR p_m = 48 kN/m^2

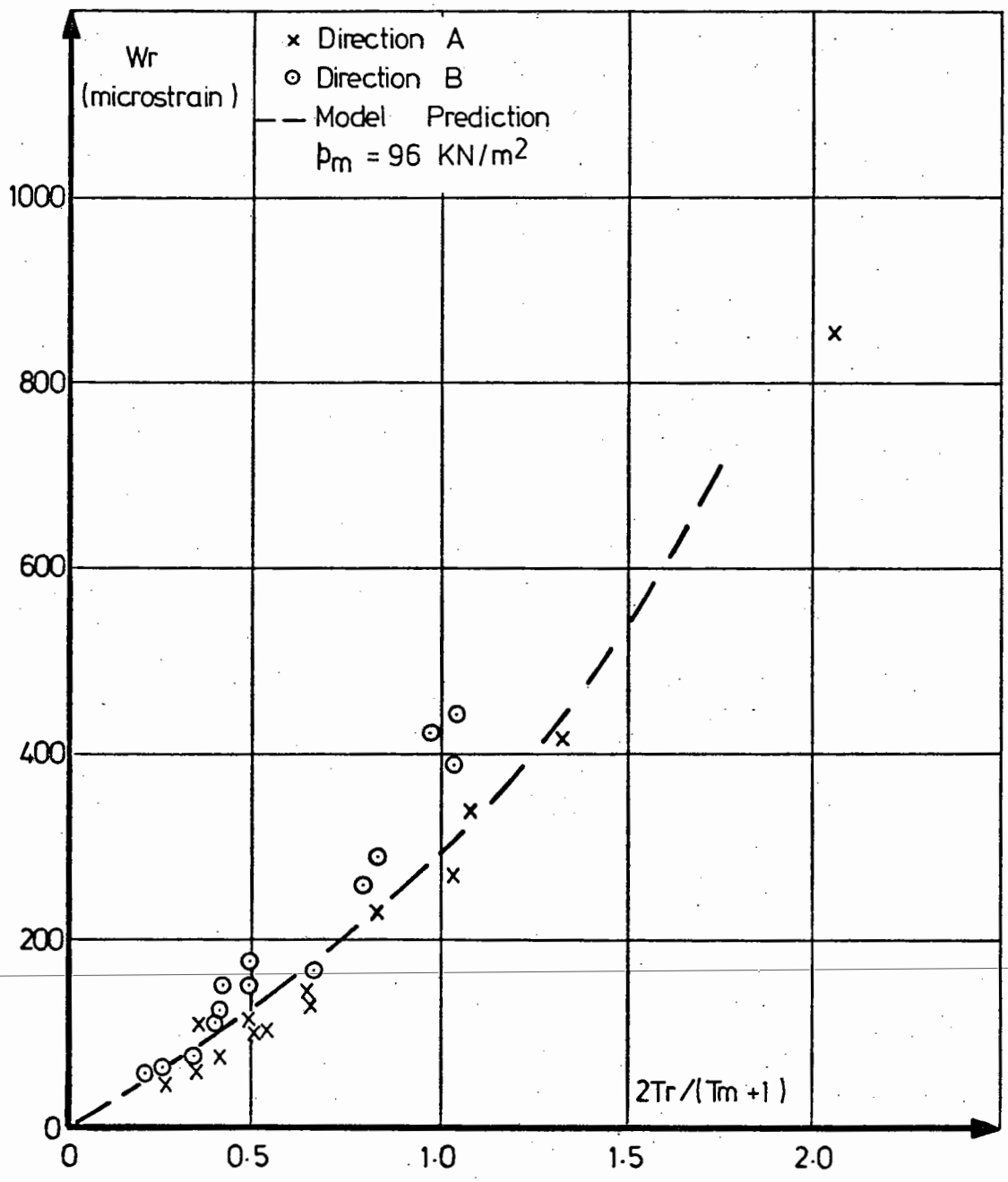

FIG. D.12 RELATIONSHIP BETWEEN THE RESILIENT STRAIN PARAMETER, W_r, AND THE STRESS FUNCTION, $2T_r/(T_m + 1)$, FOR p_m = 96 kN/m²

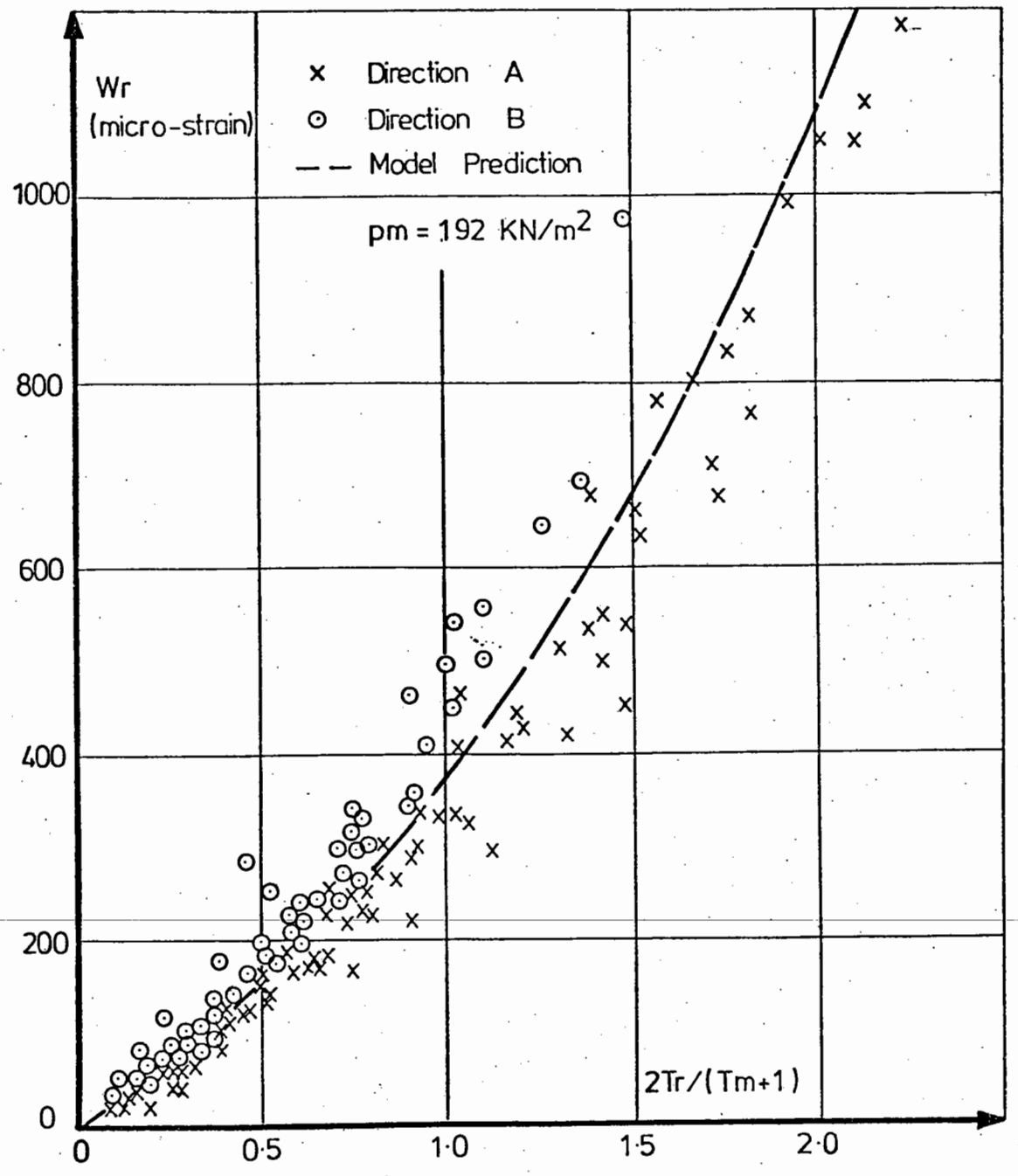

FIG. D.13 RELATIONSHIP BETWEEN THE RESILIENT STRAIN PARAMETER, W_r, AND THE STRESS FUNCTION, $2T_r/(T_m + 1)$, FOR p_m = 192 kN/m^2

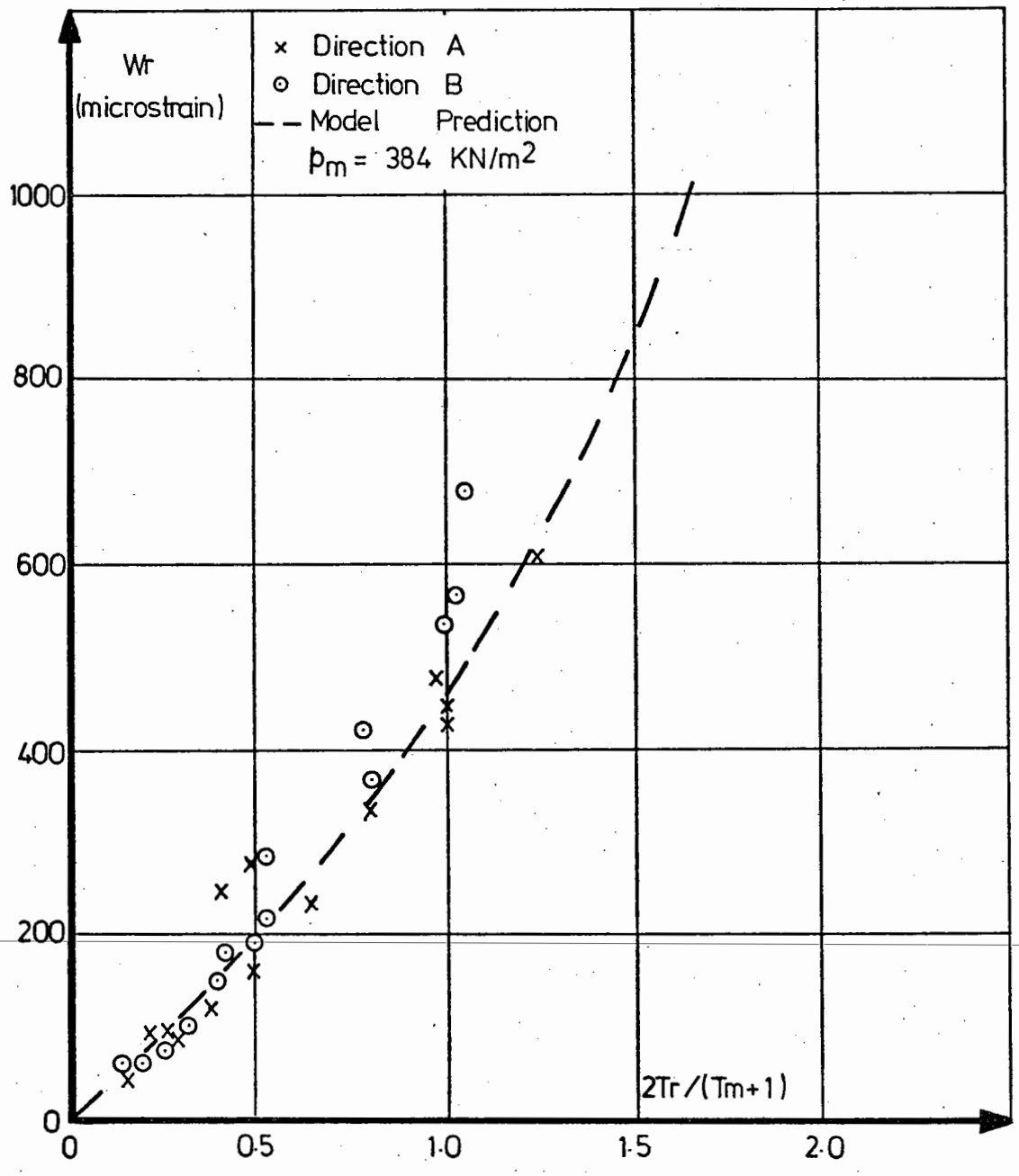

FIG. D.14 RELATIONSHIP BETWEEN THE RESILIENT STRAIN PARAMETER, W_r, AND THE STRESS FUNCTION, $2T_r/(T_m + 1)$, FOR p_m = 384 kN/m²

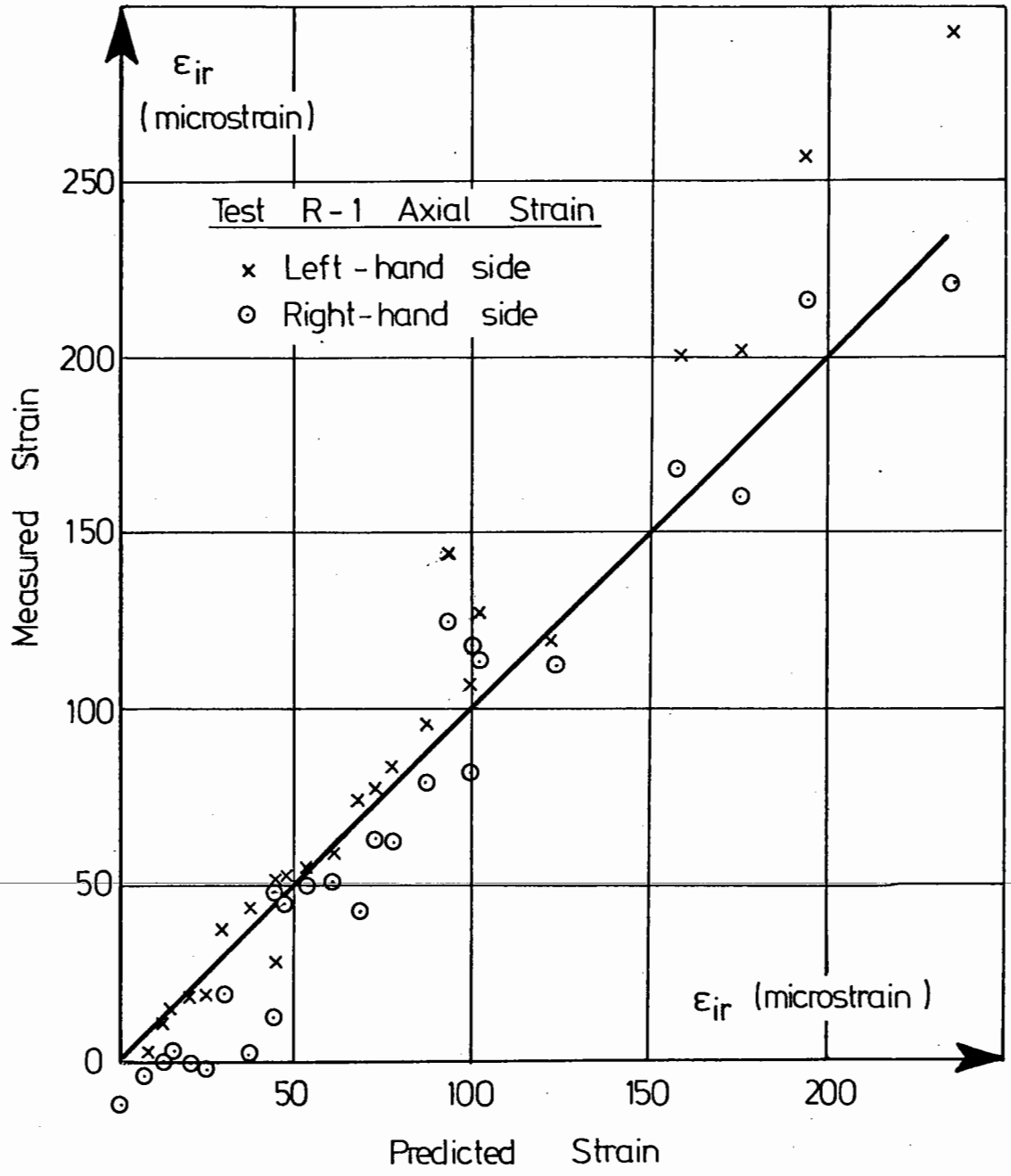

FIG. D.15 COMPARISON BETWEEN THE RESILIENT AXIAL STRAIN MEASURED ON EACH SIDE OF THE SAMPLE IN TEST R-1 AND THAT PREDICTED BY THE RESILIENT STRAIN MODEL

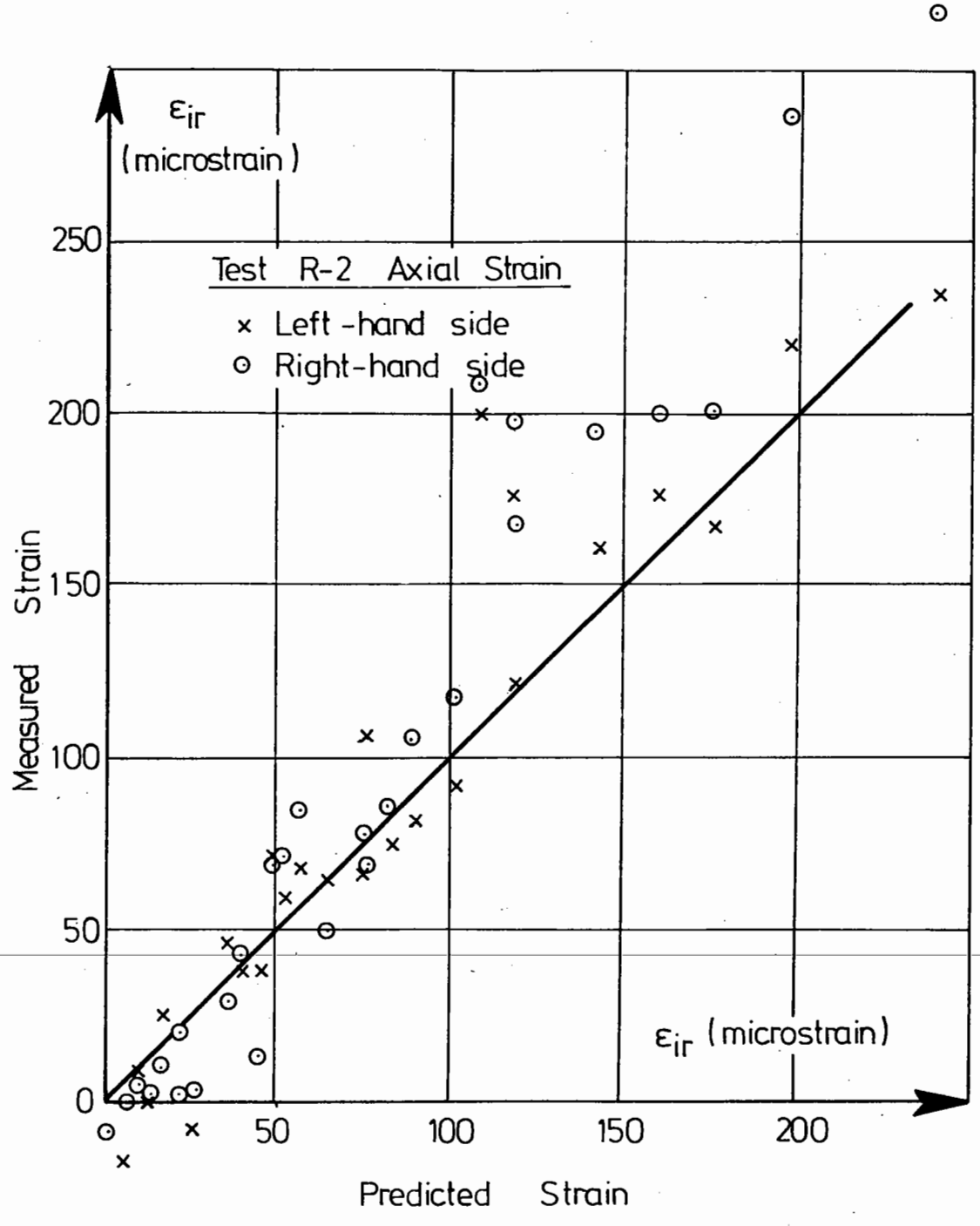

FIG. D.16 COMPARISON BETWEEN THE RESILIENT AXIAL STRAIN MEASURED ON EACH SIDE OF THE SAMPLE IN TEST R-2 AND THAT PREDICTED BY THE RESILIENT STRAIN MODEL

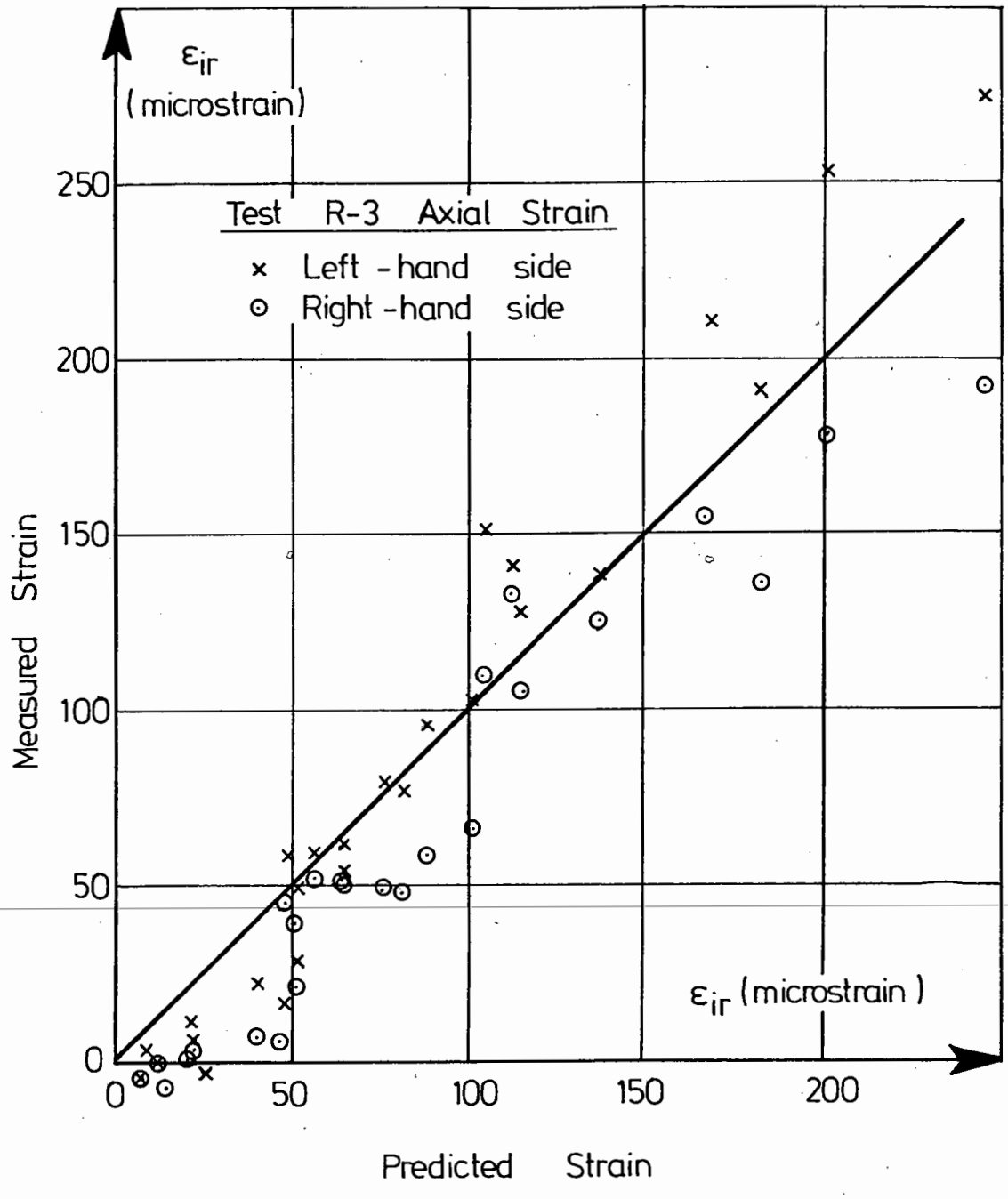

FIG. D.17 COMPARISON BETWEEN THE RESILIENT AXIAL STRAIN MEASURED ON EACH SIDE OF THE SAMPLE IN TEST R-3 AND THAT PREDICTED BY THE RESILIENT STRAIN MODEL

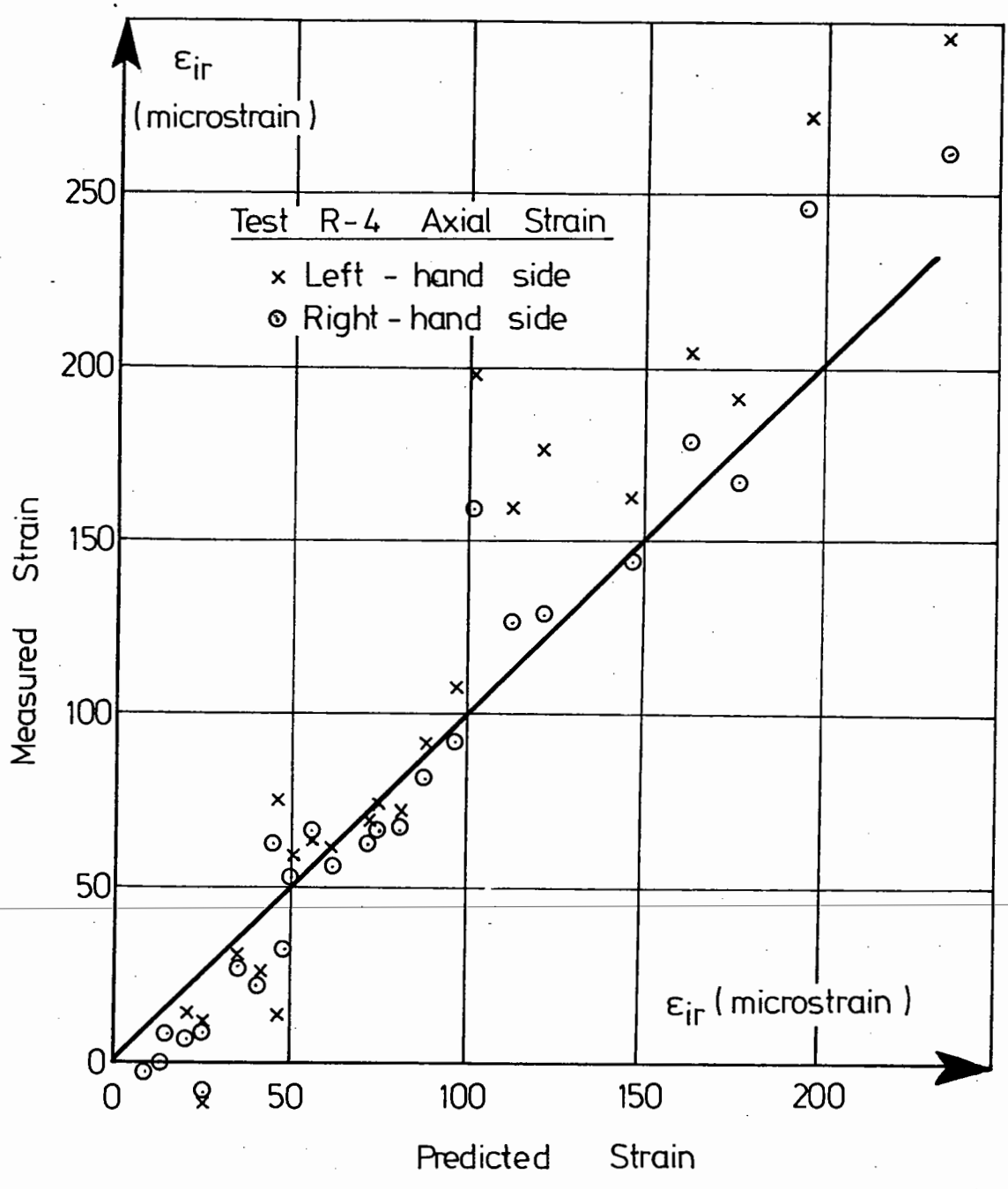

FIG. D.18 COMPARISON BETWEEN THE RESILIENT AXIAL STRAIN MEASURED ON EACH SIDE OF THE SAMPLE IN TEST R-4 AND THAT PREDICTED BY THE RESILIENT STRAIN MODEL

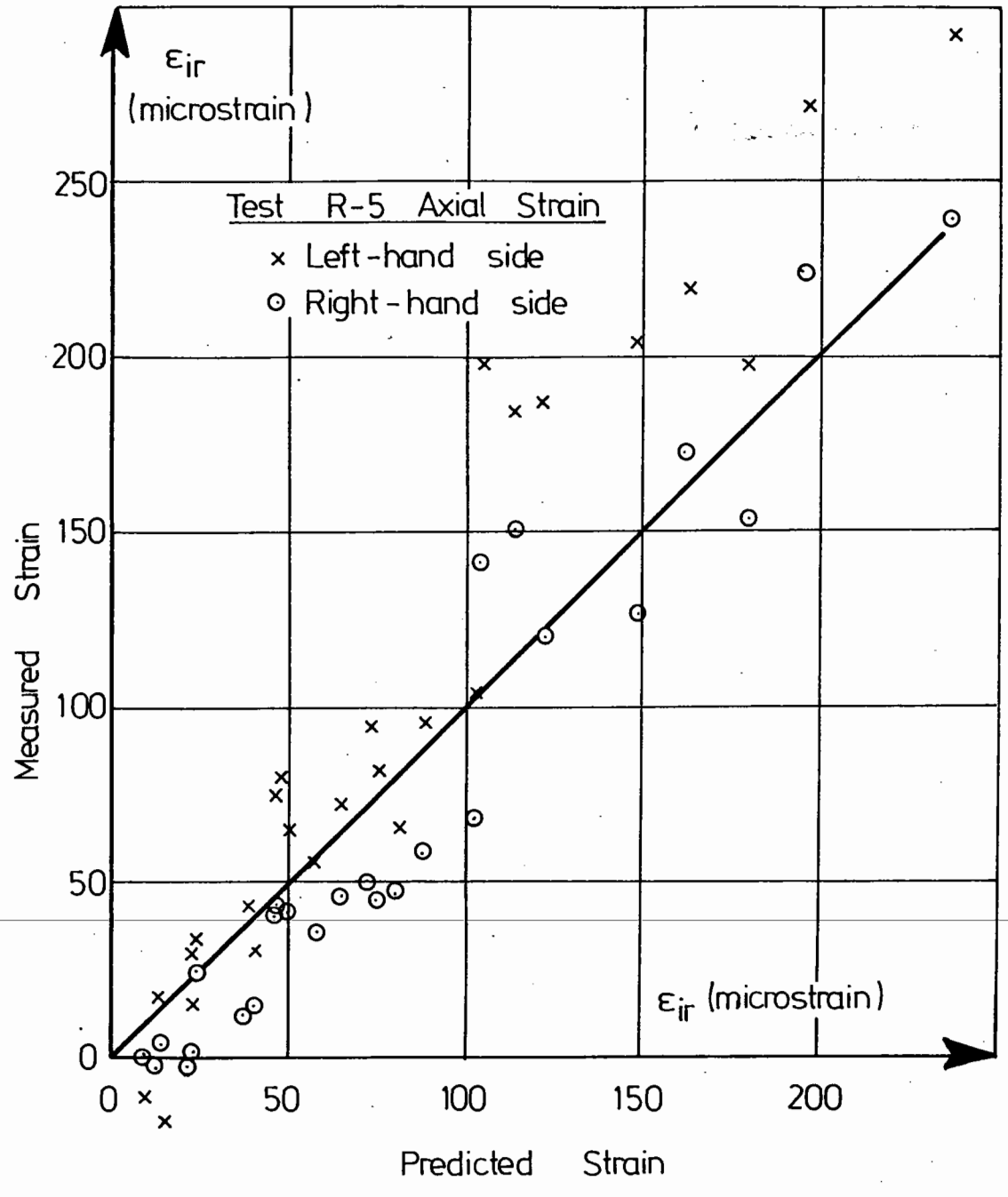

FIG. D.19 COMPARISON BETWEEN THE RESILIENT AXIAL STRAIN MEASURED ON EACH SIDE OF THE SAMPLE IN TEST R-5 AND THAT PREDICTED BY THE RESILIENT STRAIN MODEL

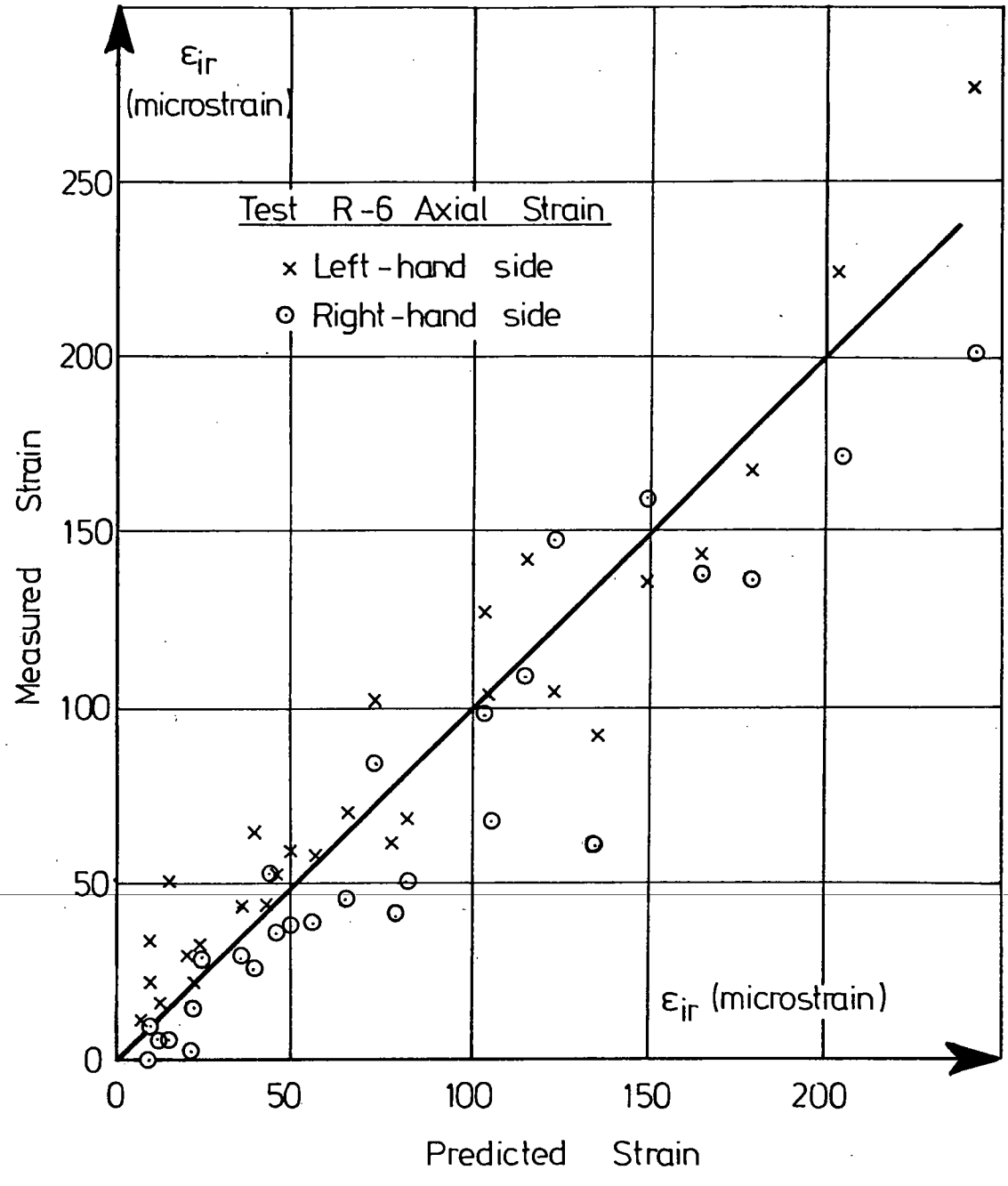

FIG. D.20 COMPARISON BETWEEN THE RESILIENT AXIAL STRAIN MEASURED ON EACH SIDE OF THE SAMPLE IN TEST R-6 AND THAT PREDICTED BY THE RESILIENT STRAIN MODEL

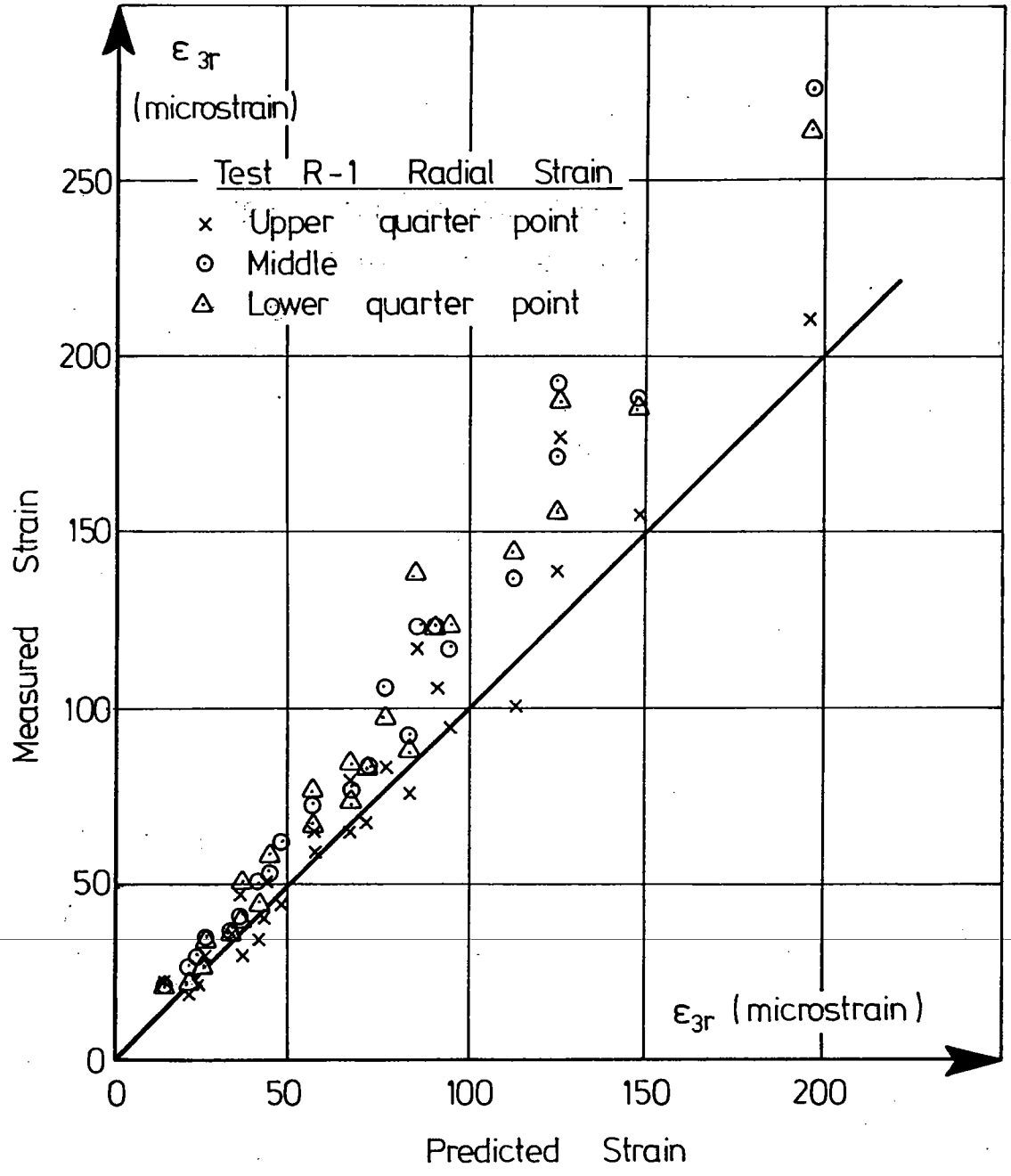

FIG. D.21 COMPARISON BETWEEN THE RESILIENT RADIAL STRAIN MEASURED AT THREE POINTS ON THE SAMPLE IN TEST R-1 AND THAT PREDICTED BY THE RESILIENT STRAIN MODEL

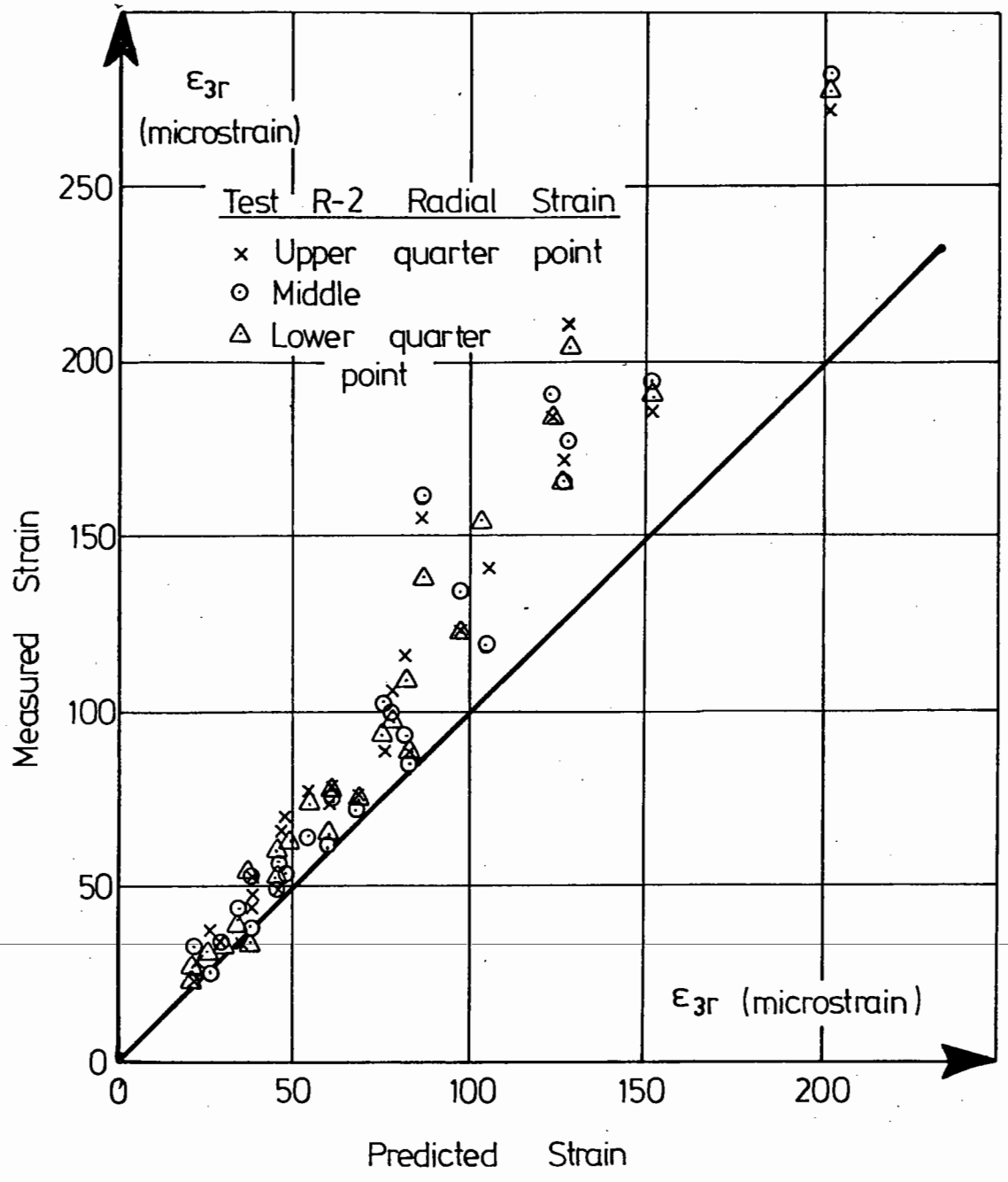

FIG. D.22 COMPARISON BETWEEN THE RESILIENT RADIAL STRAIN MEASURED AT THREE POINTS ON THE SAMPLE IN TEST R-2 AND THAT PREDICTED BY THE RESILIENT STRAIN MODEL

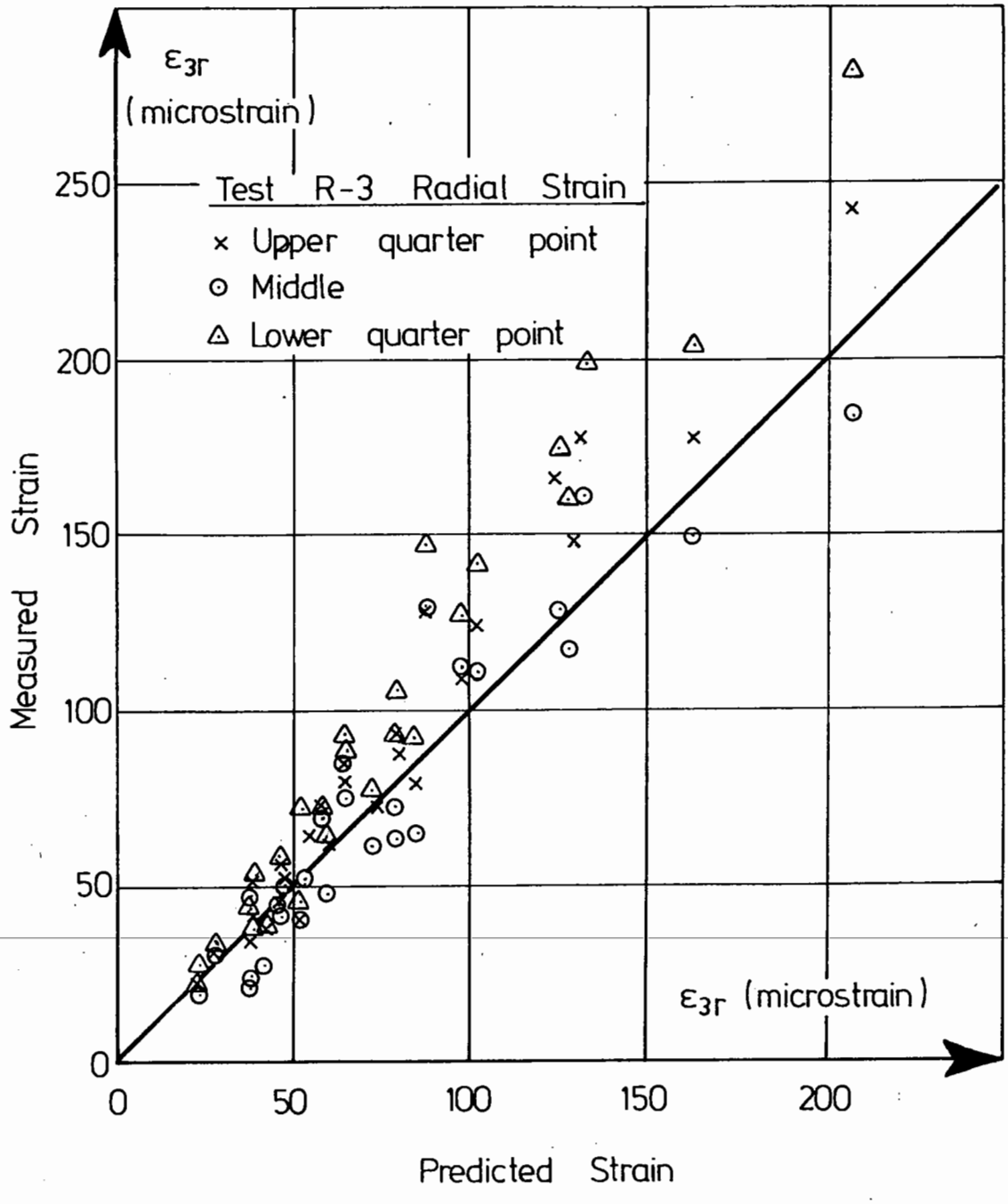

FIG. D.23 COMPARISON BETWEEN THE RESILIENT RADIAL STRAIN MEASURED AT THREE POINTS ON THE SAMPLE IN TEST R-3 AND THAT PREDICTED BY THE RESILIENT STRAIN MODEL

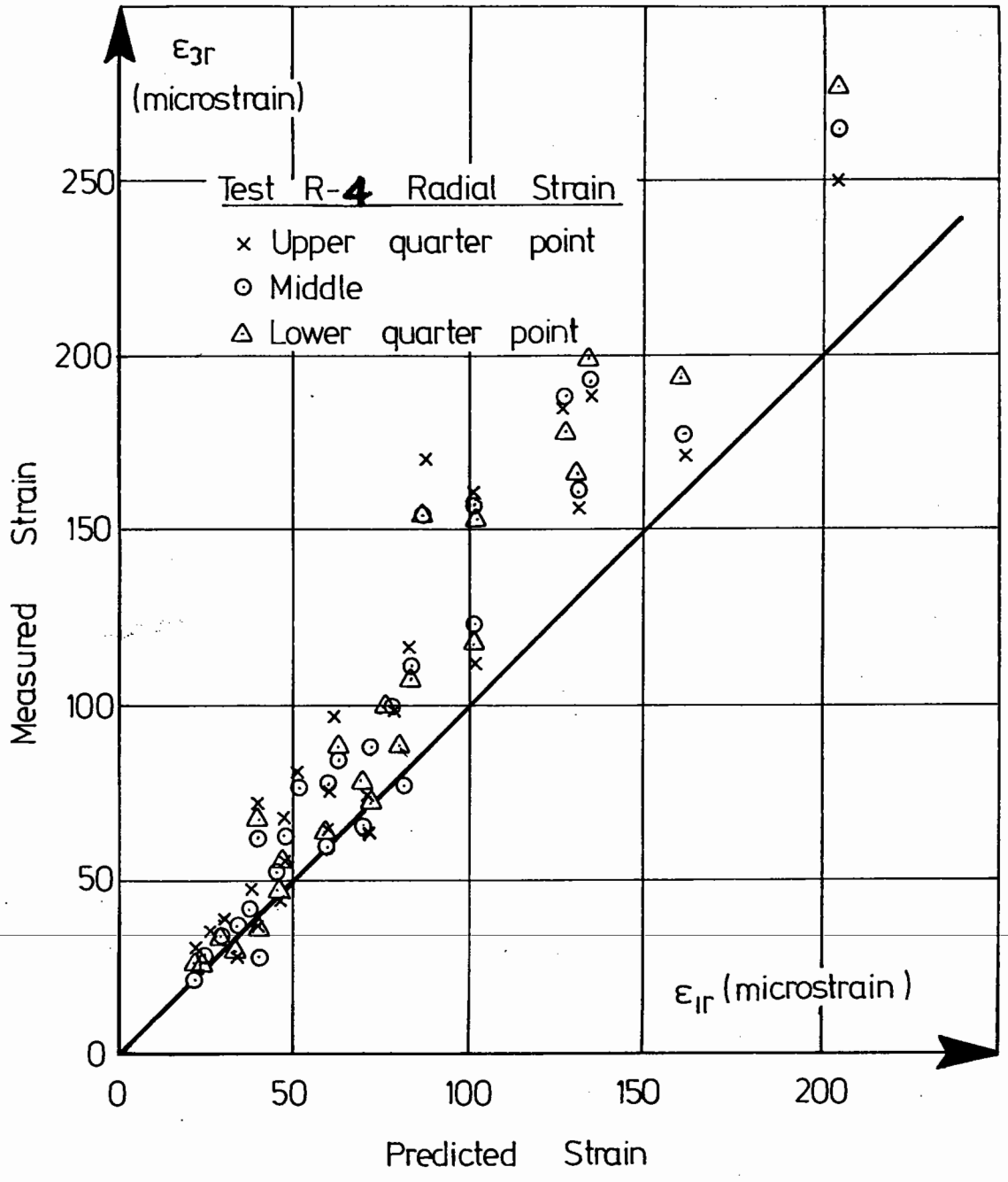

FIG. D.24 COMPARISON BETWEEN THE RESILIENT RADIAL STRAIN MEASURED AT THREE POINTS ON THE SAMPLE IN TEST R-4 AND THAT PREDICTED BY THE RESILIENT STRAIN MODEL

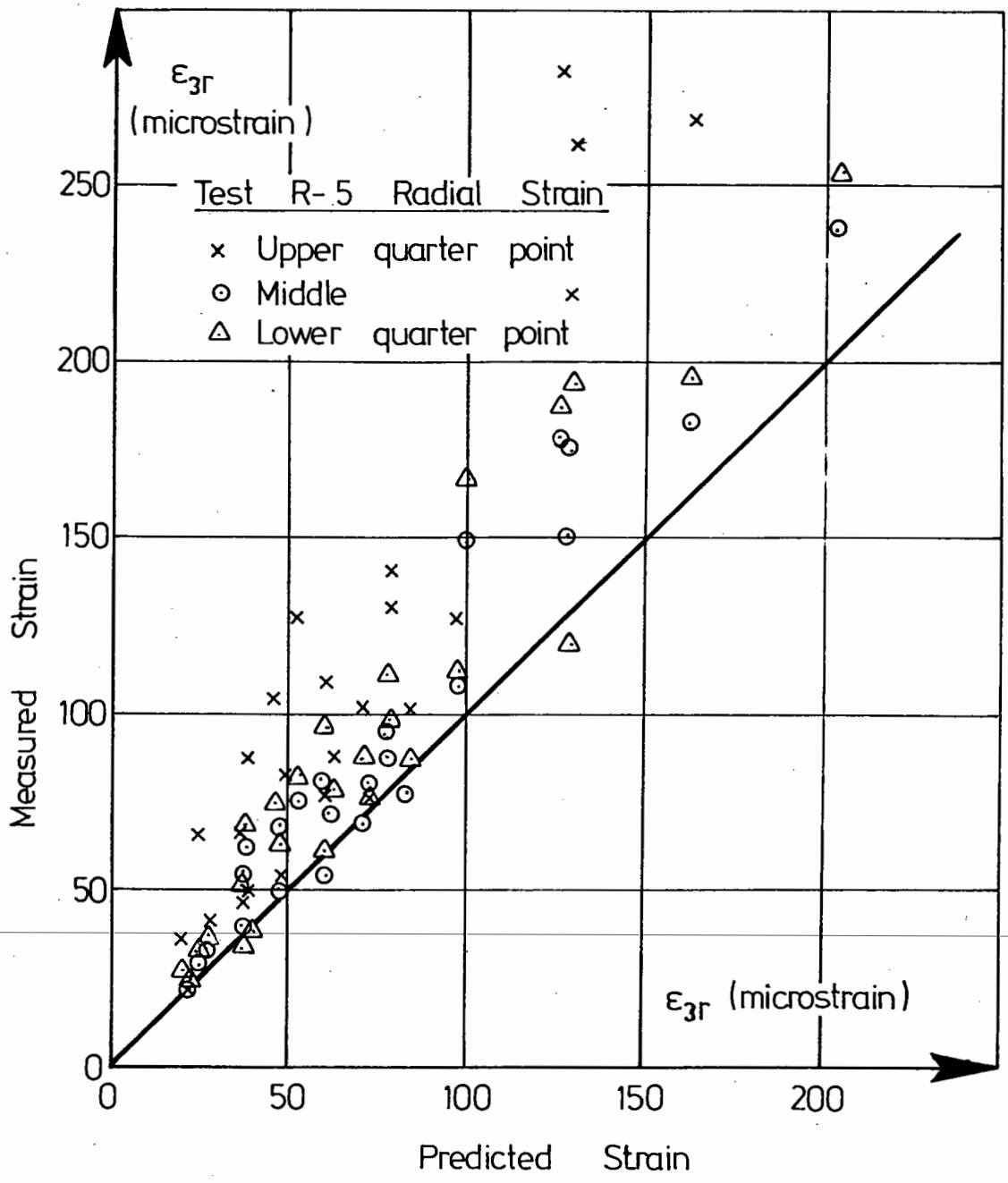

FIG. D.25 COMPARISON BETWEEN THE RESILIENT RADIAL STRAIN MEASURED AT THREE POINTS ON THE SAMPLE IN TEST R-5 AND THAT PREDICTED BY THE RESILIENT STRAIN MODEL

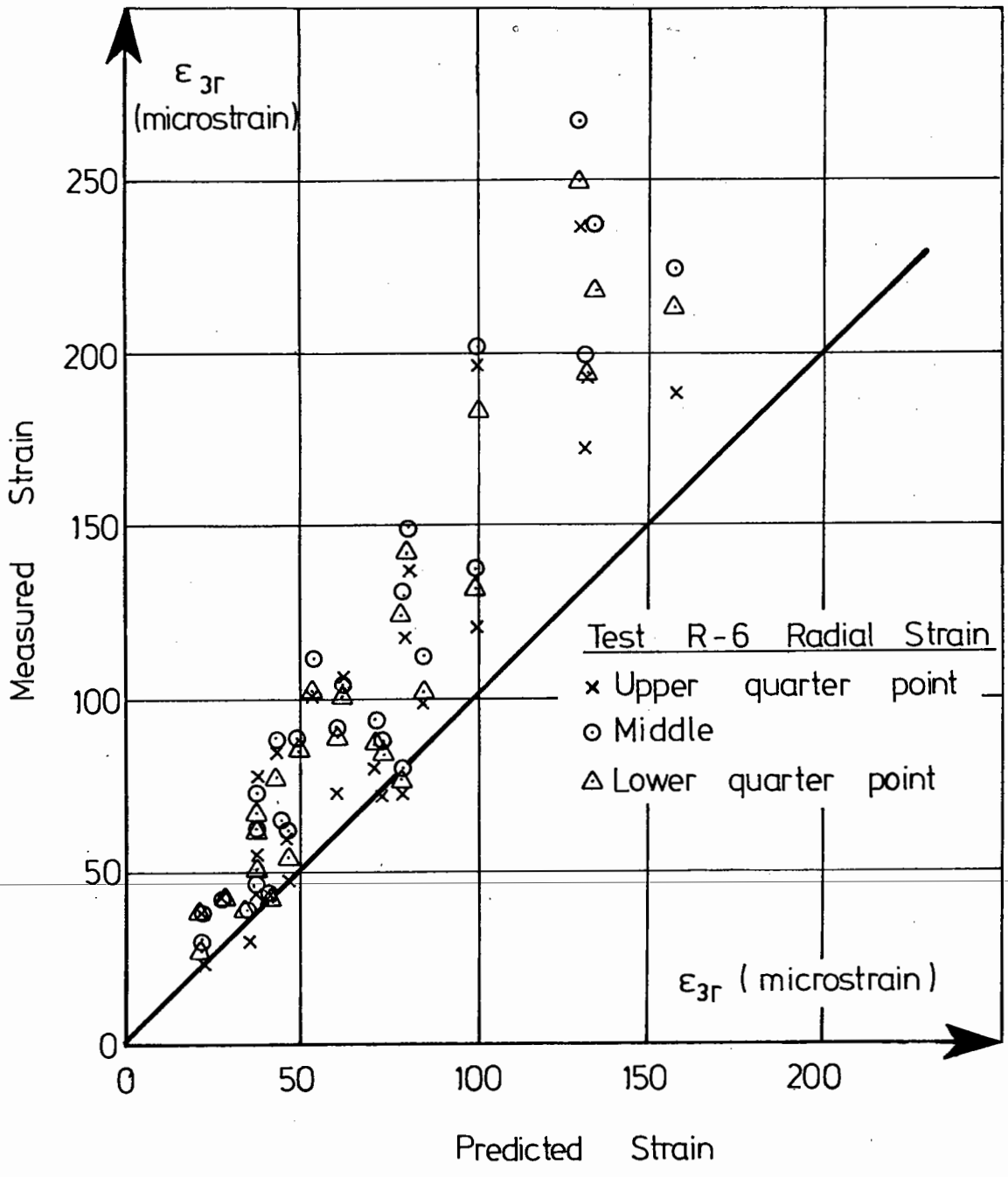

FIG. D.26 COMPARISON BETWEEN THE RESILIENT RADIAL STRAIN MEASURED AT THREE POINTS ON THE SAMPLE IN TEST R-6 AND THAT PREDICTED BY THE RESILIENT STRAIN MODEL

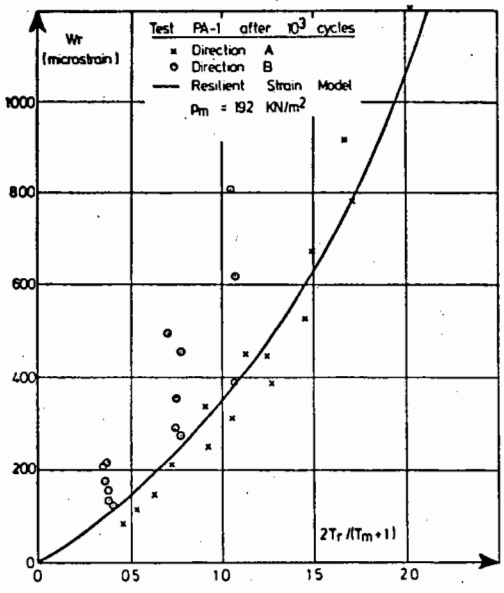

(a) After 10^3 cycles
(p_m = 192 kN/m^2)

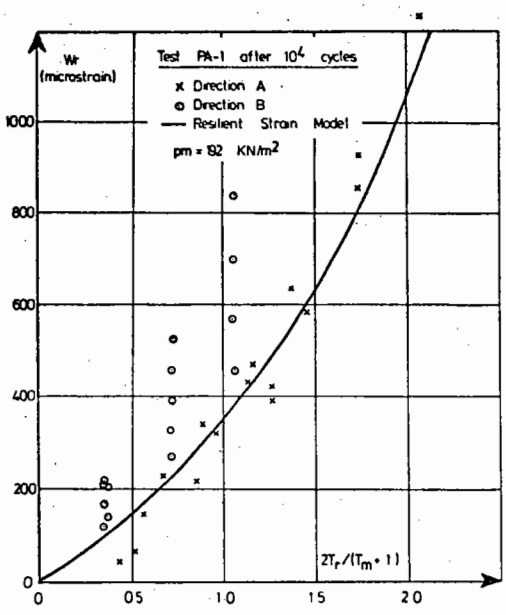

(b) After 10^4 cycles
(p_m = 192 kN/m^2)

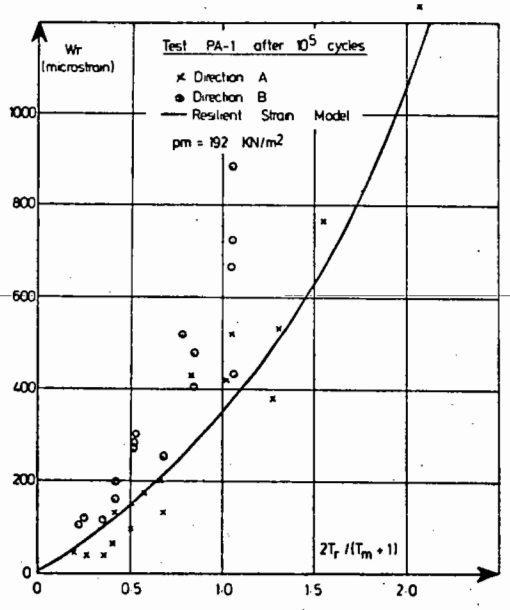

(c) After 10^5 cycles
(p_m = 192 kN/m^2)

FIG. D.27 RELATIONSHIP BETWEEN THE RESILIENT STRAIN PARAMETER, W_r, AND THE STRESS FUNCTION, $2T_r/(T_m + 1)$, FOR RESILIENT STRAIN READINGS TAKEN DURING TEST PA-1

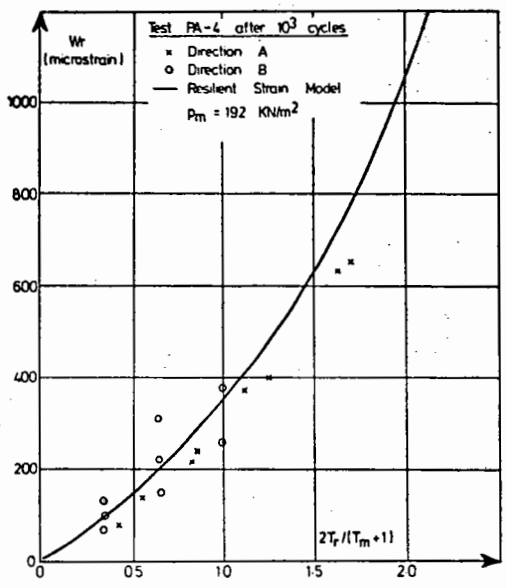

(a) After 10^3 cycles (p_m = 192 kN/m^2)

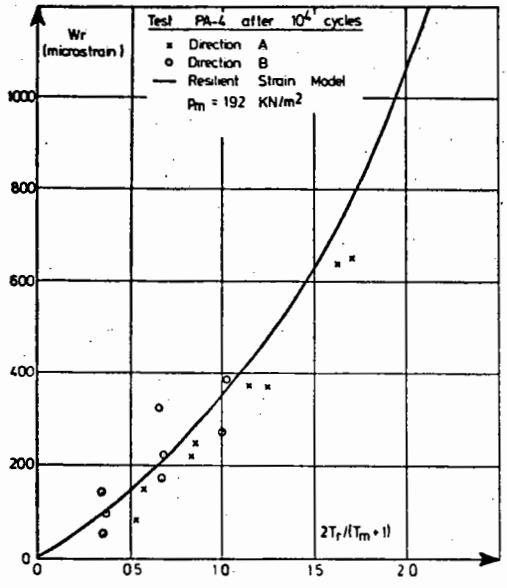

(b) After 10^4 cycles (p_m = 192 kN/m^2)

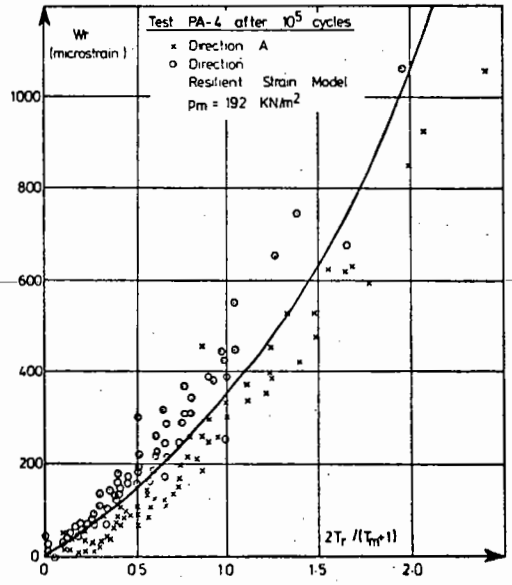

(c) After 10^5 cycles (p_m = 192 kN/m^2)

FIG. D.28 RELATIONSHIP BETWEEN THE RESILIENT STRAIN PARAMETER, W_r, AND THE STRESS FUNCTION, $2T_r/(T_m + 1)$, FOR RESILIENT STRAIN READINGS TAKEN DURING TEST PA-4

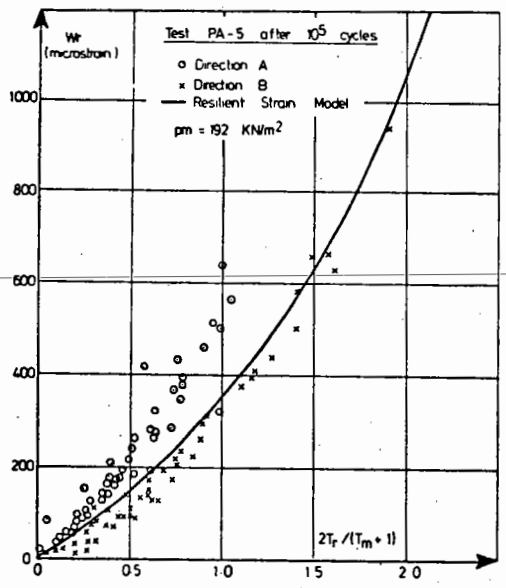

(a) After 10^5 cycles
(p_m = 192 kN/m^2)

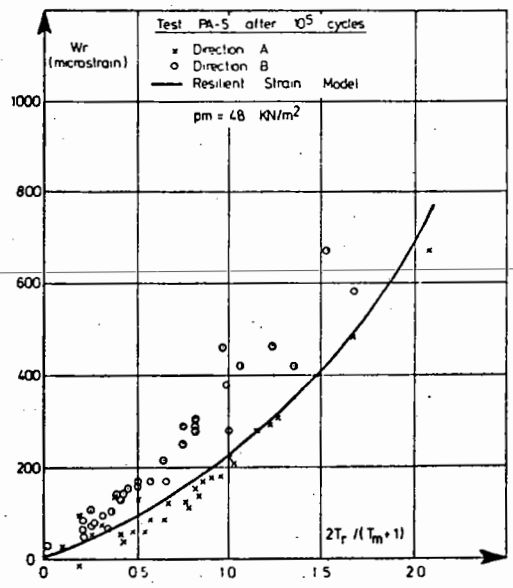

(b) After 10^5 cycles
(p_m = 48 kN/m^2)

FIG. D.29 RELATIONSHIP BETWEEN THE RESILIENT STRAIN PARAMETER, W_r, AND THE STRESS FUNCTION, $2T_r/(T_m + 1)$, FOR RESILIENT STRAIN READINGS TAKEN DURING TEST PA-5

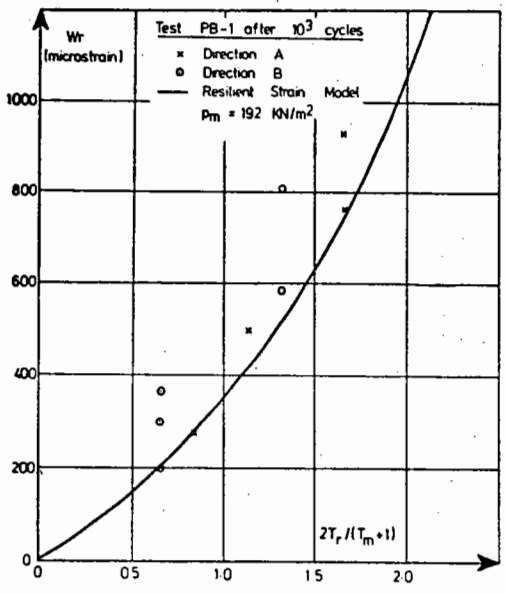

(a) After 10^3 cycles
(p_m = 192 kN/m^2)

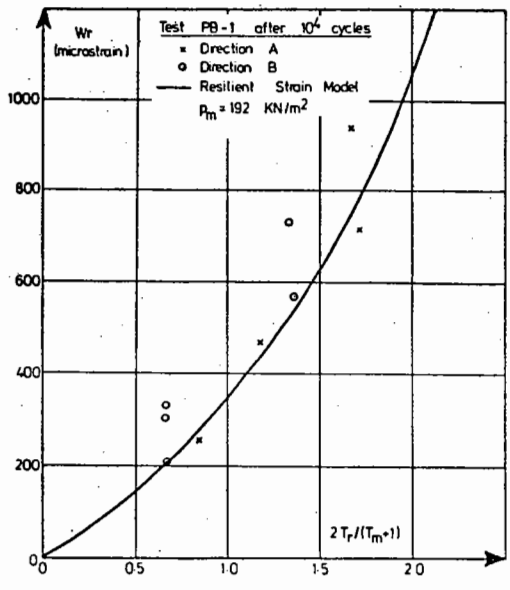

(b) After 10^4 cycles
(p_m = 192 kN/m^2)

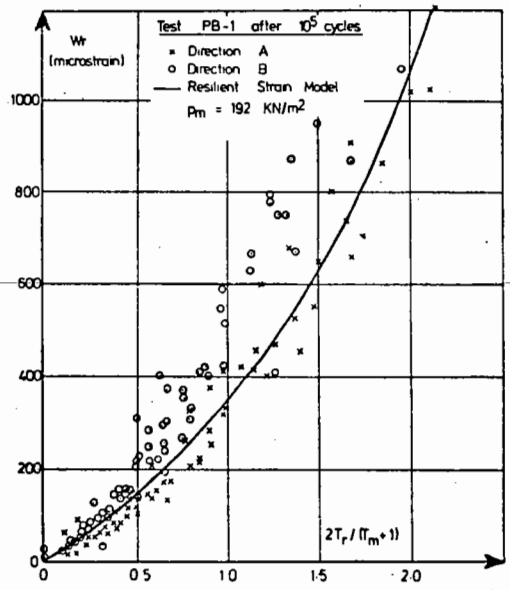

(c) After 10^5 cycles
(p_m = 192 kN/m^2)

FIG. D.30 RELATIONSHIP BETWEEN THE RESILIENT STRAIN PARAMETER, W_r, AND THE STRESS FUNCTION, $2T_r/(T_m + 1)$, FOR RESILIENT STRAIN READINGS TAKEN DURING TEST PB-1

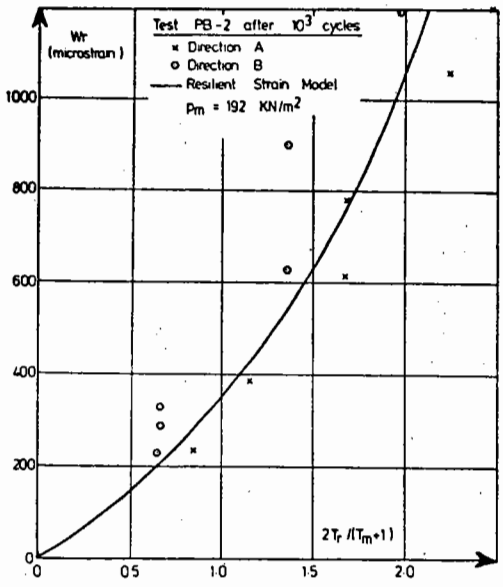

(a) After 10^3 cycles (p_m = 192 kN/m^2)

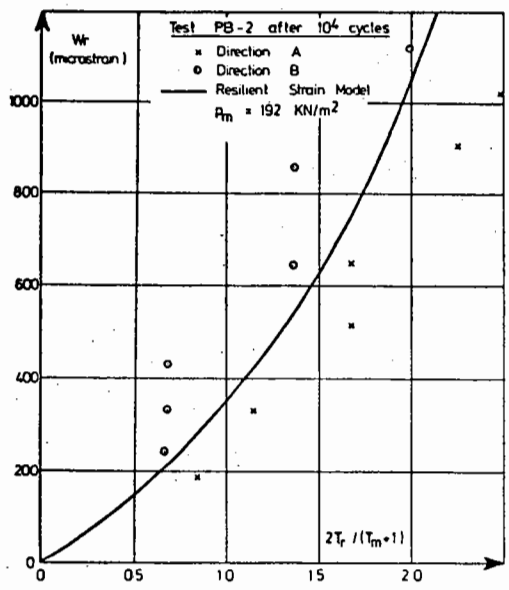

(b) After 10^4 cycles (p_m = 192 kN/m^2)

FIG. D.31 RELATIONSHIP BETWEEN THE RESILIENT STRAIN PARAMETER, W_r, AND THE STRESS FUNCTION, $2T_r/(T_m + 1)$, FOR RESILIENT STRAIN READINGS TAKEN DURING TEST PB-2

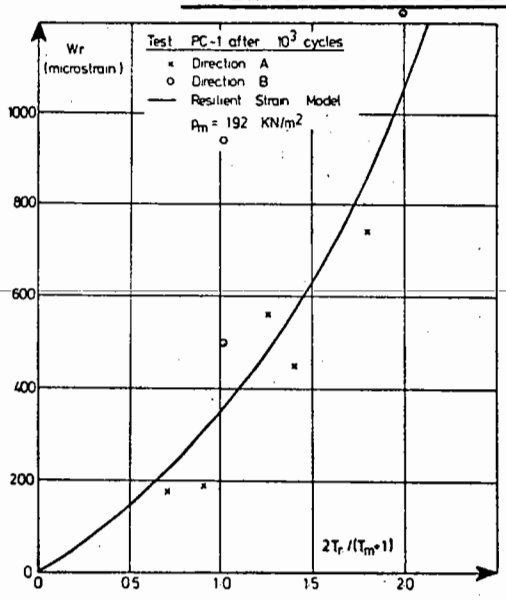

After 10^3 cycles (p_m = 192 kN/m^2)

FIG. D.32 RELATIONSHIP BETWEEN THE RESILIENT STRAIN PARAMETER, W_r, AND THE STRESS FUNCTION, $2T_r/(T_m + 1)$, FOR RESILIENT STRAIN READINGS TAKEN DURING TEST PC-1

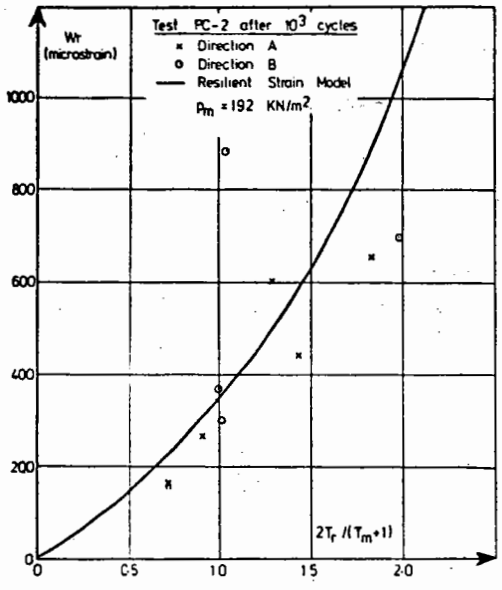

(a) After 10^3 cycles (p_m = 192 kN/m²)

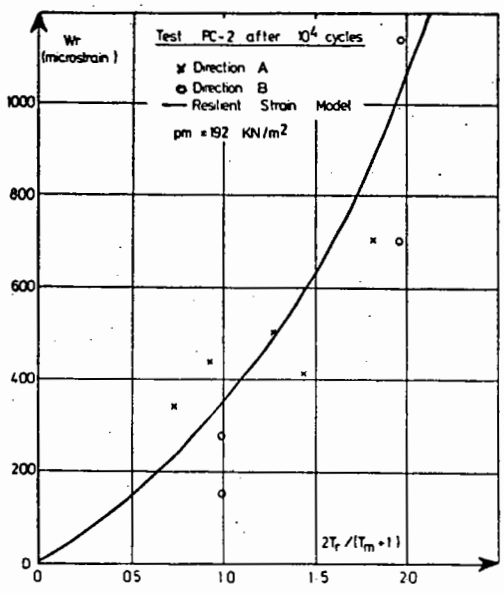

(b) After 10^4 cycles (p_m = 192 kN/m²)

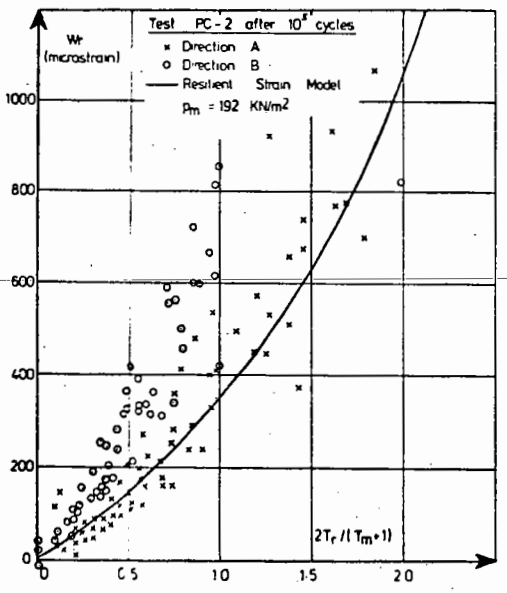

(c) After 10^5 cycles (p_m = 192 kN/m²)

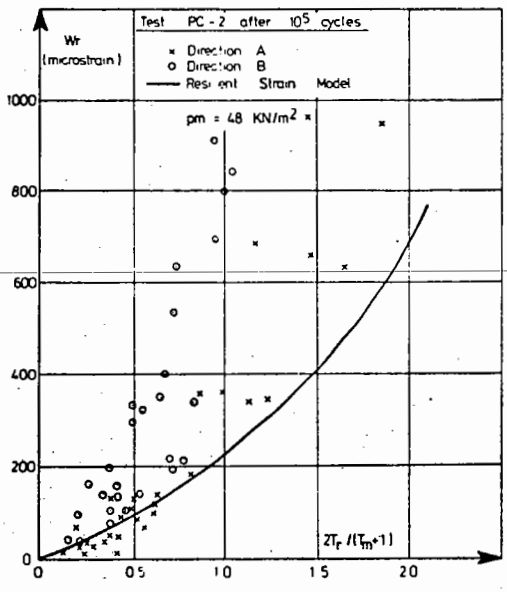

(d) After 10^5 cycles (p_m = 48 kN/m²)

FIG. D.33 RELATIONSHIP BETWEEN THE RESILIENT STRAIN PARAMETER, W_r, AND THE STRESS FUNCTION, $2T_r/(T_m + 1)$, FOR RESILIENT STRAIN READINGS TAKEN DURING TEST PC-2

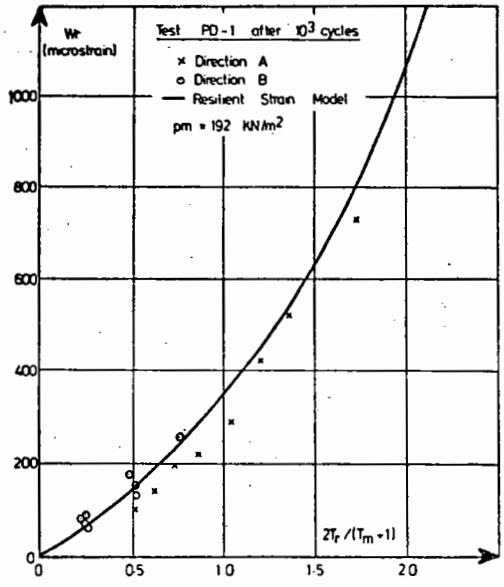

(a) After 10^3 cycles (p_m = 192 kN/m^2)

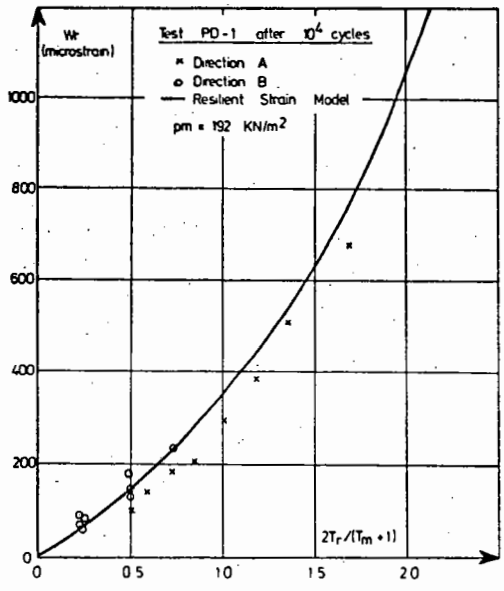

(b) After 10^4 cycles (p_m = 192 kN/m^2)

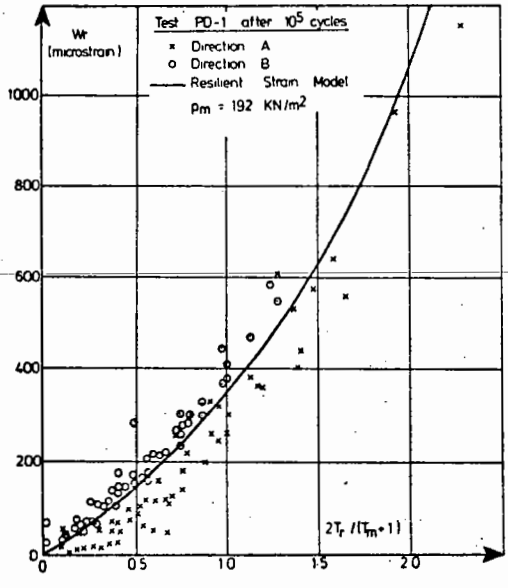

(c) After 10^5 cycles (p_m = 192 kN/m^2)

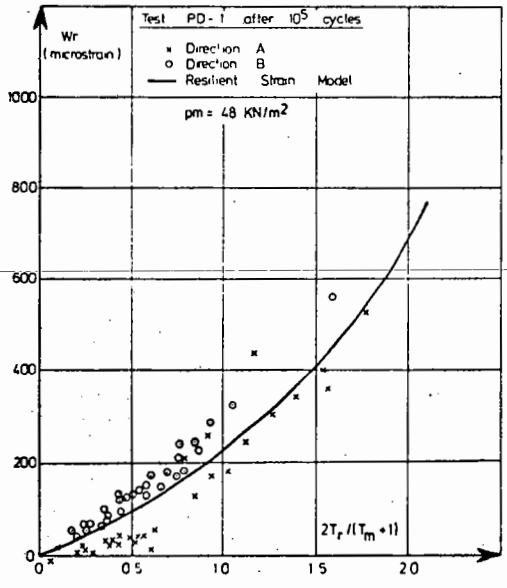

(d) After 10^5 cycles (p_m = 48 kN/m^2)

FIG. D.34 RELATIONSHIP BETWEEN THE RESILIENT STRAIN PARAMETER, W_r, AND THE STRESS FUNCTION, $2T_r/(T_m + 1)$, FOR RESILIENT STRAIN READINGS TAKEN DURING TEST PD-1

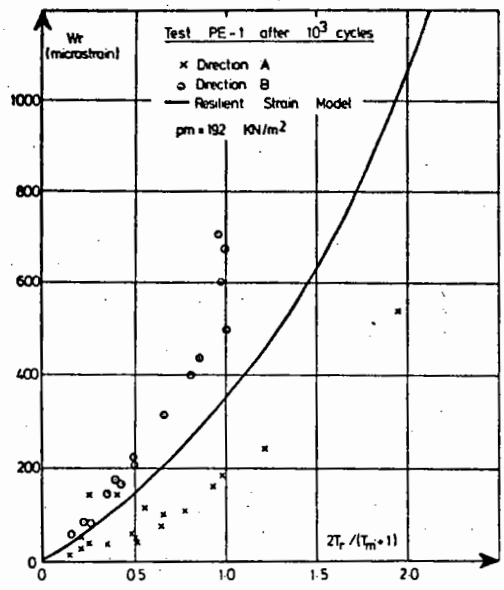

(a) After 10^3 cycles (p_m = 192 kN/m^2)

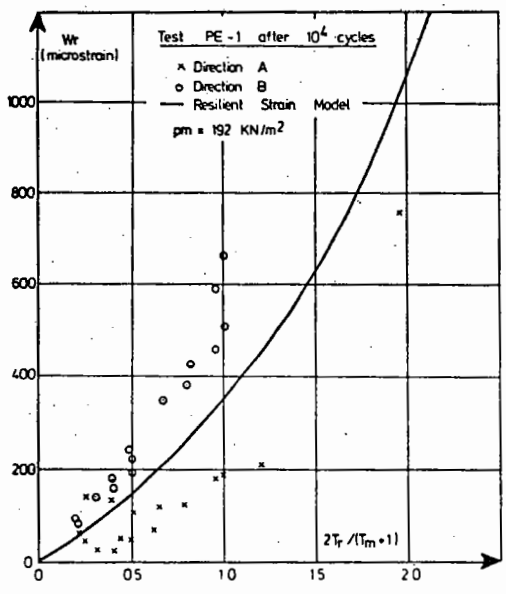

(b) After 10^4 cycles (p_m = 192 kN/m^2)

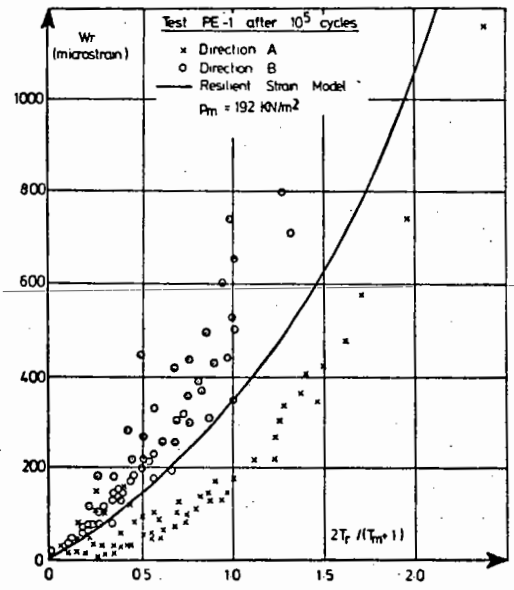

(c) After 10^5 cycles (p_m = 192 kN/m^2)

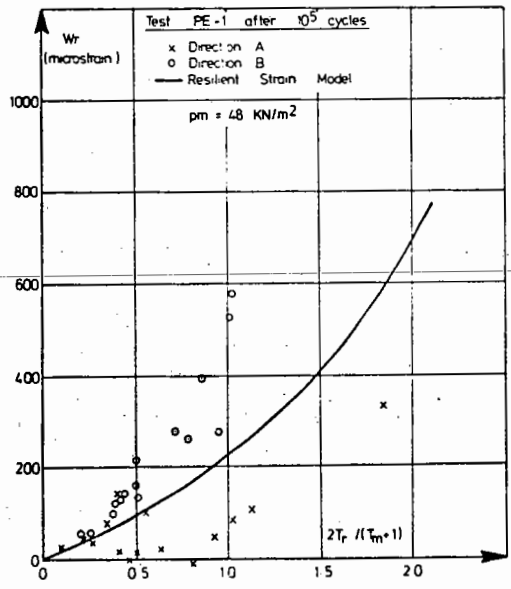

(d) After 10^5 cycles (p_m = 48 kN/m^2)

FIG. D.35 RELATIONSHIP BETWEEN THE RESILIENT STRAIN PARAMETER, W_r, AND THE STRESS FUNCTION, $2T_r/(T_m + 1)$, FOR RESILIENT STRAIN READINGS TAKEN DURING TEST PE-1

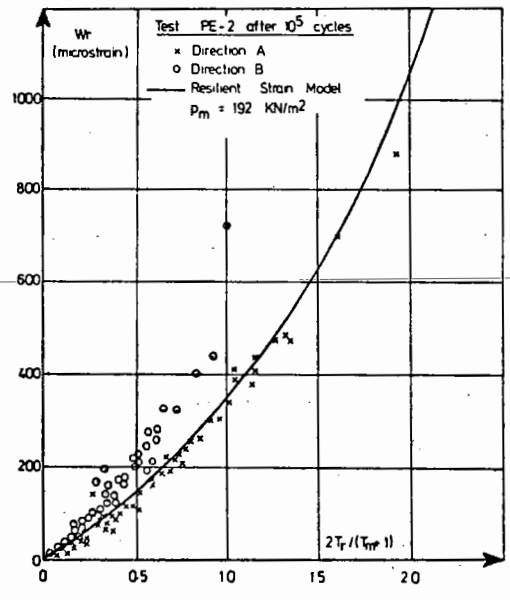

(a) After 10^5 cycles (p_m = 192 kN/m^2)

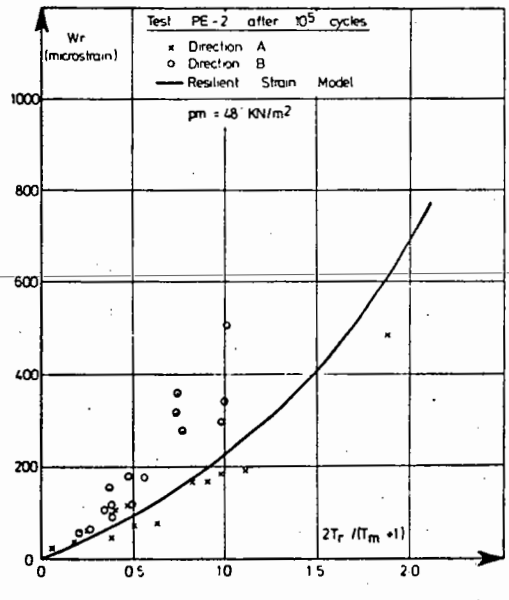

(b) After 10^5 cycles (p_m = 48 kN/m^2)

FIG. D.36 RELATIONSHIP BETWEEN THE RESILIENT STRAIN PARAMETER, W_r, AND THE STRESS FUNCTION, $2T_r/(T_m + 1)$, FOR RESILIENT STRAIN READINGS TAKEN DURING TEST PE-2

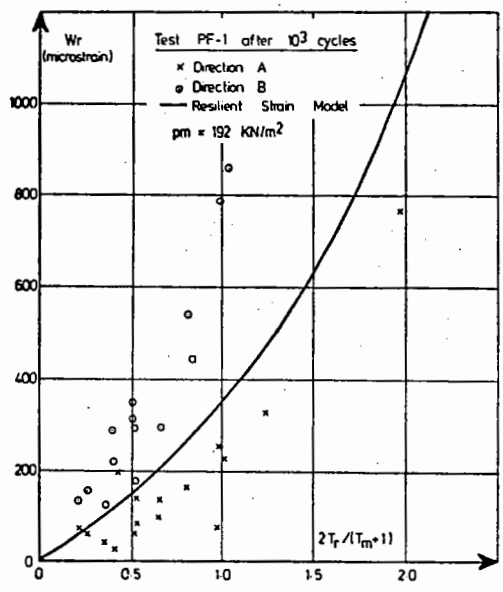

(a) After 10^3 cycles
(p_m = 192 kN/m^2)

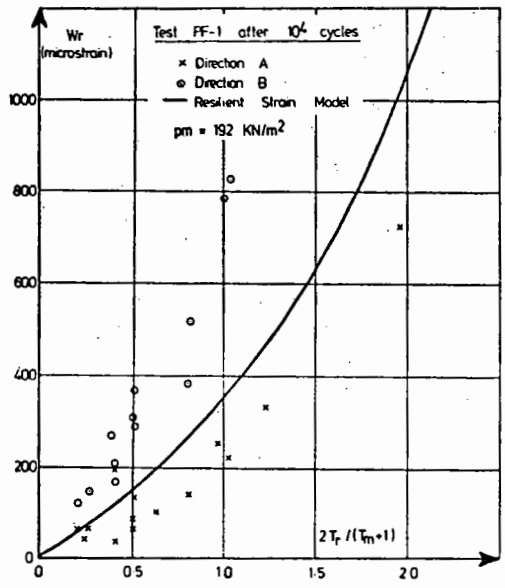

(b) After 10^4 cycles
(p_m = 192 kN/m^2)

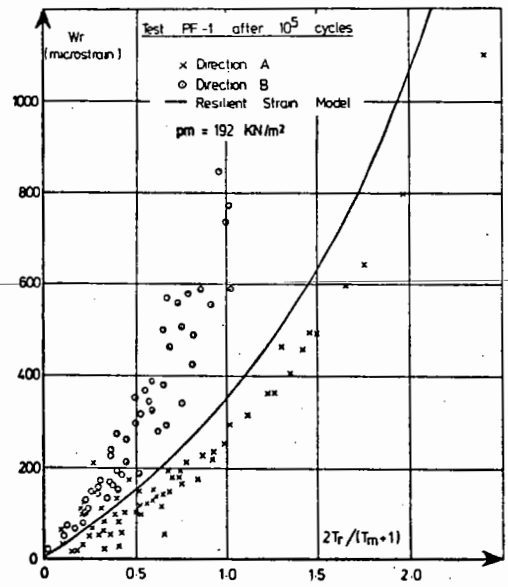

(c) After 10^5 cycles
(p_m = 192 kN/m^2)

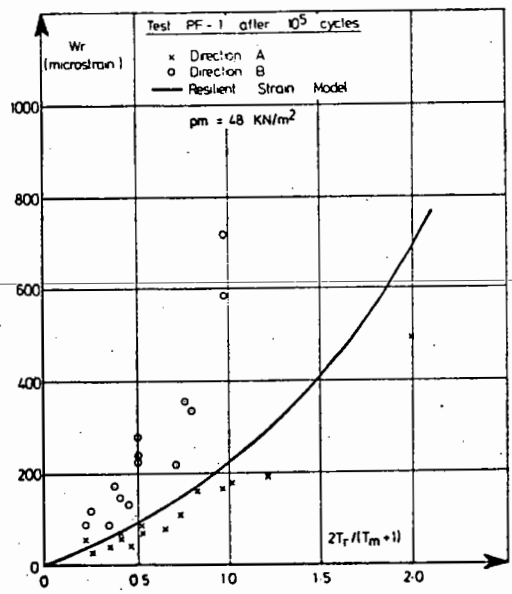

(d) After 10^5 cycles
(p_m = 48 kN/m^2)

FIG. D.37 RELATIONSHIP BETWEEN THE RESILIENT STRAIN PARAMETER, W_r, AND THE STRESS FUNCTION, $2T_r/(T_m + 1)$, FOR RESILIENT STRAIN READINGS TAKEN DURING TEST PF-1

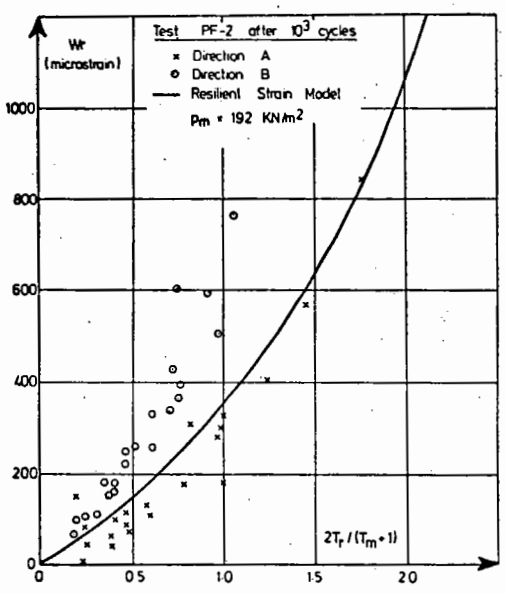

After 10^3 cycles (p_m = 192 kN/m^2)

FIG. D.38 RELATIONSHIP BETWEEN THE RESILIENT STRAIN PARAMETER, W_r, AND THE STRESS FUNCTION, $2T_r/(T_m + 1)$, FOR RESILIENT STRAIN READINGS TAKEN DURING TEST PF-2

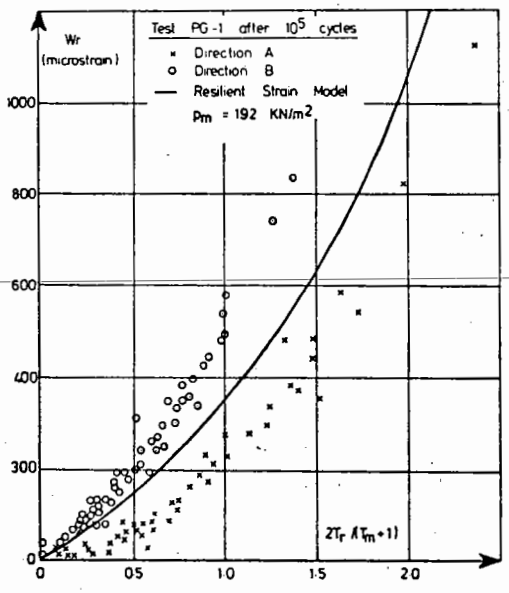

(a) After 10^5 cycles (p_m = 192 kN/m^2)

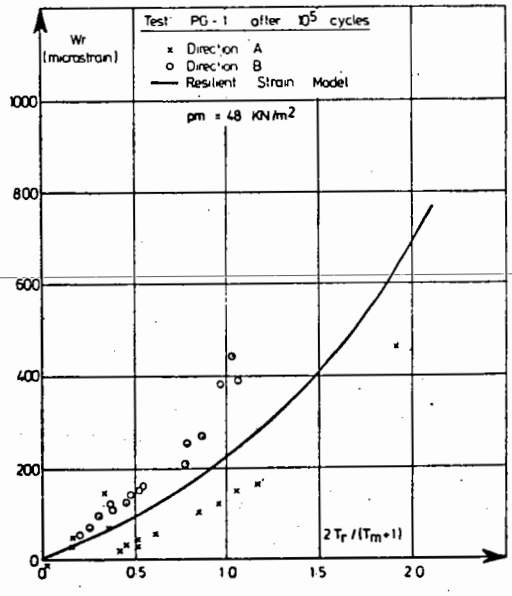

(b) After 10^5 cycles (p_m = 48 kN/m^2)

FIG. D.39 RELATIONSHIP BETWEEN THE RESILIENT STRAIN PARAMETER, W_r, AND THE STRESS FUNCTION, $2T_r/(T_m + 1)$, FOR RESILIENT STRAIN READINGS TAKEN DURING TEST PG-1

APPENDIX E

ADJUSTMENTS TO THE RESILIENT STRAIN MODEL TO GIVE A SYMMETRICAL STIFFNESS MATRIX

When the resilient strain model developed in Chapter 8 is used to define a stiffness or flexibility matrix for the material, the matrix produced (see Section 10.2.3) is not generally symmetrical. However, with small adjustments to the matrices [M] and [N] which define the stress parameter, T, and the strain parameter, W, this can be remedied. The model is then made more attractive from a theoretical point of view and more suitable for use in computation. There is no experimental justification for making this adjustment, and therefore the original model, as developed in Chapter 8, is used throughout the rest of this thesis. Parameters in the adjusted model are indicated by a prime, e.g. T′.

In the adjusted model:

$$[T'] = \left[\frac{M'}{p_m}\right] . [\sigma] \qquad \text{(E.1)}$$

where

$$[M'] = \frac{1}{4}\begin{bmatrix} 6 & -1 & -1 \\ -1 & 6 & -1 \\ -1 & 6 & -1 \end{bmatrix} \qquad \text{(E.2)}$$

and

$$[W'] = [N'] . [\epsilon] \qquad \text{(E.3)}$$

where

$$[N'] = \frac{3}{7}\begin{bmatrix} 5 & 1 & 1 \\ 1 & 5 & 1 \\ 1 & 1 & 5 \end{bmatrix} \qquad \text{(E.4)}$$

Therefore,

$$[N']^{-1} = \frac{1}{12}\begin{bmatrix} 6 & -1 & -1 \\ -1 & 6 & -1 \\ -1 & -1 & 6 \end{bmatrix} \qquad (E.5)$$

and the condition for a symmetrical flexibility matrix ($[N']^{-1} = k[M']$) is satisfied.

Considering the effect of these changes on the A and B directions in p-q space, from equations E.1 to E.4, it can be shown that:

$$T_A' = p + \frac{7}{6}q$$
$$T_B' = p - \frac{7}{12}q \qquad (E.6)$$

and

$$W_A' = v + \frac{12}{7}\epsilon$$
$$W_B' = v - \frac{6}{7}\epsilon \qquad (E.7)$$

Therefore, adjustment is indicated to the A and B direction of both stress and strain.

It is of interest to see how well the resilient strain test data agrees with the adjusted model. This is shown in Fig. E.1 in which the resilient strain parameters $(W_r)'_A$ and $(W_r)'_B$ are plotted against the stress parameter, $2T_r'/(T_m' + 1)$. It can be seen that the difference between Fig. E.1 and Fig. 8.7, which shows the same data for the original model, is insignificant compared with the scatter in the experimental points.

Changes to the coefficients in the flexibility matrix have also been evaluated. Consider the simplified situation close to the diagonal in principal stress space where $(L_r)_A = (L_r)_B = (L_r)_C$. The flexibility matrix in the principal stress directions is then $L_r.[N]^{-1}.[M]$.

For the original model:

$$L_r.[N]^{-1}.[M] = \frac{L_r}{54}\begin{bmatrix} -42 & -12 & -12 \\ -12 & 42 & -12 \\ -12 & -12 & 42 \end{bmatrix} \qquad (E.8)$$

and for the adjusted model:

$$L_r[N']^{-1}.[M'] = \frac{L_r}{48}\begin{bmatrix} 38 & -11 & -11 \\ -11 & 38 & -11 \\ -11 & -11 & 38 \end{bmatrix} \qquad (E.9)$$

It can be seen that the terms on the leading diagonal are increased by about 2% and the remainder by about 3%. This change is unlikely to be significant in a finite element calculation, although the changes may be greater away from the space diagonal.

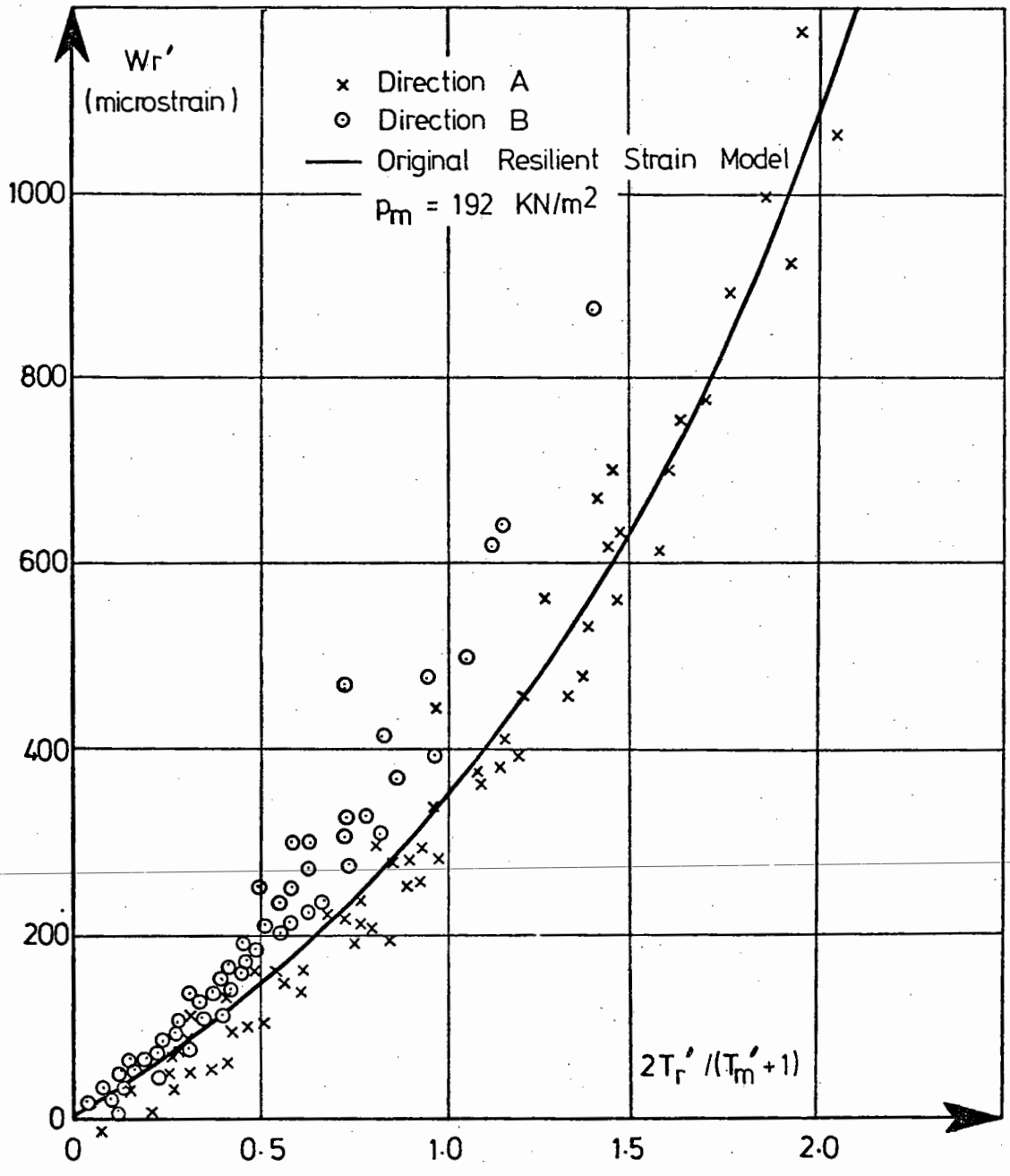

FIG. E.1 RELATIONSHIP BETWEEN THE RESILIENT STRAIN PARAMETER, W_r', AND THE STRESS FUNCTION, $2T_r'/(T_m' + 1)$, FOR THE ADJUSTED MODEL (p_m = 192 kN/m^2)

PLATE 1

SAMPLE FORMER AND VIBRATING TABLE

PLATE 2

GENERAL VIEW OF LOADING FRAME

PLATE 3

SERVO CONTROL ELECTRONICS AND

MONITORING EQUIPMENT

PLATE 4

SAMPLE READY FOR TESTING

(SHOWING ORIGINAL LOAD CELL)

PLATE 5

CLOSE-UP OF STRAIN TRANSDUCERS

PLATE 6

SAMPLE AFTER TEST PC-1

(SHOWING NEW LOAD CELL)

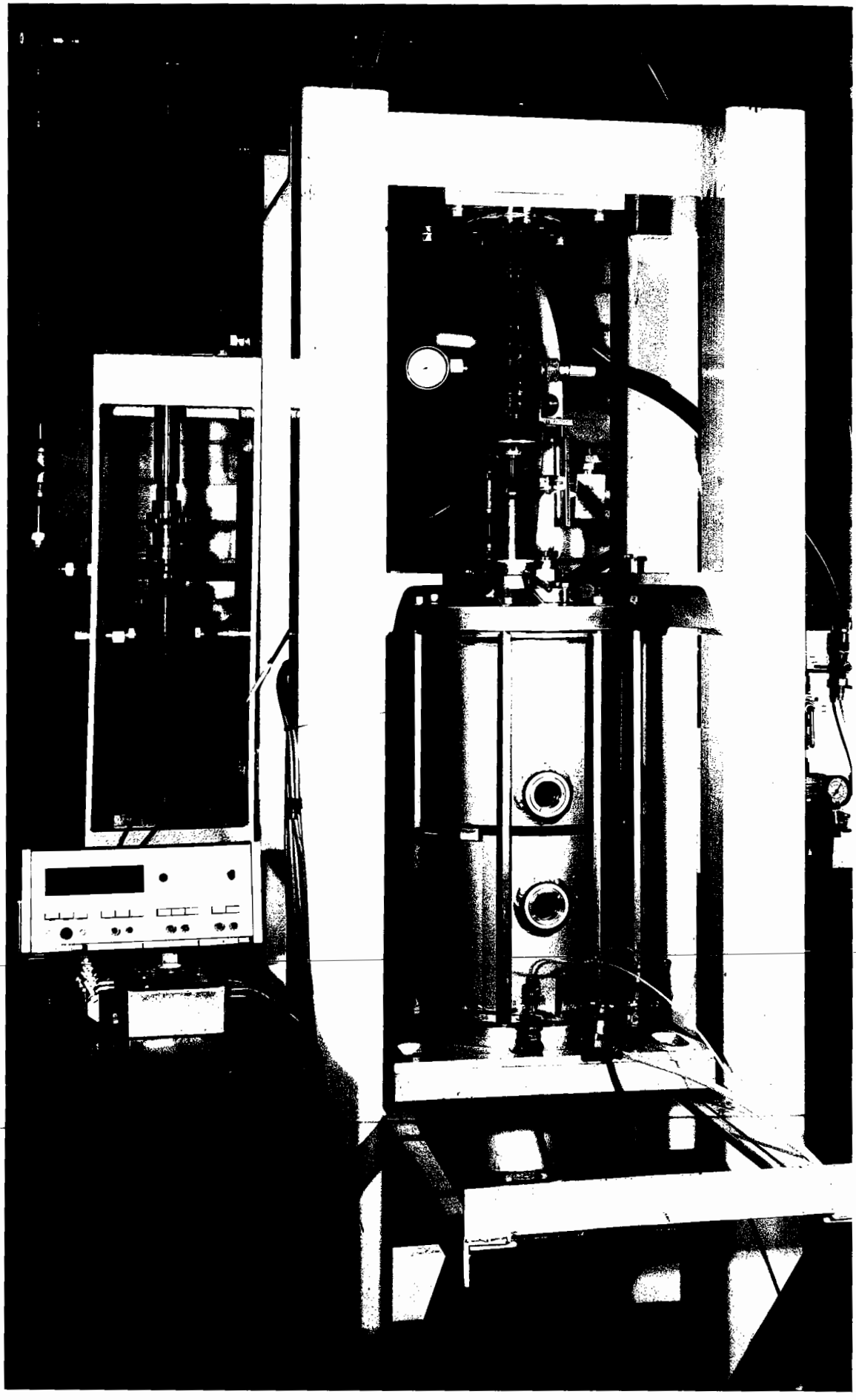

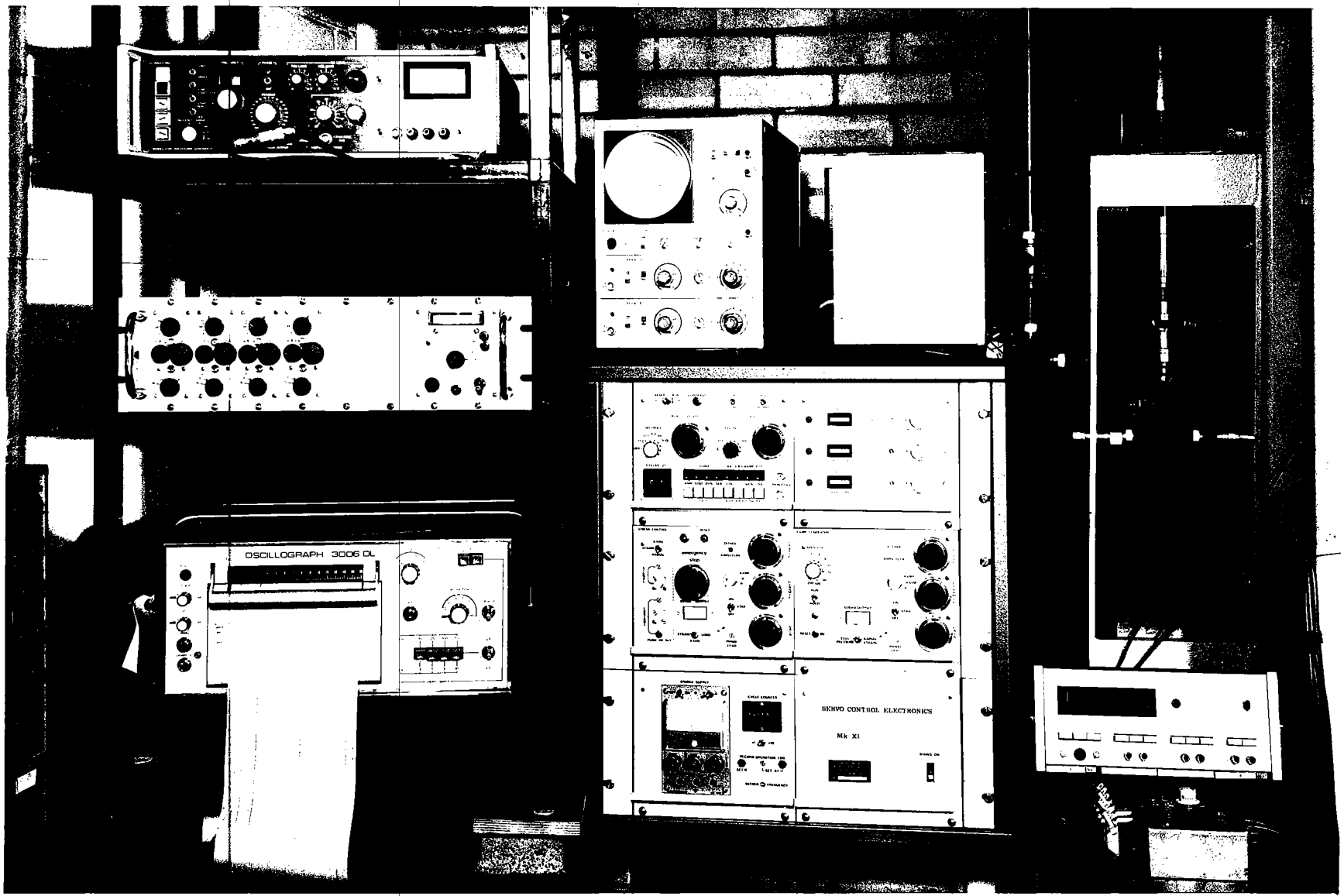
OSCILLOGRAPH 3006 DL
SERVO CONTROL ELECTRONICS
Mk XI